Universität Stuttgart

Tar Reforming over Low-cost Active Materials for Gasification Derived Syngas

A thesis accepted by the Faculty of Energy-, Process- and Bio-Engineering of the University of Stuttgart to fulfill the requirements for the degree of Doctor of Engineering Sciences (Dr.-Ing.)

By

Yen-Hau Chen

born in Neu-Taipeh City, Taiwan

Main Referee:	Univ-Prof. Dr. techn. Günter Scheffknecht
Co-Referee	Prof. Dr. Ching-Yuan Chang, National Taiwan University

Date of oral exam: 18.08.2021

Institute of Combustion and Power Plant Technology

2021

Erklärung

Hiermit versichere ich, Yen-Hau Chen, die vorliegende Arbeit ohne Hilfe Dritter und nur mit den angegebenen Quellen und Hilfsmitteln angefertigt zu haben. Alle Stellen, die Quellen entnommen wurden, sind als solche kenntlich gemacht worden. Diese Arbeit hat in gleicher oder ähnlicher Form noch keiner Prüfungsbehörde vorgelegen. In der abgegebenen Arbeit stimmen die schriftliche und elektronische Fassung überein.

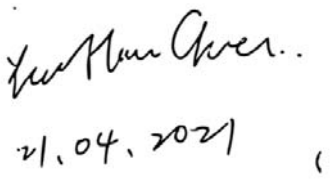

21.04.2021

Contents

SYMBOLS XI

ABBREVIATION XV

KURZFASSUNG XVIII

ABSTRACT XXI

1 INTRODUCTION 1

1.1 MOTIVATION 1

1.2 TAR DEFINITION AND FORMATION 4

1.3 TARGET GASIFICATION PROCESSES FOR TAR REDUCTION 7

1.3.1 Sorpion enhanced gasification (SEG) 7

1.3.2 Steam-oxygen gasification (SOG) 9

1.4 TAR REFORMING REACTIONS 12

1.5 TYPICAL TAR-REFORMING CATALYSTS 14

1.6 BIOCHARS AS TAR REFORMING CATALYST 15

1.7 BIOCHAR GASIFICATION DURING TAR REFORMING 17

1.8 OBJECTIVES OF PUBLISHED PAPERS 19

1.8.1 Scientific contributions 19

2 PUBLICATIONS 22

2.1 LIST OF PUBLICATIONS 22

CONTRIBUTION REPORT 23

ADDITIONAL SCIENTIFIC PUBLICATIONS 23

PAPER I 26

PAPER II 40

PAPER III 66

3 RESULTS AND DISCUSSION 80

3.1 THE PROPERTIES OF APPLIED BIOCHAR CATALYSTS 80

3.2 THE GASIFICATION REACTIVITY OF BIOCHAR DURING THE REFORMING OF TAR MODEL COMPOUNDS 85

3.3 THE GASIFICATION-CAUSED DEACTIVATION OF BIOCHAR 88

3.4 THE EFFECT OF MAIN SYNGAS COMPONENTS (H_2O AND H_2) AND THE CATALYTIC PERFORMANCE OF BIOCHARS ON THE REFORMING OF TAR MODEL COMPOUNDS 90

3.5 KINETICS OF THE REFORMING OF TAR MODEL COMPOUNDS OVER BIOCHARS 95

3.6 THE DESIGN OF THE TAR REFORMER 104

3.6.1 Heat demand for tar reforming of SEG derived syngas over wood char *105*

3.6.2 Design of the tar reformer *108*

3.6.3 Design of the preheater *112*

3.6.4 Heat source *115*

3.6.5 The diagram of the tar reformer integrated with the preheater *116*

4 SUMMARY AND CONCLUSIONS **118**

REFERENCES **121**

APPENDIX **129**

Acknowledgments

It is my pleasure to acknowledge those who made this thesis possible.

First of all, I would like to thank my advisor, Prof. Dr. techn. Günter Scheffknecht, for supporting my research and encouraging me to complete my doctoral studies.

I am very grateful to my leader, Max Schmid, M.Sc., for giving me a lot of practical guidance and assistance, allowing me to gain valuable professional experience, inspiring me, and stimulating me to think about the possibility to promote the cooperation between Taiwan and Germany. My thanks also goes to my former leader, Reinhold Spörl, for his assistance.

During my time at IFK, my colleagues - Selina Hafner, Matthias Hornberger, Felix Mangold, Joseba Moreno, Ashak Parvez, Lukas Reiner, Gebhard Waizmann, Georg Hartfuß, Thiansiri Kertthong, Heiko Holz, and Tim Seitz - were all very good partners. Thanks for the helpful comments and discussions which helped to put forward my ideas. I have learned a lot from everyone, thank you. I again appreciate Gebhard, Tim, and Thiansiri who helped me a lot with my project.

In addition, since Prof. Dr. Ching-Yuan Chang and Dr. Chia-Chi Chang of National Taiwan University encouraged me to start working in this field, their continuous and substantial cooperation have provided me with a lot of motivation for research. I would like to express my sincere thanks.

DAAD is appreciated for providing my scholarship.

Last but not least, I would like to thank my family in Taiwan for all the support they gave me along the way. Special thanks also to Regina Wittos-Liek and Dr. Werner Weins in Munich for making me feel at home in Germany. Finally, I would like to express my gratitude to my friends in Germany, you have accompanied me in my journey towards completing this research while being overseas for all these years.

Symbols

Latin Symbols

Symbol	Unit	Meaning
A	m^2	A_{ref} or A_{preH}
A_{ref}	m^2	The heat transfer area of the reformer's internal wall
A_{ref}	m^2	The heat transfer area of Pipe1's internal wall
C_{H2}	%	Initial volume concentration of hydrogen in the sample gas
C_{H2O}	%	Initial volume concentration of steam in the sample gas
C_{p_syn}	J kg^{-1} K^{-1}	The heat capacity of the syngas in the preheater
d	m	Characteristic length of the wood char
D	m	Internal diameter of the reformer pipe
da	m	Pipe1's inside diameter
d_h	m	Hydraulic diameter (m) equal to (d_a - d_i)
di	m	Pipe2's outside diameter
D_l	m^2 s^{-1}	Thermal diffusivity of the syngas in the reformer
E_a	kJ/mol	Activation energy
k_0	m^3 kg^{-1} h^{-1}	Apparent pre–exponential factor

$\dot{m}$	kg s^{-1}	The mass flow rate of inflow syngas
Nu_{preH}	-	Nusselt number of the syngas in the preheater
Nu_{ref}	-	Nusselt number of the syngas in the reformer
Pe	-	Peclet number of the syngas in the reformer
Pr_{ref}	-	Prandtl number of the syngas in the reformer
$\dot{Q}$	W	$\dot{Q}_{ref}$ or $\dot{Q}_{preH}$
$\dot{Q}_{preH}$	W	The theoretical heat demand for preheating
$\dot{Q}_{ref}$	W	The heat demand in the tar reformer
Re_{preH}	-	Reynolds number of the syngas in the preheater
Re_{ref}	-	Reynolds number of the syngas in the reformer
r_G/M_C	min^{-1}	Gasification rate
r_G/r_{20}	-	The reactivity on the basis of the reference state at conversion equal to X_C =0.2
S_{C6H6}	-	Selectivity of benzene
S_{CH4}	-	Selectivity of methane
S_{CO}	-	Selectivity of carbonmonoxide
T_a	℃	Temperature of Pipe1’s internal wall
$T_{HS,m}$	℃	The minimum temperature of heat source for the tar reformer or preheater
$T_{HS,m}$	℃	The minimum temperature of the heat source
T_i	℃	Temperature of Pipe2’s external wall

$T_{wall,in}$	℃	The temperature on the internal wall surface of the reformer or T_a on Pipe1 of the preheater
V_S	m s^{-1}	Superficial velocity of syngas in the tar reformer
X_C	-	Carbon mass conversion
X_N	-	Naphthalene conversion
X_T	-	Toluene conversion

Greek Symbols

Symbol	Unit	Meaning
α_{syn_preH}	W m^{-2} K^{-1}	The heat transfer coefficient of the syngas in the preheater
α_{syn_ref}:	W m^{-2} K^{-1}	The heat transfer coefficient of the syngas in the reformer
ΔT_P	K	The temperature difference required for preheating
ΔT_{preH}	K	The temperature variation from T_a to T_i
ΔT_{ref}	K	Temperature dropping from the internal wall of the reformer to the center
λ_{bed}	W m^{-1} K^{-1}	Thermal conductivity of wood char
λ_{syn_preH}	W m^{-1} K^{-1}	Thermal conductivity of the syngas in the preheater
λ_{syn_ref}	W m^{-1} K^{-1}	Thermal conductivity of the syngas in the reformer
σ	W m^{-2} K^{-4}	Stefan–Boltzmann constant (5.6704×10^{-8} W m^{-2} K^{-4})
$\varepsilon(d)$	-	Porosity in the catalyst bed with the function of pellet diameter d

Abbreviation

Abbreviation	Meaning
AAEMs	Alkali and alkaline earth metals
DME	Dimethyl Ether
ERPM	Extend Random Pore Model
GC-MS	Gas chromatography–mass spectrometry
NTP	Environment of 25 °C and 1 atm
PSC	Palm shell char
PAH	Polycyclic aromatic hydrocarbons
RPM	Random Pore Model
SC	Straw char
SEG	Sorption enhanced gasification
SOG	Steam-oxygen gasification
SEM	Scanning electron microscope
SEM–EDX	Scanning electron microscope–energy dispersive X–ray spectroscopy
SCFA	Straw char containing fly ash
WC	Wood char

5%K-PSC	5% potassium metal impregnated palm shell char
5%Fe-PSC	5% iron metal impregnated palm shell char

Kurzfassung

In der vorliegenden Arbeit wird das Potenzial von in-situ-Biokoksgemischen aus einem Vergasungsprozess (flugaschehaltige Strohkokse), spezial hergestellte pyrolysierte Biokokse aus Holz, Stroh und Palmkernschalen und metallimprägnierte Biokokse (Kalium- und eisenbeladene Palmkernschalen) zur Wiederverwendung als Teerreformierungskatalysatoren in Vergasungsprozessen untersucht. Die katalytische Aktivität und Reformierungsselektivität verschiedener Materialien wurden mit Toluol und Naphthalin als Teermodellkomponenten in Gegenwart von Wasserdampf und Wasserstoff (Hauptzusammensetzung des Synthesegases aus sorptionsunterstützter Wasserdampfvergasung und Wasserdampf-Sauerstoff-Vergasung) in einem Festbettreaktor im Labormaßstab bei Temperaturen bis 900 °C untersucht.

Es wurde nachgewiesen, dass flugaschehaltige Strohkokse, die aus dem Wasserdampf-Sauerstoff-Vergasungsprozess stammen, als Teerreformierungskatalysator eingesetzt werden können, um die Gesamtleistung des Wasserdampf-Sauerstoff-Vergasungsprozesses zu verbessern. Es wurde festgestellt, dass die signifikante Wirkung von Wasserstoff auf die Reformierung von Toluol durch die Bildung von Benzol durch Hydrodealkylierungsreaktion verursacht wurde. Das volumetrische Verhältnis von H_2O zu H_2 war ein wesentlicher Parameter, der die Selektivität der Reformierung von Toluol bestimmte. Obwohl die Koexistenz von Toluol und Wasserstoff die Vergasung hemmen würde, wurde bewiesen, dass die flugaschehaltigen Strohkokse während der Reformierung von Toluol vergast werden. Aus dieser Vergasung resultieren auch eine Veränderung der katalytischen Aktivität und der Reformierungsselektivität.

Bei pyrolysierten Biokoksen kann das kostengünstige Material, Holzkokse, Strohkokse und Palmkernschalenkokse erfolgreich als Teerreformierungskatalysator nach dem sorptionsunterstützten Wasserdampfvergasungsprozess verwendet werden. Die theoretische Raumzeit bis zum Erreichen der vollständigen Umwandlung von Naphthalin betrug 0,07 kg h m^{-3} bei 850 °C für Holzkokse, was eine vielversprechende katalytische Aktivität zeigt. Kalium- und eisenbeladene Palmkernschalenkokse zeigten ebenfalls eine viel bessere katalytische Aktivität als Palmkernschalenkokse, während die parallele Vergasungsreaktion von K-beladenen Palmkernschalenkoksen die Umwandlung mit ihrem drastischen Massenverlust beeinflusste.

Schließlich wurden die spontane Vergasung und die katalytische Aktivität von Holzkoksen in simulierten sorptionsunterstützten Wasserdampfvergasungsumgebungen mit Toluol und Naphthalin als Teermodellkomponenten untersucht. Zusätzlich wurde CaO als Referenzkatalysator zum Vergleich verwendet, da CaO ein häufig verwendetes Sorptionsmittel im sorptionsunterstützten Wasserdampfvergasungsprozess ist. In dieser Arbeit wurde ein Modell der Vergasungsreaktivität während der Reformierung von Teermodellkomponenten an Holzkoksen entwickelt, das auf der Reaktivität bei 20 % Kohlenstoffumsatz unter Verwendung des erweiterten Zufallsporenmodells basiert, wobei der präexponentielle Faktor, die Aktivierungsenergie und ein Strukturparameter zu $1{,}65 \cdot 10^{10}$ min^{-1}, 265,8 kJ mol^{-1} und 127 berechnet wurden. Bei der Untersuchung der katalytischen Aktivität wurde festgestellt, dass Wasserstoff die Teerreformierung an CaO hemmt, während der Einfluss von Wasserstoff an Holzkoksen unbedeutend war. Die Ergebnisse zeigten, dass eine spontane Vergasung während der Reformierung von Teersubstituten zu Massenverlust,

Porenkollaps und Agglomeration anorganischer Substanzen führte, was zur katalytischen Deaktivierung von Holzkoksen beitrug. Unter Berücksichtigung der durch die Vergasung verursachten Deaktivierung wurde der Kohlenstoffumsatz dann als Variable verwendet, um die kinetischen Gleichungen der Reformierung von Teersubstituten zu modifizieren. Die Aktivierungsenergie und der präexponentielle Faktor der Reformierung von Naphthalin (und von Toluol) auf Holzkoksen wurden mit den Werten von 422,5 kJ mol^{-1} und $2{,}92 \cdot 10^{22}$ m^3 kg^{-1} h^{-1} (284,8 kJ mol^{-1} und $1{,}90 \cdot 10^{15}$ m^3 kg^{-1} h^{-1}) berechnet, während die Werte für CaO 126,9 kJ mol^{-1} und $6{,}79 \cdot 10^{4}$ m^3 kg^{-1} h^{-1} (254,5 kJ mol^{-1} und $6{,}73 \cdot 10^{11}$ m^3 kg^{-1} h^{-1}) betrugen.

Die in dieser Arbeit entwickelten kinetischen Modelle wurden verwendet, um einen Teerreformer zu entwerfen, der in den sorptionsunterstützten Wasserdampfvergasungsprozess integriert ist.

Abstract

The present work investigated the potential of in-situ biochar mixture from gasification process (straw char containing fly ash), pyrolyzed biochars by self-production (wood char, straw char, and palm shell char), and metal impregnated biochars (potassium and iron-loaded palm shell char) to be reused as tar-reforming catalysts in gasification processes. The catalytic activity and reforming selectivity of different materials were evaluated with toluene and naphthalene as tar model compounds in the presence of steam and hydrogen (major composition in the syngas from sorption enhanced gasification and steam-oxygen gasification) in a lab-scale fixed bed reactor at high temperature up to 900 °C.

Straw char containing fly ash derived from the steam-oxygen gasification process was verified to be able to apply as a tar-reforming catalyst for enhancing the overall performance of the steam-oxygen gasification process. It was found that the significant effect of hydrogen on toluene reforming was demonstrated by the formation of benzene through hydrodealkylation reaction. The volumetric ratio of H_2O to H_2 was an essential parameter that decided the selectivity of toluene reforming. Although the coexist of toluene and hydrogen would inhibit the gasification, straw char containing fly ash was proved to be gasified during toluene reforming. The surface migration and agglomeration of inorganics due to gasification also resulted in the change of catalytic activity and reforming selectivity through time.

With regard to pyrolyzed biochars, the low-cost material, wood char, straw char, and palm shell char, can successfully be used as the tar-reforming catalyst after sorption enhanced gasification process. A theoretical space time to reach the complete naphthalene conversion was 0.07 kg h m^{-3} at 850 °C for wood char,

demonstrating a promising catalytic activity. It was also found that potassium and iron-loaded palm shell chars exhibited much better catalytic activity than palm shell char, while the parallel reaction of gasification of K-loaded palm shell char influenced the conversion with its drastic mass loss.

Lastly, the spontaneous gasification and catalytic activity of wood char were thoroughly evaluated in simulated sorption enhanced gasification environments with toluene and naphthalene as tar model compounds. Besides, CaO was used as a reference catalyst for the comparison purpose since CaO is a commonly used sorbent in the sorption enhanced gasification process. A model of gasification reactivity during reforming of tar model compounds over wood char was developed in this work based on the reactivity at 20 % carbon conversion adopting the Extended Random Pore Model, where the pre-exponential factor, activation energy, and structural parameter were calculated to be $1.65 \cdot 10^{10}$ min^{-1}, 265.8 kJ mol^{-1}, and 127, respectively. During the catalytic activity investigation, hydrogen was found to inhibit tar-reforming performance over CaO while the impact of hydrogen was insignificant over wood char. The results showed that spontaneous gasification during tar surrogates reforming led to mass loss, pore collapse, and inorganics agglomeration, which contributed to the catalytic deactivation of wood char. By considering gasification-caused deactivation, the carbon conversion was then used as a variable to modify the kinetic equations of the tar surrogates reforming. The activation energy and pre-exponential factor of naphthalene reforming (and toluene reforming) over wood char were calculated with the values of 422.5 kJ mol^{-1} and $2.92 \cdot 10^{22}$ m^3 kg^{-1} h^{-1} (284.8 kJ mol^{-1} and $1.90 \cdot 10^{15}$ m^3 kg^{-1} h^{-1}), respectively, whereas the values for CaO were 126.9 kJ mol^{-1} and $6.79 \cdot 10^4$ m^3 kg^{-1} h^{-1} (254.5 kJ mol^{-1} and $6.73 \cdot 10^{11}$ m^3 kg^{-1} h^{-1}), respectively. The kinetic models developed in this study were later used for

designing a tar reformer integrated with the sorption enhanced gasification process.

1 Introduction

Recently, the application of biochar in different research areas has gotten more and more attention. Since biochar has particular properties including high surface area, pore distribution, and alkali and alkaline earth metals (AAEMs) groups doped surface, biochar is regarded as a potential material as catalyst for various reactions. With other advantages of low cost and simple production, the possibility to replace commercial catalyst with biochar has also been discussed in various studies. This study thus investigated the catalytic activity of different biochars (pyrolyzed biochar, in-situ biochar from gasification process, metal-impregnated biochar) for tar reforming on the purpose of the further application in actual gasification processes. Sorption enhanced gasification (SEG) and steam-oxygen gasification (SOG) are two primary gasification processes carried out at the University of Stuttgart for the past few years. This research is hence based on these two gasification processes.

1.1 Motivation

With high energy efficiency and various applications of the produced syngas, biomass gasification will play a major role in an economy that ceases from using fossil fuels. The sustainably produced syngas can be used for generation of electrical power but more importantly to produce liquid (e.g. methanol, dimethyl ether (DME)) or base chemicals (e.g. C_2H_4) [1]. However, there are several barriers for the application of biomass gasification. A particularly problematic issue in this respect is the generation of tar that is associated with the gasification process. Tar can lead to severe operational problems when they condense on cold surfaces forming deposits that block the

gas path. Moreover, high tar concentrations in the syngas result in damages of downstream power generation equipment (i.e. engines, turbines) and synthesis units (i.e. catalytic reactors). This causes unscheduled standstill times and hence increases the cost of biomass gasification processes. Generally, the tar containing in raw produced gases from updraft gasifiers, with an average value of around 50 g m^{-3}_{NTP}, is more than in any other gasifier. Fluidized beds and circulating fluidized beds have an average tar loading of about 10 g m^{-3}_{NTP}. Downdraft gasifiers, when operated according to specifications, produce the cleanest gases with tar loading typically less than 1 g m^{-3}_{NTP}. In routine commercial operation downdraft units often have loadings in excess of 1 g m^{-3}_{NTP} [2]. However, the tar limitations in syngas for the typical downstream usage are less than 30, 1, and 0.1-1 mg m^{-3} for gas turbines, methanol synthesis, and Fischer–Tropsch synthesis, respectively [3, 4]. As a result, tar removal is essential in most biomass gasification processes [5–8].

The cleaning processes can be separated into physical and chemical methods [9]. Physical gas cleaning includes unit operations such as filters, scrubbers and wet electrostatic precipitators, while also chemical methods such thermal cracking and catalytic reforming can be applied. Among these methods, efficient gas cleaning processes that can be operated at high temperature are seen as energetically beneficial since they can avoid excessive gas cooling of syngas from high temperature gasification process that is required for condensing and scrubbing of tar in a water or DME scrubber. Steam reforming at high temperature is regarded as an appropriate method for syngas cleaning which can also convert tar into useful synthesis gas components such as H_2 and CO [6,8]. Syngas with suitably low tar concentration could be directly used at high temperature in a synthesis or power generation process. Such high temperature tar reduction process generally requires a suitable catalyst material with high tar conversion efficiency and a good resistance against other

syngas impurities (e.g. S and Cl species). Another promising option for catalysts is to use catalytically active material that can be generated in-situ in the gasification process or is available at a very low price. With such a process, no additional chemicals are required or their cost can be limited to a minimum. As a result, thermal catalytic steam reforming of tar in gasification process is the objective of this thesis with a special focus on the application of biochar as catalyst materials. Tar model compounds, toluene and naphthalene, were reformed in simulated gasification derived environment to evaluate the catalytic performance of biochars. The kinetics of the reforming of toluene and naphthalene over different biochars were then calculated for comparing the catalytic activity and future reformer design. On the other hand, biochar has another role as fuel which can be spontaneously gasified with steam during tar reforming. However, there is barely no research discussing the gasification reactivity of biochar during tar reforming. Therefore, an empirical gasification model for biochar gasification during tar reforming was also developed in this study. A tar reformer was finally constructed by adopting the calculated kinetics for the application combined with the actual gasification units.

1.2 Tar definition and formation

Until today, the definition of tar is different among several research groups. Typically, tar is defined as organic compounds present in product gas with a molecular weight larger than benzene after biomass gasification [10,11]. The operating temperature of biomass pyrolysis and gasification has significant influence on the formation of tar compounds. The tar transition is illustrated in Figure 1.1 as a function of process temperature from mixed oxygenates to phenolic compounds to aromatic hydrocarbons. Table 1.1 shows the classification of chemical components in each major regime based on Gas Chromatography - Mass Spectrometry Analysis (GC-MS) of collected tars. Furthermore, tar can be divided into three groups, primary, secondary, and tertiary products, based on the results from thermal cracking reactions of tar in the gas phase at different temperatures (Table 1.2). Primary products are characterized by cellulose–derived products, while the secondary products include phenolics and olefins. Benzene can be regarded as condensed tertiary products, which are aromatic compounds without substituents, like naphthalene, acenaphthylene, anthracene/phenanthrene, pyrene, and other polycyclic aromatic hydrocarbons (PAH) in this classification [2]. How tar is defined, is eventually dependent on the end-use applications of the product gas as well as tar sampling and analysis methods [12]. Various tar species formation is highly associated with the conducting ranges of gasification temperature.

Table 1.1 Chemical Components in Biomass Tars [13].

Conventional Flash Pyrolysis	High-Temperature Flash Pyrolysis	Conventional Steam Gasification	High-Temperature Steam Gasification
450–500 ℃	600–650 ℃	700–800 ℃	900–1000 ℃
Acids Aldehydes Ketones Furans Alcohols Complex Oxygenates Phenols Guaiacols Syringols Complex Phenols	Benzenes Phenols Catechols Naphthalenes Biphenyls Phenanthrenes Benzofurans Benzaldehydes	Naphthalenes Acenaphthylenes Fluorenes Phenanthrenes Benzaldehydes Phenols Naphthofurans Benzanthracenes	Naphthalene* Acenaphthylene Phenanthrene Fluoranthene Pyrene Acephenanthrylene Benzanthracenes Benzopyrenes 226 MW PAHs 276 MW PAHs
* At the highest severity, naphthalenes such as methyl naphthalene are stripped to simple naphthalene.			

Table 1.2 The classification of primary, secondary, and tertiary tars

	Formation Temperature	**Example of tar components**
Primary tars	400 - 700 °C	Light aromatics, oxygenates
Secondary tars	700 - 850 °C	Light olefins, aromatics
Tertiary tars	850 - 1000 °C	Polycyclic aromatic hydrocarbons (PAH)

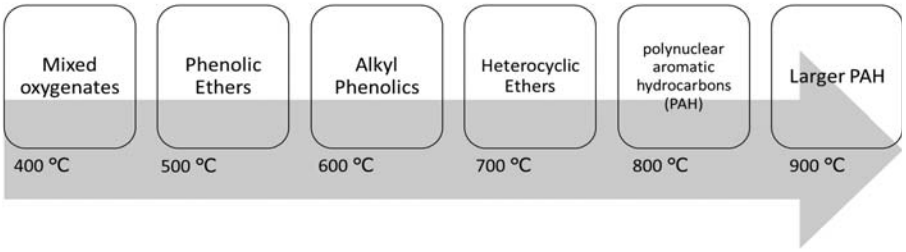

Fig. 1.1 "Tar" maturation scheme proposed by Elliott (1988).

1.3 Target gasification processes for tar reduction

Two special gasification processes, sorption enhanced gasification and steam oxygen gasification are discussed in this study. Both processes are recent-trending concepts compared to traditional gasification technologies like pyrolysis, air gasification, steam gasification in fluidized bed, or down-draft fixed bed gasification. Thus, tar reduction of SEG and SOG with different syngas composition from traditional gasification processes is worth investigating.

1.3.1 Sorption enhanced gasification (SEG)

For seeking influence of biochars on steam reforming of tar, one of effective allothermal gasification methods, sorption-enhanced gasification (SEG) [14,15], is set as the target process. This process runs in a dual fluidized bed system and is based on an absorption-desorption cycle using limestone ($CaCO_3$) as sorbent, as shown in Fig. 1.2. In the SEG, the sorbent removes CO_2 from the syngas produced in the gasification reactor at low temperature around 650 °C, resulting in a high H_2 content of the syngas which hence matches much better for a downstream synthesis (e.g. to produce CH_4 or other compounds). In a second reactor the sorbent is regenerated to CaO by heating it up by combustion of remaining char from the gasifier or of additional fuel. The sensible heat of the sorbent that is recycled to the gasifier and the reaction enthalpy of the exothermic CO_2 absorption reaction provide the required reaction heat for the endothermic gasification reaction. Since CaO and char that is catalytically active for tar conversion is inherently produced in the SEG, no additional expenses arise to provide this catalyst. At the University of Stuttgart, SEG has been studied for several years and was developed up to pilot scale

(200 kW_{th}). Syngas production via SEG has been studied targeting on the feasibility of H_2 production from renewable and waste feedstock [14]. This process features already reduced tar production of around 2 - 10 g $m^{-3}_{dry,STP}$ [16–18]. However, the tar content in syngas is still too high to pass through the downstream units for subsequent application. Although the gas composition from the SEG is dependent on different operation conditions, a typical steam to hydrogen volumetric ratio (V_{H2O}/V_{H2}) = 2 in the syngas is observed as listed in Table 1.3. The main components in the SEG derived syngas are steam and hydrogen with up to around 90 vol%. The composition of tar from the SEG can be found in Armbrust's research indicating that phenol, toluene, and naphthalene are the major tar components in the raw syngas from the gasifier at around 600 – 700 °C, and secondary tar was the primary formation (Fig. 1.3) [19].

Table 1.3 Typical product gas composition (N2 free) from SEG (wet basis).

Component	Unit	[16,17][a]	[18]
H_2O	vol %	55	60
H_2	vol %	28.4	26
CO	vol %	3.6	2.4
CO_2	vol %	6.1	3
CH_4	vol %	4.7	5.6
Tar	g m^{-3}_{NTP}	0.1–1.4	1–5

[a] Average values from reference.

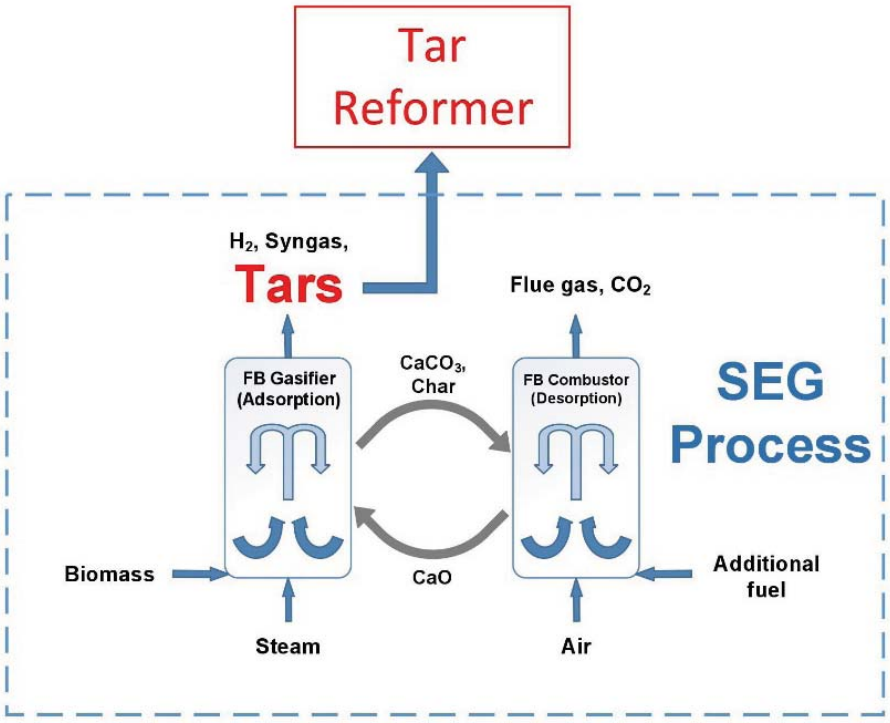

Fig. 1.2 Sorption Enhanced Gasification (SEG) process

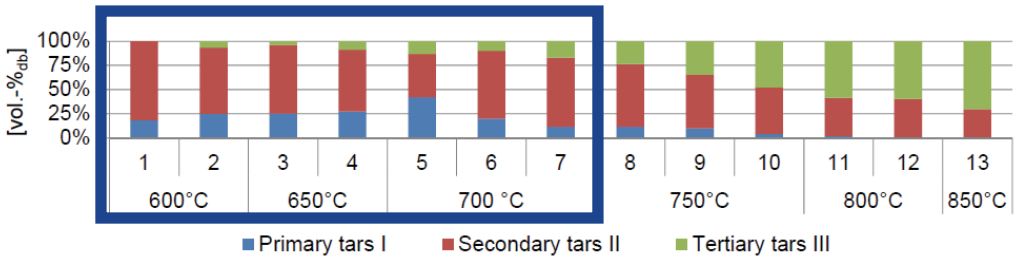

Fig. 1.3 Tar composition from SEG process

1.3.2 Steam-oxygen gasification (SOG)

Steam-oxygen gasification is an autothermal process for syngas production [20]. Steam and oxygen are applied as oxidizing (gasification) agent in a fluidized bed. The necessary heat for the endothermic gasification process is

generated from partial fuel oxidation. The gasifier is operated at high temperatures of proximately 850°C. Since the fluidized bed provides promising material and heat exchange, the fuel undergoes fast pyrolysis. It decomposes into permanent gases, tar, char, and ash. The char and primary tar are subsequently reformed by oxygen and steam. The raw product gas, leaving the gasifier, consists mainly of H_2O, H_2, CO, CO_2, CH_4, and tar. In contrast to the allothermal dual fluidized bed steam gasification, the autothermal steam-oxygen gasification is operated with one fluidized bed reactor only and thus requires less facility and cost. Apart from that, oxygen is a powerful reactant for enhancing the gas yield, char conversion, and tar reforming. Compared to conventional air gasification, the steam-oxygen gasification delivers a nitrogen-free condition and hence higher quality of product gas, which is much more suitable for downstream synthesis.

A reference SOG experiment with straw pellets as fuel conducted at the University of Stuttgart was set up as the research target [20]. The typical syngas composition and tar concentration from SOG of straw pellets at a desirable condition are listed in Table 1.4. The produced gas composition is similar to the steam-oxygen gasification of wood pellets and sewage sludge. The formed tar species were generally aromatic compounds, including naphthalene (30%), toluene (22%), indene (12%), and acenaphthylene (7%), accounted for a mass fraction of over 70 % of carbon distribution among all GC-MS detectable tar components excluding benzene. Steam and hydrogen were found to be the major components in SOG derived syngas with a volumetric ratio around 1. Since the raw syngas with a high steam concentration is produced at a high temperature of over 800 °C in the SOG process, an additional tar reformer loaded with the recycled char–based material from the process might be feasible for tar reduction through steam reforming.

Table 1.4 Typical SOG product gas composition (N_2 free; in wet basis) at the condition of gasification temperature of 850 °C, molar steam to carbon ratio of 1, and equivalence ratio (analogically to the air ratio) of 0.25 with silica sand as bed material.

Composition	H_2	CO	CH_4	CO_2	CxHy	H_2O	Tar
Unit	volume fraction, %	volume fraction, %	volume fraction, %	volume fraction, %	volume fraction, %	volume fraction, %	g m^{-3}
	28	14	4.2	22.4	1.4	30	12

1.4 Tar reforming reactions

According to above introduction of SEG and SOG, high steam concentration and high operation temperature (600 °C -900 °C) from both processes are evidently observed. As raw syngas with a high steam concentration (around 60 %) is produced at high temperature (around 700 °C) in the SEG process [16–18], thermal steam reforming of tar over proper catalyst is a suitable method for direct tar reduction. This process mainly includes oxidation of the tar components using steam with catalysts at temperatures between 650 °C and 900 °C. Tar can be converted into H_2 and CO by steam reforming, promoting the quality of syngas [6,8]. The main reaction is shown below:

$$C_xH_y + H_2O \rightarrow CO + (x + y/2)H_2 \quad \text{(R1)}$$

$$CO + H_2O \rightarrow CO_2 + H_2 \quad \text{(R2)}$$

In general, there are two reactions that occur in series during steam reforming of tar over biochar: the solid carbonaceous deposition on the solid surface by tar polymerization and coke accumulation followed by the steam gasification/reforming of the carbonaceous solid [21]. It is worth mentioning that carbon deposition is highly dependent on the reaction temperature and types of oxidizing agent. Coke can quickly accumulate on the solid surface and deactivate the catalytic activity due to low reaction temperature or weak oxidizing agent during steam reforming [22]. Toluene and naphthalene were tested as simulated tar compounds in view of the references of SEG and SOG for assessing the catalytic performance of different materials.

Many parallel and consecutive reactions occur during toluene and naphthalene reforming in high steam concentration [6,23,24]. According to the global steam reforming reaction, toluene and naphthalene can react with steam to generate H_2 and CO:

$C_7H_8 + 7H_2O \rightarrow 7CO + 11H_2$ $\Delta H°_{900\,°C} = 928\ kJ\ mol^{-1}$ (R3)

$C_{10}H_8 + 10H_2O \rightarrow 10CO + 14H_2$ $\Delta H°_{900\,°C} = 1234\ kJ\ mol^{-1}$ (R4)

The Water-Gas-Shift reaction (WGS) takes place simultaneously:

$CO + H_2O \leftrightarrow CO_2 + H_2$ $\Delta H°_{900\,°C} = -33\ kJ\ mol^{-1}$ (R5)

In the presence of steam and hydrogen, also other reactions should also be considered during tar reforming. Toluene and naphthalene can react with steam to produce C_6H_6, CO, and H_2 (R6 and R7) or with hydrogen to form C_6H_6 and CH_4 owing to hydrocracking (R8 and R9) [25]:

$C_7H_8 + H_2O \rightarrow C_6H_6 + CO + 2H_2$ $\Delta H°_{900\,°C} = 174\ kJ\ mol^{-1}$ (R6)

$C_{10}H_8 + 4H_2O \rightarrow C_6H_6 + 4CO + 5H_2$ $\Delta H°_{900\,°C} = 479\ kJ\ mol^{-1}$ (R7)

$C_7H_8 + H_2 \rightarrow C_6H_6 + CH_4$ $\Delta H^{\circ}_{900\,°C} = -53\ kJ\ mol^{-1}$ (R8)

$C_{10}H_8 + 7H_2 \rightarrow C_6H_6 + 4CH_4$. $\Delta H^{\circ}_{900\,°C} = -429\ kJ\ mol^{-1}$ (R9)

According aforementioned reactions, reforming selectivity might be highly dependent on hydrogen which is one of the main syngas components. On the other hand, the strong inhibiting effect on tar reforming in the presence of H_2 might also take place, leading to low efficiency of tar conversion [26]. Therefore, the impact of hydrogen on selectivity and conversion was investigated in this study.

1.5 Typical tar-reforming catalysts

Catalysts that can crack and convert tar to H_2, CO and other gases can be classified into calcined rocks (e.g. limestone, dolomite), clay minerals, iron ores, char, alkali-metal-based catalysts, activated alumina, transition-metal-based catalysts (e.g. Ni), etc. Calcined dolomite has a low cost and can be used in biomass gasification process with a high tar conversion of around 95%, but also has a low attrition resistance [7]. Ni-based catalysts have been known as commercial catalysts for tar cracking [7,27]. Basically, they are highly efficient in tar conversion. Nickel-based catalysts are 8 to 10 times more active than dolomite, while their limitation is relatively high expense and the rapid deactivation caused by carbon formation on the catalyst surface [7,28,29]. Their deactivation occurs easily because of sulfur and heavy tar content in the feed [7,30]. As a result, it is necessary to find other cheap materials that can substitute commercial catalysts, or can be used as a protector to eliminate most of the heavy tar before them.

1.6 Biochars as tar reforming catalyst

There have been studies indicating that biochars generated by pyrolysis have the ability to decompose organic compounds [31]. These char-based catalysts are comparably low cost and easily available from the biomass fuel and waste by pyrolysis or spent char produced in industrial processes. Moreover, the deactivated char catalyst is easy to handle because of the similar property to the spent char from the gasification process. After the application of tar reduction for SEG process, the replaced char catalysts can be combusted in the regenerator with spent char from the gasifier. On the other hand, char catalysts could be gasified spontaneously during tar reforming, which benefits the syngas production. Based on the above advantages, it is worth studying the application of char-based catalysts for tar reforming after the gasification process. The mechanism of tar cracking on biochars has also been studied recently. Feng et al. pointed out that the main factors of tar reforming are highly related to alkali and alkaline earth metal (AAEMs) contents, and the surface area of biochar [32–34]. The reaction mechanism of tar reforming with AAEMs species on biochar is comprehensively explained in their research. The presence of K and Ca elements, which lead to repeated bond-forming and bond-breaking of tar fragments, contributes to tar decomposition and the formation of light hydrocarbons and small–molecule gases. Apart from AAEM groups, Klinghoffer et al. also found that Fe sites on the char surface react obviously as active sites for the catalytic reaction. The high carbon deposition was found on the Fe site on char after applying char as a decomposing catalyst for organic compounds [35]. Kastner et al. [36] also pointed out that iron might be reduced to metallic iron (Fe) or other forms of more reduced iron (e.g., FeO) via hydrogen during steam reforming of toluene over Fe supported biochar, which is beneficial to toluene reforming as it has been already confirmed that iron in reduced forms can catalytically decompose tar [37]. The activity of chars for tar-

reforming or cracking has been studied in recent years [38]. Most published papers tested the catalytic performance of pre-manufactured char for tar reduction with a model tar component in simulated gasification conditions in a fixed or fluidized bed reactor [39–41]. The research conducted by Abu El-Rub et al. [39] shows that commercial biomass char has an apparent effect on tar reduction. When the char was tested in a fixed bed it gave 81.6% phenol conversion at a temperature of 700 °C. For naphthalene, the conversion over a fixed char and silica sand bed reached 94.4% at 900 °C. Bhandari et al. [42] have used biochar generated from downdraft gasifier (air gasification) to observe the efficiency of the biochar for toluene cracking. Toluene conversion can reach 79% at 700 °C and 81% at 800 °C, respectively.

1.7 Biochar gasification during tar reforming

During tar reforming, biochar can also go through steam reforming (gasification) during steam reforming of tar:

$$C^*(\text{carbon in biochar}) + H_2O \rightarrow CO + H_2. \qquad \Delta H°_{900\,°C} = 136\ \text{kJ mol}^{-1} \qquad \text{(R10)}$$

Several studies observed the gasification phenomenon of biochar without coke accumulation when conducting reforming of tar model compounds at the condition of over 800 °C and a steam volume fraction of 15 % [21,43,44]. Moreover, spontaneous gasification of biochar catalysts also raises the amount of H_2 and CO, which increases their contents in the bio-syngas during tar reforming. Accordingly, environmentally benign gasification of soot and char for avoiding coke deposition is regarded as a desirable condition to operate the tar reforming process over biochar. Since biochar product has been already commercialized over the world [45], the design of a bi-functional biochar-loaded reformer/gasifier for tar reduction and extra syngas production is beneficial. Zeng et al. [46] reported a novel concept of a two-stage gasification process utilizing biomass and biochar for the respective first and second stage individually, where biochar is regarded as fuel/catalyst in the second stage. The biochar is gasified in the second stage surrounding with syngas (H_2O, H_2, CO, CO_2, tar, etc.) from the first stage gasification. The gasification reactivity of biochar is therefore essential in order to assess the optimal condition and the extent of syngas production in the second-stage gasification. Recently, a method for calculating the gasification rate during the reforming of tar model substances has been developed by Chen et al. [43]. The present study adopted the aforementioned method for wood char gasification in the SEG derived environment. A model of gasification reactivity in the presence of H_2O, H_2, and tar model substances is thus established, which is conducive to the further development of the two-stage gasification process.

Although biochar gasification reveals key advantages during tar reforming, after a long-term and intense gasification, the catalytic deactivation of biochar will still take place because of several reasons: (i) since the inorganics dispersion on the char is a critical factor that influences the catalytic activity of the char, the migration and agglomeration of carbon covered inorganics during tar reforming results in a negative performance of tar conversion [38,47]; (ii) although new pores can be formed on biochar during gasification, it is found that micropores can further collapse to mesopores [48,49]. Since the activity of tar reforming is highly related to the micropore of biochar [48], in the long term or drastic gasification condition, pore collapsing also leads to deactivation; (iii) the mass loss of char catalysts due to gasification leads to a conversion drop and the reduction of the gas residence time with the requirement of fast replacement of the catalyst [43].

1.8 Objectives of published papers

Three science citation index papers were published to reveal the application of biochars in tar reforming with unique aspects. (1) An innovative idea to re-utilize in-situ biochar mixture from fluidized bed gasification was investigated to find out the performance and suitable use mode of this active mixture. (2) How reforming selectivity is affected by the ratio of two main syngas components (H_2O and H_2) were discussed. (3) Catalytic abilities of different kinds of biochars or metal impregnated biochars produced through pyrolysis were compared. (4) Innovative gasification and tar reforming models were developed. (5) The design of a tar reformer was carried out based on the findings. Such comprehensive approaches to investigate these low-cost catalysts for future validating them under practical biomass gasification conditions at technical scale is the major purpose of these papers. This will help to render biomass gasification more efficient and economical.

1.8.1 Scientific contributions

As far as we know, biochar generated from pyrolysis or gasification process can decompose organic compounds. However, in the actual gasification process with fluidized bed, pure biochar is hard to be obtained after gasification because of the existence of bed material, soot, and ash. The reutilization of the char containing fly ash as tar–reforming catalysts produced from a fluidized bed gasifier was scarcely discussed although using gasified char from the actual process for tar reduction has been reported in several publications [50–52]. Thus, in-situ char containing mixture from fluidized-bed gasification is worth to be examined for the catalytic activity of tar reforming. Moreover, as hydrogen is one of the major gas components in syngas, it is

worth investigating the effect that hydrogen has on char catalyst during tar reforming. The existence of steam and hydrogen in syngas can separately lead to steam reforming and hydro-cracking of tar, resulting in different reaction selectivity. It is hence essential to find out the effect of the steam to hydrogen ratio on tar reforming since H_2O and H_2 are main gas products from biomass gasification processes, especially SEG and SOG. To understand the aforementioned points, in **paper Ⅰ**, straw char containing fly ash (SCFA) produced inherently from SOG of straw pellets was investigated. Although SCFA is a mixture of fine particles making the application in a classical fixed bed difficult in a practical process, a lab–scale fixed–bed test conducted in this study purposely verifies the concept of potentially reutilizing SCFA as the tar–reforming catalyst in the original SOG process. SCFA was then proved to have promising catalytic activity compared to other char catalysts. SCFA was also examined under the condition of different H_2O to H_2 ratio which confirmed distinct reaction paths between the different ratios.

After figuring out the tar-reforming ability of in-situ char containing material from actual gasification process, self-produced biochar was subsequently studied for the design of a fixed bed tar reformer which will be coupled with a 20 kW gasifier in the University of Stuttgart. SEG is the target gasification process for tar reduction by utilizing self-produced biochars. Tar reforming over different biochars and metal-impregnated biochars were examined in an environment with a relatively high steam concentration based on the SEG condition. **Paper Ⅱ** applied a unique biomass category, palm shell, to produce palm shell char (PSC) by pyrolysis. PSC was further tested in the simulated SEG derived condition for tar-reforming activity and in comparison with wood char (WC) and straw char (SC). By using Fourier–transform infrared spectroscopy analyzer as an instant gas component analyzer, the main outlet gas components were recorded every 5 seconds in detail. A method for

calculating the gasification rate and carbon conversion of applied biochars during tar reforming was developed in view of the analyzed results. This method gives an opportunity for presenting the behaviour of biochar and extra syngas formation through the time at different conditions with the parallel reaction, tar reforming, where this is seldom discussed before. On the other hand, the effects of impregnated potassium and iron on tar reforming and gasification rate were also introduced in **Paper Ⅱ**. A new-discovered factor (mass loss of biochar) leading to catalytic deactivation was observed here.

When applying biochar as tar-reforming catalyst in a secondary reactor, the biochar is possible to be gasified surrounding with syngas (H_2O, H_2, CO, CO_2, tar, etc.) from the first stage gasification. The gasification reactivity of biochar is essential in order to assess the optimal condition and the extent of syngas production in the second-stage gasification of the biochar. A complete gasification model of wood char in simulated SEG derived environment were therefore established in **Paper Ⅲ** by adopting the discovery of **Paper Ⅱ**. On the other hand, three different phenomena on wood char causing catalytic deactivation were observed during the 1-h reforming. Since kinetic models of tar reforming over biochar for expressing the decline of the conversion due to the catalytic deactivation are barely discussed, **Paper Ⅲ** developed modified kinetic equations for the reforming of tar model compounds, which consider the catalytic deactivation of wood char. Finally, the tar reformer design can be referred to these kinetic models.

2 Publications

2.1 List of publications

This thesis is based on the work contained in the following papers:

Paper Ⅰ

Yen–Hau Chen, Max Schmid, Thiansiri Kertthong, Günter Scheffknecht, "Reforming of toluene as a tar model compound over straw char containing fly ash," Biomass and bioenergy, 141(2020) 105657. https://doi.org/10.1016/j.biombioe.2020.105657.

Paper Ⅱ

Yen–Hau Chen, Max Schmid, Chia-Chi Chang, Ching-Yuan Chang, Günter Scheffknecht, "Lab-scale investigation of Palm Shell Char as tar reforming catalyst," Catalysts, 10 (5) (2020) 476. https://doi.org/10.3390/catal10050476.

Paper Ⅲ

Yen–Hau Chen, Ashak Mahmud Parvez, Max Schmid, Günter Scheffknecht, "Reforming of Tar Model Compounds over Sustainable and Low-cost Biochar: Special Focus on Spontaneous Gasification Reactivity and Tar Reforming Kinetics for Reformer Design," Chemical engineering Journal, 408(2021) 127350. https://doi.org/10.1016/j.cej.2020.127350.

Contribution report

Paper Ⅰ: Principal author, responsible for the experimental works (except for solid property analyses and SEM imaging) and data evaluation.

Paper Ⅱ: Principal author, responsible for the experimental works (except for solid property analyses), method development, and data evaluation.

Paper Ⅲ: Principal author, responsible for the experimental works (except for solid property analyses and SEM imaging), data evaluation, and modeling work.

Additional scientific publications

Yen-Hau Chen, Max Schmid, Gebhard Waizmann, Selina Hafner, Günter Scheffknecht, "Tar reforming over CaO and straw char produced inherently in steam-oxygen biomass gasification processes using toluene as model component," EUBCE 2019 - 27th European Biomass Conference and Exhibition, 27-30 May 2019, Lisbon, Portugal.

Yen-Hau Chen, Max Schmid, Günter Scheffknecht, "Tar Reforming over Low-cost Bio-chars for the Application in the Biomass Gasification Process," 53. Jahrestreffen Deutscher Katalytiker. (2020, accepted, cancelled)

Yen-Hau Chen, Max Schmid, Günter Scheffknecht, "Tar Reforming over Low-cost Materials for the Application in Sorption Enhanced Gasification Process and its Kinetics," 1st FERIA Conference. (2020, accepted, cancelled)

Thiansiri Kertthong, Yen–Hau Chen, Marcel Beirow, Max Schmid, Günter Scheffknecht, "Upgrading of Synthesis Gas from Biomass Gasification by Reforming of Recycled Methane," EUBCE 2020 - 28th European Biomass Conference and Exhibition, 6-9 July 2020.

Zongpei Ye, Yen-Hau Chen, Thiansiri Kertthong, Max Schmid, Günter Scheffknecht, "CO_2 reforming of methane over Ni-based coconut char catalysts for syngas production," EUBCE 2021 - 29th European Biomass Conference and Exhibition, 26-29 April 2021.

Thiansiri Kertthong, Yen–Hau Chen, Max Schmid, Günter Scheffknecht, " Steam Reforming of Hydrocarbons from Sorption Enhanced Gasification of Biomass: Influence of Tar Model Compounds on Methane Conversion and Catalyst Behavior," EUBCE 2021 - 29th European Biomass Conference and Exhibition, 26-29 April 2021.

Chia-Chi Chang, Yen-Hau Chen, Yi-Shiou Lin, Zang-Sei Hung, Min-Hao Yuan, Ching-Yuan Chang, Yuan-Shen Li, Je-Lueng Shie, Yi-Hung Chen, Yen-Chi Wang, Chun-Han Ko, Far-Ching Lin, Chungfang Ho, Bo-Liang Liu, Kuang-Wei Liu, and Shi-Guan Wang, "A Pilot Plant Study on the Autoclaving of Food Wastes for Resource Recovery and Reutilization," Sustainability, 10(10) (2018) 3566. https://doi.org/10.3390/su10103566.

Chia-Chi Chang, Yen-Hau Chen, Wei-Ren Chang, Chao-Hsiung Wu, Yi-Hung Chen, Ching-Yuan Chang, Min-Hao Yuan, Je-Lueng Shie, Yuan-Shen Li, Sheng-Wei Chiang, Tzu-Yi Yang, Far-Ching Lin, Chun-Han Ko, Bo-Liang Liu, Kuang-Wei Liu & Shi-Guan Wang, "The emissions from co-firing of biomass and torrefied biomass with coal in a chain-grate steam boiler," Journal of the Air & Waste Management Association, 69(12) (2019) 1467-1478. https://doi.org/10.1080/10962247.2019.1668871.

Tse-Lun Chen, Yi-Xuan Xiong, Yi-Hung Chen, Pen-Chi Chiang, Yen-Hau Chen, "Performance evaluation and process simulation for synergetic removal of NOx, CO2 and PM using green alkaline solution in a high-gravity rotating packed bed," Fuel, 280 (2020) 118643. https://doi.org/10.1016/j.fuel.2020.118643.

Paper I

Biomass and Bioenergy 141 (2020) 105657

Contents lists available at ScienceDirect

Biomass and Bioenergy

journal homepage: http://www.elsevier.com/locate/biombioe

Reforming of toluene as a tar model compound over straw char containing fly ash

Yen-Hau Chen *, Max Schmid, Thiansiri Kertthong, Günter Scheffknecht

Institute of Combustion and Power Plant Technology, University of Stuttgart, Germany

ARTICLE INFO

Keywords:
Catalytic reforming of toluene
Tar reduction
Char catalyst
Biomass gasification

ABSTRACT

The present work focuses on confirming that straw char containing fly ash (SCFA) produced from steam–oxygen gasification (SOG) of straw pellets has the potential to be reused as a tar–reforming catalyst in the original process. The catalytic activity and reforming selectivity of SCFA was evaluated with toluene as a tar model compound in the presence of steam and hydrogen in a lab–scale fixed bed reactor at high temperature up to 900 °C. The kinetic results showed that SCFA was effective in toluene reforming with a complete toluene conversion at a space time of 0.05 kg h m^{-3} under 850 °C and a steam volume fraction of 15%. On the other hand, when hydrogen was present, the significant effect of hydrogen on toluene reforming was demonstrated by the formation of benzene through hydrodealkylation reaction. The volumetric ratio of H_2O to H_2 was an essential parameter that decided the selectivity of toluene reforming. Although the coexist of toluene and hydrogen would inhibit the gasification, SCFA was proved to be gasified during toluene reforming. The surface migration and agglomeration of inorganics due to gasification also resulted in the change of catalytic activity and reforming selectivity through time. In conclusion, this study demonstrated the potential utilization of SCFA derived from the SOG process as a tar–reforming catalyst to enhance the overall performance of the SOG process.

1. Introduction

With high energy efficiency and various applications of the produced syngas, biomass gasification might play a major role in an economy that ceases using fossil fuels. Sustainably produced syngas can be used for the generation of electrical power but, more importantly, to produce chemicals (e.g., methanol and dimethyl ether) or gaseous (CH_4) fuels or base chemicals (e.g., C_2H_4) [1]. However, there are several barriers to the application of biomass gasification. A particularly problematic issue in this respect is the generation of tar that is associated with the gasification process.

Until today, the definition of tar is different among several research groups. Typically, tar is defined as organic compounds present in product gas with a molecular weight larger than benzene after biomass gasification [1,2]. Furthermore, tar can be divided into three groups, primary, secondary, and tertiary products, based on the results from thermal cracking reactions of tar in the gas phase. Primary products are characterized by cellulose–derived products, while the secondary products include phenolics and olefins. Benzene can be regarded as condensed tertiary products, which are aromatic compounds without substituents, like naphthalene, acenaphthylene, anthracene/phenanthrene, and pyrene in this classification [3]. How tar is defined, is eventually dependent on the end-use applications of the product gas as well as tar sampling and analysis methods [4]. Tar can lead to severe operational problems when they condense on cold surfaces forming deposits that block the gas path. Moreover, high tar concentration in the syngas damages downstream power generation equipment (e.g., engines and turbines) and synthesis units (e.g., catalytic reactors) and causes unscheduled downtimes, hence increases the cost of biomass gasification processes. The tar limitations in syngas for the typical downstream usage are less than 30, 1, and 0.1–1 mg m^{-3} for gas turbines, methanol synthesis, and Fischer–Tropsch synthesis, respectively [5,6]. As a result, tar removal is essential in most biomass gasification processes [7–10].

The tar removal process can be separated into physical and chemical methods [7]. Physical gas cleaning includes unit operations such as filters, scrubbers, and wet electrostatic precipitators, while chemical methods such as thermal cracking and catalytic reforming can also be applied. Among these methods, efficient gas cleaning processes that can

* Corresponding author.
E-mail addresses: Yen-Hau.Chen@ifk.uni-stuttgart.de (Y.-H. Chen), max.schmid@ifk.uni-stuttgart.de (M. Schmid), thiansiri.kertthong@ifk.uni-stuttgart.de (T. Kertthong), guenter.scheffknecht@ifk.uni-stuttgart.de (G. Scheffknecht).

https://doi.org/10.1016/j.biombioe.2020.105657
Received 16 September 2019; Received in revised form 27 May 2020; Accepted 14 June 2020
Available online 25 August 2020

Table 1
Typical SOG product gas composition (N_2 free; in wet basis) at the condition of gasification temperature of 850 °C, molar steam to carbon ratio of 1, and equivalence ratio (analogically to the air ratio) of 0.25 with silica sand as bed material [23].

Composition	H_2	CO	CH_4	CO_2	CxHy	H_2O	Tar
Unit	volume fraction, %	volume fraction, %	volume fraction, %	volume fraction, %	volume fraction, %	volume fraction, %	g m^{-3}
	28	14	4.2	22.4	1.4	30	12

be operated at high temperatures are seen as energetically beneficial because they can avoid excessive gas cooling that is required for condensing and scrubbing of tar in a water scrubber. As far as we know, steam reforming at high temperature converts tar into useful synthesis gas components such as H_2 and CO [9,10]. Such a high–temperature tar reduction process generally requires a suitable catalyst material with high tar conversion efficiency and exceptional resistance against other syngas impurities (e.g., S and Cl species). Another promising option for catalysts is to use catalytically active material, biochar, which is also suitably used as a protector to eliminate most of the heavy tar before the commercial catalyst. The performance of tar reforming over biochar is highly connected with alkali and alkaline earth metals (AAEMs) groups on the biochar and the surface area [11–13]. So far, there have been studies indicating that biochar generated from pyrolysis or thermal steam activation can decompose organic compounds [8,14–19]. Biochar has also been proven that it has a better ability to decompose the aromatic ring than mineral materials [19]. However, in the actual gasification process with fluidized bed, pure biochar is hard to be obtained after gasification because of the existence of bed material, soot, and ash. The reutilization of the char containing fly ash as tar–reforming catalysts produced from a fluidized bed gasifier was scarcely discussed, although using gasified char from the actual process for tar reduction has been reported in several publications [20–22]. In this study, straw char containing fly ash (SCFA) from steam–oxygen gasification (SOG) of straw pellets was investigated. Although SCFA is a mixture of fine particles making the application in a classical fixed bed difficult in a practical process, a lab–scale fixed–bed test conducted in this study purposely proves the concept of potentially reutilizing SCFA as the tar–reforming catalyst in the original SOG process. After verifying the performance of SCFA, these fine particles can be suitably used in an additional fluidized–bed tar reformer connected with the gasifier or in the "freeboard" of gasifier where the syngas should pass through with many fine particles, contributing to tar reforming.

According to Schmid et al. [23], the typical syngas composition and tar concentration from SOG of straw pellets at a desirable condition are listed in Table 1. The formed tar species were generally aromatic compounds, including naphthalene (30%), toluene (22%), indene (12%), and acenaphthylene (7%), accounted for a mass fraction of over 70% of carbon distribution among all GC-MS detectable tar components excluding benzene. Steam and hydrogen were found to be the major components in SOG derived syngas with a volumetric ratio around 1. Since the raw syngas with a high steam concentration is produced at a high temperature of over 800 °C in the SOG process, an additional tar reformer loaded with the recycled char–based material from the process might be feasible for tar reduction through steam reforming.

With SCFA as a tar–reforming catalyst after the SOG process, char gasification can be a spontaneous reaction during tar reforming [24,25]. Thus, the overall carbon conversion of the biomass fuel in the whole process might be enhanced due to the gasification of the recycled char mixture during tar reforming, and the syngas quality can be improved with extra H_2/CO production. The spontaneous gasification of SCFA while reforming the tar model compound, toluene, was thus investigated. Moreover, since hydrogen is one of the major gas components in SOG derived syngas, it is worth investigating the effect that hydrogen has on SCFA during tar reforming. According to Fushimi's research [25], hydrogen leads to inhibition of steam gasification of biochar. The model established by Barrio et al. indicated that the partial pressures of H_2O and H_2 are highly correlated with the gasification rate of wood char, and high partial pressure of H_2 results in potent inhibition of gasification [26]. Besides the inhibition effect on gasification, a comprehensive study targeting the influence of hydrogen on toluene reforming over SCFA was also reported in this study. Apart from H_2O and H_2, it was found that CO_2 concentration occupied a considerable fraction with a volume proportion of around 20% in SOG derived syngas shown in Table 1. The presence of CO_2 has been proven to have a positive effect on catalytic tar reforming, and char can also be gasified by CO_2 [27,28]. Nonetheless, reforming of tar and gasification of char with CO_2 have been reported to be not so significant compared to H_2O. CO_2 and other low–concentration gas components in SOG derived syngas were then not considered here in the simulated test of SCFA.

Table 2
Operating conditions of steam–oxygen gasification of straw pellets.

Parameters	Values	Unit
S/C[a]	1.1	mol/mol
ER[b]	0.26	mol/mol
Temperature	800	°C

[a] The steam to carbon ratio, S/C, describes the ratio of the total mole flow of water, including the fuel's moisture, per mole flow of biomass carbon introduced into the gasifier.

[b] The equivalence ratio, ER (analogous to the air ratio in combustion processes), expresses the ratio of the amount of oxygen used to the amount of oxygen that would be required for stoichiometric oxidation of the fuel.

For the downstream synthesis applications of syngas, light unsaturated hydrocarbons are undesirable because it can react with the synthesis catalysts and deactivate them by carbon deposition. It is recommended to remove all the light unsaturated hydrocarbons, including benzene, to avoid the deactivation of synthesis catalysts, which are typically nickel catalysts [29]. Benzene is known as a stable intermediate that is cracked mainly from aromatic tar substances, and it is also one of the primary content of aromatics formed from the SOG process [23]. Benzene selectivity from toluene reforming over SCFA was hence discussed here to figure out the ability of SCFA on breaking down the aromatic ring. With the further decomposition of benzene from original syngas and intermediate formed from heavy tar cracking, more syngas production can be expected.

2. Materials and methods

2.1. Materials

SCFA was produced, referring to the experiment (Table 1) conducted by Schmid et al. [23]. Silica sand was chosen here as the bed material because it has been proven to have a weak tar cracking ability compared to other bed materials, which is appropriate while investigating the catalytic activity of the char side in the recycled mixture [30]. Straw pellets, which were also used in the reference experiment, were then gasified by the SOG process applying the same fluidized bed and method described by Schmid et al. The 20 kW fuel input bubbling fluidized bed facility was used for conducting the gasification, and details of the configuration and process can be found elsewhere [23]. The operating conditions of steam–oxygen fluidized bed gasification are listed in Table 2, where they were all similar to the reference experiment. SCFA was the fly ash from the primary cyclone of the 20 kW facility. The

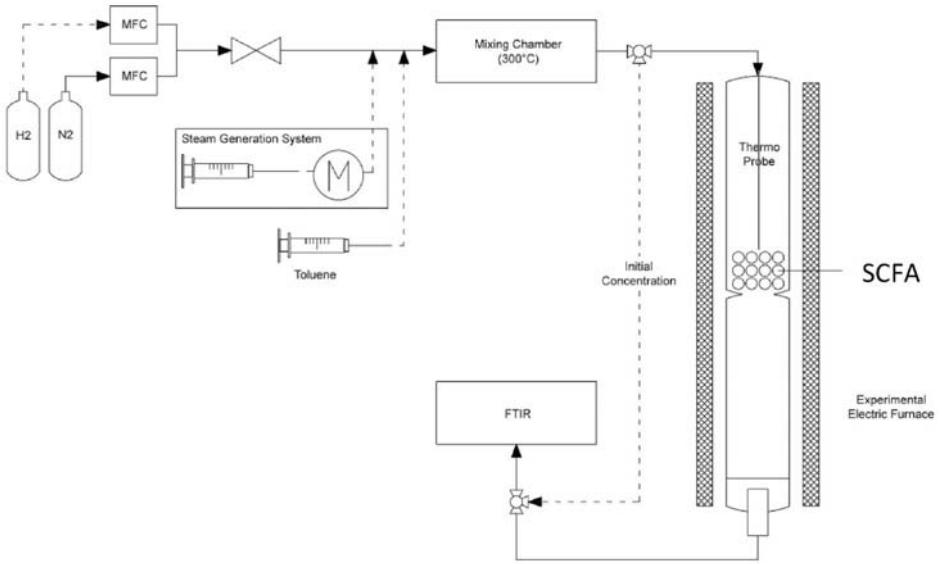

Fig. 1. Schematic diagram of the toluene–reforming system.

Table 3
Operating conditions of each experiment with $Q_{NTP} = 0.3\ m^3\ h^{-1}$. (T: Reforming temperature; V_i: Volume fraction of component i (i = H_2O and H_2) in inlet flow).

T	V_{H2O}	V_{H2}	$y_{C7H8,in}$
°C	%	%	dm^3/m^3
750	15	0	2.43
850	15	0	2.43
900	15	0	2.43
850	5	0	2.43
850	30	0	2.43
850	5	2.5	2.43
850	5	5	2.43
850	5	10	2.43
850	10	10	2.43
850	20	10	2.43
850	15	15	2.43

cyclone efficiently collected SCFA during SOG, which did not return to the bubbling fluidized bed. Reutilizing this straw char based mixture as the catalytic material for tar reduction was the main objective of this study. It was a mixture of spent straw char, soot, ash, and silica sand attrition. After the experiment, the material was removed and put into a sealed container under the air atmosphere for further testing. No other treatment, such as sieving, was performed.

2.2. The experimental set–up and conditions

A high–temperature laboratory-scale catalytic tar reduction reactor capable of operating at various conditions was designed and set up in this study, as shown in Fig. 1. Since the main tar components from the SOG process are aromatic carbons [23], toluene was used as the tar model compound in this study because it represents the aromatics and is one of the primary tar components from the SOG process [23]. SCFA was tested as the catalyst in the toluene reforming process. All pipes were heated up above 180 °C to avoid condensation of toluene. The inner diameter of the glass reactor is 12 mm. Relevant test gases with different concentrations of H_2O, H_2, and toluene listed in Table 3 were premixed in N_2 and then flowed through SCFA with 1 cm bed length. Pure steam reforming of toluene was first carried out to evaluate the tar reforming ability of SCFA. The addition of hydrogen for toluene reforming was subsequently tested. Although steam and hydrogen concentrations tested in this study were lower than those in actual SOG-derived syngas, the influence of steam to hydrogen volumetric ratio (V_{H2O}/V_{H2}) on toluene reforming over SCFA was still detectable here. A test of simulated SOG derived environment with $V_{H2O}/V_{H2} = 1$ also gave a rough model on applying SCFA in the original SOG process. The space time of the gas (τ_{NTP}) over the SCFA was 0.8 g h m^{-3}, calculated by the weight of catalysts (0.25 g of SCFA) and constant total flow rate (Q_{NTP} equal to 0.3 $m^3\ h^{-1}$ at NTP) fixed at every condition. The flow rate of carrier gas N_2 was altered to maintain the same total flow rate (Q_{NTP}) according to different volume fractions of steam and hydrogen. 2.43 dm^3/m^3 (ca 10 g m^{-3}) [23] was set as the initial toluene concentration to simulate the average tar concentration after the SOG process, regarding Table 1.

As SCFA reacted with steam and subsequently proceeded with char gasification during toluene reforming, gas concentrations were not stable in the beginning. The time measured for each toluene reforming experiment over SCFA was 60 min. The time range selected for calculating toluene conversion, selectivities, and kinetics was from the 30th min to 40th min. In this time range, gas concentrations at all conditions were stable, and the influence of char gasification was neglected (explained in section 3.5.1). Change of SCFA property due to gasification during toluene reforming was not considered for the calculation of these basic indicators at different conditions. However, the in-depth exploration of the connection between the property change on the surface of SCFA and toluene reforming selectivity is discussed in Section 3.5.3.

2.3. Detection of gas components

By Fourier–transform infrared spectroscopy analyzer (FTIR–Gas analyzer, GASMET DX4000), toluene concentrations were recorded continuously. C_6H_6, CO, CO_2, and CH_4 were also transferred with the transmitting pipe of FTIR (5 m length) at 180 °C and had their concentrations detected. The initial concentration was also recorded at the beginning of each test.

2.4. Analytical and characterization methods

Elemental, ultimate analyses, and metal oxide compositions of SCFA were performed following standard methods DIN (the German Institute for Standardization) EN ISO 18134–3, 18122, 18123, 16948, 16967, and 16994 [31]. Thermal gravimetric analysis (TGA) was tested in the same condition described by Chen et al. [32]. The particle size distribution and the BET surface area were measured by Mastersizer 3000 laser diffraction particle size analyzer and Micromeritics ASAP2020,

respectively.

In this study, a scanning electron microscope (SEM) (JEOL field emission microscope JSM–7200F) equipped with energy dispersive X–ray spectroscopy (EDX) (Quantax XFlash6/60, Bruker Nano GmbH) was used to image the straw char and map the elemental composition of the surface. The resolution of SEM for specific char surface in SCFA was 10 μm.

2.5. Toluene reforming with steam and hydrogen over SCFA

Many parallel and consecutive reactions occur during toluene reforming over SCFA [9,33,34]. According to the global steam reforming reaction, toluene reacts with steam to generate H_2 and CO (R1):

$$C_7H_8 + 7H_2O \rightarrow 7CO + 11H_2;\ \Delta H_{\circ}^{900\ ^{\circ}C} = 928\ kJ\ mol^{-1} \quad (R1)$$

The Water–Gas Shift reaction also takes place simultaneously (R2):

$$CO + H_2O \leftrightarrow CO_2 + H_2;\ \Delta H_{\circ}^{900\ ^{\circ}C} = -33\ kJ\ mol^{-1} \quad (R2)$$

Two reactions are occurring in series for R1: The solid carbonaceous deposition on the solid surface by tar polymerization and coke accumulation followed by the steam gasification/reforming of the carbonaceous solid [24]. It is worth mentioning that carbon deposition reactions are highly dependent on the reaction temperature and types of oxidizing agent. When the reaction temperature is low, or the oxidizing agent does not contain enough steam during steam reforming, coke will quickly accumulate on the solid surface [35]. Several studies observed the gasification phenomenon of biochars without coke accumulation when conducting reforming of tar model compounds at the condition of over 850 °C and a steam volume fraction of 15% [19,24].

With the presence of steam and hydrogen, other reactions should also be considered during toluene reforming. Toluene can react with steam to produce benzene, CO, and H_2 (from the reaction of steam dealkylation (R3)) or with hydrogen to form benzene and CH_4 owing to the hydrodealkylation reaction (R4) [36]:

$$C_7H_8 + H_2O \rightarrow C_6H_6 + CO + 2H_2;\ \Delta H_{\circ}^{900\ ^{\circ}C} = 174\ kJ\ mol^{-1} \quad (R3)$$

$$C_7H_8 + H_2 \rightarrow C_6H_6 + CH_4;\quad \Delta H_{\circ}^{900\ ^{\circ}C} = -53\ kJ\ mol^{-1} \quad (R4)$$

Straw char may also go through steam reforming (gasification) concurrently with toluene:

$$C*(char) + H_2O \rightarrow CO + H_2;\ \Delta H_{\circ}^{900\ ^{\circ}C} = 136\ kJ\ mol^{-1} \quad (R5)$$

2.6. Performance indicators

The general formulas used to calculate toluene conversion, carbon distribution, and selectivity are listed below [18,37]. In this study, a constant total volume flow rate is assumed. A short space time was applied in this study, resulting in the negligible flow of products and reactants, and improved the accuracy of results based on the assumption of a constant flow.

Toluene conversion (X_{C7H8}) was calculated using Eq. (1).

$$X_{C7H8}(-) = \frac{Q_{C7H8,in} - Q_{C7H8}}{Q_{C7H8,\ in}} = \frac{Q_{in} \times y_{C7H8,in} - Q \times y_{C7H8}}{Q_{in} \times y_{C7H8,in}} \approx \frac{y_{C7H8,in} - y_{C7H8}}{y_{C7H8,in}}, \quad (1)$$

where X_{C7H8} = toluene conversion, $Q_{C7H8,\ in}$ = inlet toluene volume flow rate, Q_{C7H8} = outlet toluene volume flow rate, Q_{in} = inlet total volume flow rate, Q = outlet total volume flow rate, $y_{C7H8,\ in}$ = inlet toluene volume concentration, and y_{C7H8} = outlet toluene volume concentration. (Assumption: $Q_{in} = Q = Q_{NTP}$).

Carbon distribution (D_{C_i}) is defined in Eq. (2) as the ratio of carbon content in each main carbon–containing product (i = C_7H_8, C_6H_6, CO, CO_2, and CH_4) to the carbon content in toluene at the inlet. The carbon distributions of these components were summed up for different conditions of toluene reforming are between 98% and 106% exhibiting credible carbon balance assuming that the main carbon–containing species only involve C_7H_8, C_6H_6, CO, CO_2 and CH_4 during toluene reforming over SCFA.

$$D_{C\_i}\ (-) = \frac{r_i \times y_i}{7 \times y_{C7H8,in}}, \quad (2)$$

where r_i represents the number of carbon atoms, and y_i represents the outlet volume concentration for the component i (i = C_6H_6, CO, CO_2, and CH_4).

The selectivity (S_i, Eq. (3)) of carbon–containing products is obtained by calculating the D_C of product i to a toluene–free basis.

$$Si\ (-) = \frac{D_{C\_i}}{\sum_i D_{C\_i}} \quad (3)$$

Table 4
Basic properties of materials.

Analyses	Compositions	SCFA	Straw pellet
Proximate Analysis[a] (mass fraction, %)	Fixed carbon	20.4	17.2
	Volatile matters	8.9	71.7
	Ash	67.8	5.6
	Equilibrium moisture[b]	3.0	5.5
Ultimate Analysis[a] (mass fraction, %)	C	25.7	44.0
	H	0.7	6.3
	O[c]	0.5	37.2
	N	0.4	0.8
	S	0.5	0.2
	Cl	1.5	0.4
Ash components[a] (mass fraction, %)	Al_2O_3	2.6	0.5
	BaO	0.1	0.1
	CaO	8.6	12.7
	Fe_2O_3	2.0	0.5
	K_2O	6.5	45.0
	MgO	1.5	4.1
	MnO_2	0.1	0.1
	Na_2O	0.2	0.2
	P_2O_5	2.1	1.8
	SO_3	1.4	4.7
	SiO_2	38.0	30.1
	SrO	–	0.1
	TiO_2	0.1	–
BET total surface area ($m^2\ g^{-1}$)		116.6	–

[a] In wet basis.
[b] Equilibrium moisture content of the sample in air.
[c] Balance of C, H, N, S, Cl, equilibrium moisture, and ash.

3. Results and discussion

3.1. Characterization of SCFA

The basic properties of straw pellets and SCFA are shown in Table 4. The particle size of straw char was in the range of 0.01–0.3 mm. The intercepts of particle sizes for 10, 50, and 90% mass (D_{10}, D_{50}, and D_{90}) from an S–curve of cumulative mass retained against sieve mesh size were 0.011, 0.070, and 0.239 mm, respectively, indicating a form of fine particles in SCFA. According to the elemental analysis of SCFA, as presented in Table 4, SCFA has a significant carbon mass fraction of 26% after SOG, while the highest mass fraction is ash with 68%. It was found that potassium occupied the most content in the ash of straw pellets. However, the ash component analysis shows that SiO_2 is the highest component between all metal oxides in SCFA with a mass fraction of 38% much more than the mass fraction of 6.5% for K_2O among the total ash content of 68%, suggesting a contribution of silica sand attrition. According to Blott et al. [38], the specific surface area of quartz sands is in the range of 1.0–4.0 $m^2\ g^{-1}$. However, a much higher surface area of

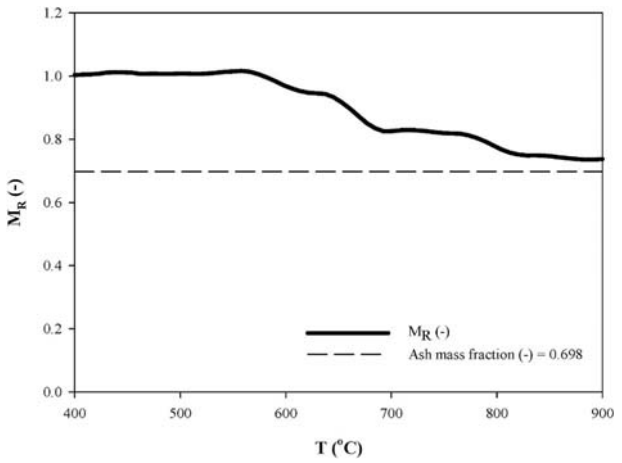

Fig. 2. TGA diagram of the residual mass fraction (M_R) vs. temperature (T) of SCFA (conducted with a N_2 flow rate of $5{\cdot}10^{-5}$ m^3 min^{-1}).

116.6 m^2 g^{-1} for SCFA is observed, compared to the sand. As biochar has been confirmed to possess a higher surface area than mineral materials [19], straw char might have a dominant distribution in SCFA, which contributes the most of the surface area. Regarding the findings above, SCFA was mainly a mixture of straw char and silica sand.

When applying SCFA as a catalyst, the carbon inside decomposed due to high temperatures. TGA results of SCFA shown in Fig. 2 present the mass–loss rate during pyrolysis from 400 to 900 °C. During the gasification process, most hemicellulose and cellulose (volatiles) in straw were removed [32], causing the TGA mass loss occurring in the high–temperature range, roughly 600 °C. The temperature range for SCFA to decompose thus covers the temperature for conducting toluene reforming in this study from 750 to 900 °C. The residual mass fraction (M_R) of SCFA decreases gradually to 0.7 at 900 °C, which is close to the ash content (70%) on a dry basis of SCFA.

SEM diagrams give evident information on the elemental composition and the surface property of SCFA particles. SEM–EDX applied a color distribution for exhibiting the presence of the element on the material's surface. The shades of the colors on SEM diagrams correspond to the quantity of the particular element, while a deeper color refers to a higher concentration on the surface. Fig. 3 (a) and (b) demonstrate an evenly distributed carbon and silica with the colors of green and light blue, respectively, on a flat of SCFA particles, proving a char/silica structure. Since char can contribute much better catalytic activity than silica sand [30], the SEM diagram in Fig. 3 (c) specifically depicts the char surface of SCFA for further investigation. Sub–diagrams (d), (e), (f), and (g) illustrate the SEM–EDX results of C, K, Ca, and Si, respectively, with colors of green, yellow, blue, and light blue to show the distribution of these elements. The surface of the char has no regular structure, and most components are carbon on the surface because of the large explicit green area, with only a few dispersion of K and Ca regarding Fig. 3 (e) and (f). High ash content in the straw char might be covered by carbon, which can migrate to the surface through thermal treatment [39]. Some Silica lumps from silica sand attrition can also be observed in Fig. 3 (g) in the red circle.

3.2. Toluene reforming with steam over SCFA in the absence of H_2

SCFA was first tested with different steam concentrations to evaluate its catalytic activity of toluene reforming. Since temperature is an essential parameter for the toluene conversion [10,19], toluene reforming at different temperatures was first conducted in a fixed V_{H2O} = 15%. The toluene conversion and selectivities of C_6H_6, CO, CO_2, and CH_4 during toluene reforming at 750, 850, and 900 °C are shown in Fig. 4. It was found that X_{C7H8} increased along with rising temperature, where the highest X_{C7H8} in this test was 0.21 at the highest temperature of 900 °C. Because of the short space time of 0.8 g h m^{-3}, conversions were not prominent in the experimental test. However, by developing the kinetic model from the result, the catalytic activity of SCFA can still be compared with other research. Fig. 4 also illustrates that toluene mainly converts into CO and CO_2, indicating that R1 and R2 are the major reactions with SCFA as the catalyst. Since R3 also happens at high temperatures, S_{C6H6} gradually increases from 0 to 0.19 along with the increasing temperature. In comparison to the reference [18], S_{C6H6} and S_{CO2} have similar trends to those obtained from pine bark biochar carried out with a relatively long space time of 0.09 kg h m^{-3}. S_{CH4} decreases from 0.07 at 750 °C to 0.03 at 900 °C, as the same reference has a similar decline at a high–temperature range from 800 to 900 °C. At 900 °C, toluene reforming prefers to form CO rather than CO_2 because the reverse water–gas shift reaction takes place at extremely high temperatures over 850 °C [40].

Reforming conversion and selectivity over SCFA with different V_{H2O} at 850 °C was also depicted in Fig. 5. Although no significant change of toluene conversion occurred by adding more steam, V_{H2O} had an impact on the selectivity of toluene reforming. According to Fig. 5, S_{CO} rises along with the increasing V_{H2O} and then turns out to be higher than the S_{CO2} at V_{H2O} = 15% in Fig. 4, suggesting that R2 is gradually weakened by increasing V_{H2O}. On the other hand, benzene tends to be decomposed at high V_{H2O} due to reinforced R1 with more reactant steam. S_{C6H6} decreases from 0.14 to almost 0 until V_{H2O} reaches 30%. This result suggests that toluene reforming over SCFA is better to be carried out at high steam volume fraction since the intermediate, benzene, can be further transformed into light gas components due to enhanced reaction of steam reforming. Moreover, selectivity obtained from steam reforming of toluene over SCFA is entirely different from that over sand with a primary selectivity to C_6H_6 [37]. A major formation of CO and CO_2 over SCFA suggests straw char would have a significant contribution to toluene reforming and the decomposition of the aromatic ring. Since straw char provides the main surface area in SCFA, active sites on straw char can promote steam reforming of toluene and influence the mechanism of toluene reforming, leading to a low benzene selectivity.

3.3. Toluene reforming with steam over straw char in the presence of H_2

Since H_2 is one of the main gas components from the SOG process, the effect of hydrogen concentration on toluene reforming over SCFA was detected. Fig. 6 shows toluene conversion and reaction selectivity during toluene reforming over SCFA at various V_{H2} from 0 to 10% (850 °C; V_{H2O} fixed at 5%). X_{C7H8} has no significant difference when V_{H2} = 0, 2.5, 5, and 10% in this research. It is worth mentioning that hydrogen has an enormous influence on the selectivity of toluene reforming based on the result. S_{C6H6} and S_{CH4} increase from 0.14 to 0.44 and from 0.03 to 0.07, respectively, along with rising V_{H2}, indicating that toluene hydrodealkylation plays a major role. Therefore, at a high range of V_{H2} (above 5%), C_6H_6 was the major component formed from toluene reforming, among other carbon–containing species. In the presence of H_2, steam reforming of toluene was suppressed, and hence less and less CO and CO_2 were produced. According to Fig. 6, S_{CO} and S_{CO2} decrease from 0.37 to 0.28 and from 0.46 to 0.21, respectively, when V_{H2} increases to 10%. This result suggests that R1 was drastically weakened by increasing V_{H2} because the primary reaction was switched to R4. This effect might also lead to the change of X_{C7H8} when hydrogen is present. A fixed V_{H2} = 10% was also tested with three different V_{H2O} = 5%, 10%, and 20% to investigate the influence of the steam to hydrogen volumetric ratio (V_{H2O}/V_{H2}) on the selectivity. S_{C6H6} and S_{CO} at different V_{H2O}/V_{H2} are illustrated in Fig. 7, suggesting that V_{H2O}/V_{H2} has a significant influence on the selectivity. Higher V_{H2O}/V_{H2} leads to the preference of steam reforming of toluene rather than hydrodealkylation of toluene. As a result, S_{CO} significantly increases while S_{C6H6} drops along with V_{H2O}/V_{H2} increasing in the range from 0.5 to 2. At high V_{H2O}/V_{H2} = 2, SCFA exhibited better activity on the breakdown of the

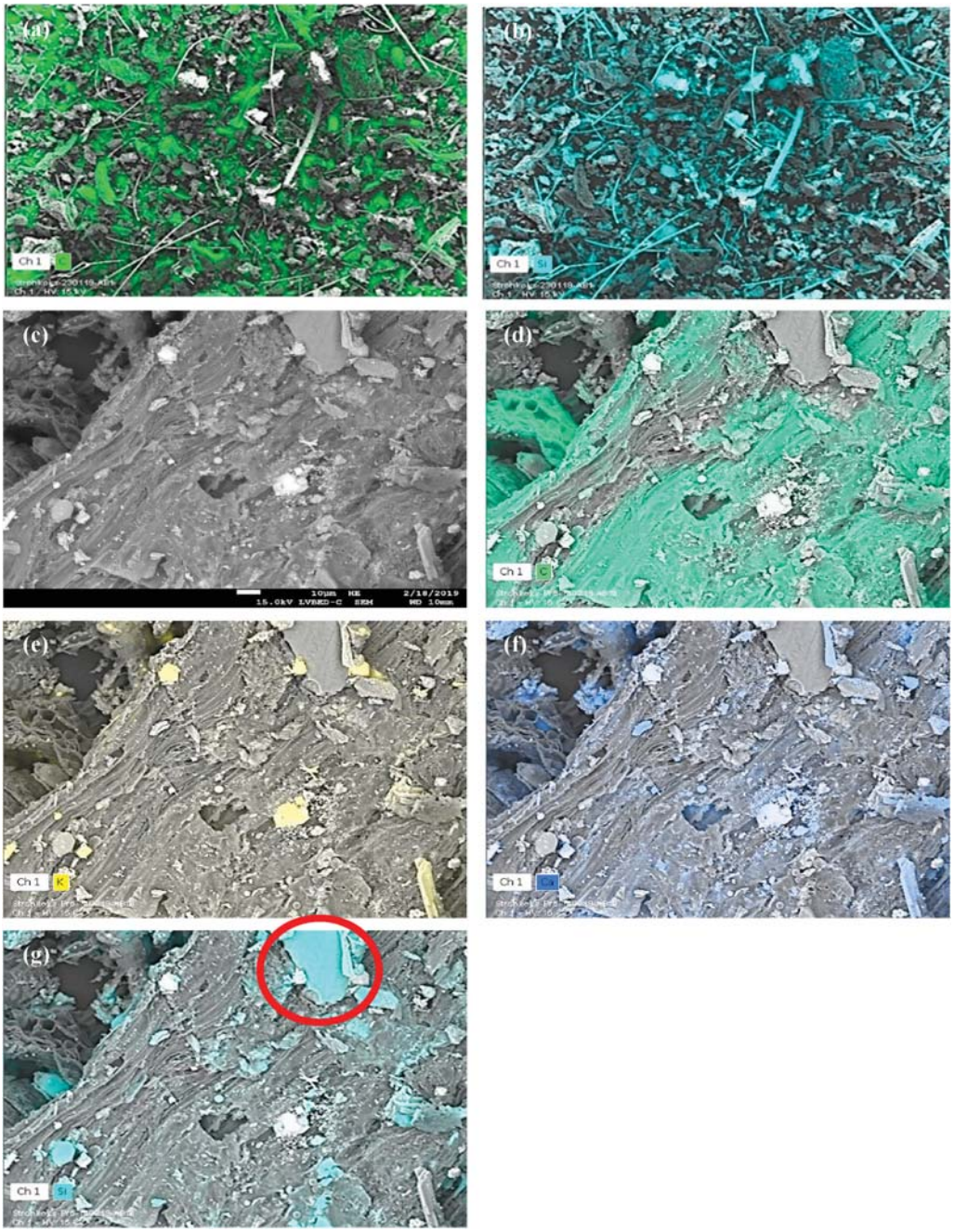

Fig. 3. (a) SEM–EDX analysis of C on a flat of SCFA particles (b) SEM–EDX analysis of Si on a flat of SCFA particles (c) Specific SEM analysis of char in SCFA (d) Specific SEM–EDX analysis of char in SCFA with C distribution (e) Specific SEM–EDX analysis of char in SCFA with K distribution (f) Specific SEM–EDX analysis of char in SCFA with Ca distribution (g) Specific SEM–EDX analysis of char in SCFA with Si distribution.

aromatic ring, which is one of the main challenges in tar reforming, with a lower S_{C6H6} below 0.35 compared to S_{C6H6} of 0.45 at $V_{H2O}/V_{H2} = 0.5$. Chen et al. also observed that the S_{C6H6} of toluene/naphthalene reforming at $V_{H2O}/V_{H2} = 2$ over different biochars had a low value below 0.2 [19]. The finding here suggests that the conversion from aromatics to light gas components over SCFA can be enhanced with an additional steam flow for raising the value of V_{H2O}/V_{H2} in raw syngas. With different V_{H2O}/V_{H2} of syngas derived from various biomass gasification processes, the selectivity of tar reforming might also have different trends.

3.4. Kinetics

With toluene conversions and reaction temperatures, kinetic constants can also be calculated using kinetic models. In this work, the first–order kinetic model, which is generally followed by tar reforming over char, was used in this study [18,30]. Under plug flow conditions, the apparent kinetic rate constant (k) is shown below,

$$k = \frac{\ln(1 - X_{C7H8})}{\tau_{NTP}} \quad (4)$$

By substituting respective k and reforming temperature (T_r) into Arrhenius' law (5), the activation energy (Ea) (assumed to be constant in the studied temperature range), and the apparent pre–exponential factor

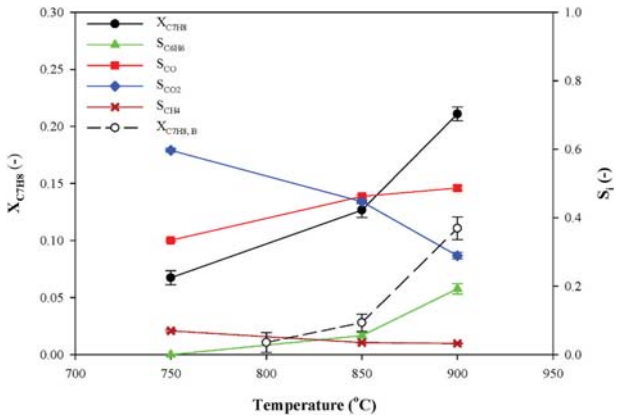

Fig. 4. Toluene conversion and selectivity from toluene reforming over SCFA at different temperatures (V_{H2O} = 15%). ($X_{C7H8,B}$: X_{C7H8} of blank testing).

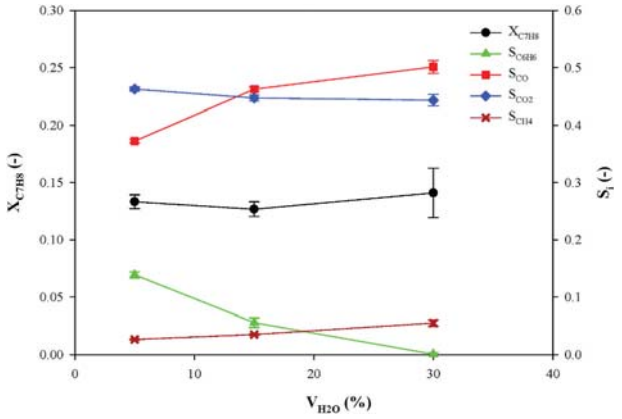

Fig. 5. Toluene conversion and selectivity from toluene reforming over SCFA at different steam volume fractions (T = 850 °C).

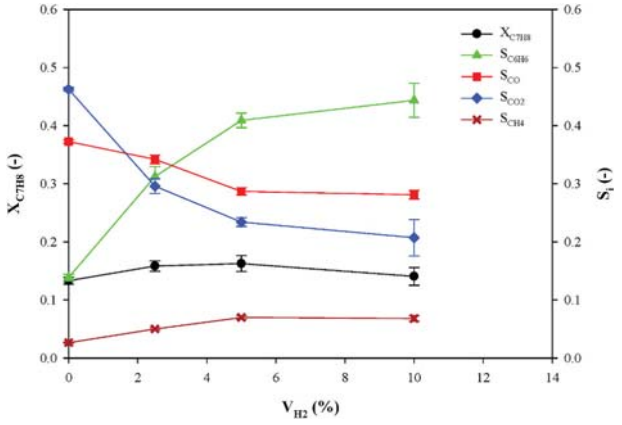

Fig. 6. Effect of volume fraction of hydrogen on selectivity during toluene reforming over SCFA (T = 850 °C; V_{H2O} = 5%).

(k_0) can be calculated. Then both kinetic parameters can be compared with the results of other studies to evaluate the activity of the applied catalysts for tar reforming.

$$k = k_0 \times e^{(-Ea/RT_r)}, \quad (5)$$

where R is the ideal gas constant (8.314 J K^{-1} mol^{-1}).

Kinetic constants of different biochars and mineral materials from different researches are listed in Table 5. In this research, the gas space time for SCFA is much shorter than other studies, so a relatively low toluene conversion is expected. However, with two parameters Ea and k_0 (Table 5), the performance of different catalysts at 850 °C can be easily compared by constructing the relationship between the space time and the conversion of tar compounds (X) of these catalysts. Since SCFA is fine particles with a particle size below 0.5 mm, biochars with the similar size listed in Table 5 are then compared with SCFA in Fig. 8, although the reforming processes, conditions, and tested tar compounds in different research are distinct. At 850 °C, all chars have high X exceeding 0.8 with space time above 0.1 kg h m^{-3}, while only SCFA and sawdust biochar [8] reach complete conversion of the tar compound at 0.05 kg h m^{-3}, confirming that SCFA can be regarded as a suitable catalyst for tar reduction as demonstrated by high conversion rate in short space time.

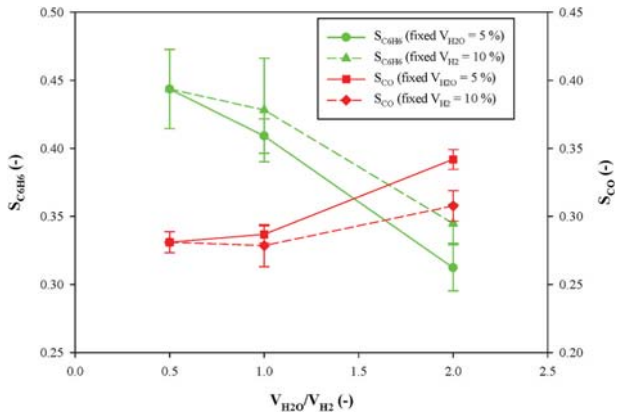

Fig. 7. Effect of steam to hydrogen volumetric ratio on selectivity during toluene reforming over SCFA (T = 850 °C).

3.5. Toluene reforming over SCFA in a simulated SOG derived condition

The gasification of SCFA, toluene conversion, and benzene selectivity during 1–h toluene reforming in a simulated SOG derived condition were investigated here. In this study, the sample gas for simulating SOG derived syngas was made up of the main gas composition from the SOG process, H_2O and H_2, with the volumetric ratio = 1 (15%/15%) referring to Table 1. CO_2 and other gas components were neglected in the simulated environment regarding the description in Section 1. SCFA steam gasification without toluene and the steam reforming of toluene over SCFA in the absence of hydrogen are also demonstrated.

3.5.1. SCFA gasification during toluene reforming

Char gasification during tar reforming is barely found in literature, and thus this research referred to the method developed by Chen et al. [19] to elucidate the influence of toluene and H_2 on SCFA gasification by the gasification rate at the same temperature. The representative experimental conditions are as follows: (1) T = 850 °C and V_{H2O} = 15%; (2) T = 850 °C, V_{H2O} = 15%, y_{C7H8} = 2.43 dm^3/m^3 and (3) T = 850 °C, V_{H2O} = 15%, V_{H2} = 15%, y_{C7H8} = 2.43 dm^3/m^3. Condition (3) is a simulated gas composition with V_{H2O}/V_{H2} = 1 referring to SOG derived syngas.

The gasification rate (r_G) of SCFA in condition (1) can be calculated with Eq. (6) by defining r_G equals to the production rate of carbon in CO and CO_2 stemming from SCFA on the basis of gasification reactions R2 and R5 [43], where A_{C_CO} and A_{C_CO2} are the accumulated concentration of carbon from CO and CO_2 which are arising from SCFA gasification (y_{G_CO} and y_{G_CO2}) during time t. In condition (1), y_{G_CO} and y_{G_CO2} are equal to the outlet volume concentration of CO and CO_2 detected directly by FTIR (y_{CO} and y_{CO2} in Fig. 9), respectively, since SCFA is the only reactant for steam gasification.

Table 5
Comparison of first–order rate constants for toluene reforming using SCFA as catalyst ($y_{C7H8} = 2.43\ dm^3/m^3$; $V_{H2O} = 15\%$) with the literature.

Catalyst type	Reactants	T (°C)	X (–)	Ea (kJ/mol)	k_0 ($m^3\ kg^{-1}\ h^{-1}$)	τ_{NTP}(kg h m^{-3})	Pellet size (mm)
SCFA (this research)	Toluene, H_2O	750–900	0.06–0.21	78	$8.7{\cdot}10^5$	0.0008	0.01–0.3
Straw char[a] [19]	Toluene &Naphthalene, H_2O, H_2	830–880	0.21–0.56	260	$2.3{\cdot}10^{13}$	0.02	2–5
Palm shell char[a] [19]	Toluene &Naphthalene, H_2O, H_2	850–900	0.31–0.81	319	$7.8{\cdot}10^{15}$	0.03	2–5
Wood char[a] [19]	Toluene &Naphthalene, H_2O, H_2	730–880	0.26–0.70	89	$1.3{\cdot}10^6$	0.01	2–5
Pine bark biochar [18]	Toluene, H_2O	650–900	0.19–0.94	91	$2.6{\cdot}10^5$	0.09	0.212–0.42
Commercial biochar [30]	Naphthalene, H_2O	700–900	~0.75–1.0	61	$7.6{\cdot}10^4$	0.04	0.5–0.8
Coal char[a] [24]	Toluene & Naphthalene, H_2, H_2O	750–950	–	91	$4.0{\cdot}10^6$	0.014[b]	1–2.8
Coconut char[a] [24]	Toluene & Naphthalene, H_2, H_2O	750–950	–	75	$2.8{\cdot}10^5$	0.044[b]	1–2.8
Dried sewage sludge char[a] [24]	Toluene & Naphthalene, H_2, H_2O	750–950	–	88	$6.0{\cdot}10^5$	0 .048[b]	2–2.8
Sawdust biochar [16]	Tar from pyrolysis of biomass, H_2O	650–800	0.81–0.96	35	$1.8{\cdot}10^4$	~0.009	0.15–0.25
18.7% Fe–biochar [41]	Toluene, H_2O	450–900	–	48	$5.4{\cdot}10^3$	0.09	0.2–0.4
Olivine [42]	Naphthalene, H_2O, CO_2, CO, H_2	825–900	~0.3–0.75	141	$1.7{\cdot}10^7$	–	–
Ni/olivine [9]	Toluene, H_2O	560–850	0.3–1.0	196	$3.1{\cdot}10^{13}$	–	0.25–0.315
CaO[a] [19]	Toluene &Naphthalene, H_2O, H_2	750–900	0.14–0.98	218	$1.5{\cdot}10^{11}$	0.135	2–5

[a] Data from toluene conversion.
[b] Calculated by bulk density (kg m^{-3}) and residence time (s).

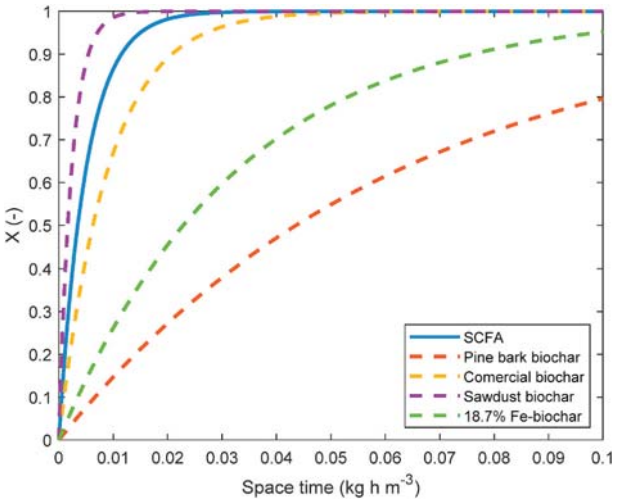

Fig. 8. Theoretical conversion of the tar compound over different fine char-based materials as a function of gas space time at 850 °C, calculated from the kinetics given in Table 5.

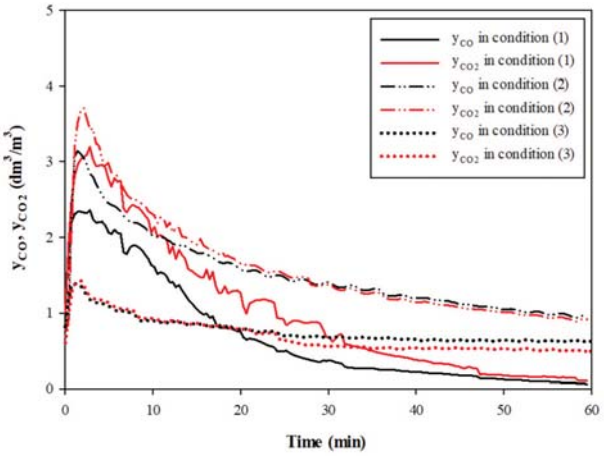

Fig. 9. Volume fractions of carbon monoxide and carbon dioxide as a function of time during testing at the following conditions (1) T = 850 °C and V_{H2O} = 15%, (2) T = 850 °C, V_{H2O} = 15%, $y_{C7H8,\ in} = 2.43\ dm^3/m^3$, and (3) T = 850 °C, V_{H2O} = 15%, V_{H2} = 15%, $y_{C7H8,in} = 2.43\ dm^3/m^3$.

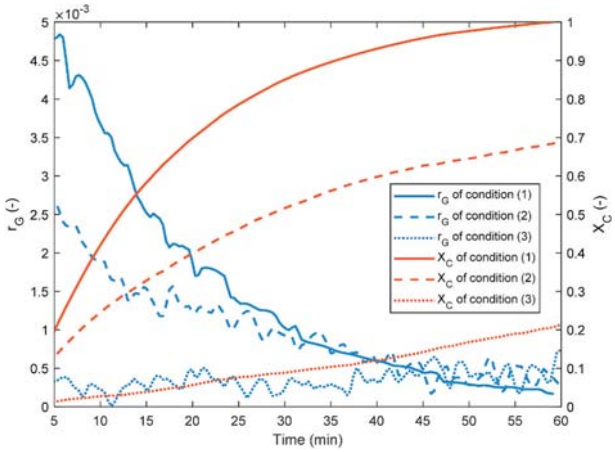

Fig. 10. Comparison of gasification rate and carbon conversion of SCFA from calculation during 1–h testing time at the following conditions (1) T = 850 °C and V_{H2O} = 15%, (2) T = 850 °C, V_{H2O} = 15%, $y_{C7H8,\ in} = 2.43\ dm^3/m^3$, and (3) T = 850 °C, V_{H2O} = 15%, V_{H2} = 15%, $y_{C7H8,in} = 2.43\ dm^3/m^3$.

$$r_G(-) = \frac{d(A_{C\_CO} + A_{C\_CO2})}{dt} \tag{6}$$

A_{C_CO} and A_{C_CO2} at time t are computed by the integration of y_{G_CO} and y_{G_CO2} with t in Eqs. (7) and (8):

$$A_{C\_CO} = 10^{-3} \cdot \int_0^t y_{G\_CO} dt, \tag{7}$$

$$A_{C\_CO2} = 10^{-3} \cdot \int_0^t y_{G\_CO2} dt \tag{8}$$

Finally, r_G can be calculated by differentiation of A_{C_CO} and A_{C_CO2} with respect to t shown in Eq. (6).

When it comes to gasification of SCFA in condition (2), y_{G_CO} and y_{G_CO2} can not be directly obtained from y_{CO} and y_{CO2} because toluene reforming also contributes to CO and CO_2 production due to R1 and R2. As a result, they are enumerated by y_{CO} and y_{CO2} depicted in Fig. 9 subtracting concentrations of CO and CO_2 from toluene (y_{T_CO} and y_{T_CO2}) at time t, presented as Eq. (9). With the same assumption as Chen et al. [19], y_{T_CO} and y_{T_CO2} can be calculated by fractions of C from reacted tar model compound deducting those from CH_4 and C_6H_6 (Eq. (10)). r_G of SCFA at time t in condition (2) is then calculated by Eqs. (6)–(8) and is presented in Fig. 10.

$$y_{G\_CO} + y_{G\_CO2} = y_{CO} + y_{CO2} - (y_{T\_CO} + y_{T\_CO2}) \tag{9}$$

Table 6
Comparison of gasification related parameters in different conditions.

Conditions	r_{G_10} (10^{-3})	[a]C_C %
1. 850 °C; V_{H2O} = 15%; 1 h	3.6	<0.02
2. 850 °C; V_{H2O} = 15%; $y_{C7H8,in}$ = 2.43 dm^3/m^3; 1 h	1.9	2.7
3. 850 °C; V_{H2O} = 15%; V_{H2} = 15%; $y_{C7H8,in}$ = 2.43 dm^3/m^3; 1 h	0.22	15.5

[a] Carbon content from the elemental analysis on a wet basis.

$$y_{T\_CO} + y_{T\_CO2} = 7 \cdot \left(y_{C7H8,\ in} - y_{C7H8}\right) - 6 \cdot y_{C6H6} - y_{CH4} \quad (10)$$

In the light of Fig. 10, r_G in the condition (1) is much higher in the beginning until approximately t = 30 min than r_G in condition (2), which confirms the phenomenon of inhibition of char gasification with the presence of toluene. This result corresponds to previous research, which also proves that the presence of tar inhibits the gasification of biochar [25]. After 30 min, r_G of condition (1) and (2) decrease to values below $1{\cdot}10^{-3}$ from $4.8{\cdot}10^{-3}$ and $2.7{\cdot}10^{-3}$ (t = 5 min), respectively, indicating that the first 30 min is the prime time for SCFA gasification whether with toluene or not. After 30 min, gas product stems mostly from steam reforming of toluene, where y_{CO} and y_{CO2} both stabilize at approximately 1 dm^3/m^3.

By using the same method, the r_G of condition (3) is also illustrated in Fig. 10. The production of CO and CO_2 with H_2 present is much lower than that without H_2 during the whole testing period, reporting that H_2 hinders the steam reforming reactions R2 and R5. According to Fig. 10, r_G in toluene reforming with hydrogen is much lower than that without hydrogen and remains roughly constant below $1{\cdot}10^{-3}$, indicating that the presence of hydrogen can strongly inhibit the gasification of SCFA during toluene reforming.

The carbon molecular conversion (X_C) of SCFA can also be calculated. Through condition (1), the carbon in SCFA was almost converted into CO and CO_2 (carbon content < a mass fraction of 0.02% shown in Table 6) in 60 min. The value of $A_{C\_CO} + A_{C\_CO2}$ (A_{C_Max}) at t = 60 min in condition (1) is considered as the maximum production of CO and CO_2 from all SCFA carbon. According to Avogadro's law, assuming all gas components after toluene reforming over SCFA are ideal gases, the molecular ratio of carbon is regarded to be proportional to volume ratio,

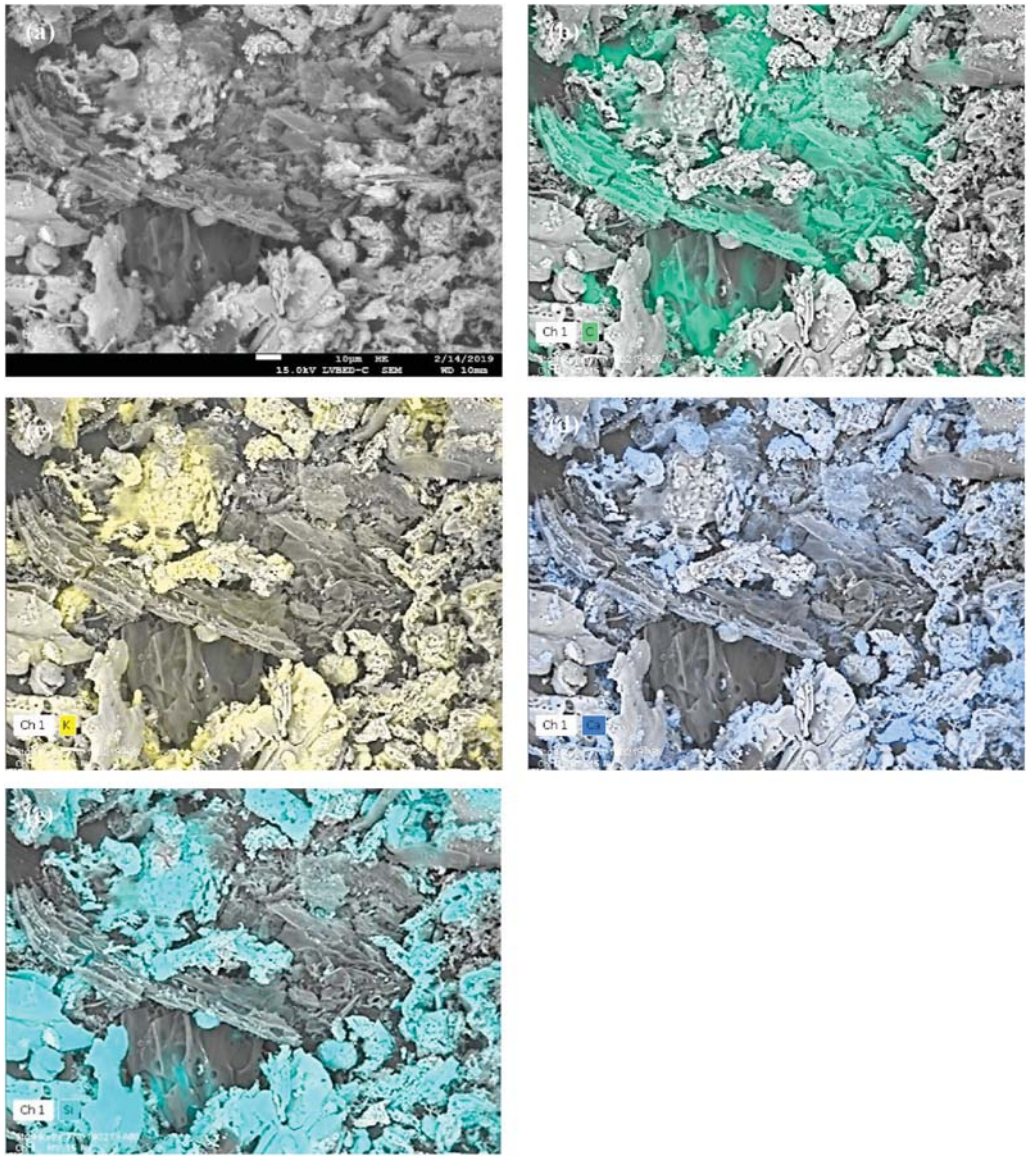

Fig. 11. (a) SEM analysis (b) SEM–EDX analysis of C with green distribution (c) SEM–EDX analysis of K with yellow distribution (d) SEM–EDX analysis of Ca with blue distribution (e) SEM–EDX analysis of Si with light blue distribution of SCFA generated from 1–h steam reforming of toluene at the condition of V_{H2O} = 15% and T = 850 °C. (For interpretation of the references to color in this figure legend, the reader is referred to the Web version of this article.)

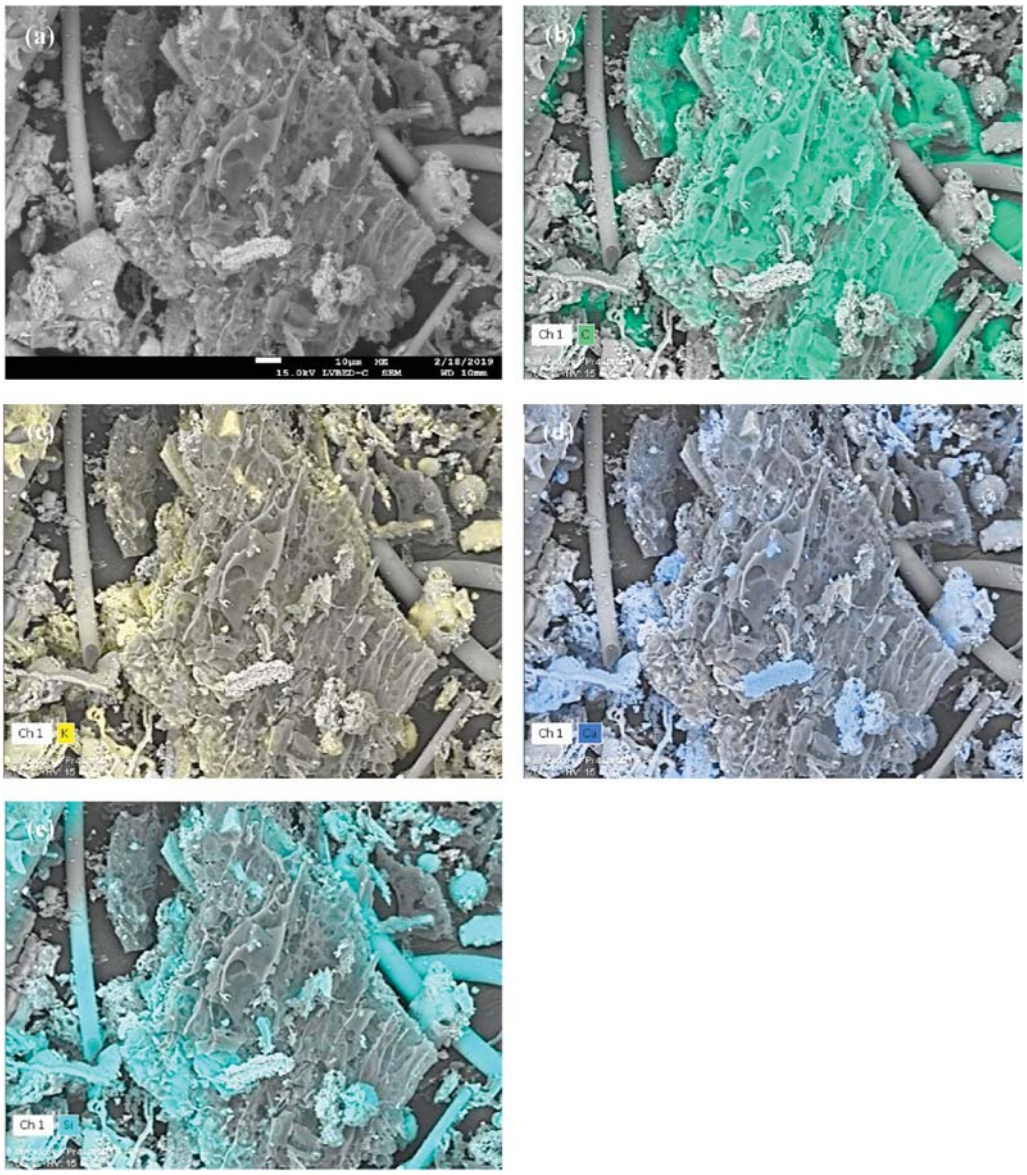

Fig. 12. (a) SEM analysis (b) SEM–EDX analysis of C with green distribution (c) SEM–EDX analysis of K with yellow distribution (d) SEM–EDX analysis of Ca with blue distribution (e) SEM–EDX analysis of Si with light blue distribution of SCFA generated from 1–h toluene reforming at the condition with V_{H2O} = 15%, V_{H2} = 15%, and T = 850 °C. (For interpretation of the references to color in this figure legend, the reader is referred to the Web version of this article.)

so Xc at time t can be calculated by Eq. (11) and illustrated in Fig. 10, which indicates that carbon in SCFA can be gasified in 1–h testing with X_C = 0.70 and 0.22 in the conditions (2) and (3) during toluene reforming.

$$X_C \approx \frac{A_{C\_CO} + A_{C\_CO2}}{A_{C\_Max}} \tag{11}$$

Table 6 lists two gasification related parameters to compare the application of SCFA as the tar–reforming catalyst in different conditions. Toluene and hydrogen can reduce the gasification rate of SCFA according to r_G of SCFA at t = 10 min (r_{G_10}). Hydrogen strongly inhibited char gasification, and a low constant r_G was thus observed throughout the whole reforming time in condition (3). The mass fraction of carbon content in SCFA (C_C) from these three conditions also presents apparent differences. Without hydrogen in toluene reforming, gasification of SCFA decomposes most of the carbon (C_C = 2.7%) from the original SCFA with C_C = 26%, while carbon with a mass fraction of 15% remains on the SCFA after toluene reforming in the presence of H_2. As steam has been verified that it has a positive effect on increasing the gasification rate, V_{H2O}/V_{H2} of syngas might be an important parameter for the gasification of char–based catalysts in tar reforming and avoiding carbon deposition. In conclusion, when applying SCFA as the catalyst for toluene reforming at 850 °C, gasification of SCFA was found to be a spontaneous reaction, indicating a possible enhancement of carbon conversion in the SOG process of straw pellets when using recycled SCFA as the tar–reforming catalyst.

3.5.2. SEM diagrams of char surface of SCFA after toluene reforming

SEM diagrams shown in Fig. 11 point out that during 1–h steam reforming of toluene over SCFA at 850 °C and V_{H2O} = 15%, carbon can remain on the char surfaces surrounded by large agglomerated inorganic groups as can be seen in Fig. 11 (b), (c), (d), and (e) because of SCFA gasification. In contrast, sole char gasification without toluene and hydrogen at 850 °C and V_{H2O} = 15% consumed almost all the carbon, and thus carbon concentration was so low that SEM–EDX could not detect the distribution of carbon on the surface (not shown).

SEM diagrams obtained in 1–h toluene reforming at V_{H2O} = 15%, V_{H2} = 15%, and T = 850 °C suggest that more carbon remains on the

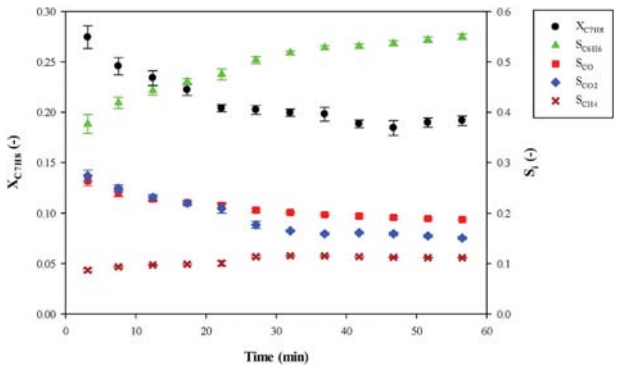

Fig. 13. Conversion and selectivities of toluene reforming during 1–h testing in the condition: T = 850 °C, V_{H2O} = 15%, V_{H2} = 15%, $y_{C7H8,in}$ = 2.43 dm^3/m^3.

char surface compared to the condition in the absence of H_2. Although Fig. 12 shows that carbon occupies the large area, agglomeration of metal is found at some stretches on the surface, especially on the edge of the char surface. Si appears evidently on the surface of SCFA shown in Fig. 12 (e). Both findings indicated that the carbon-covered ash in the char migrated on the surface during toluene reforming, which might result in an influence on the performance of toluene reforming. The inorganics dispersion on the char is a critical factor that influences the catalytic activity of the char. With the disappearance of carbon and large agglomeration of metals on the surface, a decrease in the catalytic activity of chars can be expected [39].

3.5.3. The change of toluene conversion and benzene selectivity through the time

By testing the simulated SOG derived environment with a H_2 volume fraction of 15%, a steam volume fraction of 15%, and 2.43 dm^3/m^3 of toluene, the X_{C7H8} and selectivities of the carbon–containing products during 1–h reforming are displayed in Fig. 13. Char gasification was neglected here due to a low constant r_G through the 1–h test. The much higher X_{C7H8} shown in Fig. 13 than that in the blank test (Fig. 4) confirms that toluene can be catalytically reformed over SCFA in the simulated SOG environment. Because of a low V_{H2O}/V_{H2} ratio in this condition, high S_{C6H6} can be found in Fig. 13. In comparison between the condition here and the condition absent of H_2 (V_{H2O} = 15%, $y_{C7H8,in}$ = 2.43 dm^3/m^3, and T = 850 °C), a significant difference of the reforming selectivity was observed at the sample-taken time range for indicator calculations. The presence of hydrogen led to the high selectivity of benzene (S_{C6H6} = 0.52), while light gas components like CO (S_{CO} = 0.46) are the main products when H_2 is absent.

Fig. 13 illustrates that X_{C7H8} decreases from 0.3 to around 0.2 when time increases, and S_{C6H6} has a gradual rise from 0.40 to 0.55. The change in the conversion and selectivity is highly related to the alternation of the surface property of SCFA verified from sections 3.5.1 and 3.5.2. Spontaneous gasification of char caused char decreasing and ash agglomeration on the surface of SCFA. More intensive inorganic areas covered on the surface were discovered in Fig. 12 with a decrease in carbon content from a mass fraction of 25.6 to 15.5%. It has been proven that the thermal treatment of char causes inorganics to migrate and agglomerate on the surface, and the activity is thus significantly reduced [39]. This phenomenon might also affect the selectivity during toluene reforming according to the observation in this study. The increase of S_{C6H6} and S_{CH4}, along with the decrease of S_{CO} and S_{CO2} through the time indicated hydrodealkylation became more dominant than other reactions. Thus, continuous replacement of deactivated SCFA with fresh SCFA is essential in a long–term process for maintaining high conversion rate and desired selectivity of tar reforming.

4. Conclusions

Straw char containing fly ash (SCFA) produced from steam–oxygen fluidized bed gasification exhibits promising catalytic activity for steam reforming of toluene compared to other chars derived from different conditions. Char surface, which provides the main surface area in SCFA, plays a big role in toluene reforming. SCFA gasification and selectivity of toluene reforming over SCFA are highly related to the steam to hydrogen volumetric ratio in the sample gas. Although toluene can be catalytically reformed over SCFA accompanied with the spontaneous gasification in a simulated SOG environment with V_{H2O}/V_{H2} = 1, adding additional steam into the SOG derived syngas before the tar reformer should be considered for formulating V_{H2O}/V_{H2} larger than 1 when applying recycled SCFA as tar–reforming catalyst. The reduction of the aromatic structure and enhancement of the gasification rate by increasing V_{H2O}/V_{H2} are beneficial for the downstream utilization and the total carbon conversion of the fuel. This study suggests that toluene reforming over SCFA should be conducted in the environment with high V_{H2O}/V_{H2} (>2) and residence time over 0.05 kg h m^{-3} at temperatures over 850 °C to achieve high toluene conversion with excellent selectivity of light gas components. Moreover, the alternation of the surface property due to the gasification is highly related to the deactivation of SCFA and the change of the reforming selectivity, suggesting that the replacement of the deactivated SCFA for a long–term tar reforming is necessary. This research gives a principle concept for using recycled SCFA as a tar–reforming catalyst in the original SOG process. A field test should be conducted for treating actual syngas in the future by constructing an optimized tar reformer that can realize the extra steam infusion with a convenient system to substitute fresh SCFA for deactivated SCFA.

Acknowledgement

The authors gratefully acknowledge the support from DAAD (German Academic Exchange Service) and the project NuCA (0324342A) funded by the German Ministry of Economic Affairs and Energy (BMWi).

Nomenclature

τ_{NTP}	Space time (g h m^{-3} or kg h m^{-3})
A_{C_CO} and A_{C_CO2}	The accumulated concentration of carbon from CO and CO_2 which are arising from straw char gasification during time t (m^3/m^3·min)
A_{C_Max}	$A_{C\_CO} + A_{C\_CO2}$ (T = 850 °C and V_{H2O} = 15%) at t = 60 min (m^3/m^3·min)
C_C	Mass fraction of carbon content (%)
D_{C_i}	Carbon distribution of component i (−)
Ea	Activation energy (kJ/mol)
ER	The equivalence ratio (mol/mol)
k	Apparent kinetic constant (m^3 kg^{-1} h^{-1})
k_0	Apparent pre–exponential factor (m^3 kg^{-1} h^{-1})

M_R Residual mass fraction (−)
Q Outlet total volume flow rate ($m^3\ h^{-1}$)
$Q_{C7H8,\ in}$ Inlet toluene volume flow rate ($m^3\ h^{-1}$)
Q_{C7H8} Outlet toluene volume flow rate ($m^3\ h^{-1}$)
Q_{in} Inlet total volume flow rate ($m^3\ h^{-1}$)
Q_{NTP} Constant total flow rate (0.3 $m^3\ h^{-1}$)
R The ideal gas constant (8.314 J K^{-1} mol^{-1})
r_G Gasification rate of SCFA (−)
r_{G_10} Gasification rate of SCFA at t = 10 min (−)
r_i The number of carbon atoms of component i (−)
S/C The steam to carbon ratio (mol/mol)
S_i Selectivity of component i (−)
T Reaction temperature (°C)
T_r Reforming temperature in Arrhenius' law (K)
t Reaction time (min)
V_i Volume fraction of component i (i = H_2O and H_2) in inlet flow (%)
X Conversion of the tar model compound (−)
X_{C7H8} Toluene conversion (−)
X_C Carbon molcular conversion (−)
y_{C7H8} Outlet toluene volume concentration (dm^3/m^3)
$y_{C7H8,\ in}$ Inlet toluene volume concentration (dm^3/m^3)
y_{G_CO} and y_{G_CO2} Volume fractions of CO and CO_2 arising from gasification of SCFA (dm^3/m^3)
y_i Outlet volume concentration of component i (dm^3/m^3)
y_{T_CO} and y_{T_CO2} Volume fractions of CO and CO_2 from toluene reforming (dm^3/m^3)

Abbreviation
AAEMs Alkali and alkaline earth metals
DIN The German Institute for Standardization
FTIR Fourier–transform infrared spectroscopy analyzer
SCFA Straw char containing fly ash
SEM Scanning electron microscope
EDX Energy dispersive X–ray spectroscopy
SEM–EDX Scanning electron microscope–energy dispersive X–ray spectroscopy
SOG Steam–oxygen gasification
TGA Thermal gravimetric analysis

References

[1] W.L. van de Kamp, P.J. de Wild, H.A.M. Knoef, J.P.A. Neeft, J.H.A. Kiel, Tar Measurement in Biomass Gasification, Standardisation and Supporting R&D, Research Centre of the Netherlands, 2006 report ECN-C—06-046.
[2] J.P.A. Neeft, H.A.M. Knoef, G.J. Buffinga, U. Zielke, K. Sjöström, C. Brage, P. Hasler, P.A. Smell, M. Suomalainen, M.A. Dorrington, C. Greil, Guideline for sampling and analysis of tar and particles in biomass producer gases, in: A. V. Bridgwater (Ed.), Progress in Thermochemical Biomass Conversion, Blackwell Science Ltd, Oxford, 2001, p. 162, https://doi.org/10.1002/9780470694954.ch11.
[3] T.A. Milne, R.J. Evans, N. Abatzoglou, Biomass Gasifier "Tars": Their Nature, Formation, and Conversion, National Renewable Energy Laboratory, Colorado, 1998. Report No. NREL/TP570-25357.
[4] D. Dayton, A Review of the Literature on Catalytic Biomass Tar Destruction, National Renewable Energy Laboratory, Colorado, 2002. Report No. NREL/TP-510-32815.
[5] V.S. Sikarwar, M. Zhao, P. Clough, J. Yao, X. Zhong, M.Z. Memon, N. Shah, E. J. Anthony, P.S. Fennell, An overview of advances in biomass gasification, Energy Environ. Sci. 9 (10) (2006) 2939–2977, https://doi.org/10.1039/C6EE00935B.
[6] A.V. Bridgwater, The technical and economic feasibility of biomass gasification for power generation, Fuel 74 (5) (1995) 631–653, https://doi.org/10.1016/0016-2361(95)00001-L.
[7] S. Anis, Z.A. Zainal, Tar reduction in biomass producer gas via mechanical, catalytic and thermal methods: a review, Renew. Sustain. Energy Rev. 15 (5) (2011) 2355–2377, https://doi.org/10.1016/jsser.2011.02.018.
[8] Z. Abu El-Rub, E.A. Bramer, G. Brem, Review of catalysts for tar elimination in Biomass gasification processes, Ind. Eng. Chem. Res. 43 (22) (2004) 6911–6919, https://doi.org/10.1021/ie0498403.
[9] D. Swierczynski, S. Libs, C. Courson, A. Kiennemann, Steam reforming of tar from a biomass gasification process over Ni/olivine catalyst using toluene as a model compound, Appl. Catal., B 74 (3–4) (2007) 211–222, https://doi.org/10.1016/j.apcatb.2007.01.017.
[10] R. Coll, J. Salvado, X. Farriol, D. Montane, Steam reforming model compounds of biomass gasification tars: conversion at different operating conditions and tendency towards coke formation, Fuel Process. Technol. 74 (1) (2001) 19–31, https://doi.org/10.1016/S0378-3820(01)00214-4.
[11] D. Feng, Y. Zhao, Y. Zhang, S. Sun, S. Meng, Y. Guo, Y. Huang, Effects of K and Ca on reforming of model tar compounds with pyrolysis biochars under H2O or CO2, Chem. Eng. J. 306 (2016) 422–432, https://doi.org/10.1016/j.cej.2016.07.065.
[12] D. Feng, Y. Zhao, Y. Zhang, Z. Zhang, H. Che, S. Sun, Experimental comparison of biochar species on in-situ biomass tar H2O reforming over biochar, Int. J. Hydrogen Energy 42 (38) (2017) 24035–24046, https://doi.org/10.1016/j.ijhydene.2017.08.013.
[13] D. Feng, Y. Zhao, Y. Zhang, Z. Zhang, S. Sun, Roles and fates of K and Ca species on biochar structure during in-situ tar H2O reforming over nascent biochar, Int. J. Hydrogen Energy 42 (34) (2017) 21686–21696, https://doi.org/10.1016/j.ijhydene.2017.07.096.
[14] Y. Shen, Y. Fu, Advances in in situ and ex situ tar reforming with biochar catalysts for clean energy production, Sustain. Energy Fuels 2 (2) (2018) 326–344, https://doi.org/10.1039/c7se00553a.
[15] P.N. Bhandari, A. Kumar, D.D. Bellmer, R.L. Huhnke, Synthesis and evaluation of biochar-derived catalysts for removal of toluene (model tar) from biomass-generated producer gas, Renew. Energy 66 (2014) 346–353, https://doi.org/10.1016/j.renene.2013.12.017.
[16] D. Feng, Y. Zhao, Y. Zhang, Z. Zhang, L. Zhang, S. Sun, In-situ steam reforming of biomass tar over sawdust biochar in mild catalytic temperature, Biomass Bioenergy 107 (2017) 261–270, https://doi.org/10.1016/j.biombioe.2017.10.007.
[17] N.B. Klinghoffer, M.J. Castaldi, A. Nzihou, Catalyst properties and catalytic performance of char from biomass gasification, Ind. Eng. Chem. Res. 51 (40) (2012) 13113–13122, https://doi.org/10.1021/ie3014082.
[18] S. Mani, J.R. Kastner, A. Juneja, Catalytic decomposition of toluene using a biomass derived catalyst, Fuel Process. Technol. 114 (2013) 118–125, https://doi.org/10.1016/j.fuproc.2013.03.015.
[19] Y.-H. Chen, M. Schmid, C.-C. Chang, C.-Y. Chang, G. Scheffknecht, Lab-scale investigation of palm shell char as tar reforming catalyst, Catalysts 10 (5) (2020) 476, https://doi.org/10.3390/catal10050476.
[20] P. Brandt, E. Larsen, U. Henriksen, High tar reduction in a two-stage gasifier, Energy Fuels 14 (4) (2000) 816–819, https://doi.org/10.1021/ef990182m.
[21] G. Ravenni, Application of Biomass Char to Tar Conversion and Producer Gas Upgrading to Syngas, Ph.D. Thesis, Technical University of Denmark, Kgs, Lyngby, 2018.
[22] G. Ravenni, O.H. Elhami, J. Ahrenfeldt, U.B. Henriksen, Y. Neubauer, Adsorption and decomposition of tar model compounds over the surface of gasification char

and active carbon within the temperature range 250–800 °C, Appl. Energy 241 (2019) 139–151, https://doi.org/10.1016/j.apenergy.2019.03.032.
[23] M. Schmid, M. Beirow, D. Schweitzer, G. Waizmann, R. Spörl, G. Scheffknecht, Product gas composition for steam-oxygen fluidized bed gasification of dried sewage sludge, straw pellets and wood pellets and the influence of limestone as bed material, Biomass Bioenergy 117 (2018) 71–77, https://doi.org/10.1016/j.biombioe.2018.07.011.
[24] D. Fuentes-Cano, A. Gomez-Barea, S. Nilsson, P. Ollero, Decomposition kinetics of model tar compounds over chars with different internal structure to model hot tar removal in biomass gasification, Chem. Eng. J. 228 (2013) 1223–1233, https://doi.org/10.1016/j.cej.2013.03.130.
[25] C. Fushimi, T. Wada, A. Tsutsumi, Inhibition of steam gasification of biomass char by hydrogen and tar, Biomass Bioenergy 35 (1) (2011) 179–185, https://doi.org/10.1016/j.biombioe.2010.08.017.
[26] M. Barrio, B. Gbel, H. Rimes, U. Henriksen, J.E. Hustad, L.H. Srensen, Steam gasification of wood char and the effect of hydrogen inhibition on the chemical kinetics, in: A.V. Bridgwater (Ed.), Progress in Thermochemical Biomass Conversion, Blackwell Science Ltd, Oxford, 2001, p. 32.
[27] D. Feng, Y. Zhao, Y. Zhang, S. Sun, Effects of H2O and CO2 on the homogeneous conversion and heterogeneous reforming of biomass tar over biochar, Int. J. Hydrogen Energy 42 (18) (2017) 13070–13084, https://doi.org/10.1016/j.ijhydene.2017.04.018.
[28] C. Guizani, M. Jeguirim, R. Gadiou, F.J. Escudero Sanz, S. Salvador, Biomass char gasification by H2O, CO2 and their mixture: evolution of chemical, textural and structural properties of the chars, Energy 112 (2016) 133–145, https://doi.org/10.1016/j.energy.2016.06.065.
[29] H. Boerrigter, R.W.R. Zwart, E.P. Deurwaarder, C.M. van der Meijden, S.V.B. van Paasen, Production of Synthetic Natural Gas (SNG) from Biomass—Development and Operation of an Integrated Bio-SNG System—Non-Confidential Version, Research Centre of the Netherlands, 2006 report ECN-E—06-018.
[30] Z. Abu El-Rub, E.A. Bramer, G. Brem, Experimental comparison of biomass chars with other catalysts for tar reduction, Fuel 87 (10–11) (2008) 2243–2252, https://doi.org/10.1016/j.fuel.2008.01.004.
[31] The German Institute for Standardization, DIN EN ISO 18134-3, 18122, 18123, 16948, 16967, and 16994 [2019]. Available from: https://www.din.de/de.
[32] Y.-H. Chen, C.-C. Chang, C.-Y. Chang, M.-H. Yuan, D.-R. Ji, J.-L. Shie, C.-H. Lee, Yi-H. Chen, W.-R. Chang, T.-Y. Yang, T.-C. Hsu, M. Huang, C.-H. Wu, F.-C. Lin, C.-H. Ko, Production of a solid bio-fuel from waste bamboo chopsticks by torrefaction for cofiring with coal, J. Anal. Appl. Pyrolysis 126 (2017) 315–322, https://doi.org/10.1016/j.jaap.2017.05.015.
[33] G. Taralas, M.G. Kontominas, Kinetic modelling of VOC catalytic steam pyrolysis for tar abatement phenomena in gasification/pyrolysis technologies, Fuel 83 (9) (2004) 1235–1245, https://doi.org/10.1016/j.fuel.2003.11.010.
[34] G. Taralas, M.G. Kontominas, Numerical modeling of tar species/VOC dissociation for clean and intelligent energy production, Energy Fuels 19 (1) (2005) 87–93, https://doi.org/10.1021/ef040048o.
[35] D. Shekhawat, J.J. Spivey, D.A. Berry (Eds.), Fuel Cells: Technologies for Fuel Processing, first ed., Elsevier Science, London, 2011.
[36] G. Taralas, M.G. Kontominas, X. Kakatsios, Modeling the thermal destruction of toluene (C7H8) as tar-related species for fuel gas cleanup, Energy Fuels 17 (2) (2003) 329–337, https://doi.org/10.1021/ef0201533.
[37] M. Morin, X. Nitsch, S. Pecate, M. Hemati, Tar conversion over olivine and sand in a fluidized bed reactor using toluene as model compound, Fuel 209 (2017) 25–34, https://doi.org/10.1016/j.fuel.2017.07.084.
[38] S.J. Blott, A.M. Al-Dousari, K. Pye, S.E. Saye, Three-dimensional characterization of sand grain shape and surface texture using a nitrogen gas adsorption technique, J. Sediment. Res. 74 (1) (2004) 156–159, https://doi.org/10.1306/052403740156.
[39] N.B. Klinghoffer, M.J. Castaldi, A. Nzihou, Influence of char composition and inorganics on catalytic activity of char from biomass gasification, Fuel 157 (2015) 37–47, https://doi.org/10.1016/j.fuel.2015.04.036.
[40] F. Bustamante, R.M. Enick, A.V. Cugini, R.P. Killmeyer, B.H. Howard, K. S. Rothenberger, M.V. Ciocco, B.D. Morreale, S. Chattopadhyay, S. Shi, High-temperature kinetics of the homogeneous reverse water-gas shift reaction, AIChE J. 50 (5) (2004) 1028–1041, https://doi.org/10.1002/aic.10099.
[41] J.R. Kastner, S. Mani, A. Juneja, Catalytic decomposition of tar using iron supported biochar, Fuel Process. Technol. 130 (2015) 31–37, https://doi.org/10.1016/j.fuproc.2014.09.038.
[42] L. Devi, Catalytic removal of biomass tars: olivine as prospective in-bed catalyst for fluidized-bed biomass gasifiers, Technische Universiteit Eindhoven, The Netherlands, 2005, https://doi.org/10.6100/IR583960.
[43] S. Nilsson, A. Gomez-Barea, D. Fuentes Cano, Gasification reactivity of char from dried sewage sludge in a fluidized bed, Fuel 92 (1) (2012) 346–353, https://doi.org/10.1016/j.fuel.2011.07.031.

Paper II

catalysts

MDPI

Article

Lab-Scale Investigation of Palm Shell Char as Tar Reforming Catalyst

Yen-Hau Chen [1,*], Max Schmid [1], Chia-Chi Chang [2], Ching-Yuan Chang [2] and Günter Scheffknecht [1]

[1] Institute of Combustion and Power Plant Technology, University of Stuttgart, 70569 Stuttgart, Germany; max.schmid@ifk.uni-stuttgart.de (M.S.); guenter.scheffknecht@ifk.uni-stuttgart.de (G.S.)

[2] Graduate Institute of Environmental Engineering, National Taiwan University, Taipei 106, Taiwan; d92541005@ntu.edu.tw (C.-C.C.); cychang3@ntu.edu.tw (C.-Y.C.)

* Correspondence: yen-hau.chen@ifk.uni-stuttgart.de; Tel.: +49-711-685-69498

Received: 25 March 2020; Accepted: 24 April 2020; Published: 27 April 2020

Abstract: This research investigated the application of palm shell char as a catalyst for the catalytic steam reforming of tar after the sorption enhanced gasification (SEG) process. The catalytic activities of palm shell char and metal-supported palm shell char were tested in a simulated SEG derived syngas with tar model compounds (i.e., toluene and naphthalene) at a concentration of 10 g m^{-3}_{NTP}. The results indicated that palm shell char had an experimentally excellent catalytic activity for tar reforming with toluene and naphthalene conversions of 0.8 in a short residence time of 0.17 s at 900 °C. A theoretical residence time to reach the complete naphthalene conversion was 1.2 s at 900 °C for palm shell char, demonstrating a promising activity similar to wood char and straw char, but better than CaO. It was also found that potassium and iron-loaded palm shell chars exhibited much better catalytic activity than palm shell char, while the parallel reaction of gasification of K-loaded palm shell char influenced the conversion with its drastic mass loss. Moreover, contrary to CaO, palm shell char presented relatively low selectivity to benzene, and its spontaneous gasification generated extra syngas. In summary, the present study demonstrated that the low-cost material, palm shell char, can successfully be used as the tar-reforming catalyst after SEG process.

Keywords: biomass gasification; tar reduction; cost-effective catalytically active biochar; catalytic steam reforming

1. Introduction

Steam gasification is one of the gasification processes for syngas production. An enhanced process, so-called sorption enhanced gasification (SEG), is regarded as an attractive process for hydrogen-rich syngas generation. This process runs in a dual fluidized bed system and is based on a sorption-desorption cycle using calcined limestone (CaO) as the sorbent. In the SEG, the sorbent removes CO_2 from the syngas produced in the gasification reactor at a low-temperature range from 600 °C to 700 °C, resulting in a high hydrogen content in the syngas which hence matches much better for a downstream synthesis (e.g., to produce CH_4 or other products). In a second reactor, the sorbent is regenerated to CaO by heating it via combustion of the remaining char from the gasifier or the additional fuel. The sensible heat of the sorbent that is recycled to the gasifier and the reaction enthalpy of the exothermic CO_2 sorption reaction provide the required reaction heat for the endothermic gasification reactions. The SEG process, covering lab-scale and pilot-scale facilities, has been studied for several years at the Institute of Combustion and Power Plant Technology (IFK), University of Stuttgart [1–3]. In this process, tar production is still a problem because the tar concentration on a dry basis in raw syngas still can reach around 10 g $m^{-3}_{dry, STP}$ [4]. However, downstream units, such as gas

engines or turbines require a reduction of the tar content down to 30 mg $m^{-3}_{dry, STP}$, or even lower [5]. Tar can be firmly adsorbed on the surface of catalysts for syngas synthesis, inhibiting the production of other chemicals [6–8]. Hence, further tar reduction is necessary, particularly where the syngas is used in synthesis.

Since the raw syngas is produced at a high temperature of 600–700 °C in the SEG process with a high steam concentration, an additional tar reformer loaded with tar cracking catalysts is suitable for coupling with SEG process for tar reduction by steam reforming. This efficient gas cleaning process that can be operated at high temperatures is seen as energetically beneficial. Excessive gas cooling, that is required for condensing and scrubbing of tar in heated syngas, can be avoided. Moreover, tars can be converted into H_2 and CO by steam reforming, promoting the quality of syngas. This study aimed to examine the catalytic steam reforming of tar model compounds, carried in simulated SEG derived syngas, by using low-cost biochars as catalysts that have the potential to be applied in the tar reformer after SEG process.

Although the gas composition from SEG process is dependent on different operation conditions, the ratio of steam volume fraction to hydrogen volume fraction (V_{H2O}/V_{H2}, -) = 2 in the simulated syngas was chosen in this study, referring to the typical product gas composition in Table 1. Further, gas components, such as CO, CO_2, methane, and other hydrocarbons were not considered for the tar reforming reaction as the main components in SEG syngas are steam and hydrogen with up to 90 vol %. With a high content of steam in the raw syngas, steam reforming of tar might become the dominant reaction for tar reduction. The composition of tar from the SEG process can be found in Armbrust's research indicating that phenol, toluene, and naphthalene are the major tar components in raw syngas [9]. As phenol is able to be decomposed at high temperatures above 800 °C without any catalysts [10], this study examined the tar reforming with toluene and naphthalene, representing also secondary and tertiary tars [4], of circa 10 g m^{-3}_{NTP} based on the typical tar concentration in SEG syngas. Naphthalene concentration around 250 ppmv was considered in this study based on a representative SEG derived tar fraction [8].

Table 1. Typical SEG product gas composition (N2 free).

Component	Unit	[11,12]	[13]
H_2O	vol %	50–60	60
H_2	vol %	55–71 [a]	26
CO	vol %	5–11 [a]	2.4
CO_2	vol %	7–20 [a]	3
CH_4	vol %	8–13 [a]	5.6
Tar	g m^{-3}_{NTP}	0.3–3 [a]	1–5

[a] On the dry basis.

Ni-based catalysts have been known as commercial catalysts for tar cracking [14,15]. Basically, they are highly efficient in tar conversion. However, Ni-based catalysts are more expensive than active natural materials, and their deactivation occurs easily because of sulfur and heavy tar content in the feed [15,16]. As a result, it is necessary to find other cheap materials that can substitute commercial catalysts, or can used as a protector to eliminate most of the heavy tar before them. So far, there have been studies indicating that biochars generated by pyrolysis have the ability to decompose organic compounds [17]. These char-based catalysts are comparably low cost and easily available from the biomass fuel and waste by pyrolysis or spent char produced in industrial processes. Moreover, the deactivated char catalyst is easy to handle because of the similar property to the spent char from the gasification process. After the application of tar reduction for SEG process, the replaced char catalysts can be combusted in the regenerator with spent char from the gasifier. On the other hand, char catalysts could be gasified spontaneously during tar reforming, which benefits the syngas production. Based on the above advantages, it is worth studying the application of char-based catalysts for tar reforming after the gasification process.

In this study, palm shell (PS) was considered a potential biomass for producing tar-cracking active biochar by pyrolysis. The production of palm oil has more than doubled in the past two decades, given it is the most widely traded edible oil. In obtaining edible oils from palms, a large amount of PS waste is produced. In recent years, PS waste has been a commercial and cheap biomass to be used as fuel in Asia [18–20]. In addition, activated carbon with high surface area, which is also preferable for tar reforming, can be obtained from palm shell [21]. Consequently, with high production and good properties following carbonization, it is worth investigating the catalytic activity of palm shell char for the special issue of tar reforming and then comparing the catalytic activity with other biochars. According to several references, biochars were manufactured by similar methods for the purpose of tar reforming. For example, (1) biochar was prepared by pyrolyzing pine bark at 950 °C for 2 h with nitrogen [22]; (2) pyrolysis of sawdust was carried out in 2.0 L min^{-1} Ar atmosphere at a slow heating rate of 10 °C min^{-1} and a final pyrolysis temperature of 800 °C with the residence time 30 min [23]; (3) rice husk was then pyrolyzed with a slow heating rate of 10 °C min^{-1} to a final pyrolysis temperature of 800 °C. The hold time was 10 min [24]. This study then established a pyrolysis procedure for the manufacturing of palm shell char according to the above methods.

The mechanism of tar cracking on biochars has also been studied recently. Feng et al. pointed out that the main factors of tar reforming are highly related to alkali and alkaline earth metal (AAEMs) contents, and the surface area of biochar [24–26]. The reaction mechanism of tar reforming with AAEMs species on biochar is comprehensively explained in their research. The presence of K and Ca elements, which lead to repeated bond-forming and bond-breaking of tar fragments, contributes to tar decomposition and the formation of light hydrocarbons and small–molecule gases. Apart from AAEM groups, Klinghoffer et al. also found that Fe sites on the char surface react obviously as active sites for the catalytic reaction. The high carbon deposition was found on the Fe site on char after applying char as a decomposing catalyst for organic compounds [27]. Kastner et al. [28] also pointed out that iron might be reduced to metallic iron (Fe) or other forms of more reduced iron (e.g., FeO) via hydrogen during steam reforming of toluene over Fe supported biochar, which is beneficial to toluene reforming as it has been already confirmed that iron in reduced forms can catalytically decompose tar [29]. This study investigated the reforming ability of potassium in tar and iron-loaded palm shell chars. Another low-cost material, CaO, which is used as the sorbent in the SEG process, was also tested here as the reference catalyst, as compared with biochar catalysts. Since Chen et al. found that CaO performed well on toluene cracking through steam reforming [30], CaO might be applicable as the tar-reforming catalyst in a downstream reformer after SEG process. For better understanding the role of individual catalysts, sole catalyst-sorbents were examined. This information provides the basic knowledge for further testing the possibility of using mixed catalyst-sorbents, which would complicate the preparation of catalysts.

2. Results

2.1. Characteristics of Palm Shell Char (PSC), 5%K-Loaded Palm Shell Char (5%K-PSC), 5%Fe-Loaded Palm Shell Char (5%Fe-PSC), Wood Char (WC), and Straw Char (SC)

All bio-chars were manufactured by the pyrolysis process described in Section 3.1. According to Table 2, after the pyrolysis of PS, its contents of equilibrium moisture and volatile matters decreased significantly, while that of fixed carbon content increased, as expected. Since the higher volatile matter makes biomass more susceptible to tar formation during steam reforming, the low content of only 3.4 wt.% in PSC is suitable for the following tar-reforming catalyst usage. Fixed carbon and carbon content increased from 4.7 to 89.7 wt.%, and from 38.8 to 89.8 wt.%, respectively, proving that the carbonization during pyrolysis increased carbon content. According to Klinghoffer et al. [31], the presence of carbon in biochar promoted the catalytic activity. After intense carbonization by pyrolysis, the performance of tar reforming over PSC and WC might be enhanced. It was also found that PSC had much lower oxygen content of 1.82 wt.% compared to that of PS of 35.3 wt.%, suggesting that more hydrophobic solid was formed after pyrolysis [32].

Both K and Fe-supported PSC had higher ash contents of 16.9 wt.%, and 17.8 wt.%, respectively, than PSC with 4.61 wt.%. After PSC was impregnated with potassium and iron-containing solutions, 11.0 wt.% of K_2O and 12.1 wt.% of Fe_2O_3 were observed by metal analysis in 5%K-PSC and 5%Fe-PSC, respectively, while PSC had only 0.532 wt.% of K_2O and 0.939 wt.% of Fe_2O_3 in ash. These results verify that the metal loading method used in this study can successfully load potassium or iron on the PSC. Although ash content had a significant rise after PS was soaked with K and Fe, the major component in both, metal-loaded PSC is still carbon, as can be seen in Table 2.

Among three biochars produced from palm shell, wood, and straw, SC had the highest ash content of 31.1 wt.% resulting in the lowest carbon content among three biochars. In comparison to PSC and WC, SC possessed more AAEM contents, which can promote the activity of biochars for gasification and tar reforming [24,33]. Moreover, the equilibrium moisture content of PSC was only 2.0 wt.% much lower than those of WC and SC with a value of around 7 wt.%, which was better for storage and transportation when applying it as catalysts.

PSC possessed a much higher BET surface area (469.6 $m^2\ g^{-1}$) compared to that of CaO with only 8.8 $m^2\ g^{-1}$. However, a negative effect of potassium was found in the pyrolysis process for producing char catalysts. Char lumps were formed from the individual pellet, which might be caused by the agglomeration of potassium. At such a high temperature as in this case, excessive impregnation of potassium on biochar can lead to agglomeration during pyrolysis [34]. A blockage in the pyrolyzer was observed, causing the difficulty of manufacturing K-loaded PSC. According to the surface area analysis of three PSCs, 5%K-PSC has a tiny surface area of 6.9 $m^2\ g^{-1}$, which might be due to agglomeration, resulting in the disappearance of the porous structure, while the surface areas of 5%Fe-PSC and PSC are both above 200 $m^2\ g^{-1}$ shown in Table 2.

Table 2. Characteristics of PS, PSC, 5%K-PSC, 5%Fe-PSC, WC, and SC.

Analyses	Compositions	PS [c]	PSC	5%K-PSC	5%Fe-PSC	WC	SC
Proximate Analysis [a] (wt.%)	Fixed carbon	4.73	89.7	59.8	69.3	77.54	53.5
	Volatile matters	80.21	3.38	13.4	7.32	10.50	8.09
	Ash	2.64	4.61	16.9	17.8	5.36	31.1
	Equilibrium moisture [b]	12.42	2.00	9.94	5.58	6.58	7.30
Ultimate Analysis [a] (wt.%)	C	38.8	89.8	67.5	75.3	83.8	56.7
	H	6.00	0.708	1.70	0.974	1.23	1.15
	O	35.3	1.82 [d]	3.02 [d]	-	2.57 [d]	1.81 [d]
	N	0.298	0.905	0.873	0.745	0.428	1.02
	S	0.038	0.075	0.017	0.047	0.009	0.345
	Cl	0.044	0.079	0.047	0.028	0.020	0.579
Ash components [a] (wt.%)	Al_2O_3	-	1.72	0.014	0.058	0.095	0.407
	BaO	-	0.004	0.0001	0.0001	0.019	0.008
	CaO	-	0.215	0.430	2.08	2.03	1.62
	Fe_2O_3	-	0.939	0.021	12.1	0.059	0.656
	K_2O	-	0.532	11.0	0.340	1.24	4.24
	MgO	-	0.054	0.057	0.087	0.342	1.10
	MnO_2	-	0.002	0.004	0.020	0.255	0.525
	Na_2O	-	0.060	0.033	0.016	0.014	0.685
	P_2O_5	-	0.028	0.029	0.045	0.215	0.731
	SO_3	-	0.17	0.031	0.071	0.008	0.803
	SiO_2	-	3.22	1.74	2.68	0.656	18.1
	SrO	-	0.008	0.001	0.002	0.006	0.005
	TiO_2	-	0.077	0.001	0.00	0.004	0.028
BET total surface area (m^2/g)		-	469.6	6.93	220.7	-	-

[a] In wet basis. [b] Equilibrium moisture content of sample in air. [c] Data of the report [35]. [d] Balance of C, H, N, S, Cl, equilibrium moisture, and ash.

It is essential to predict the remaining mass from the pyrolysis of PS for catalyst production. Therefore, thermal gravimetric analysis (TGA) and derivative thermal gravimetric analysis (DTG) of PS, in an N_2 environment, were carried out to analyze weight loss with increasing temperature.

Since metal impregnation might influence the pyrolysis rate of biomass, it is also worth understanding the effect of K and Fe on the pyrolysis of PS. Generally, hemicellulose has a sharp pyrolysis rate of around 277–312 °C [32]. As soon as arriving at 355 °C, the intense decomposition of cellulose can be observed. However, decomposition of lignin would be difficult to be identified because of overlapping temperatures with cellulose. Figure 1 presents the temperature variation of the residual mass fraction (M_R) of PS, 5%K-PS, and 5%Fe-PS in TGA curves. It shows K and Fe reduce the required temperature for the decomposition of PS while Fe-impregnated PS starts to have apparent weight loss at a much lower temperature of around 206 °C than K-impregnated PS at 254 °C. The first and second peaks (P1 and P2) of DTG curves of 5%K-PS and 5%Fe-PS are all at lower temperatures (temperatures of P1 and P2 of 5%K-PS = 266 °C and 332 °C; temperatures of P1 and P2 of 5%Fe-PS = 277 °C and 341 °C) compared to those of PS (temperatures of P1 and P2 of PS = 284 °C and 361 °C), indicating that the pyrolysis temperature of iron- and potassium-loaded PS can be conducted at lower temperatures for converting the hemicellulose and cellulose of PS into liquids and gases. The TGA results indicate that PS, through the first step pyrolysis at 450 °C in the manufacturing process of this study, had a significant mass loss, and most volatiles was removed at this stage. Then, the increase in temperature to 850 °C caused only a little drop in the mass. Eventually, TGA curves tend to M_R = 0.3–0.4 at 850 °C for three types of PSs, which gives a rough concept for PSC production by pyrolysis of PS.

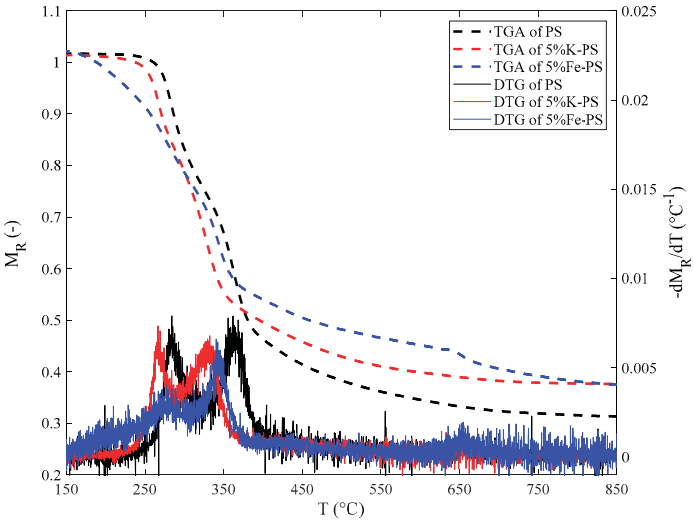

Figure 1. TGA and DTG diagrams from pyrolysis of PS, 5%K-PS, and 5%Fe-PS of residual mass fraction (M_R) and -dM_R/dT vs. temperature at heating rate = 30 °C min^{-1} in N_2.

2.2. Tar Reforming over PSC, WC, and SC

2.2.1. Conversions of Tar and Gasification Rates of PSC at Different Temperatures

In 90 min reforming of tar model compounds over PSC, the trends of toluene (X_T, -) and naphthalene conversion (X_N, -) at 850 °C and 900 °C are depicted in Figure 2. It is apparent that higher X_T and X_N of roughly 0.8 can be reached at 900 °C at the end of testing. However, conversions needed some time to approach the stable state from low conversions. This phenomenon was also observed when using WC and SC as catalysts (shown in Section 2.2.2). For example, X_N at 900 °C in Figure 2, increases from 0.24 to 0.80 during the initial 15 min, which suggests that the catalytic activity can be enhanced in this time range. After pyrolysis, high porosity is not accessible as the pores fill from disorganized carbon from the deposited tar, which reduces the surface area and pore distribution on the char surface [36]. However, with a high content of steam and high temperature during tar reforming, the gasification of char can take place and change the surface property of chars. According

to Fuentes-Cano et al. [37], when the rate of carbon (char and soot) gasification is higher than that of coking during tar reforming, the surface area and porosity of the char are increased, resulting in a better activity of the char. Consequently, with high steam content in SEG derived syngas, the steam activation process (gasification) for more surface area of chars might be directly carried out at elevated temperatures during tar reforming. In order to verify this phenomenon, a method was established here, for presenting the gasification of palm shell char during the reforming of tar model, compounds. The gasification rate (r_G, g min^{-1}) of the char was then calculated here during 90 min reforming.

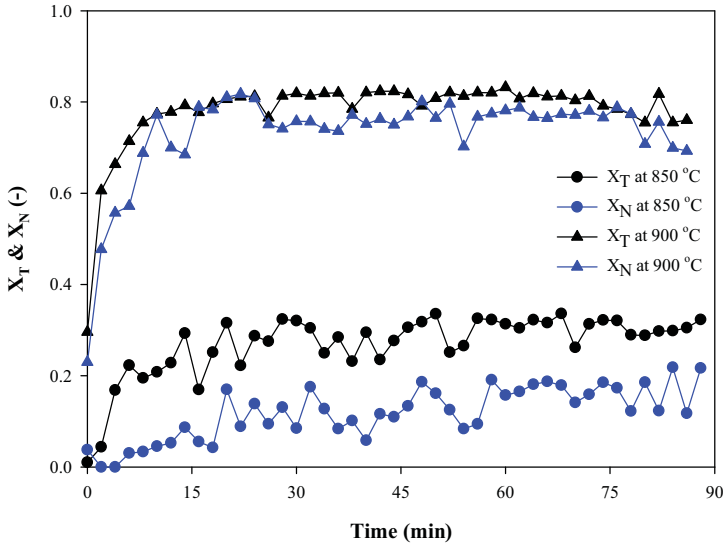

Figure 2. Conversions during 90 min tar reforming over PSC.

r_G of PSC is defined as the rate of reacted carbon from PSC, while r_G can also be assumed equal to the rate of production of CO and CO_2 stemming from PSC presented in Equation (1) on the basis of gasification reactions as shown in Equations (13) and (18) (Reactions are described in Section 3.5) [38], where m_{C^*}, m_{C_CO}, and m_{C_CO2} (g) are the mass of carbon in the char, in the produced CO, and in the produced CO_2 at time t, respectively:

$$r_G = \frac{-dm_{C^*}}{dt} = \frac{d(m_{C\_CO} + m_{C\_CO2})}{dt}. \quad (1)$$

m_{C_CO} and m_{C_CO2} at time t are computed by the integration of volume fractions of CO and CO_2 arising from PSC gasification (y_{G_CO} and y_{G_CO2}, ppmv) with t, which is substituted into the ideal gas Equation at NTP (assuming CO and CO_2 are ideal gases), according to Equations (2) and (3):

$$m_{C\_CO} = \frac{P\overline{M}V}{RT} = \frac{P\overline{M}}{RT} \times (\dot{Q}_{NTP} \times \int_0^t y_{G\_CO} dt) \quad (2)$$

$$m_{C\_CO2} = \frac{P\overline{M}V}{RT} = \frac{P\overline{M}}{RT} \times (\dot{Q}_{NTP} \times \int_0^t y_{G\_CO2} dt), \quad (3)$$

where P is pressure (assumed at 101.3 kPa), $\overline{M}$ is the molar mass of carbon (12 g mol^{-1}), R is the ideal gas constant (8.314 Pa·m^3·K^{-1}·mol^{-1}), temperature (T) is 298 K here, and Q_{NTP} = 0.3 m^3 h^{-1} = 5 L min^{-1} at NTP.

y_{G_CO} and y_{G_CO2} can not be directly obtained from the outlet volume concentration of CO and CO_2 (y_{CO} and y_{CO2}, ppmv) detected by FTIR because toluene and naphthalene also contributed to CO and CO_2 production due to Equations (11), (12), and (13). As a result, they are enumerated by

y_{CO} and y_{CO2} subtracting concentrations of CO and CO_2 from tar model components (y_{T_CO} and y_{T_CO2}, ppmv) at time t, presented as Equation (4). This method assumes that PSC only converted into CO and CO_2 (the main product of gasification of PSC from Equations (13) and (18)) during 90 min reforming, and carbon-containing species of products from the conversion of tar model components existed only as CO, CO_2, C_6H_6, and CH_4. Hence, C_7H_8, $C_{10}H_8$, CH_4, and C_6H_6 analyzed by FTIR were all assumed originating from the infused tar model compounds. y_{T_CO} and y_{T_CO2} can be then calculated by fractions of C from reacted toluene and naphthalene deducting those from CH_4 and C_6H_6 (Equation (5)). The gasification rate of PSC during reforming of tar model compounds at time t is subsequently calculated by Equations (1), (2), and (3). Finally, r_G of PSC at 850 and 900 °C against time is then illustrated in Figure 3:

$$y_{G\_CO} + y_{G\_CO2} = y_{CO} + y_{CO2} - (y_{T\_CO} + y_{T\_CO2}) \quad (4)$$

$$y_{T\_CO} + y_{T\_CO2} = 7 \times (y_{C7H8,\ in} - y_{C7H8}) + 10 \times (y_{C10H8,\ in} - y_{C10H8}) - 6 \times y_{C6H6} - y_{CH4}. \quad (5)$$

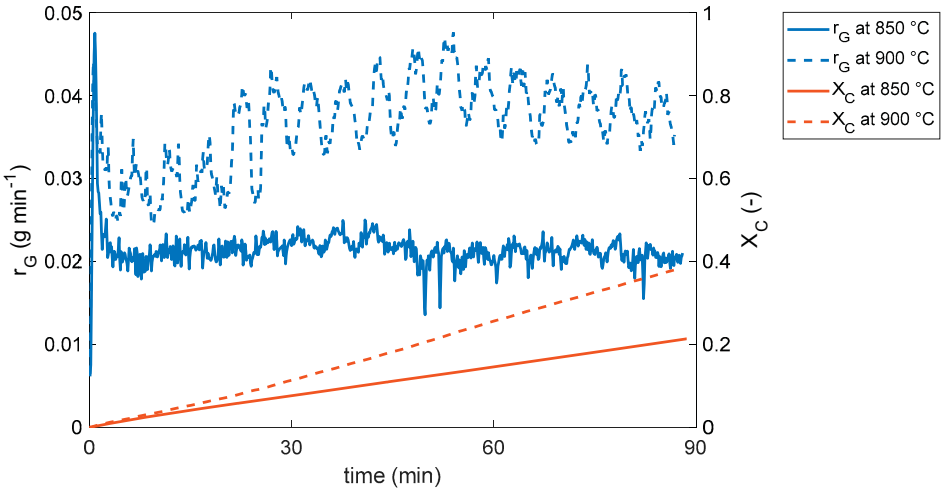

Figure 3. Comparison of calculated r_G and Xc during 90 min tar reforming over PSC.

The conversions of carbon mass (X_C, -) of PSC is also calculated also by this method. By Equations (2) and (3), the mass of carbon in PSC transforming to CO and CO_2 ($m_{C\_CO} + m_{C\_CO2}$) is obtained, so X_C at time t can be calculated by Equation (6) and illustrated in also Figure 3, where M_C is the initial carbon mass in the biochar (g). The diagram shows that carbon in PSC is gasified apparently in 90 min test with X_C = 0.20 and 0.40 at 850 and 900 °C, respectively. The error of this method is estimated by the difference between X_C calculated from this method and real X_C. The real X_C after 90 min reforming ($X_{C,real}$, -) is calculated by the mass loss (Δm, g) of PSC measured after the experiment divided by M_C (Equation (7)). X_C at 90 min (= 0.20 and 0.40) has an excellent compromise to $X_{C,real}$ (= 0.20 and 0.45) at 850 and 900 °C suggesting this method can be used for constructing the first concept of mass loss of carbon catalysts during steam reforming of tar. This method is also helpful for the establishment of the change of the residence time in the course of tar reforming:

$$X_C = \frac{m_{C\_CO} + m_{C\_CO2}}{M_C} \quad (6)$$

$$X_{C\_real} = \frac{\Delta m}{M_C}. \quad (7)$$

According to Figure 3, a higher gasification rate can be observed at 900 °C in 90 min reforming with a constant r_G = 0.039 higher than r_G = 0.022 g min^{-1} at 850 °C. Hence, more surface area and pore volume might be formed at 900 °C, while twice the loss of carbon mass occurs compared to 850 °C in 90 min. In order to figure out the relationship between gasification and surface area, the result of internal structure analyses is shown in Table 3. After 850 °C reforming, the surface area and micropore area all increase. With strong gasification at 900 °C reforming, the surface area and the micropore surface area become more than 850 °C reforming, which is consistent with the previous hypothesis that gasification activates the char surface and high gasification rate leads to more surface area and micropores. However, the ratio of micropore to mesopore area has a decrease from 5 to 2 after 900 °C tar reforming, indicating a possible micropore collapsing through long-time strong gasification. This phenomenon, which is related to the deactivation of char catalyst, was also found by Zeng et al. [39].

Table 3. The internal structure of PSC and PSCs after 90 min test.

Sample	BET Total Surface Area (m^2 g^{-1})	Micropore Area (m^2 g^{-1})	Mesopore Area (m^2 g^{-1})	The Ratio of Micropore to Mesopore Area	Micropore Volume (cm^3 g^{-1})	Pore Average Diameter (nm)
PSC	469.6	331.8	66.1	5.0	0.199	2.5
PSC-850	532.6	430.1	82.0	5.2	0.2	2.13
PSC-900	813.7	511.3	253.1	2.0	0.26	2.68

2.2.2. Comparison of Conversions of Tar and Gasification Rates between PSC, WC, and SC

X_N of naphthalene reforming over PSC, WC, and SC is depicted in Figure 4, which illustrates that naphthalene reforming over wood char presenting the best activity of naphthalene reforming at 850 °C in the whole 90 min. Here only X_N is depicted in Figure 4 to avoid the interference of showing toluene conversions. The toluene conversion trends, from each biochar, also indicated that WC had the best catalytic activity at 850 °C. The method described in Section 2.2.1 was also adopted to 90 min reforming of tar model compounds over WC and SC to compare the gasification rate and carbon conversion of different biochars. Due to the difference in bulk density of different biochars, r_G is then divided by individual M_C (r_G/M_C, min^{-1}) of them for the comparable rate of gasification. Figure 5 shows that SC has the most drastic gasification with X_C = 0.60 in 90 min reforming, which may be due to the highest ash content among these three biochars with abundant AAEM groups. Some research has confirmed that AAEM groups enhance the gasification rate of biochars [40,41]. This surmise also agrees with WC, which is more susceptible to steam for gasification with X_C = 0.35 in 90 min reforming than PSC because of a higher content of AAEM groups. With the least content of AAEM groups, r_G/M_C of PSC remains almost constant during the whole time reforming range. At 850 °C, X_C at 90 min of PSC (=0.21) is much lower than those of WC and SC, demonstrating a stabilized characteristic at high temperature and rich steam concentration environments.

In light of Figure 5, the primary gasification of WC and SC takes place in the beginning, and r_G/M_C becomes constant afterward. The surface area might soar tensely in this gasification time range, explaining the increase of activity of biochars at the starting time range, as can be seen in Figure 4. This study also proves that biochar catalysts can be parallelly gasified to raise the amount of H_2 and CO to increase their contents in the bio-syngas during the reforming of tar model compounds.

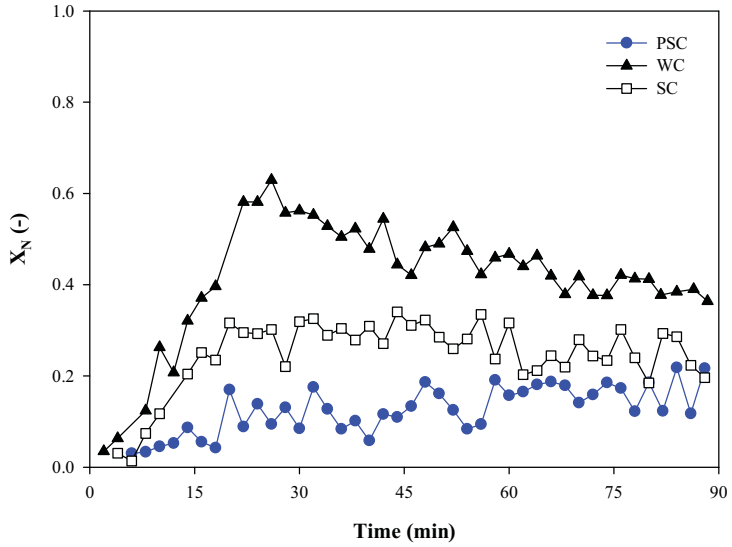

Figure 4. Naphthalene conversions during 90 min tar reforming over PSC, WC, and SC at 850 °C.

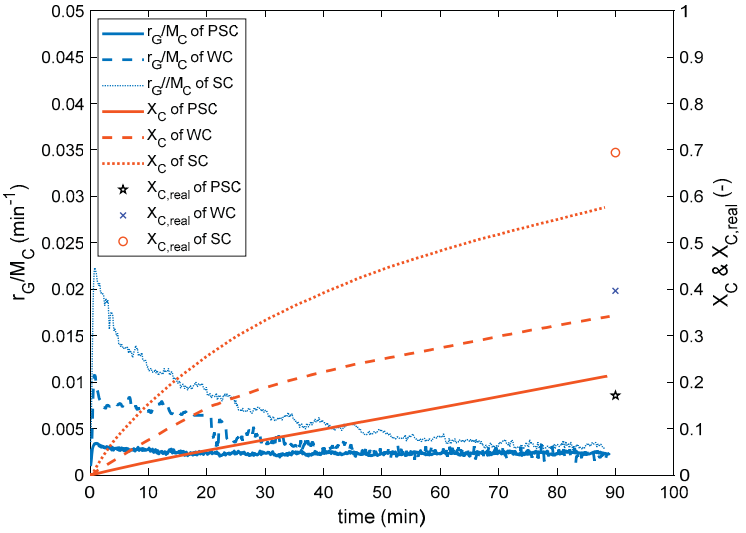

Figure 5. Comparison of calculated r_G/M_C and Xc during 90 min tar reforming over PSC, WC, and SC at 850 °C.

2.3. Tar Reforming over 5%K-PSC and 5%Fe-PSC

Loading metal on biochars is a time-consuming process with extra cost, so quick mass loss of biochar catalysts due to gasification should be avoided in a long-duration reaction. A drastic mass loss also means a decrease in residence time. Therefore, tar conversion can drop. According to reference [40], impregnated potassium and iron can significantly increase the gasification rate of the biochar. A continuous three-stage tar reforming at three temperatures was thus conducted to investigate the effect of T and r_G/M_C on tar conversion. At different stages, only nitrogen went through the reformer. As soon as the stage temperature was reached and maintained constant, simulated syngas with tar model compounds then flowed into the reformer for roughly 8 min reforming. r_G/M_C, X_C, and X_N in three stages for 5%K-PSC and 5%Fe-PSC are depicted in Figure 6a,b. A significant difference in the gasification rate between iron- and potassium-loaded chars was thus observed in this research.

At each stage, steam activation of Fe-loaded PSC quickly occurs with an extremely high gasification rate in the beginning, while the mass loss is much less than 5%K-PSC during long-term reforming on account of a rapid drop of r_G/M_C. Regarding the reforming of tar model compounds at 840 °C as an example, 5%Fe-PSC has a considerable decrease of r_G/M_C from 0.035 to 0.003 min^{-1}, and the value then maintains constant close to r_G/M_C of PSC depicted in Figure 5. According to Yu et al. [42], iron in its reduced forms on the char surface can be oxidated into magnetite during short reforming time with steam, which reduces the activity of char for reacting with steam and hence leads to a sink of r_G/M_C. In contrast, with potassium on the surface of PSC, a high gasification rate, which is twelve times greater than that of PSC at 850 °C, appears with nearly a constant value through the reforming.

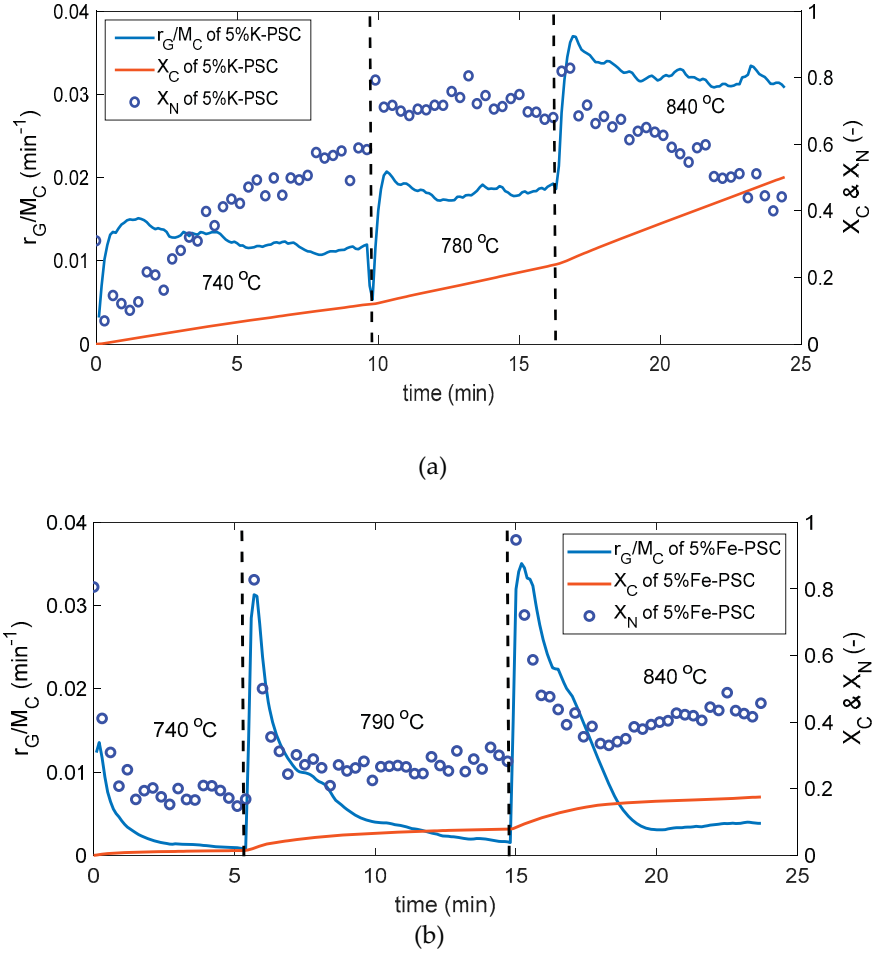

Figure 6. The tendency of calculated r_G/M_C and X_N during tar reforming over; (**a**) 5%K-PSC; and (**b**) 5%Fe-PSC at a continuous three-stage tar reforming.

X_N has a rapid increase to 0.54 at the first stage due to the strong steam activation of 5%K-PSC. At the second stage, conversion approaches a much higher value of 0.70. However, a considerable drop of X_N at 850 °C is found. This is not consistent with the general trend of K-loaded char in other research [43], which suggests that conversion increases along with rising temperatures. Through three stages, the carbon conversion of 5%K-PSC quickly reaches 0.5 in only 24 min. Therefore, the enormous mass loss of 5%K-PSC through three-stage reforming might be the main reason for the conversion drop with the need for fast replacement of the catalyst. According to the references [39,44], although new micropores can be formed on biochars during gasification, it is found that micropores can further

collapse to mesopore because of continuously intense gasification. Since the activity of tar reforming is highly related to the micropore of biochar [39], in the long term or drastic gasification situation, pore collapsing might also lead to deactivation. With the highest gasification rate at the final stage where naphthalene conversion starts to decrease, an intense gasification rate might also result in the collapse of micropores. In comparison to 5%K-PSC, the X_C value of 5%Fe-PSC is only 0.19 at the end of three-stage reforming without the decline of naphthalene conversion.

As a result, rapid mass loss of char catalysts because of gasification during tar reforming must be avoided to maintain the activity of char catalysts. In the site of reforming at a low temperature of 750 °C, the gasification rate of K-loaded PSC is still much faster than that of PSC at 850 °C. Consequently, the proper temperature (below 750 °C) should be considered to reduce the severe mass loss of 5%K-loaded PSC while applying them as a catalyst in tar reforming.

Although potassium has been commonly tested as a promoter for char catalyst, agglomeration in pyrolysis for the catalyst production and strong gasification during tar reforming have to be considered as problems. Iron is a relatively tender promoter on the biochar suitable for long-term operation with a quick activation only at the very beginning during the reforming of tar model compounds. However, this research only gives a general concept for applying metal-supported biochars in tar reforming. Further investigation of these metal-loaded PSCs should still be carried out.

2.4. Catalytic Activities of Different Biochar at Different Temperatures

By sorting average conversions at different temperatures, the catalytic activities of the reforming of tar model compounds over all biochars are compared here. As can be seen in Figure 7, conversions of both, toluene and naphthalene over WC, SC, and PSC are observed at temperatures above 800 °C, where WC has the best catalytic activity for tar reforming with the highest X_T and X_N of roughly 0.7 at 880 °C in τ_{NTP} = 0.17 s. On the other hand, X_T and X_N increase along with the temperature, suggesting that naphthalene and toluene can be better reformed at high temperatures.

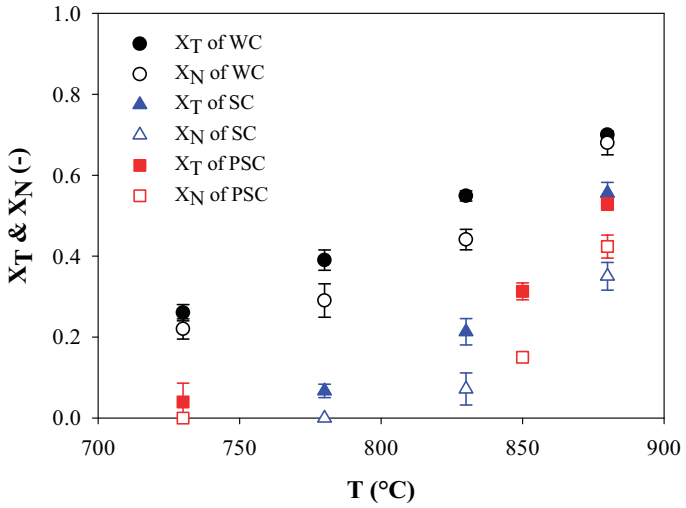

Figure 7. X_T and X_N from tar reforming over PSC, WC, and SC at different temperatures.

The average conversions of 5%K- and 5%Fe-PSC from the tests in Figure 6 are depicted in order to understand whether conversion can be enhanced in the presence of additional K and Fe. Figure 8 shows that 5%K-PSC has an excellent catalytic activity with high X_T and X_N = 0.7 at moderate temperature = 780 °C. However, both conversions decrease to 0.54, and 0.47, respectively, at 840 °C, caused by rapidly decreasing char amount owing to drastic char gasification, which has been explained in Section 2.3. With the iron on the surface, the catalytic activity was also promoted,

giving higher conversions of toluene and naphthalene than PSC. These findings correspond to the references [24–26,28] that potassium and iron enhance the ability of tar decomposition over biochars in a steam-hydrogen rich environment.

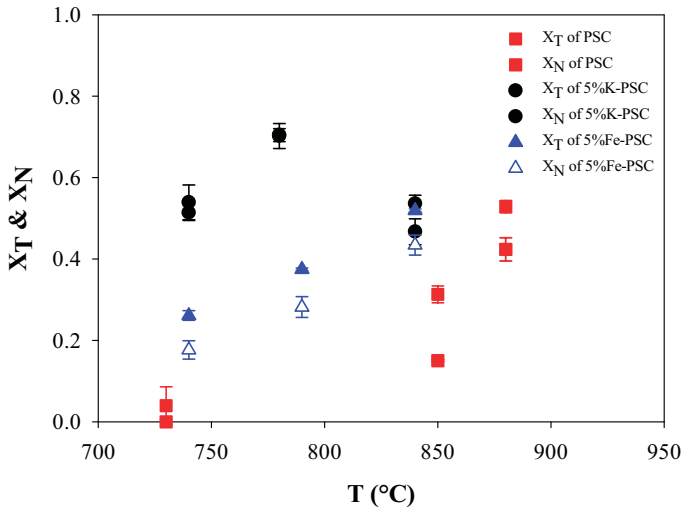

Figure 8. X_T and X_N from tar reforming over PSC, 5%K-PSC, and 5%Fe-PSC at different temperatures.

According to references [45,46], char-based catalysts have been reported that the content of oxygen-containing functional groups on the surface enhanced its activity for tar reforming. These groups were mainly in the acidic form and increased the acidity of the char-based catalyst [47]. Therefore, the acidity of the char-based catalyst is then regarded as an essential characteristic for improving the removal efficiency of tar. Since the tar-reforming activity of PSC was enhanced after dopped with K and Fe, the acidity on the surface of 5%K-PSC and 5%Fe-PSC might be higher compared to PSC. Hazmi et al. also indicated that after moderate impregnation of K and Fe on the rice husk char, a significant increase of the acidity was observed on its surface [48].

2.5. Benzene Selectivities of Different Biochars

Benzene has been known as an intermediate which is cracked mainly from aromatic tars through dealkylation. With better catalysts, benzene can be further decomposed to light gas components indicating that benzene selectivity (S_{C6H6}, -) can also be regarded as a proper index to evaluate whether tar tends to decompose to light gas components with certain catalysts or not. Figure 9 shows that S_{C6H6} of three different PSCs are smaller than 0.2 compared to relatively high values between 0.20 and 0.54 obtained from CaO in the temperature range from 700 to 900 °C. Moreover, the reforming of tar model compounds over WC and SC also exhibited similar selectivity of benzene with values below 0.2, suggesting that biochars are inclined to break down benzene further and present high selectivity to light components due to unique surface possessing AAEM groups. In addition, apparent drops of S_{C6H6} of PSC and CaO occur at 850 °C to 900 °C, meaning that, at a high-temperature range above 850 °C, not only high conversion rate can be approached over PSC and CaO, but benzene is also much easier to decompose.

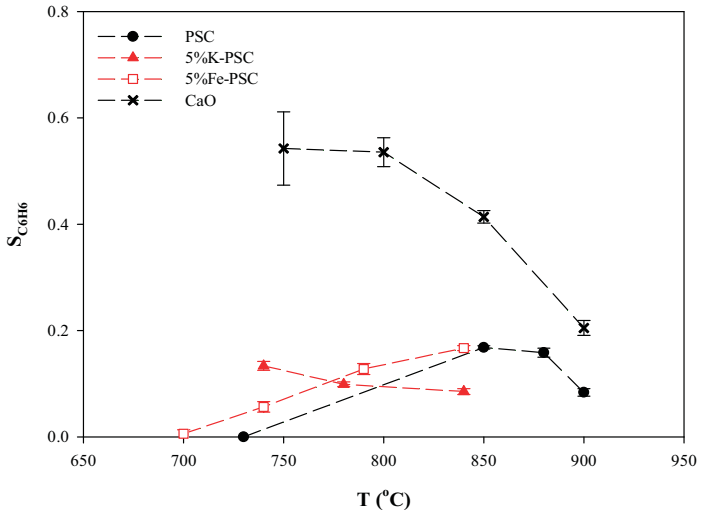

Figure 9. S_{C6H6} of PSC, 5%K-PSC, 5%Fe-PSC, and CaO at different temperatures.

2.6. Kinetics

Kinetic constants can be calculated using kinetic models, along with the relationship between tar concentration and reaction temperature. In a recent review paper [17], the kinetics of tar model compounds reforming over char catalysts were assessed from the previous publication. It indicated that the research on reaction kinetics of tar removal is very scarce at present. Generally, for the typical tar model compounds, such as phenol, toluene, and naphthalene, the first-order reaction model is appropriate in describing the reaction process. By using the same model, it is also beneficial for comparing the results with the literature [22,49]. As a result, the first-order kinetic model presented in Equation (8) was then applied in this study,

$$-\mathrm{r} = \mathrm{k} \cdot C_{tar} \tag{8}$$

where r is the rate of model tar conversion (kmol m^{-3} s^{-1}), k is the apparent kinetic constant (s^{-1}) and C_{tar} is the model tar concentration (kmol m^{-3}). The validity of the model can be justified by the R-square value (R^2, -) of the model fitting with data.

Plug-flow behavior and negligible diffusion in the catalyst pellets are assumed for determining the kinetic parameters. k is then integrated as below,

$$\mathrm{k} = \frac{\ln(1-X)}{\tau_{NTP}} \tag{9}$$

where X is the conversion of tar model compounds (-), and τ_{NTP} is the gas residence time (s) in the catalytic bed based on gas flow rate. X of materials at different temperatures is based on Figures 7 and 8. For 5%K-PSC, the conversions at 840 °C were excluded due to the intense gasification of char.

By substituting respective k and reforming temperature (T_r, k) into Arrhenius' law (Equation (9)), the activation energy (E_a, kJ/mol) (assumed to be constant in the studied temperature range) and the apparent pre-exponential factor (k_0) can be computed. Then both kinetic parameters can be compared with the results of other researchers to evaluate the activity of the applied catalysts for tar reforming,

$$\mathrm{k} = k_0 \cdot e^{\frac{-E_a}{R \cdot T_r}} \tag{10}$$

where R is the ideal gas constant (8.314 J K^{-1} mol^{-1}).

The apparent rate constant was varied with temperature by an Arrhenius-type relationship, as shown in Figure 10. Linear regressions were then established for toluene and naphthalene reforming over different materials based on the Arrhenius-type relationship. According to Table 4, high R^2, which are derived from these linear regressions, confirmed a good fit for the first-order kinetic model. With two parameters E_a and $k_{0,}$ as listed in Table 4, the performance of different active materials, tested in this study, can be easily compared by establishing the relationship between residence time and conversion (Figures 11–13). 850 °C and 900 °C were selected as the standard temperatures for the comparison of catalytic activity of natural materials because they have been regarded as effective temperatures for tar reforming.

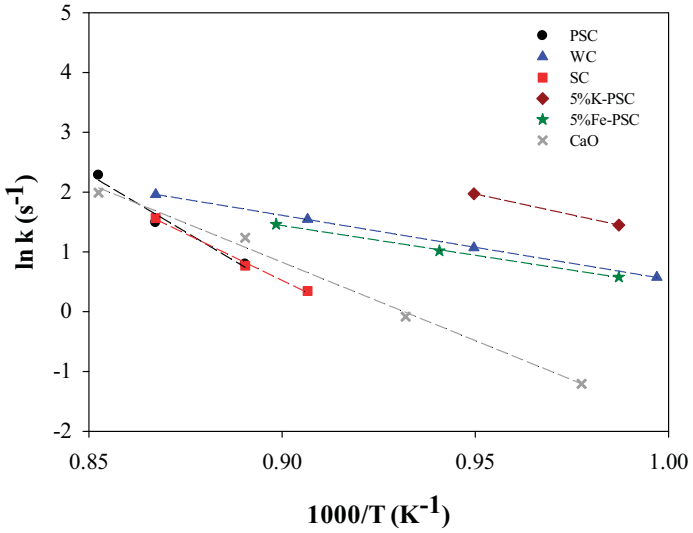

(a)

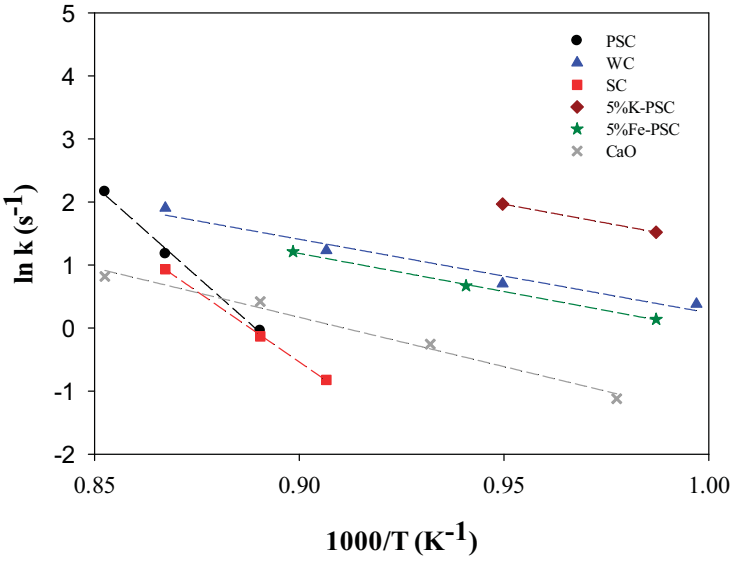

(b)

Figure 10. Temperature dependency of the apparent reaction rate constant according to Arrhenius' law. Calculation by; (**a**) toluene conversions; and (**b**) naphthalene conversions.

Table 4. Effect of temperature on fractional conversions and first-order rate constants for tar reforming over different catalysts. Calculation by toluene conversions and naphthalene conversions.

Tar Model Compound	Catalyst Type	T_r (°C)	X_T (-)	Ea (kJ/mol)	k_0 (s^{-1})	R^2 *
Toluene	PSC	850–900	0.31–0.81	318.9	1.44×10^{15}	0.973
	WC	730–880	0.26–0.70	89.0	7.66×10^{4}	0.999
	SC	830–880	0.21–0.56	259.7	2.73×10^{12}	0.995
	5%K-PSC	740–780	0.51–0.70	116.3	4.22×10^{6}	-
	5%Fe-PSC	740–850	0.26–0.52	82.7	3.26×10^{4}	0.999
	CaO	750–950	0.14–0.98	218.0	4.06×10^{10}	0.994
Naphthalene	PSC	850–900	0.15–0.77	478.9	1.76×10^{22}	0.996
	WC	730–880	0.22–0.68	97.2	1.51×10^{5}	0.963
	SC	830–880	0.07–0.35	372.2	1.83×10^{17}	0.999
	5%K-PSC	740–780	0.54–0.70	99.1	5.88×10^{5}	-
	5%Fe-PSC	740–850	0.18–0.43	100.6	1.74×10^{5}	0.999
	CaO	750–950	0.15–0.68	130.1	1.56×10^{6}	0.986

*R^2: The percentage of the response variable variation that is explained by a linear model. This value is derived from Figure 10.

According to Figures 11 and 12, the theoretical residence time (τ_T, s) for the complete conversion of naphthalene is longer than that of toluene, indicating that this tertiary tar with a stable structure is harder to break down. At 850 °C, WC has the best catalytic activity for naphthalene reforming among natural materials, and CaO demonstrates a better activity than PSC and SC.

As temperature increases to 900 °C, four low-cost materials are much more inclined to reform toluene and naphthalene. X_T and X_N rapidly arrive at 100% conversion with less residence time than at 850 °C. It is also found that biochars possess better catalytic activity for naphthalene reforming than CaO at 900 °C, according to Figure 12. Among four materials, PSC exhibits an excellent activity for naphthalene reforming at 900 °C, which reached complete conversion at τ_T = 1.2 s much shorter than 10.6 s at 850 °C. The temperature is then confirmed to be one of the most crucial parameters for tar reforming regarding the result. The bulk volume of PSC with the value above 3.33×10^{-4} m^3 per m^3 h^{-1} of SEG-derived syngas is theoretically required for tar reforming at 900 °C, based on the kinetic constant of naphthalene reforming over PSC.

The advantage of loading with potassium and iron on biochar is that Ea for the reforming of tar model compounds becomes much lower (shown in Table 4), meaning that tar reforming over K- and Fe-PSC can be accomplished at more moderate temperatures compared to PSC. The energy consumption thus decreases for a long-time reforming. In order to avoid considerable mass loss of PSC due to gasification at high temperatures, metal-loaded PSC is, therefore, more suitable for low-temperature tar reforming. 5%K-PSC and 5%Fe-PSC are hence compared to PSC at a low temperature of 750 °C with the relationship between residence time and conversion, as can be seen in Figure 13. A complete conversion of naphthalene for 5%K- and Fe-loaded PSC is reached with τ_T = 1.7 and 6.9 s, respectively, while PSC shows a weak activity with X_N = 0.06 at τ_T = 10 s. In comparison to required τ_T (10.6 s) for complete conversion over PSC at 850 °C, 5%K-PSC and 5%Fe-PSC show still better catalytic activities at 750 °C, proving potassium and iron are prominent promoters for not only reducing the reforming temperature, but also significantly enhancing the catalytic activity of PSC.

On account of the above findings, PSC is applicable as tar-reforming catalysts at the high-temperature range around 900 °C, which can theoretically achieve complete tar conversion with short residence time. Besides, the catalytic activity of PSC can be enhanced after impregnated with potassium and iron. For design purposes, the mass of active materials required in the reformer for SEG derived syngas can be deduced from Figures 11–13 to approach the target conversion at specific temperatures.

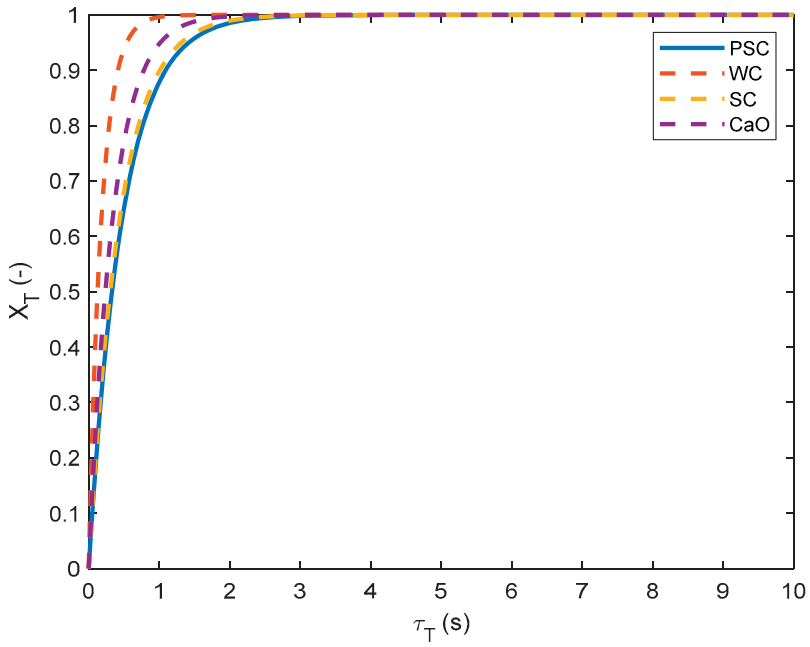

(a)

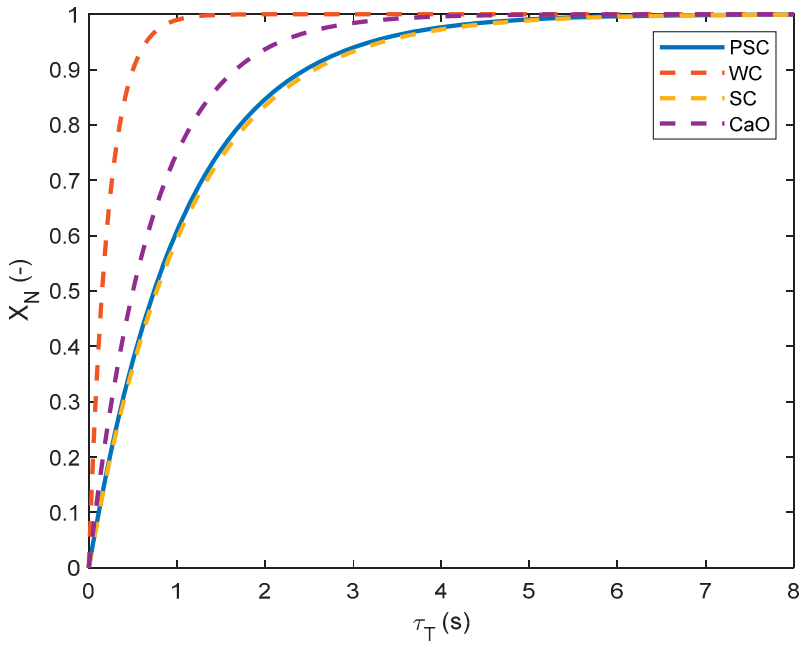

(b)

Figure 11. (**a**) Toluene; and (**b**) naphthalene conversion as a function of theoretical residence time at 850 °C for different active materials.

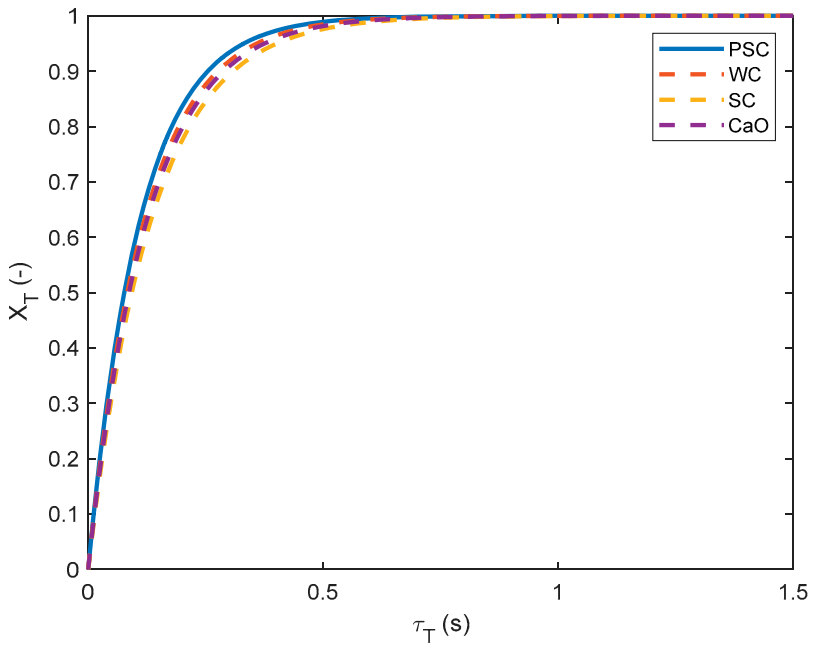

(a)

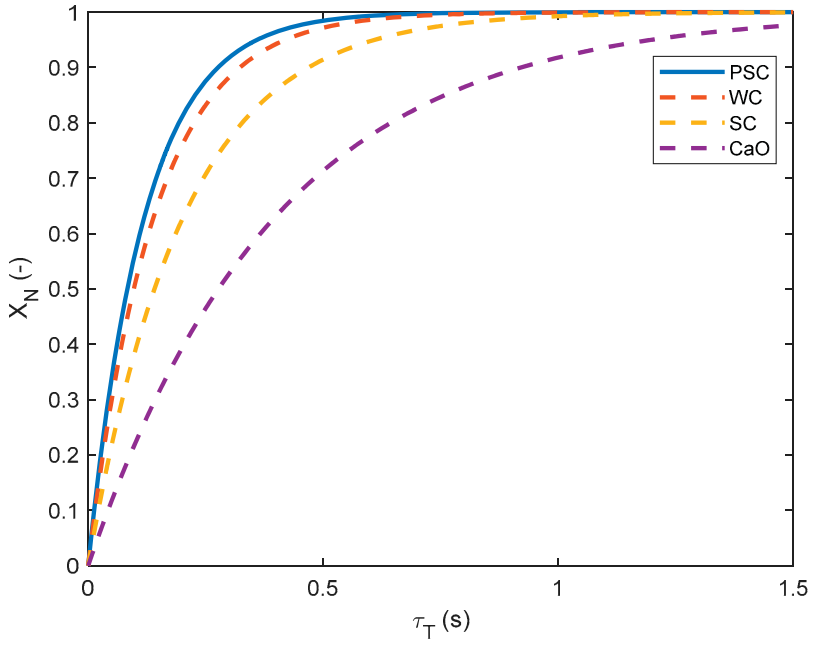

(b)

Figure 12. (**a**) Toluene; and (**b**) naphthalene conversion as a function of theoretical residence time at 900 °C for different active materials.

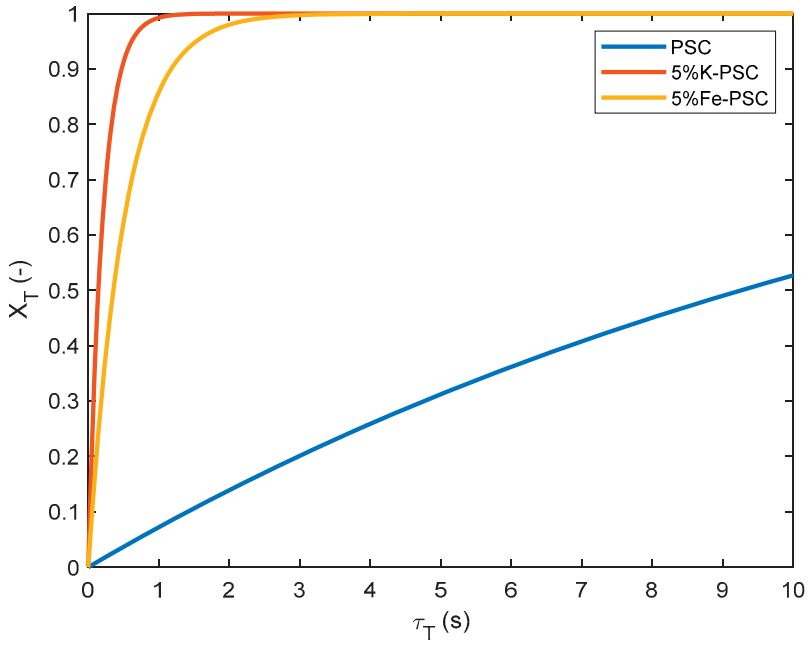

(a)

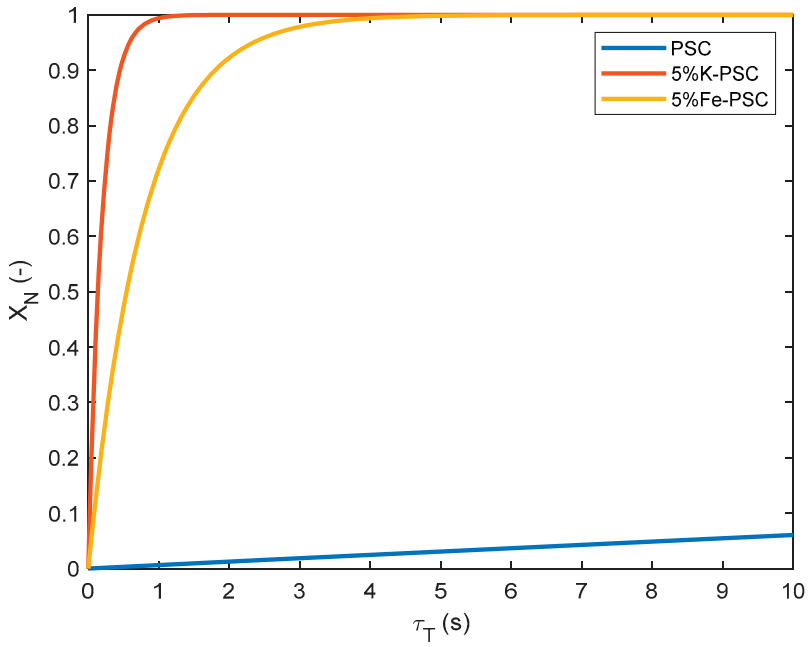

(b)

Figure 13. (**a**) Toluene; and (**b**) naphthalene conversion as a function of theoretical residence time at 750 °C for PSC, 5%K-PSC, and 5%Fe-PSC.

3. Material and Methods

3.1. Materials

PSs imported from Malaysia by Liang Xin Energy Co., Ltd. (New Taipei City, Taiwan) were carbonized at 450 °C in the self-generated atmosphere for 30 min with nitrogen to remove most of the volatiles. This range of temperature has also been applied as bio-oil production by pyrolysis of PSs. The temperature then rose to 850 °C, reaching the temperature range of tar reforming to produce final palm shell chars (PSCs). PSCs were then sieved to the size of 2–5 mm for tar reforming. Moreover, this research adopted a low-cost impregnation method with K_2CO_3 (99.5%, SHOWA CHEMICAL CO., LTD., Nihombashihoncho, Tokyo, Japan) and $Fe(NO_3)_3$-$9H_2O$ (98%, VETEC, Merck KGaA, Darmstadt, HE, Germany) to prepare K- and Fe-loaded PSC. Solutions of potassium and iron salt, prepared by dissolving K_2CO_3 and $Fe(NO_3)_3$-$9H_2O$ in an appropriate amount of DI water, were mixed with PSs for 12 h under continuous intense agitation using a magnetic stirrer, and then dried at 105 °C for 24 h. The amounts of K_2CO_3 and $Fe(NO_3)_3$-$9H_2O$ added in the solution were decided by making K and Fe occupy 5 wt.% of the metal impregnated PS assuming that all potassium or iron ions in the solution could evenly cover on the surface of PSs. The metal impregnated PSs were subsequently pyrolyzed in a similar method as adopted for PSCs. K- and Fe-loaded PSC were named 5%K-PSC, and 5%Fe-PSC, respectively. Tar reforming was also carried out with wood char (WC), straw char (SC), and CaO as catalysts with similar pellet diameter (2–5 mm) to PSC to observe the difference of these materials by using them as tar-reforming catalysts. The same pyrolysis method was adopted for straw pellets (GIEE, National Taiwan University, Taipei, Taiwan) to manufacture SCs, while WCs were produced by pyrolysis of wood pellets (SCHARR WÄRME, Stuttgart, BW, Germany) in a fluidized bed at a constant temperature of 850 °C for 1 hr. The bed material of the SEG process, CaO, has been proved that it can reduce tar production and convert heavy tar into light tar. CaO, which is obtained from the calcination of limestone (Lhoist Germany Rheinkalk GmbH, Wülfrath, NW, Germany) at 900 °C, was also tested here as the reference catalyst representing mineral rock catalyst. The calcined limestone, which is regarded as "CaO" in this study, consisted of over 90% CaO.

3.2. Experiment Method

A high-temperature laboratory-scale catalytic tar reduction system capable of operating at various conditions was developed in this study, as shown in Figure 14. Low-cost materials (PSC, 5%K-PSC, 5%Fe-PSC, WC, SC, and CaO) were tested as the catalysts filled in the reactor. All pipes were heated up above 180 °C to avoid condensation of tar. A relevant test gas with 15 vol % H_2O, 7.5 vol % H_2 (99.9%, Westfalen AG, Münster, NW, Germany), and tar model compounds was premixed in N_2 (99.999%, Westfalen AG, Münster, NW, Germany) simulating the essential components of the raw syngas from the SEG process [2–4]. The tar model components were toluene (99.5%, Merck KGaA, Darmstadt, HE, Germany) and naphthalene (Riedel-de Haën AG, Seelze, NI, Germany), amounting to total tar concentration of circa 10 g $m^{-3}{}_{NTP}$. The residence times of the gas (τ_{NTP}, s) over the biochars and CaO were 0.17 and 0.51 s, respectively, calculated by the bulk volume of the catalyst bed (V_{bed}, m^3) divided by total flow rate (Q_{NTP}, m^3 s^{-1}). Long-term tests of PSC, WC, and SC with 90 min reforming were conducted at different temperatures.

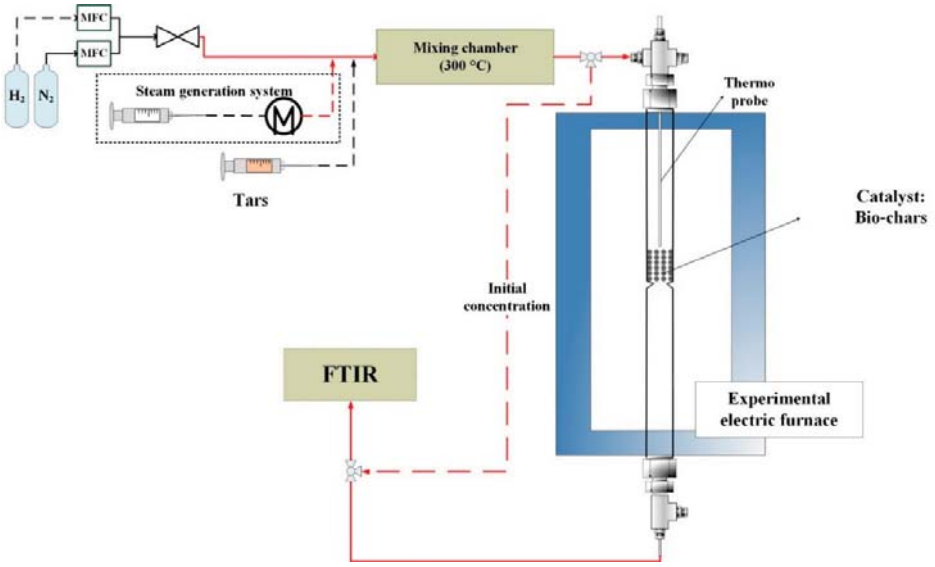

Figure 14. Diagram of tar reforming system.

3.3. Detection of Gas Components

By Fourier–transform infrared spectroscopy analyzer (FTIR–Gas analyzer, GASMET DX4000, Gasmet Technologies Oy, Mestarintie, Vantaa, Finland), continuous toluene and naphthalene concentrations were recorded, and concentrations of C_6H_6, CO, CO_2, and CH_4 were also detected with a transmitting pipe (5 m length) at 180 °C. The initial concentration was also recorded at the beginning of every test.

3.4. Analytical and Characterization Methods

Elemental, ultimate analyses and metal oxide compositions of biochars were performed following standard methods DIN (the German Institute for Standardization) EN ISO 18134–3, 18122, 18123, 16948, 16967, and 16994 [50]. Thermal gravimetric analysis (TGA) and derivative thermal gravimetric analysis (DTG) were tested in the same condition described by Chen et al. [32]. The porous structure of the char sample, including BET surface area, pore volume, and average pore diameter, was measured by an automatic volumetric analyzer (Micromeritics ASAP 2420, Micromeritics Instrument Corp., Norcross, GA, U.S.A.) using liquid N_2 as the adsorption agent. The catalyst sample was degassed at 200 °C to remove adsorbed contaminants and water vapor on the surface of the catalyst. The information of micropore and mesopore was calculated by the approaches of t-plot and Barrett-Joyner-Halenda (BJH) [51,52].

3.5. Toluene and Naphthalene Reforming

Many parallel and consecutive reactions can occur during toluene and naphthalene reforming in the environment with high steam concentration [53–55]. According to the global steam reforming reaction, toluene and naphthalene can react with steam to generate H_2 and CO:

$$C_7H_8+7H_2O\rightarrow 7CO+11H_2 \quad (11)$$

$$C_{10}H_8+10H_2O\rightarrow 10CO+14H_2. \quad (12)$$

The Water-Gas-Shift reaction (WGS) takes place simultaneously:

$$CO+H_2O\leftrightarrow CO_2+H_2. \quad (13)$$

Some work in the literature suggested that Equations (11) and (12) may be divided into two different reactions in series: The solid carbonaceous deposition on the solid surface by tar polymerization or coke accumulation followed by the steam gasification/reforming of the carbonaceous solid [37]. It is worth mentioning that carbon deposition reactions highly depend on the temperature and the concentration of the oxidizing component (steam). When the reaction temperature is too low, or not enough steam is present, coke can quickly accumulate on the solid surface [56].

In the presence of steam and hydrogen, also other reactions should be considered during tar reforming. Toluene and naphthalene can react with steam to produce C_6H_6, CO, and H_2 from the reaction of steam dealkylation (Equations (14) and (15)) or with hydrogen to form C_6H_6 and CH_4 owing to the hydrodealkylation reaction (Equations (16) and (17)) [57]:

$$C_7H_8+H_2O \rightarrow C_6H_6+CO+2H_2 \quad (14)$$

$$C_{10}H_8+4H_2O \rightarrow C_6H_6+4CO+5H_2 \quad (15)$$

$$C_7H_8+H_2 \rightarrow C_6H_6+CH_4 \quad (16)$$

$$C_{10}H_8+7H_2 \rightarrow C_6H_6+4CH_4. \quad (17)$$

Biochar can also go through steam reforming (gasification) during steam reforming of tar:

$$C^*(\text{carbon in biochar}) + H_2O \rightarrow CO + H_2. \quad (18)$$

3.6. Calculation Formulas

The concentrations obtained from FTIR were able to quantify the present reagents and products. AS biochar was simultaneously gasified during the reforming of tar model compounds, carbon balance was hard to prove with the parallel production of carbon-containing species from biochar. As a result, CaO was also used as a reference catalyst for confirming that the experimental process in this study gave a credible carbon balance during the reforming. Figure 15 depicts the carbon balance of the reforming of tar model compounds over CaO at 850 °C between reacted tar model mixture and majorly produced carbon-containing species (CO, CO_2, CH_4, and C_6H_6). Since there is a good fit between carbon conversed and carbon produced, a constant total volume flow rate before and after the reaction was then assumed in this study. Here, gasification of biochar catalysts was also assumed to have no influence on total volume flow.

Toluene conversion (X_T, -) and naphthalene conversion (X_N, -) were then computed using Equations (19), and (20), respectively,

$$X_T = \frac{y_{C7H8,in} - y_{C7H8,\ out}}{y_{C7H8,in}} \quad (19)$$

$$X_N = \frac{y_{C10H8,in} - y_{C10H8,out}}{y_{C10H8,in}} \quad (20)$$

where $y_{C7H8,in}$, ppmv = inlet toluene volume concentration, $y_{C7H8,out}$, ppmv = outlet toluene volume concentration, $y_{C10H8,in}$, ppmv = inlet naphthalene volume concentration, and $y_{C10H8,out}$, ppmv = outlet naphthalene volume concentration.

Benzene selectivity (S_{C6H6}, -) was defined by Equation (21), assuming that benzene all produced from tar model compounds,

$$S_{C6H6} = \frac{6 \cdot y_{C6H6}}{7 \cdot (y_{C7H8,in} - y_{C7H8,out}) + 10 \cdot (y_{C10H8,in} - y_{C10H8,out})} \quad (21)$$

where y_i (ppmv) represents the outlet volume concentration of the product i (y_{C6H6}: the outlet volume concentration of benzene.)

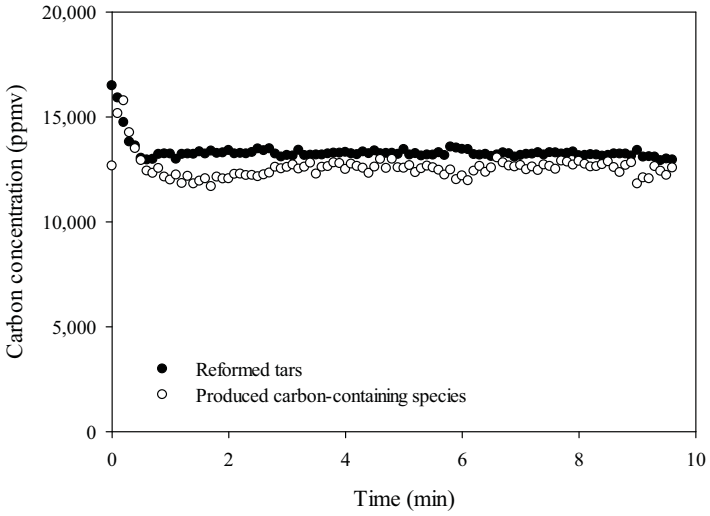

Figure 15. Carbon balance of toluene and naphthalene reforming over CaO at 850 °C. (Reformed toluene and naphthalene: $7{\cdot}(y_{C7H8,in} - y_{C7H8,out}) + 10{\cdot}\left(y_{C10H8,\ in} - y_{C10H8,out}\right)$; Produced carbon-containing species: $y_{CO} + y_{CO2} + y_{CH4} + 6{\cdot}y_{C6H6}$).

4. Conclusions

Pyrolysis of PS removes most volatiles of PS and produces PSC with a high surface area and good hydrophobicity. PSC performed significantly in tar reforming at 900 °C, with a theoretically required bulk volume of 3.33×10^{-4} m^3, for the complete tar conversion per m^3 h^{-1} of SEG-derived syngas, which proves that it has a good potential applied in a tar reformer after SEG process. As for the reforming selectivity, toluene and naphthalene over PSC are mainly decomposed to light components with low benzene selectivity. Parallel gasification of biochars during the reforming of tar model compounds is highly related to the activation and deactivation of biochars. Initial gasification can increase the surface area and micropores. However, mass loss and pore collapsing after continuous gasification lead to the deactivation of biochars. With low reactivity to steam, palm shell char is a suitable choice for applying the catalyst, compared to wood char and straw char, as it avoids drastic mass loss in the long-term toluene and naphthalene reforming. Moreover, it is worth developing K- and Fe- loaded palm shell char for reducing the reforming temperature. These metal promoters significantly enhance the catalytic activity of palm shell char, while intense gasification carried out on potassium loaded palm shell char results in a rapid mass loss. Iron is a relatively tender promoter on the palm shell char suitable for long-term operation with a quick activation only at the very beginning during the reforming of toluene and naphthalene mixture.

Author Contributions: Y.-H.C. and M.S. conceived and designed the experiments; Y.-H.C. performed the experiments; Y.-H.C. analyzed the data; C.-C.C. and G.S. contributed reagents/materials/analysis tools; M.S. and C.-Y.C. discussed the results and provided the suggestion. Y.-H.C. wrote the paper. All authors have read and agreed to the published version of the manuscript.

Funding: This research was funded by the project NuCA (0324342A) of the German Ministry of Economic Affairs and Energy (BMWi).

Acknowledgments: The authors gratefully acknowledge the support from DAAD (German Academic Exchange Service) and the project NuCA (0324342A) funded by the German Ministry of Economic Affairs and Energy (BMWi).

Conflicts of Interest: The authors declare no conflict of interest.

References

1. Hawthorne, C.; Poboss, N.; Dieter, H.; Gredinger, A.; Zieba, M.; Scheffknecht, G. Operation and results of a 200-kWth dual fluidized bed pilot plant gasifier with adsorption-enhanced reforming. *Biomass Conv. Bioref.* **2012**, *2*, 217–227. [CrossRef]
2. Schweitzer, D.; Beirow, M.; Gredinger, A.; Armbrust, N.; Waizmann, G.; Dieter, H.; Scheffknecht, G. Pilot-Scale Demonstration of Oxy-SER steam Gasification: Production of Syngas with Pre-Combustion CO^2 Capture. *Energy Procedia* **2016**, *86*, 56–68. [CrossRef]
3. Poboss, N. Experimental investigation of the absorption enhanced reforming of biomass in a 20 kWth dual fluidized bed system. *Int. J. Thermodyn.* **2012**, *15*. [CrossRef]
4. Milne, T.A.; Evans, R.J.; Abatzoglou, N. *Biomass Gasifier "Tars": Their Nature, Formation, and Conversion*; National Renewable Energy Laboratory: Golden, CO, USA, 1998.
5. Bridgwater, A.V. The technical and economic feasibility of biomass gasification for power generation. *Fuel* **1995**, *74*, 631–653. [CrossRef]
6. Jess, A. Catalytic upgrading of tarry fuel gases: A kinetic study with model components. *Chem. Eng. Process* **1996**, *35*, 487–494. [CrossRef]
7. Depner, H. Untersuchungen Zur Katalytischen Umsetzung Flüchtiger Schwelprodukte in Rohgasen Der Verkokung Und Vergasung Fester Brennstoffe. Ph.D. Thesis, TH Karlsruhe, Karlsruhe, Germany, 1998.
8. Speidel, M.; Fischer, H. Steam reforming of tars at low temperature and elevated pressure for model tar component naphthalene. *Int. J. Hydrog. Energy* **2016**, *41*, 12920–12928. [CrossRef]
9. Armbrust, N.; Poboss, N.; Eder, T.; Zieba, M.; Scheffknecht, G. Comparison of Two Methods of Sampling and Analyzing Tars during AER Biomass Gasification. In Proceedings of the 19th European Biomass Conference and Exhibition, Berlin, Germany, 6–10 June 2011.
10. Diehl, A. Experimentelle Untersuchung der Reformierung von Teeren an Katalystisch Aktiven Substanzen. Ph.D. Thesis, Uni Stuttgart, Stuttgart, Germany, 2012.
11. Soukup, G.; Pfeifer, C.; Kreuzeder, A.; Hofbauer, H. In Situ CO 2 Capture in a Dual Fluidized Bed Biomass Steam Gasifier—Bed Material and Fuel Variation. *Chem. Eng. Technol.* **2009**, *32*, 348–354. [CrossRef]
12. Pfeifer, C.; Koppatz, S.; Hofbauer, H. Steam gasification of various feedstocks at a dual fluidised bed gasifier: Impacts of operation conditions and bed materials. *Biomass Conv. Bioref.* **2011**, *1*, 39–53. [CrossRef]
13. Steiert, S. *FuE-Plattform "Biomass-to-Gas"—Energetische Nutzung biogener Reststoffe mit AER-Technologie zur Poly-Generation von Strom, Wasserstoff, Erdgassubstitut und Wärme, Schlussbericht*; Zentrums für Sonnenenergie-und Wasserstoff-Forschung Baden-Württemberg (ZSW): Stuttgart, Germany, 2013.
14. Aznar, M.P.; Caballero, M.A.; Gil, J.; Martín, J.A.; Corella, J. Commercial Steam Reforming Catalysts To Improve Biomass Gasification with Steam−Oxygen Mixtures. 2. Catalytic Tar Removal. *Ind. Eng. Chem. Res.* **1998**, *37*, 2668–2680. [CrossRef]
15. Abu El-Rub, Z.; Bramer, E.A.; Brem, G. Review of Catalysts for Tar Elimination in Biomass Gasification Processes. *Ind. Eng. Chem. Res.* **2004**, *43*, 6911–6919. [CrossRef]
16. Kostyniuk, A.; Grilc, M.; Likozar, B. Catalytic Cracking of Biomass-Derived Hydrocarbon Tars or Model Compounds To Form Biobased Benzene, Toluene, and Xylene Isomer Mixtures. *Ind. Eng. Chem. Res.* **2019**, *58*, 7690–7705. [CrossRef]
17. Zeng, X.; Ueki, Y.; Yoshiie, R.; Naruse, I.; Wang, F.; Han, Z.; Xu, G. Recent progress in tar removal by char and the applications: A comprehensive analysis. *Carbon Resour. Convers.* **2020**, *3*, 1–18. [CrossRef]
18. Prasertsan, S.; Prasertsan, P. Biomass residues from palm oil mills in Thailand: An overview on quantity and potential usage. *Biomass Bioenergy* **1996**, *11*, 387–395. [CrossRef]
19. Ani, F.N.; Zailani, R. Characteristics of Pyrolysis Oil and Char from Oil Palm Shells. In *Developments in Thermochemical Biomass Conversion*, 1st ed.; Bridgwater, A.V., Boocock, D.G.B., Eds.; Springer Netherlands: Dordrecht, The Netherlands, 1997; pp. 425–432.
20. Kim, S.-J.; Jung, S.-H.; Kim, J.-S. Fast pyrolysis of palm kernel shells: Influence of operation parameters on the bio-oil yield and the yield of phenol and phenolic compounds. *Bioresour. Technol.* **2010**, *101*, 9294–9300. [CrossRef] [PubMed]
21. Wan Daud, W.M.A.; Ali, W.S.W.; Sulaiman, M.Z. Effect of activation temperature on pore development in activated carbon produced from palm shell. *J. Chem. Technol. Biotechnol.* **2003**, *78*, 1–5. [CrossRef]

22. Mani, S.; Kastner, J.R.; Juneja, A. Catalytic decomposition of toluene using a biomass derived catalyst. *Fuel Process. Technol.* **2013**, *114*, 118–125. [CrossRef]
23. Feng, D.; Zhao, Y.; Zhang, Y.; Zhang, Z.; Zhang, L.; Sun, S. In-situ steam reforming of biomass tar over sawdust biochar in mild catalytic temperature. *Biomass Bioenergy* **2017**, *107*, 261–270. [CrossRef]
24. Feng, D.; Zhao, Y.; Zhang, Y.; Sun, S.; Meng, S.; Guo, Y.; Huang, Y. Effects of K and Ca on reforming of model tar compounds with pyrolysis biochars under H_2O or CO_2. *Chem. Eng. J.* **2016**, *306*, 422–432. [CrossRef]
25. Feng, D.; Zhao, Y.; Zhang, Y.; Zhang, Z.; Che, H.; Sun, S. Experimental comparison of biochar species on in-situ biomass tar H2O reforming over biochar. *Int. J. Hydrog. Energy* **2017**, *42*, 24035–24046. [CrossRef]
26. Feng, D.; Zhao, Y.; Zhang, Y.; Zhang, Z.; Sun, S. Roles and fates of K and Ca species on biochar structure during in-situ tar H_2O reforming over nascent biochar. *Int. J. Hydrog. Energy* **2017**, *42*, 21686–21696. [CrossRef]
27. Klinghoffer, N.B.; Castaldi, M.J.; Nzihou, A. Catalyst Properties and Catalytic Performance of Char from Biomass Gasification. *Ind. Eng. Chem. Res.* **2012**, *51*, 13113–13122. [CrossRef]
28. Kastner, J.R.; Mani, S.; Juneja, A. Catalytic decomposition of tar using iron supported biochar. *Fuel Process. Technol.* **2015**, *130*, 31–37. [CrossRef]
29. Nordgreen, T.; Liliedahl, T.; Sjostrom, K. Metallic iron as a tar breakdown catalyst related to atmospheric, fluidised bed gasification of biomass. *Fuel* **2006**, *85*, 689–694. [CrossRef]
30. Chen, Y.-H.; Schmid, M.; Waizmann, G.; Hafner, S.; Scheffknecht, G. Tar Reforming over CAO and Straw Char Produced Inherently in Steam-oxygen Biomass Gasification Processes Using Toluene as Model Component. In Proceedings of the 27th European Biomass Conference and Exhibition, Lisbon, Portugal, 27–30 May 2019. [CrossRef]
31. Klinghoffer, N.B.; Castaldi, M.J.; Nzihou, A. Influence of char composition and inorganics on catalytic activity of char from biomass gasification. *Fuel* **2015**, *157*, 37–47. [CrossRef]
32. Chen, Y.-H.; Chang, C.-C.; Chang, C.-Y.; Yuan, M.-H.; Ji, D.-R.; Shie, J.-L.; Lee, C.-H.; Chen, Y.-H.; Chang, W.-R.; Yang, T.-Y.; et al. Production of a solid bio-fuel from waste bamboo chopsticks by torrefaction for cofiring with coal. *J. Anal. Appl. Pyrolysis* **2017**, *126*, 315–322. [CrossRef]
33. Kajita, M.; Kimura, T.; Norinaga, K.; Li, C.-Z.; Hayashi, J.-i. Catalytic and Noncatalytic Mechanisms in Steam Gasification of Char from the Pyrolysis of Biomass. *Energy Fuels* **2010**, *24*, 108–116. [CrossRef]
34. Guo, F.; Liu, Y.; Wang, Y.; Li, X.; Li, T.; Guo, C. Pyrolysis kinetics and behavior of potassium-impregnated pine wood in TGA and a fixed-bed reactor. *Energy Convers. Manag.* **2016**, *130*, 184–191. [CrossRef]
35. Industrial Development Bureau of Taiwan. *Regional Energy Resource Integration and Efficiency Enhancement Demonstration Counseling Project*; Industrial Development Bureau: Taipei, Taiwan, 2016.
36. Prakash Kumar, B.G.; Shivakamy, K.; Miranda, L.R.; Velan, M. Preparation of steam activated carbon from rubberwood sawdust (Hevea brasiliensis) and its adsorption kinetics. *J. Hazard. Mater.* **2006**, *136*, 922–929. [CrossRef]
37. Fuentes-Cano, D.; Gómez-Barea, A.; Nilsson, S.; Ollero, P. Decomposition kinetics of model tar compounds over chars with different internal structure to model hot tar removal in biomass gasification. *Chem. Eng. J.* **2013**, *228*, 1223–1233. [CrossRef]
38. Nilsson, S.; Gomez-Barea, A.; Fuentes Cano, D. Gasification reactivity of char from dried sewage sludge in a fluidized bed. *Fuel* **2012**, *92*, 346–353. [CrossRef]
39. Zeng, X.; Wang, F.; Han, Z.; Han, J.; Zhang, J.; Wu, R.; Xu, G. Assessment of char property on tar catalytic reforming in a fluidized bed reactor for adopting a two-stage gasification process. *Appl. Energy* **2019**, *248*, 115–125. [CrossRef]
40. Suzuki, T.; Nakajima, H.; Ikenaga, N.-o.; Oda, H.; Miyake, T. Effect of mineral matters in biomass on the gasification rate of their chars. *Biomass Conv. Bioref.* **2011**, *1*, 17–28. [CrossRef]
41. Yip, K.; Tian, F.; Hayashi, J.-I.; Wu, H. Effect of Alkali and Alkaline Earth Metallic Species on Biochar Reactivity and Syngas Compositions during Steam Gasification. *Energy Fuels* **2010**, *24*, 173–181. [CrossRef]
42. Yu, J.; Tian, F.; Chow, M.; Mckenzie, L.; Li, C. Effect of iron on the gasification of Victorian brown coal with steam:enhancement of hydrogen production. *Fuel* **2006**, *85*, 127–133. [CrossRef]
43. Guo, F.; Liu, Y.; Liu, Y.; Guo, C. Catalytic reforming of tar using corncob char and char-supported potassium catalysts. *J. Therm. Anal. Calorim.* **2017**, *130*, 1297–1306. [CrossRef]
44. Fu, P.; Hu, S.; Xiang, J.; Yi, W.; Bai, X.; Sun, L.; Su, S. Evolution of char structure during steam gasification of the chars produced from rapid pyrolysis of rice husk. *Bioresour. Technol.* **2012**, *114*, 691–697. [CrossRef]

45. Song, Y.; Wang, Y.; Hu, X.; Hu, S.; Xiang, J.; Zhang, L.; Zhang, S.; Min, Z.; Li, C.-Z. Effects of volatile–char interactions on in situ destruction of nascent tar during the pyrolysis and gasification of biomass. Part I. Roles of nascent char. *Fuel* **2014**, *122*, 60–66. [CrossRef]
46. Song, Y.; Wang, Y.; Hu, X.; Xiang, J.; Hu, S.; Mourant, D.; Li, T.; Wu, L.; Li, C.-Z. Effects of volatile–char interactions on in-situ destruction of nascent tar during the pyrolysis and gasification of biomass. Part II. Roles of steam. *Fuel* **2015**, *143*, 555–562. [CrossRef]
47. Ducousso, M.; Weiss-Hortala, E.; Nzihou, A.; Castaldi, M.J. Reactivity enhancement of gasification biochars for catalytic applications. *Fuel* **2015**, *159*, 491–499. [CrossRef]
48. Zhang, Y.; Feng, D.; Zhao, Y.; Dong, H.; Chang, G.; Quan, C.; Sun, S.; Qin, Y. Evolution of Char Structure During In-Situ Biomass Tar Reforming: Importance of the Coupling Effect Among the Physical-Chemical Structure of Char-Based Catalysts. *Catalysts* **2019**, *9*, 711. [CrossRef]
49. El-Rub, Z.A.; Bramer, E.A.; Brem, G. Experimental comparison of biomass chars with other catalysts for tar reduction. *Fuel* **2008**, *87*, 2243–2252. [CrossRef]
50. The German Institute for Standardization: DIN EN ISO 18134-3, 18122, 18123, 16948, 16967, and 16994. Available online: https://www.din.de/de (accessed on 4 November 2019).
51. Barrett, E.P.; Joyner, L.G.; Halenda, P.P. The Determination of Pore Volume and Area Distributions in Porous Substances. I. Computations from Nitrogen Isotherms. *J. Am. Chem. Soc.* **1951**, *73*, 373–380. [CrossRef]
52. Storck, S.; Bretinger, H.; Maier, W.F. Characterization of micro- and mesoporous solids by physisorption methods and pore-size analysis. *Appl. Catal. A* **1998**, *174*, 137–146. [CrossRef]
53. Taralas, G.; Kontominas, M.G. Kinetic modelling of VOC catalytic steam pyrolysis for tar abatement phenomena in gasification/pyrolysis technologies. *Fuel* **2004**, *83*, 1235–1245. [CrossRef]
54. Swierczynski, D.; Libs, S.; Courson, C.; Kiennemann, A. Steam reforming of tar from a biomass gasification process over Ni/olivine catalyst using toluene as a model compound. *Appl. Catal. B* **2007**, *74*, 211–222. [CrossRef]
55. Taralas, G.; Kontominas, M.G. Numerical modeling of tar species/VOC dissociation for clean and intelligent energy production. *Energy Fuels* **2005**, *19*, 87–93. [CrossRef]
56. Shekhawat, D.; Spivey, J.J.; Berry, D.A. *Fuel Cells: Technologies for Fuel Processing*, 1st ed.; Elsevier Science: Amsterdem, The Netherlands, 2011.
57. Taralas, G.; Kontominas, M.G.; Kakatsios, X. Modeling the thermal destruction of toluene (C7H8) as tar-related species for fuel gas cleanup. *Energy Fuels* **2003**, *17*, 329–337. [CrossRef]

Paper III

Chemical Engineering Journal 408 (2021) 127350

Contents lists available at ScienceDirect

Chemical Engineering Journal

journal homepage: www.elsevier.com/locate/cej

Reforming of tar model compounds over sustainable and low-cost biochar: Special focus on spontaneous gasification reactivity and tar reforming kinetics for reformer design

Yen–Hau Chen *, Ashak Mahmud Parvez, Max Schmid, Günter Scheffknecht

Institute of Combustion and Power Plant Technology (IFK), University of Stuttgart, Pfaffenwaldring 23, D-70569 Stuttgart, Germany

ARTICLE INFO

Keywords:
Wood char
Sustainable catalyst
Gasification reactivity
Tar reforming kinetics
Renewable syngas

ABSTRACT

In this study, the spontaneous gasification and catalytic activity of wood char were experimentally evaluated in simulated sorption enhanced gasification (SEG) environments with toluene and naphthalene as tar model compounds. Besides, CaO was used as a reference catalyst for the comparison purpose since CaO is a commonly used sorbent in the SEG process. A model of gasification reactivity during reforming of tar model compounds over wood char was developed in this work based on the reactivity at 20% carbon conversion adopting the Extended Random Pore Model, where the pre-exponential factor, activation energy, and structural parameter were calculated to be $1.65{\cdot}10^{10}$ min^{-1}, 265.8 kJ mol^{-1}, and 127, respectively. During the catalytic activity investigation, hydrogen was found to inhibit tar-reforming performance over CaO while the impact of hydrogen was insignificant over wood char. The results showed that spontaneous gasification during tar surrogates reforming led to mass loss, pore collapse, and inorganics agglomeration, which contributed to the catalytic deactivation of wood char. By considering gasification-caused deactivation, the carbon conversion was then used as a variable to modify the kinetic equations of the tar surrogates reforming. The activation energy and pre-exponential factor of naphthalene reforming (and toluene reforming) over wood char were calculated with the values of 422.5 kJ mol^{-1} and $2.92{\cdot}10^{22}$ m^3 kg^{-1} h^{-1} (284.8 kJ mol^{-1} and $1.90{\cdot}10^{15}$ m^3 kg^{-1} h^{-1}), respectively, whereas the values for CaO were 126.9 kJ mol^{-1} and $6.79{\cdot}10^{4}$ m^3 kg^{-1} h^{-1} (254.5 kJ mol^{-1} and $6.73{\cdot}10^{11}$ m^3 kg^{-1} h^{-1}), respectively. The kinetic models developed in this study were later used for designing a tar reformer integrated with the SEG process.

1. Introduction

Over the years, syngas production via sorption enhanced gasification (SEG) has been studied targeting on the feasibility of H_2 production from renewable and waste feedstock [1]. This process features already reduced tar production of around 2–10 g $m^{-3}_{dry,STP}$ [2–4]. However, the tar limitations in syngas for the typical downstream usage are less than 30, 1, and 0.1–1 mg m^{-3}_{NTP} for gas turbines, methanol synthesis, and Fischer–Tropsch synthesis, respectively [5,6]. Besides, heavy tar, such as naphthalene, can be firmly adsorbed on the surface of catalysts for syngas synthesis, inhibiting the catalyst performance [7,8]. Hence, further tar reduction is necessary, particularly where the syngas is used in various synthesis applications.

As raw syngas with a high steam concentration (around 60%) is produced at high temperature (around 700 °C) in the SEG process [2–4], thermal steam reforming of tar is suitable for direct tar reduction. Tar can be converted into H_2 and CO by steam reforming, promoting the quality of syngas. Although the gas composition from the SEG is dependent on different operation conditions, a typical steam to hydrogen volumetric ratio (V_{H2O}/V_{H2}) = 2 in the syngas is observed as listed in Table 1. In this research, gas components, such as CO, CO_2, methane, and other hydrocarbons, were not considered for the tar reforming reaction as the main components in the SEG derived syngas are steam and hydrogen with up to 90 vol%. The composition of tar from the SEG can be found in Armbrust's research indicating that phenol, toluene, and naphthalene are the major tar components in the raw syngas [9]. As phenol is able to be decomposed at high temperatures above 800 °C without any catalysts [10], this study investigated the tar reforming with only toluene and naphthalene, representing also secondary and tertiary tars, respectively [11]. The total concentration of tar model compounds was 10 g m^{-3}_{NTP} based on the typical tar

* Corresponding author.
E-mail address: yen-hau.chen@ifk.uni-stuttgart.de (Y. Chen).

https://doi.org/10.1016/j.cej.2020.127350
Received 20 July 2020; Received in revised form 20 September 2020; Accepted 10 October 2020
Available online 16 October 2020

Nomenclature

M^-	The molar mass of carbon (12 g mol^{-1})
τ_{NTP}	Space time (kg h m^{-3})
φ	The pore surface parameter
a, c, and p	The constants of $F(X_C)$ in Eq. (15) (–)
A	The constant orders of C_{H2} in Eqs. (16) and (17) (–)
C_i	Volume concentration of component i (i = H_2O and H_2) in inlet flow (%)
C_S	A constant value in Eq. (13) (–)
$E_{a,i}$	Activation energy (kJ/mol) (i = G, CaO, and WC representing for gasification, tar surrogates reforming over CaO, and tar surrogates reforming over WC)
$F(X_C)$	A function taking into account the variation of reactivity with conversion (–)
$k_{0,i}$	Apparent pre–exponential factor ($m^3\ kg^{-1}h^{-1}$) (i = G, CaO, and WC representing for gasification, tar surrogates reforming over CaO, and tar surrogates reforming over WC)
k_i	Apparent kinetic constant ($m^3\ kg^{-1}h^{-1}$) (i = G, CaO, and WC representing for gasification, tar surrogates reforming over CaO, and tar surrogates reforming over WC)
m_{C^*}	The mass of carbon in the char through gasification at time t (g)
M_C	The initial carbon mass in WC (g)
m_{C_CO} and m_{C_CO2}	The accumulated mass of carbon from CO and CO_2 produced from WC through gasification at time t (g)
n and m	The constant orders of C_{H2O} and C_{H2} in Eqs. (12), (13), and (14) (-)
P	Pressure (101.3 kPa)
Q_{NTP}	Constant total flow rate (0.2 $m^3\ h^{-1}$)
R	The ideal gas constant (8.314 J $K^{-1}\ mol^{-1}$)
r_G	Gasification rate of WC (g min^{-1})
r_{TMC}	The reforming rate of tar model compounds ($m^3\ kg_{cat}^{-1}h^{-1}$)
r_{XC}	The reactivity at the reference state at conversion equal to X_C (min^{-1})
S_{C6H6}	Selectivity of benzene (–)
T	Reaction temperature (°C)
t	Reaction time (min)
T_r	Reforming temperature in Arrhenius' law (K)
$X_{C,E}$	The experimental carbon mass conversion after 1-h reforming (–)
X_C	Carbon mass conversion (–)
X_N	Naphthalene conversion (–)
X_T	Toluene conversion (–)
X_{TMC}	Conversion of the tar model compounds (–)
Y	A coefficient in Eq. (13)
$y_{C10H8,in}$	Inlet naphthalene volume concentration (ppmv)
y_{C10H8}	Outlet naphthalene volume concentration (ppmv)
$y_{C7H8,in}$	Inlet toluene volume concentration (ppmv)
y_{C7H8}	Outlet toluene volume concentration (ppmv)
y_{G_CO} and y_{G_CO2}	Volume fractions of CO and CO_2 arising from gasification of WC (ppmv)
y_i	Outlet volume concentration of component i (ppmv)
y_{T_CO} and y_{T_CO2}	Volume fractions of CO and CO_2 from toluene reforming (ppmv)
y_{TMC}	Initial total concentration of tar model compounds in this study (10 g $m^{-3}{}_{NTP}$)
Δm	mass loss (g)

Abbreviation

AAEMs	Alkali and alkaline earth metals
BJH	Barrett-Joyner-Halenda
DIN	The German Institute for Standardization
EDX	Energy dispersive X-ray spectroscopy
ERPM	Extend Random Pore Model
FTIR	Fourier–transform infrared spectroscopy analyzer
RPM	Random Pore Model
SEG	Sorption enhanced gasification
SEM	Scanning electron microscope
SEM–EDX	Scanning electron microscope–energy dispersive X–ray spectroscopy
WC	Wood char

Table 1
Typical product gas composition (N2 free) from SEG (wet basis).

Component	Unit	[2,3][a]	[4]
H_2O	vol %	55	60
H_2	vol %	28.4	26
CO	vol %	3.6	2.4
CO_2	vol %	6.1	3
CH_4	vol %	4.7	5.6
Tar	g $m^{-3}{}_{NTP}$	0.1–1.4	1–5

[a] Average values from reference.

concentration in the SEG derived syngas. Naphthalene concentration of 250 ppmv was considered in this study based on a representative SEG derived tar fraction [12]. Hence, a mass ratio of toluene to naphthalene applied in this study is 90%/10%.

Thermal steam reforming of tar generally requires a suitable catalyst material. A promising option for catalysts is to use catalytically active material, biochar, which is also suitably used as a protector to eliminate most of the heavy tar before raw syngas passes through the commercial catalyst. The performance of tar reforming over biochar is highly connected with alkali and alkaline earth metals (AAEMs) groups on the biochar and the surface area [13–16]. So far, there have been studies indicating that biochar generated from pyrolysis or thermal steam activation can decompose organic compounds [17–23]. Biochar has also been proven a better ability to decompose the aromatic ring than mineral materials [23]. Therefore, an in-depth exploration of the application of wood char as a tar-reforming catalyst was conducted in this study. On the other hand, CaO was also tested as the reference catalyst representing mineral rock catalysts since it has been used as the sorbent in the SEG process for enhancing the gasification performance. As CaO and wood pellets are typically used as sorbent and fuel, respectively, in the SEG process, CaO and wood char are easily available for the tar reforming application.

In general, there are two reactions that occur in series during steam reforming of tar over biochar: the solid carbonaceous deposition on the solid surface by tar polymerization and coke accumulation followed by the steam gasification/reforming of the carbonaceous solid [24]. It is worth mentioning that carbon deposition reactions are highly dependent on the reaction temperature and types of oxidizing agent. Coke can quickly accumulate on the solid surface and deactivate the catalytic activity due to low reaction temperature or weak oxidizing agent during steam reforming [25]. When the rate of carbon (char and soot) gasification is higher than that of coking during tar reforming, the surface area and porosity of the char are increased, resulting in a better activity of the char [24]. Consequently, the steam activation process (gasification) for increasing surface area of chars is possible to be directly carried out at elevated temperatures during steam reforming of tar. Several studies observed the gasification phenomenon of biochar without coke accumulation when conducting reforming of tar model compounds at

the condition of over 800 °C and a steam volume fraction of 15% [23,24,26]. Moreover, spontaneous gasification of biochar catalysts also raises the amount of H_2 and CO, which increases their contents in the bio-syngas during tar reforming. Accordingly, environmentally benign gasification of soot and char for avoiding coke deposition is regarded as a desirable condition to operate the tar reforming process over biochar. Since biochar product has been already commercialized over the world [27], the design of a bi-functional biochar-loaded reformer/gasifier for tar reduction and extra syngas production is beneficial. Zeng et al. [28] reported a novel concept of a two-stage gasification process utilizing biomass and biochar for the respective first and second stage individually, where biochar is regarded as fuel/catalyst in the second stage. The biochar is gasified in the second stage surrounding with syngas (H_2O, H_2, CO, CO_2, tar, etc.) from the first stage gasification. The gasification reactivity of biochar is therefore essential in order to assess the optimal condition and the extent of syngas production in the second-stage gasification. Recently, a method for calculating the gasification rate during the reforming of tar model substances has been developed by Chen et al. [23]. The present study adopted the aforementioned method for wood char gasification in the SEG derived environment. A model of gasification reactivity in the presence of H_2O, H_2, and tar model substances is thus established, which is conducive to the further development of the two-stage gasification process.

Although biochar gasification reveals key advantages during tar reforming, after a long-term and intense gasification, the catalytic deactivation of biochar will still take place because of several reasons: (i) since the inorganics dispersion on the char is a critical factor that influences the catalytic activity of the char, the migration and agglomeration of carbon covered inorganics during tar reforming results in a negative performance of tar conversion [16,29]; (ii) although new pores can be formed on biochar during gasification, it is found that micropores can further collapse to mesopores [30,31]. Since the activity of tar reforming is highly related to the micropore of biochar [30], in the long term or drastic gasification condition, pore collapsing also leads to deactivation; (iii) the mass loss of char catalysts due to gasification leads to a conversion drop and the reduction of the gas residence time with the requirement of fast replacement of the catalyst [23]. Apart from the negative influence of long-term gasification, hydrogen, as one of the main gas components in the SEG derived syngas, has an inhibiting effect on the surface of catalysts and thus weaken the catalytic activity [32]. So far, kinetic models of tar reforming over biochar for expressing the decline of the conversion due to the catalytic deactivation are barely discussed. Thus, this study dedicated to developing modified kinetic equations for the reforming of tar model compounds, which consider the catalytic deactivation of wood char. Afterwards, the design of a wood char-loaded tar reformer is performed using the modified kinetic model established in this research.

2. Materials and methods

2.1. Materials

Wood char (WC) was prepared in a fluidized bed reactor with a diameter of 70 mm and a height of 155 mm. First, 300 g of wood pellets (SCHARR WÄRME, Germany) were pyrolyzed in the reactor with 1 kg of silica sand as bed material at 850 °C. The fluidizing rate was around 0.3 m s^{-1} with nitrogen as fluidizing gas. The particle size of bed material was 0.1–0.5 mm, and the theoretical minimum fluidization velocity with nitrogen at STP was around 0.04 m s^{-1}.

After pyrolysis for 1 h, WC was cooled down to room temperature with N_2 and then sieved out from the sand. The wood char pellets were then cut into a size of 4.4 ± 0.6 mm for testing. CaO was produced by calcinating limestone (Lhoist Germany Rheinkalk GmbH, Germany) in an oven at 900 °C for 1 h under the air. The calcined limestone possessed high content of CaO, therefore, regarded as "CaO" in this study. CaO was tested as a catalyst with a diameter of 3.2 ± 0.8 mm.

2.2. Methods

Wood char and CaO materials were tested as catalysts in a fixed-bed steel reactor at temperatures ranging from 700 to 900 °C. The detail of the experimental rig can be found elsewhere [23]. A relevant test gas with steam, hydrogen (Volume concentration ratio of steam to hydrogen, $C_{H2O}/C_{H2} = 2$), and tar model compounds were premixed in N_2 simulating the essential components of the raw syngas from the SEG process [2–4]. The weights of materials used here were 3.1 g and 27 g for WC and CaO, respectively, and the total flow rate (Q_{NTP} equal to 0.2 m^3 h^{-1} at NTP) was fixed at every condition. The flow rate of carrier gas N_2 was altered to maintain the same total flow rate according to different volume concentrations of steam and hydrogen. The model tar components were toluene and naphthalene with a respective mass fraction ratio of 90% : 10%, and an initial total concentration (y_{TMC}) of 10 g m^{-3}_{NTP} was used according to tar concentration and composition in the SEG derived syngas [9]. In order to investigate the influence of steam and hydrogen volume concentrations (C_{H2O} and C_{H2}) on the gasification rate of WC and the tar surrogates reforming conversions, C_{H2} was tested in the range from 7.5% to 20% with the same $C_{H2O}/C_{H2} = 2$ for maintaining a simulated SEG derived condition. Each test was conducted in 1 h.

2.3. Analytical and characterization methods

Toluene and naphthalene concentrations were continuously recorded by a Fourier–transform infrared spectroscopy analyzer (FTIR–Gas analyzer, GASMET DX4000). C_6H_6, CO, CO_2, and CH_4 were also continuously detected by FTIR. The initial concentration was first recorded at the beginning of each test. Elemental, ultimate analyses, and metal oxide compositions of CaO and WC were conducted by adopting the method introduced by Chen et al. [23]. The porous structure of the char sample, including BET surface area, pore volume, and average pore diameter, was measured by an automatic volumetric analyzer (Micromeritics ASAP 2420, Micromeritics Instrument Corp., Norcross, GA, U.S.A.) using liquid N_2 as the adsorption agent. The WC samples were first ground to powder form and then degassed at 200 °C to remove adsorbed contaminants and water vapor on the surface of the catalyst. The information related to micropore and mesopore was calculated by the approaches of t-plot and Barrett-Joyner-Halenda (BJH) [33,34]. In this study, a scanning electron microscope (SEM) (JEOL field emission microscope JSM–7200F) equipped with energy dispersive X-ray spectroscopy (EDX) (Quantax XFlash6/60, Bruker Nano GmbH) was used to image WC and map the elemental composition of the surface. The resolutions of SEM for specific WC surface were 100 μm and 10 μm with magnifications of 120X and 600X, respectively.

2.4. Toluene and naphthalene reforming

Many parallel and consecutive reactions occur during toluene and naphthalene reforming in high steam concentration [35–37]. According to the global steam reforming reaction, toluene and naphthalene can react with steam to generate H_2 and CO:

$$C_7H_8 + 7H_2O \rightarrow 7CO + 11H_2 \quad H°_{900\ °C} = 928\ kJ\ mol^{-1} \tag{R1}$$

$$C_{10}H_8 + 10H_2O \rightarrow 10CO + 14H_2 \quad H°_{900\ °C} = 1234\ kJ\ mol^{-1} \tag{R2}$$

The Water-Gas-Shift reaction (WGS) takes place simultaneously:

$$CO + H_2O \leftrightarrow CO_2 + H_2. \quad H°_{900\ °C} = -33\ kJ\ mol^{-1} \tag{R3}$$

In the presence of steam and hydrogen, also other reactions should also be considered during tar reforming. Toluene and naphthalene can react with steam to produce C_6H_6, CO, and H_2 from the reaction of steam dealkylation (R4 and R5) or with hydrogen to form C_6H_6 and CH_4 owing to the hydrodealkylation reaction (R6 and R7) [38]:

$$C_7H_8 + H_2O \rightarrow C_6H_6 + CO + 2H_2\ H°_{900\ °C} = 174\ kJ\ mol^{-1} \quad (R4)$$

$$C_{10}H_8 + 4H_2O \rightarrow C_6H_6 + 4CO + 5H_2\ H°_{900\ °C} = 479\ kJ\ mol^{-1} \quad (R5)$$

$$C_7H_8 + H_2 \rightarrow C_6H_6 + CH_4\ H°_{900\ °C} = -53\ kJ\ mol^{-1} \quad (R6)$$

$$C_{10}H_8 + 7H_2 \rightarrow C_6H_6 + 4CH_4.\ H°_{900\ °C} = -429\ kJ\ mol^{-1} \quad (R7)$$

Biochar can also go through steam reforming (gasification) during steam reforming of tar:

$$C*(\text{carbon in biochar}) + H_2O \rightarrow CO + H_2.\ H°_{900\ °C} = 136\ kJ\ mol^{-1} \quad (R8)$$

2.5. Performance indicators

The formulas used to calculate toluene and naphthalene conversion, benzene selectivity, gasification rate, and carbon conversion are listed below [22,39]. In this study, a constant total volume flow rate is assumed. All equations are calculated based on the constant total volume flow. This assumption is proved to be credible, according to section 3.1.1. Toluene conversion (X_T) and naphthalene conversion (X_N) are computed using Eq. (1) and Eq. (2), respectively.

$$X_T = \frac{y_{C7H8,in} - y_{C7H8}}{y_{C7H8,in}} \quad (1)$$

$$X_N = \frac{y_{C10H8,in} - y_{C10H8}}{y_{C10H8,in}} \quad (2)$$

where X_T = toluene conversion, $y_{C7H8,in}$ = inlet toluene volume concentration, y_{C7H8} = outlet toluene volume concentration, X_N = naphthalene conversion, $y_{C10H8,in}$ = inlet naphthalene volume concentration, and y_{C10H8} = outlet naphthalene volume concentration.

Benzene selectivity (S_{C6H6}) was defined by Eq. (3), assuming that benzene all produced from tar model compounds.

$$S_{C6H6} = \frac{6 \cdot y_{C6H6}}{7 \cdot (y_{C7H8,in} - y_{C7H8}) + 10 \cdot (y_{C10H8,in} - y_{C10H8})} \quad (3)$$

where y_i represents the outlet volume concentration of the product i (y_{C6H6}: the outlet volume concentration of benzene.).

Moreover, this study focused on the development of a kinetic model of gasification reactivity for WC during the tar surrogates reforming. Gasification rate (r_G) and carbon conversion (X_C) of WC were then calculated with the experimental data by the methods introduced by Chen et al. [23]. Gasification rate (r_G) of WC is defined as the rate of reacted carbon from WC, while r_G can also be assumed equal to the rate of production of CO and CO_2 stemming from WC presented in Eq. (4) based on gasification reactions R8 and R3 (explanation in detail later) [40], where m_{C*}, m_{C_CO}, and m_{C_CO2} are the mass of carbon in the char, in the produced CO, and in the produced CO_2 at time t, respectively.

$$r_G = \frac{-dm_{C*}}{dt} = \frac{d(m_{C\_CO} + m_{C\_CO2})}{dt}. \quad (4)$$

m_{C_CO} and m_{C_CO2} at time t are computed by the integration of volume concentrations of CO and CO_2 arising from WC gasification (y_{G_CO} and y_{G_CO2}) with t, which are substituted into the ideal gas equation at NTP (assuming CO and CO_2 are ideal gases) according to equations (5) and (6):

$$m_{C\_CO} = \frac{PM^- V}{RT} = \frac{PM^-}{RT} \times (Q_{NTP} \times \int_0^t y_{G\_CO} dt) \quad (5)$$

$$m_{C\_CO2} = \frac{PM^- V}{RT} = \frac{PM^-}{RT} \times (Q_{NTP} \times \int_0^t y_{G\_CO2} dt) \quad (6)$$

where P is pressure (assumed at 101.3 kPa), M^- is the molar mass of carbon (12 g mol^{-1}), R is the ideal gas constant (8.314 $Pa \cdot m^3 \cdot K^{-1} \cdot mol^{-1}$), temperature (T) is 298 K here, and $Q_{NTP} = 0.2\ m^3\ h^{-1}$ at NTP.

Volume concentrations of CO and CO_2 from WC gasification (y_{G_CO} and y_{G_CO2}) cannot be directly obtained from the outlet volume concentrations of CO and CO_2 (y_{CO} and y_{CO2}) detected by FTIR because toluene and naphthalene also contributed to CO and CO_2 production due to R1, R2, and R3. As a result, y_{G_CO} and y_{G_CO2} are calculated by y_{CO} and y_{CO2} subtracting concentrations of CO and CO_2 from tar model components (y_{T_CO} and y_{T_CO2}) at time t as presented in Eq. (7). With high steam to carbon (in wood char and tar model compound) ratio in 1-h reforming (3.3–8.8 mol/mol), WC was mostly converted into CO and CO_2 via R8 and R3. According to other researches, steam gasification of biochar generally formed H_2, CO and CO_2 with neglectable amounts of CH_4 and other hydrocarbons at high temperatures over 800 °C [41,42]. In the presence of H_2, methane can still be produced from tar model substances (R6 and R7) and wood char (methanation [43]). However, compared to total CO and CO_2 production, relatively much lower CH_4 was detected at different experimental conditions in this study. According to the reforming at 900 °C, the total concentration of CO and CO_2 is much higher than CH_4 (<0.3%), with around 10–20 times difference through 1-h reforming. CH_4 production from wood char gasification was thus ignored for simplifying the calculation of the gasification rate. Based on the above-mentioned reasons, it was assumed that carbon in WC only converted into CO and CO_2 during 1-h reforming, and carbon-containing species in the products through the conversion of tar model components existed only as CO, CO_2, C_6H_6, and CH_4 referring to the main tar-reforming reactions as shown in Section 2.4. Hence, C_7H_8, $C_{10}H_8$, CH_4, and C_6H_6 analyzed by FTIR were assumed to originate from the introduced tar model substances without considering methane production from wood char. y_{T_CO} and y_{T_CO2} can be then calculated by fractions of C from reacted toluene and naphthalene deducting those from CH_4 and C_6H_6 (Eq. (8)). The gasification rate of WC during reforming of tar model compounds at time t is subsequently calculated by Eqs. (4), (5), and (6). The deviation exists expectedly between the actual and calculated gasification rates due to these assumptions. The error caused by the calculation is justified in Section 3.2.1.

$$y_{G\_CO} + y_{G\_CO2} = y_{CO} + y_{CO2} - (y_{T\_CO} + y_{T\_CO2}) \quad (7)$$

$$y_{T\_CO} + y_{T\_CO2} = 7 \times (y_{C7H8,in} - y_{C7H8}) + 10 \times (y_{C10H8,in} - y_{C10H8}) - 6 \times y_{C6H6} - y_{CH4} \quad (8)$$

The carbon conversion (X_C) of WC is also calculated here. By Eqs. (5) and (6), the carbon mass of CO and CO_2 from WC gasification ($m_{C\_CO} + m_{C\_CO2}$) is obtained, so X_C at time t can be calculated by Equation (9), where M_C is the initial carbon mass in WC calculated by the mass of applied wood char multiplying the carbon content of wood char detected via elementary analysis. The experimental carbon conversion after 1-h reforming ($X_{C,E}$) is calculated by the mass loss (Δm) of WC measured after the experiment divided by M_C (Eq. (10)).

$$X_C = \frac{m_{C\_CO} + m_{C\_CO2}}{M_C} \quad (9)$$

$$X_{C,E} = \frac{\Delta m}{M_C} \quad (10)$$

3. Results and discussion

3.1. Characteristics of wood char and CaO

According to Table 2, the volatile matters of wood pellets decrease significantly after pyrolysis while fixed carbon content increases as expected. Since the higher volatile matter makes biomass more susceptible to tar formation during steam reforming, a low mass fraction of only 10.5% in WC is suitable for following tar-reforming catalyst usage. Fixed carbon and carbon content increased from 17.0 to 77.5% and from 47.3

Table 2
Properties of wood char and CaO.

		Wood pellet	Wood char	CaO[d]
Proximate analysis[a] (mass fraction %)	Fixed carbon	17.0	77.54	–
	Volatile matters	75.3	10.50	–
	Ash	0.39	5.36	94.4
	Equilibrium moisture[b]	7.25	6.58	6.40
Ultimate analysis[a] (mass fraction %)	C	47.3	83.8	0.313
	H	6.65	1.23	0.679
	O[c]	38.18	2.57	–
	N	0.175	0.428	<0.4
	S	0.036	0.009	–
	Cl	0.018	0.020	–
Ash components[a] (mass fraction %)	Al_2O_3	0.010	0.095	0.384
	BaO	–	0.019	–
	CaO	0.096	2.03	91.6
	Fe_2O_3	0.010	0.059	0.224
	K_2O	0.065	1.24	0.059
	MgO	0.014	0.342	0.579
	MnO_2	0.010	0.255	0.007
	Na_2O	–	0.014	0.017
	P_2O_5	0.007	0.215	0.050
	SO_3	0.017	0.008	0.059
	SiO_2	0.245	0.656	1.95
	SrO	–	0.006	0.026
	TiO_2	–	0.004	0.019
BET surface area (m^2 g^{-1})		–	350.71	8.77

[a] In wet basis.
[b] Equilibrium moisture content of sample in air.
[c] Balance of C, H, N, S, Cl, H_2O, including ash.
[d] Sum of H_2O, oxides, organics = 100.5%

to 83.8%, respectively, indicating that wood converted into high carbon content char (wood char) through pyrolysis. Extra production of H_2 and CO by spontaneous gasification of the carbon during tar reforming can be thus expected. It was also found that WC had a much lower oxygen content of 2.57% compared to that of wood of 38.2%, suggesting that more hydrophobic solid was formed after pyrolysis [44]. AAEMs group is found to be the primary ash components in WC with K_2O of 1.24% and CaO of 2.03%, as can be seen in Table 2. This result suggests a potential dispersion of AAEMs groups on the WC's surface, which can enhance the catalytic activity of WC [13–15]. On the other hand, the calcined limestone tested in this study is regarded as CaO since it contained more than 90% CaO. A considerable difference between the surface area of WC and CaO is noticed in Table 2. WC possesses a much higher BET surface area (351 m^2 g^{-1}) compared to that of CaO with only 8.8 m^2 g^{-1}. Since the surface area is also highly related to the catalytic activity of active materials for tar reforming, CaO is expected to exhibit less tar-reforming ability.

3.2. Wood char gasification during the reforming of tar model compounds

3.2.1. Gasification rate and carbon conversion

The gasification rate (r_G) of wood char was enumerated by the method as described in Section 2.5. The error of this method is estimated by the difference between carbon conversion (X_C) calculated from this method and experimental carbon conversion ($X_{C,E}$). X_C at 60 min has an excellent compromise to $X_{C,E}$ at different conditions (as seen in Figs. 1 and 2), suggesting credible gasification rates of WC through the whole reforming test are demonstrated by this method. The assumptions adapted to the calculations detailed in Section 2.5 are thus convincible. The results show that WC is gasified normally in the simulated SEG environment at over 800 °C and more than 15% C_{H2O} with 10 g m^{-3}_{NTP} of tar model substances, which avoids the phenomenon of coke accumulation on the WC's surface and beneficial for extra H_2 and CO production. Although r_G drops through the time at each condition, the carbon in WC is continuously gasified during the 1-h test. It is found that

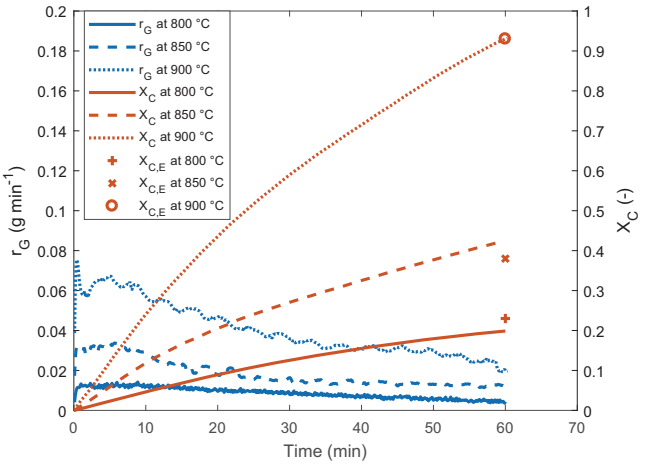

Fig. 1. Comparison of calculated r_G and X_C during 1-h reforming of toluene and naphthalene over wood char at different temperatures (C_{H2O} = 30%, C_{H2} = 15%, y_{TMC} = 10 g m^{-3}_{NTP}).

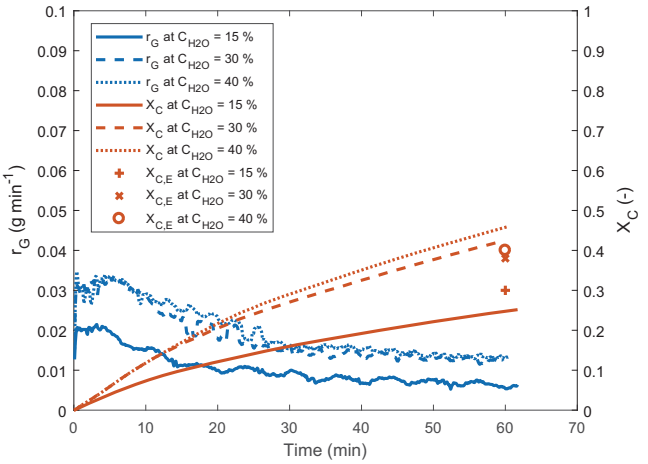

Fig. 2. Comparison of calculated r_G and X_C during 1-h reforming of toluene and naphthalene over wood char at different volume concentrations of H_2O and H_2 (T = 850 °C, C_{H2O}/C_{H2} = 2, y_{TMC} = 10 g m^{-3}_{NTP}).

temperature plays a big role in promoting the gasification rate of carbon during the reforming. According to Fig. 1, drastic gasification can be observed at 900 °C in 1-h reforming with an X_C = 0.93 much higher than X_C = 0.20 and 0.42 at 800 and 850 °C, respectively. The increase of steam concentration from C_{H2O} = 15% to 40% at 850 °C also promotes the gasification rate, and X_C at t = 60 min rises from 0.25 to 0.46 according to Fig. 2. However, there is no significant increase in the gasification rate during the 1-h test when C_{H2O} rises from 30% to 40%, indicating that gasification reactivity is moderated at a high steam concentration (>30%). On the other hand, according to Fushimi's research [45], H_2 leads to inhibition of steam gasification of biochar. The model established by Barrio et al. indicated that the partial pressures of H_2O and H_2 are highly correlated with the gasification rate of WC, and high partial pressure of H_2 results in strong inhibition of gasification [46]. Although C_{H2} also raised along with increasing C_{H2O} for maintaining C_{H2O}/C_{H2} = 2, the dominant reaction on WC was still steam gasification at each condition. Based on the above findings, sufficient steam concentration (60%) in SEG derived syngas is verified to be beneficial for carbon gasification. With a fixed steam concentration in SEG derived syngas, the temperature is therefore regarded as a crucial control variable when applying WC as a tar-reforming catalyst to promote the gasification rate and prevent coke deposition.

3.2.2. Kinetic model of gasification reactivity

Since the hydrogen and tar model compounds can reduce the gasification reactivity during steam gasification of biochar [16], the trends of gasification rate versus time and versus carbon conversion rate deduced from this study are different from those derived from steam gasification of woodchips char [47]. However, the trends are comparable to CO_2 gasification with a prolonged gasification time for complete conversion [47]. CO_2, which is a weak oxidizing agent [47,48], exhibits similar gasification effect to steam gasification in the presence of tar model species and hydrogen. Therefore, the modified gasification model during the reforming of tar model compounds in the SEG derived environment was founded on the presently existed CO_2 gasification models [40,47–50]. A kinetic model of gasification reactivity of WC in the environment with H_2O, H_2, and tar model components were established by modifying the original model of char gasification with CO_2, as can be seen in Eqs. (11) and (12), according to Nilsson et al. [40]. This method has been verified by fitting CO_2 gasification of sewage sludge char with a size of 1.2 mm at different conditions. The reactivity is assumed to be obtained without diffusion effects. Eqs. (11) and (12) thus allow for a simplified and practical expression to fit the measurements. In the equations, r_{XC} accounts for the dependence of reactivity on temperature and concentration of the gas reactants (C_{H2O} and C_{H2}) at the reference state with carbon conversion equal to X_C, whereas $F(X_C)$ is a function taking into account the variation of reactivity with the conversion [49]. Although the steam and hydrogen concentrations and reaction heat were continuously changed at different positions while passing the char bed due to steam reforming, zero-dimension model (mass and heat balances are made over the entire char bed) is applied here for the development of the gasification model according to the reference [49]. All calculations are formulated for the fixed concentration of toluene and naphthalene. On the other hand, the data at the condition of $C_{H2O} = 40\%$ is not used for modeling the gasification rate as high steam concentration (>30%) shows no significant influence on the gasification rate as seen in Fig. 2.

Since the current study focuses on WC gasification in a unique environment with $C_{H2O}/C_{H2} = 2$, Eq. (12) can be simplified by substituting the standard concentrations of H_2O and H_2 ($C_{H2O\_S} = 30\%$ and $C_{H2\_S} = 15\%$) for C_{H2O} and C_{H2}. A constant C_S and a coefficient Y ($=C_{H2O}/C_{H2O\_S} = C_{H2}/C_{H2\_S}$) are thus obtained as shown in Eq. (13) for idealizing Eq. (12) to Eq. (14). Because X_C only reaches around 0.2 in the 1-h test at 800 °C as seen in Fig. 1, this model adopts r_{20} as the reactivity of reference state, which is the actual gasification rate obtained at $X_C = 0.2$. The parameters of the orders (n + m), activation energy at $X_C = 0.2$ ($E_{a,G}$), and the modified pre-exponential factor at $X_C = 0.2$ ($K_{O,G}$), are computed and listed in Table 3. The modified model is then developed by fitting the r_G/r_{20} into the function $F(X_C)$. This function is purposely applied for adjusting Eq. (12) to match the actual gasification rate at different X_C. Random Pore Model (RPM) has been proven to give a good agreement with CO_2 gasification [47]. However, the Extended Random Pore Model (ERPM) was applied in the present study as this extended model can better fit the gasification rate at the low X_C value as presented in Eq. (15) [49,50]. The changes in structure and surface area of the pores during the reaction with H_2O, H_2 and tar model compounds are considered to be controlled by constant c and p, and the pore surface parameter (φ). A constant a is added to modify the difference between r_G/r_{20} and the developed ERPM. The maximal r_G/r_{20} at different conditions were found to appear below $X_C = 0.1$, while the values varied from 1 to 3 in different cases. As a result, the developed model cannot be so accurate in this X_C range, as depicted in Fig. 3 (a). However, after X_C = 0.1, the trends at different conditions can match well in ERPM. A similar phenomenon was also found by Nilsson et al. [40]. The r_G/r_{30} curves obtained at different temperatures show the same trends with increased conversion. However, the deviation is observed when $X_C < 0.15$ [40]. The unstable transient period in the beginning (when the composition of the gas surrounding the char pellets reaches the steady-state value) of each experimental condition might be the reason for the deviation. The derived activation energy in this research is higher than those from Nilsson's study (163.5 and 171.0 kJ mol^{-1} for CO_2 and H_2O gasification, respectively [40]). As can be seen that more energy might be required because of the presence of hydrogen and tar model compounds which can suppress the gasification of wood char. On the other hand, although ERPM behaves well in denoting a maximum at a lower (like this research) or higher carbon conversion, the extra constants of c and p (modified from RPM) in ERPM actually have no chemical meaning or irregularity. The constants thus have significant differences among distinct materials and conditions [50,51].

According to Fig. 3 (b), the model curves have high consistency with the experimental data, suggesting a predictable X_C with increasing time.

Table 3
Kinetic parameters of wood char gasification during tar reforming.

n + m	$E_{a,G}$	$K_{O,G}$	a	c	p	φ
–	kJ mol^{-1}	min^{-1}	–	–	–	–
1.17	265.8	1.65×10^{10}	0.124	−1.25	10	127

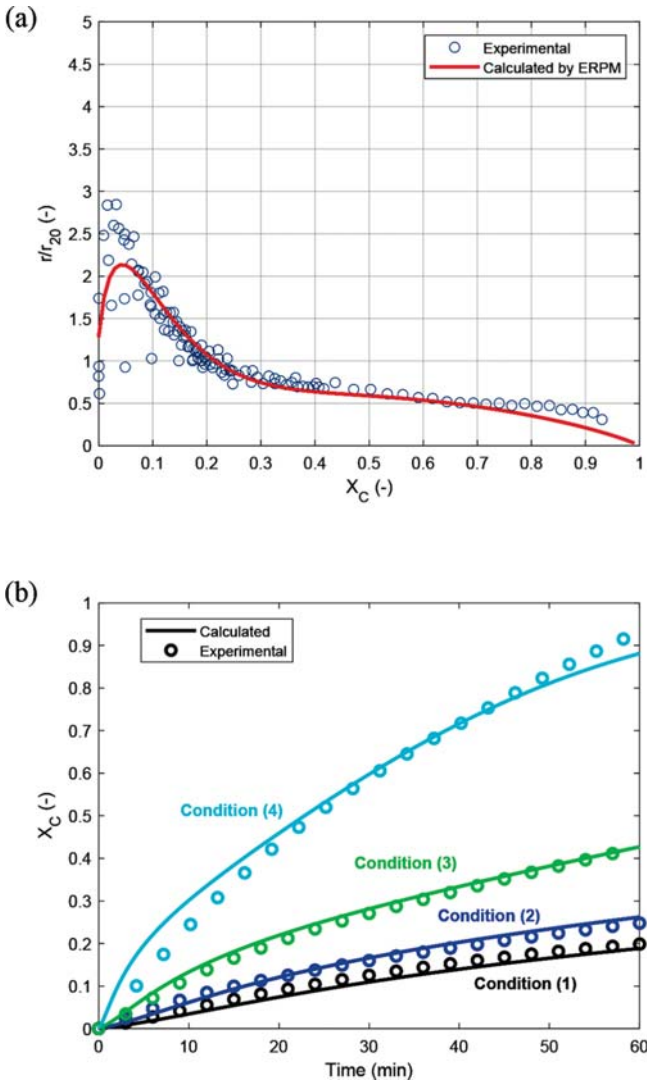

Fig. 3. (a) Normalized reactivity r/r_{20} as a function of carbon conversion at different conditions. (b) Comparison between experimental and theoretical curves of carbon conversion of wood char versus time in simulated SER derived syngas at different conditions (1) T = 800 °C; C_{H2O}/C_{H2} = 30%/15% (2) T = 850 °C; C_{H2O}/C_{H2} = 15%/7.5% (3) T = 850 °C; C_{H2O}/C_{H2} = 30%/15% (4) T = 900 °C; C_{H2O}/C_{H2} = 30%/15%; all with $y_{TMC} = 10$ g m^{-3}_{NTP}.

ERPM is thus confirmed to be a suitable model for gasification of biochar in the presence of steam, hydrogen, and tar. Additional production of H_2 and CO from biochar catalyst and the time interval for the dosing of fresh biochar catalyst to maintain a stable gas space time are then possible to predict by this method. This model also can be further improved for the application in the two-stage gasification process (described in Section 1) for simulating the gasification reactivity of biochar in the second-stage gasifier.

$$r_G = \frac{dX_C}{dt} = r_{XC}(T, C_{H2O}, C_{H2}) \cdot F(X_C) \tag{11}$$

$$r_{XC} = k_{O,G} \cdot e^{-\frac{E_{a,G}}{R \cdot T_r}} \cdot {C_{H2O}}^n \cdot {C_{H2}}^m \tag{12}$$

$${C_{H2O}}^n \cdot {C_{H2}}^m = (Y \cdot C_{H2O\_S})^n \cdot (Y \cdot C_{H2\_S})^m = Y^{n+m} \cdot {C_{H2O\_S}}^n \cdot {C_{H2\_S}}^m = Y^{n+m} \cdot C_S \tag{13}$$

$$r_{20} = \left(k_{O,G} \cdot C_S\right) \cdot Y^{(n+m)} \cdot e^{-\frac{E_{a,G}}{R \cdot T_r}} = K_{O,G} \cdot Y^{(n+m)} \cdot e^{-\frac{E_{a,G}}{R \cdot T_r}} \tag{14}$$

$$F(X_C) = a \cdot (1 - X_c) \cdot (1 - \varphi \cdot (1 - X_c))^{0.5} \cdot (1 + (c \cdot (1 - X_c)^p) \tag{15}$$

3.2.3. Surface property change of wood char through gasification

As one of the negative influences on tar reforming, mass loss of wood char has been proven through the tar surrogates reforming as can be seen in Figs. 1 and 2. Other deactivation factors were then investigated by surface property analyses. According to the surface structure of WCs (listed in Table 4), although the surface area had a slight increase after the reforming at 850 °C, micropore surface area is found to drop from 266 to 155 $m^3\ g^{-1}$. In contrast, the mesopore surface area rises from 26 to 297 $m^3\ g^{-1}$. The ratio of micropore to mesopore area has a decrease from 10.2 to 0.52 after the reforming, indicating a collapse of micropores through the long-time gasification. This phenomenon, which is related to the catalytic deactivation of char catalyst, was also found by Zeng et al. [30]. As micropores are highly related to the efficiency of tar reforming over chars, the conversion of tar model compounds might also be affected by the change of the pore distribution.

In addition, SEM diagrams provide sufficient information on the elemental composition and the surface property of the fresh and reacted WC. Fig. 4 (a) and (b) demonstrate comb-like surface structures of both fresh WC and reacted WC at 850 °C with a magnification of 120 X. It can be seen that no coke or pore blockage are observed on the surface. Higher magnification of 600 X was also applied for detecting the elemental distribution and ash agglomeration on these WC's surface, as can be seen in Fig. 5. High numbers of white inorganic clusters are observed on the reacted WC, suggesting that the inorganics agglomeration on the char surface took place during the 1-h test of tar surrogates reforming. SEM–EDX was applied to prove the presence of the elements and show the inorganics dispersion on the material's surface by a color distribution. The shades of the colors on SEM diagrams correspond to the quantity of the particular element (e.g., Ca and K), while a deeper color refers to a higher concentration on the surface. More intensive distribution of Ca and K, which are the major ash components in WC, are found on the surface of the reacted WC. The images illustrate that the reacted WC shows a completely different surface property with densely concentrated inorganics agglomeration compared to fresh WC. More inorganics migrated on the surface during the reforming that can result in negative impacts on the performance of tar reforming.

In summary, the factors for the catalytic deactivation of WC, including mass loss, pore collapse, and inorganics agglomeration, were all detected after the 1-h reforming. Thus, a decline in the conversion of tar model compounds can be anticipated during the reforming.

3.3. The reforming of tar model compounds in simulated SEG derived environment

3.3.1. Conversion of tar model compounds over wood char and CaO

Since tar surrogates conversions over the reference material (CaO) had no apparent change in 1-h testing, average conversions at different conditions are then presented here for the comparison purpose. According to Fig. 6, X_T and X_N are observed to increase along with the temperature, suggesting that temperature is an essential parameter for toluene and naphthalene reforming. CaO exhibited a better catalytic activity on toluene reforming with a high X_T of 0.91 at 900 °C, while only 0.37 of X_N was achieved for naphthalene. This result verifies that naphthalene, which is a heavier tar specie than toluene, is harder to break down because of its stable structure. The test results at different C_{H2} conducted at 850 °C are depicted in Fig. 7 in order to investigate the impacts of hydrogen on the tar surrogates reforming. When the concentrations increased from C_{H2O}/C_{H2} = 15%/7.5% to 40%/20%, conversions of toluene and naphthalene decreased considerably. X_N over CaO dropped drastically from 0.54 to 0.12 as C_{H2} increased. According to Chen et al. [52], when steam volume concentration approached to over 5%, no obvious change of toluene conversion was observed by applying CaO as the catalyst at 850 °C. The effect of steam concentration on the reforming was thus neglected since this study adopted a high C_{H2O} (>15%). The strong inhibiting effect on tar reforming in the presence of H_2 was therefore confirmed while applying CaO as a catalyst. Low surface area and strong adsorption of H_2 on CaO might lead to the low tar-reforming performance [32].

On the other hand, because of the carbon-based surface characteristics of WC, X_T and X_N over WC were not stable during the 1-h test. As can be seen in Fig. 8, a two-step reforming is confirmed. An activation step is observed at the beginning where X_T and X_N increase to a maximum value, and a deactivation step takes place subsequently with gradually sinking conversions. At the first step, the steam activation of WC for increasing surface area and pores is directly carried out. However, at the second step, considerable carbon loss, the collapse of micropores, and inorganics agglomeration (detailed in Section 3.2.3) lead to the catalytic inactivation of WC and a decline of tar surrogates conversions. For example, at condition (5) (900 °C; 30%/15%) in Fig. 8, naphthalene conversion increases rapidly from 0.73 to 1 in 10 min and maintains at $X_N = 1$ in the period of t = 10–20 min, indicating a rapid activation of the char surface compared to other temperatures. However, deactivation of WC subsequently results in a sharp decreasing trend from the complete conversion to $X_N = 0.63$ during the 1-h test. In comparison with naphthalene reforming, toluene reforming over WC exhibits a better resistance of inactivation on the WC's surface. After the 1-h test at condition (5), X_T only diminishes to 0.75 from 0.89. This finding indicates naphthalene, which represents as a tertiary tar and a heavy tar, might be more susceptible to the catalytic deactivation of WC. When tests conducted at 850 °C under different H_2O and H_2 volume concentrations, no apparent difference in maximum conversions was detected. Thus, inhibition impact on the reforming performance of tar over WC from hydrogen could not be considered in the SEG derived

Table 4
The surface properties of powder-form fresh and reacted wood chars after the 1-h test.

Sample	BET total surface area $m^2\ g^{-1}$	Micropore area $m^2\ g^{-1}$	Mesopore area $m^2\ g^{-1}$	The ratio of micropore to mesopore area –	Micropore volume $cm^3\ g^{-1}$	Pore average diameter nm
WC	309.2	265.6	26.1	10.2	0.13	2.14
WC-850	486.1	154.5	297.2	0.52	0.08	3.74

*WC-850: Reacted WCs at the reforming temperature at 850 °C. (C_{H2O}/C_{H2} = 30%/15%; $y_{TMC} = 10\ g\ m^{-3}{}_{NTP}$).

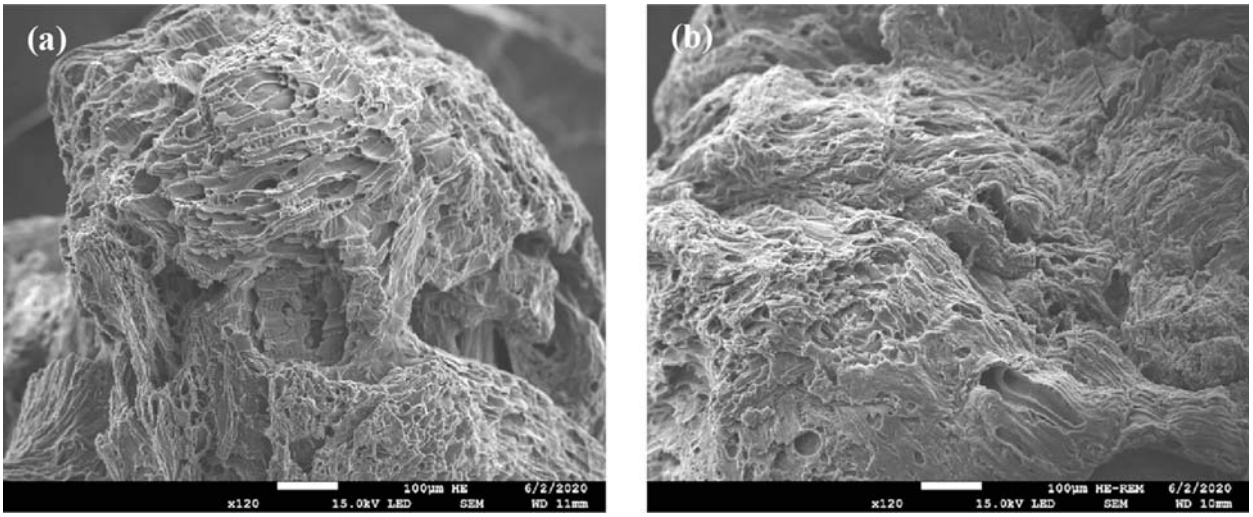

Fig. 4. SEM analysis of (a) raw wood char and (b) reacted wood char (T = 850 °C; C_{H2O} = 30%, C_{H2} = 15%, y_{TMC} = 10 g $m^{-3}{}_{NTP}$) with a magnification of 120 X.

environment. With a promising catalytic activity and a negligible effect by hydrogen inhibition, WC was therefore confirmed to be a more suitable catalyst than CaO for the reduction of tar presented in SEG derived syngas. In addition, it was found that X_T and X_N increased along with rising temperature over both CaO and WC from 800 to 900 °C. At the lowest temperature of 800 °C, X_T and X_N over CaO can still reach 0.25 and 0.12 while those over WC are 0.29 and 0.1 (after 1-h reforming) according to Figs. 6 and 8.

3.3.2. Benzene selectivity over wood char

Benzene has been known as an intermediate which is cracked mainly from aromatic tars through dealkylation. With suitable catalysts, benzene can be further decomposed to light gas components. Thus, S_{C6H6} can be regarded as a proper index to evaluate whether the aromatic ring has been broken under the influence of certain catalysts. Fig. 9 shows that S_{C6H6} of WC is smaller than 0.2 in the 1-h test at the temperature range from 850 to 900 °C. S_{C6H6} at 900 °C is lower than that at 850 °C, suggesting that at a high-temperature range above 850 °C not only high conversion rate can be approached over WC, but benzene is also much easier to decompose. However, it is observed that S_{C6H6} has a gradual rise after t = 30 min at both conditions. Since spontaneous gasification caused carbon loss and inorganics agglomeration on the WC surface, the reaction pathway of the tar surrogates reforming might also be affected through the progress of gasification. A relatively high average S_{C6H6} of 0.43 and 0.31 were found from the reforming over CaO at respective 850 and 900 °C compared to those from WC (below 0.2 at both temperatures). This finding shows that WC is more inclined to break down the aromatic ring and present high selectivity to light gas components due to large surface area (309 m^2 g^{-1}) and the dispersion of AAEM groups on the char surface (Fig. 5).

3.4. Modified kinetic model of the reforming of model tar compounds

3.4.1. Kinetics of CaO

Generally, the first-order reaction model is reported to be suitable to describe the reforming of typical tar model compounds (such as phenol, toluene, and naphthalene) [53]. This study thus developed modified kinetic models designed for the reforming rate of tar model compounds (r_{TMC}) based on the first-order kinetic model [54,55], assuming that toluene and naphthalene reforming occurred independently over CaO and WC. As discussed, the severe inhibition of reforming caused by H_2 has to be considered when applying CaO as the catalyst. Therefore, a modified first-order kinetic equation is then presented in Eq. (16). The space time (τ_{NTP}), conversions of tar model compounds (X_{TMC}) and C_{H2} are then able to express the apparent kinetic rate constant (k_{CAO}) as shown in Eq. (17), where the order of H_2 (A) can be determined with the conversions at different C_{H2} from Fig. 7. A linear relation with high R^2 = 0.97 and 0.95 between ln(C_{H2}) and ln(-ln(1- X_{TMC})/τ_{NTP}) shown in Fig. 10 verifies a reasonable derivation of A by this modified model. The temperature dependency of rate constant can be represented by Arrhenius law (Eq. (18)), which can be combined with Eq. (17) for calculating the pre-exponential factor ($k_{o,CaO}$) and activation energy ($E_{a,CaO}$) as shown in Fig. 6 at constant C_{H2} = 15%. The combined equation is then presented in Eq. (19). The apparent kinetic rate constant is varied with temperature by an Arrhenius-type relationship, as shown in Fig. 11. This modified first-order kinetic model is then proved to be a reliable model at different temperatures because of linear regressions with R^2 = 0.99 and 0.98, and the derived kinetic parameters can be seen in Table 5. The $k_{o,CaO}$ and $E_{a,CaO}$ calculated in this study are similar to those from the literature (CaO and olivine) listed in Table 5.

$$r_{TMC} = k_{CaO} \cdot C_{TMC} \cdot {C_{H2}}^{A} \tag{16}$$

$$k_{CaO} = \frac{\ln(1 - X_{TMC})}{{C_{H2}}^{A} \cdot \tau_{NTP}} \tag{17}$$

$$k_{CaO} = k_{o,CaO} \cdot e^{-\frac{E_{a,CaO}}{R \cdot T_r}} \tag{18}$$

$$\ln\left(\frac{-\ln(1 - X_{TMC})}{\tau_{NTP}}\right) = A \cdot \ln C_{H2} + \ln k_{CaO} \tag{19}$$

3.4.2. Kinetics of wood char

The reasons for char deactivation, including char mass loss, micropore collapsing, and carbon disappearance on the surface (agglomeration of inorganics), are directly related to the gasification of wood char during the reforming of tar surrogates. Thus, X_C, which is associated with the extent of gasification, has been regarded as a crucial parameter to determine the catalytic deactivation of WC taking place after the maximum conversion. As no coke deposition on the WC surface has been observed because of spontaneous gasification, the catalytic deactivation due to soot formation was not considered. An empirical equation of the reforming rate of model tar species over WC in the time range of the deactivation was thus derived based on the first-order kinetic model and X_C. As the catalytic activity of WC is highly dependent on the carbon content, the space time for kinetic calculation is substituted with the carbon space time (M_C/Q_{NTP}, carbon mass of WC divided by total gas flow rate) neglecting the mass of ash which occupies only 5.7% in a dry basis.

Since the change of C_{H2O} and C_{H2} has no noticeable influence on the

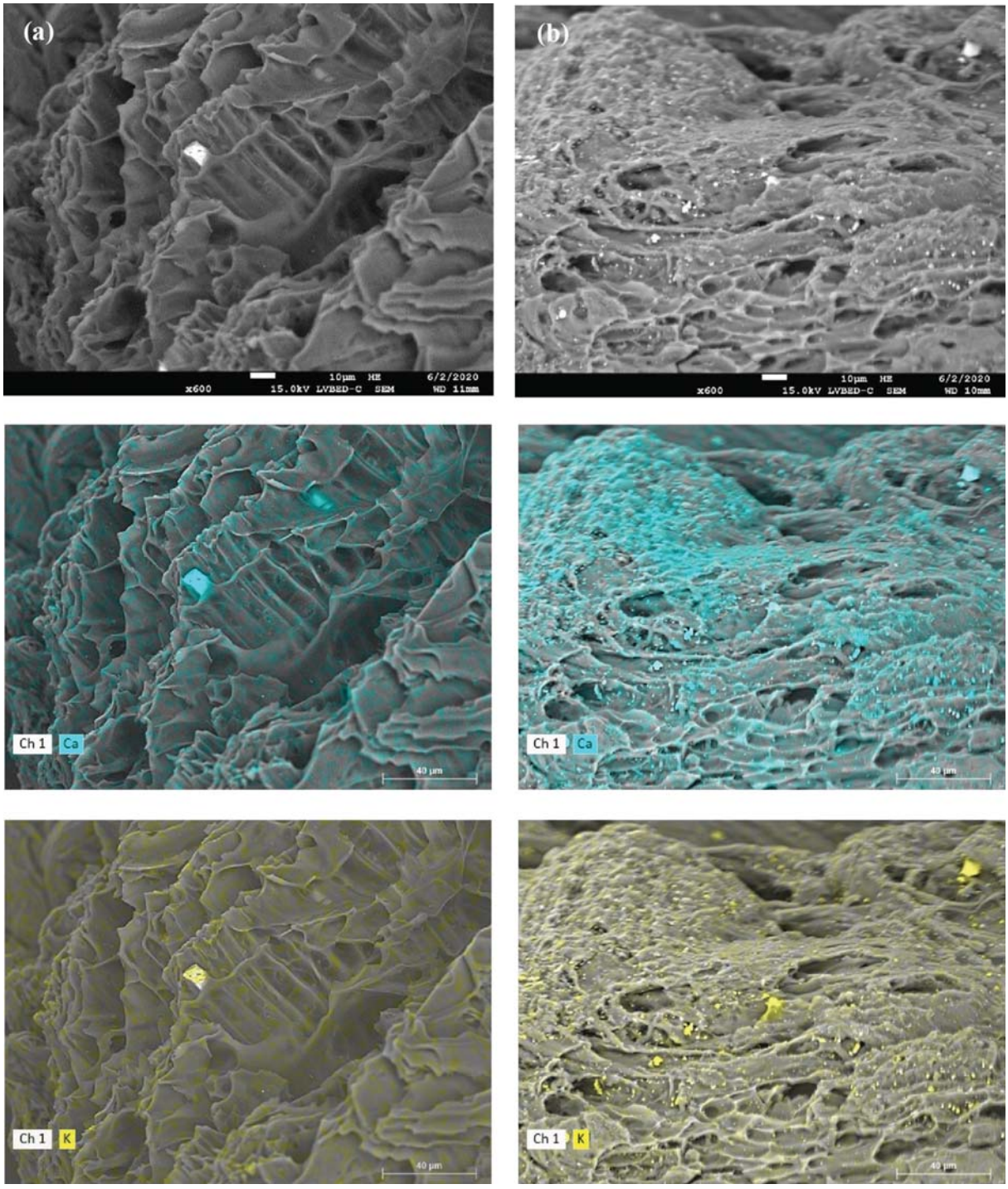

Fig. 5. SEM and SEM-EDX analyses of (a) raw wood char and (b) reacted wood char (T = 850 °C; C_{H2O} = 30%, C_{H2} = 15%, y_{TMC} = 10 g $m^{-3}{}_{NTP}$) with a magnification of 600 X. (SEM–EDX analyses of Ca and K with blue and yellow distribution). (For interpretation of the references to color in this figure legend, the reader is referred to the web version of this article.)

tar surrogates conversion presented in Fig. 8, X_C, M_C/Q_{NTP}, and T are assumed to be the main variables for the calculation of the reforming rate by modifying the first-order kinetic equations based on Eq. (20). Toluene and naphthalene conversions (Fig. 8) in the deactivation time range (X_T and X_N after the respective maximums during the 1-h test) and their corresponding X_C (Figs. 1 and 2) are then substituted into Eq. (21) and (22) to calculate the pre-exponential factor ($k_{o,WC}$) and the activation energy ($E_{a,WC}$) (Table 6). 1-X_C is used as a deactivation function in Eq. (22) for adjusting the apparent kinetic rate constant (k_{WC}). An Arrhenius-type relationship between the apparent rate constant and the temperature is shown in Fig. 12. High R^2 = 0.94 and 0.98, which are derived from the linear regressions, confirm a credible modified kinetic model. This model is also compared with all the data from experiments. Although calculated toluene conversions are found to be lower than experimental conversions at high X_C (>0.8), the model conversions still fit reasonably well to those given by experimental measurements under various conditions, as seen in Fig. 13. X_C is therefore proved to be a vital parameter for predicting the conversion rate. In comparison with the kinetics of wood char, pine bark biochar, and commercial biochar from other literature [17,23,57], the activation energy and pre-exponential

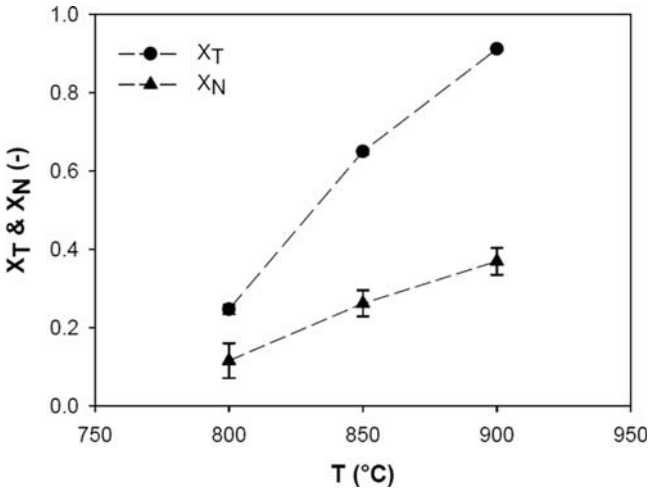

Fig. 6. Conversion of toluene and naphthalene over CaO at different temperature (C_{H2O} = 30%, C_{H2} = 15%, y_{TMC} = 10 g m^{-3}_{NTP}).

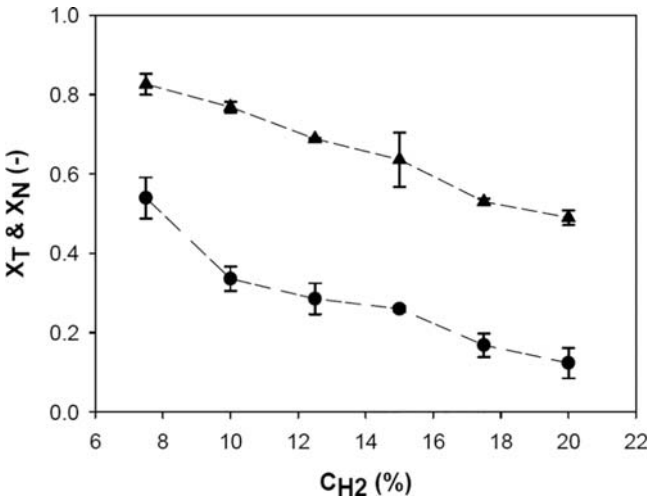

Fig. 7. Conversion of toluene and naphthalene over CaO at 850 °C with different C_{H2} (T = 850 °C, C_{H2O}/C_{H2} = 2, y_{TMC} = 10 g m^{-3}_{NTP}).

factor are found to increase considerably after considering the catalytic deactivation of wood char in this study. Thus, high energy condition is actually required for tar reforming over wood char. Elevated temperature is thus essential to maintain high tar conversion during the time range of the catalytic deactivation.

$$r_{TMC} = k_{WC} \cdot C_{TMC} \tag{20}$$

$$k_{WC} = k_{o,WC} \cdot e^{-\frac{E_{a,WC}}{R \cdot T_r}} \tag{21}$$

$$(1 - X_C) \cdot k_{WC} = \frac{-\ln(1 - X_{TMC})}{\frac{M_C}{Q_{NTP}}} \tag{22}$$

3.5. Design of a tar reformer loaded with wood char

Based on the above mentioned developed models, the required volume of the tar reformer loaded with wood char or CaO at a typical SEG condition (C_{H2O}/C_{H2} = 60%/30%) can be calculated. Since high-temperature operation can reduce the volume required for the reformer, and enhance the qualities of the syngas (e.g., hydrogen concentration and heating value) by WC gasification, 900 °C was chosen as a suitable temperature for the tar reforming. The carbon conversion of

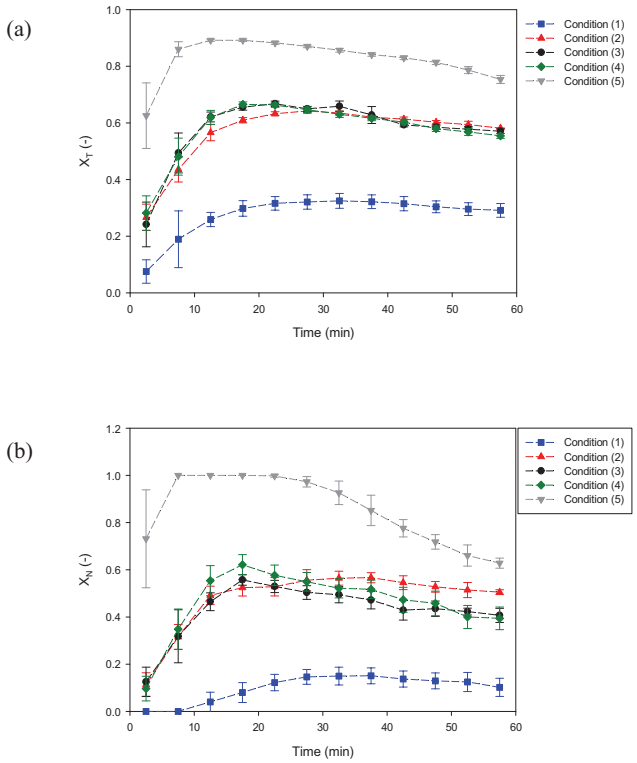

Fig. 8. (a) Toluene and (b) naphthalene conversion over wood char at different conditions at T and C_{H2O}/C_{H2} = (1) 800 °C; 30%/15% (2) 850 °C; 15%/7.5% (3) 850 °C; 30%/15% (4) 850 °C; 40%/20% (5) 900 °C; 30%/15%; all with y_{TMC} = 10 g m^{-3}_{NTP}.

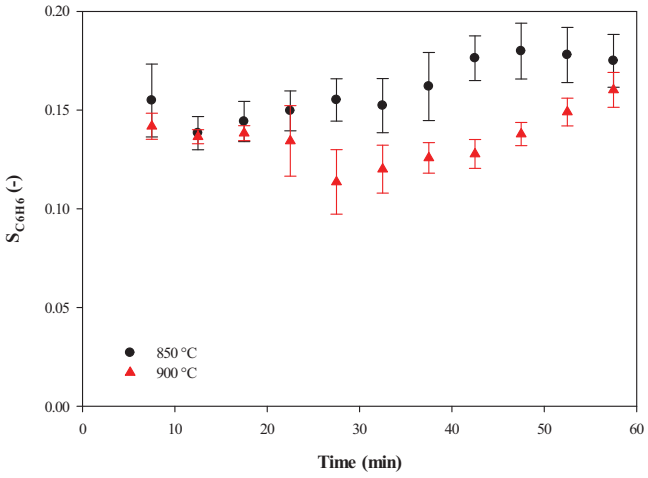

Fig. 9. Benzene selectivity of the reforming of toluene and naphthalene at 850 and 900 °C during 1–h testing in the condition: C_{H2O} = 30%, C_{H2} = 15%, y_{TMC} = 10 g m^{-3}_{NTP}.

wood char is assumed to be acceptable until X_C = 0.9, and then the reacted WC should be replaced by the fresh WC for maintaining stable bed space time and reforming performance. The reforming of model tar species over CaO is compared to WC by setting up the relationship between conversion rate and the space time (τ_{NTP} for CaO; M_C/ Q_{NTP} for WC). As can be seen in Fig. 14, the mass of WC required for a high conversion rate is far less than that needed for CaO. This result indicates that WC is more sustainable and cost-effective tar reforming material than CaO. Approximately 0.3 kg_{WC} / m^3 $h^{-1}_{NTP,syngas}$ (0.3 kg of WC per

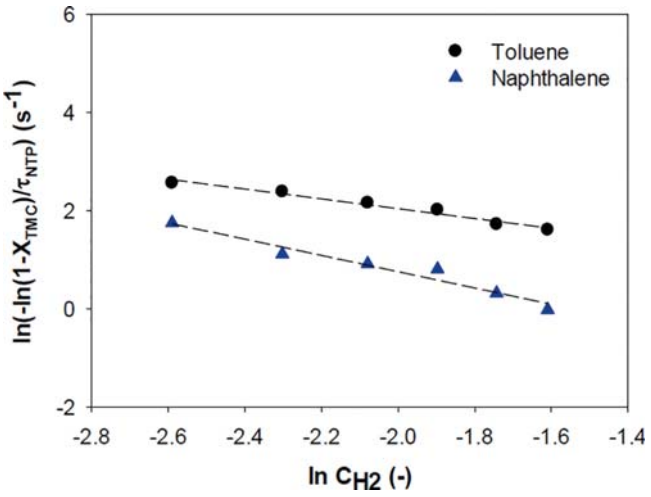

Fig. 10. The relation between $\ln(C_{H2})$ and $\ln(-\ln(1-X_{TMC})/\tau_{NTP})$ ($R^2 = 0.97$ and 0.95 for toluene and naphthalene, respectively).

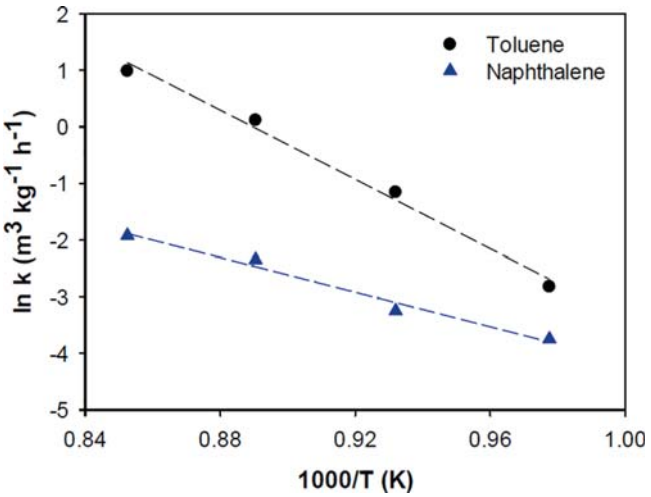

Fig. 11. Temperature dependency of the apparent reaction rate constant according to Arrhenius' law. Calculation by toluene conversions and naphthalene conversions over CaO. (R^2 = 0.99 and 0.98 for toluene and naphthalene, respectively).

Table 5
Kinetic parameters of toluene and naphthalene over CaO in this research compared to literature.

Materials	Tar species	A –	$k_{o,CaO}$ $m^3\ kg^{-1}h^{-1}$	$E_{a,CaO}$ $kJ\ mol^{-1}$
CaO	Toluene	−1.00	$6.73{\cdot}10^{11}$	254.5
	Naphthalene	−1.66	$6.79{\cdot}10^{4}$	126.9
CaO* [23]	Toluene	–	$1.53{\cdot}10^{11}$	218.0
	Naphthalene	–	$5.87{\cdot}10^{6}$	130.1
Olivine [56]	Naphthalene	–	$1.7{\cdot}10^{7}$	141

*Calculated at fixed C_{H2O}/C_{H2} = 15%/7.5% with y_{TMC} = 10 g $m^{-3}{}_{NTP}$ (mass fraction of toluene to naphthalene = 90%: 10%).

$m^3\ h^{-1}$ of syngas at NTP) is regarded as a minimum required load in the tar reformer as seen in Fig. 14, where a complete conversion of toluene and naphthalene is achieved. Since the bulk density of WC used in this study was roughly 213 kg m^{-3}, the value with $1.17{\cdot}10^{-3}$ m^3 / $m^3\ h^{-1}$ $_{NTP,syngas}$ should be considered for the volume design of the tar reformer. As for CaO, 8.85 kg_{CaO} / $m^3\ h^{-1}$ $_{NTP,syngas}$ is required for a complete conversion of naphthalene, which means the estimated volume design is

Table 6
Kinetic parameters of toluene and naphthalene over wood char in this research compared to literature.

Materials	Tar species	$k_{o,WC}$ $m^3\ kg^{-1}h^{-1}$	$E_{a,WC}$ $kJ\ mol^{-1}$
Wood char	Toluene	$1.90{\cdot}10^{15}$	284.8
	Naphthalene	$2.92{\cdot}10^{22}$	442.5
Wood char* [23]	Toluene	$1.30{\cdot}10^{6}$	89.0
	Naphthalene	$2.57{\cdot}10^{6}$	97.2
Pine bark biochar [17]	Toluene	$2.6{\cdot}10^{5}$	91
Commercial biochar [57]	Naphthalene	$7.6{\cdot}10^{4}$	61

*Calculated at fixed C_{H2O}/C_{H2} = 15%/7.5% with y_{TMC} = 10 g $m^{-3}{}_{NTP}$ (mass fraction of toluene to naphthalene = 90%: 10%).

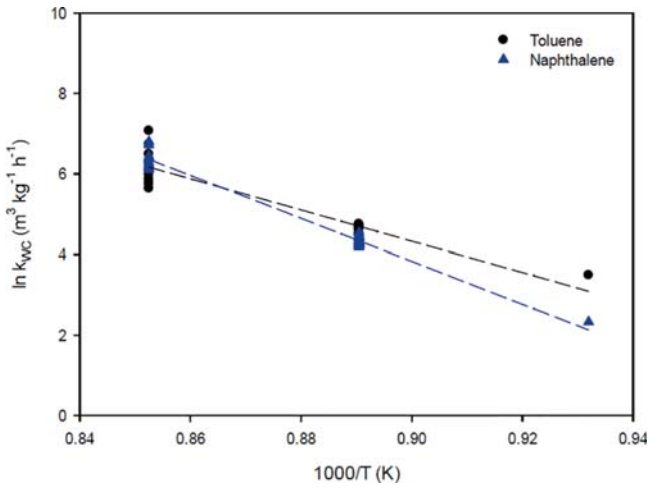

Fig. 12. Temperature dependency of the apparent reaction rate constant according to Arrhenius' law. Calculation by toluene conversions and naphthalene conversions over WC. (R^2 = 0.94 and 0.98 for toluene and naphthalene, respectively).

$9.27{\cdot}10^{-3}$ m^3 / $m^3\ h^{-1}$ $_{NTP,syngas}$ (bulk density of CaO is roughly 955 kg m^{-3}). On the other hand, it is still a challenge to predict the actual carbon loss in a pilot-scale WC reformer by using the gasification reactivity model developed in this study since a large amount of WC (0.3 kg) is required for 1 $m^3\ h^{-1}$ of the syngas. There is a 20 times difference in the space time between the value adopted in this lab-scale study (0.015 kg h m^{-3}) and the calculated value for the practical reformer (0.3 kg h m^{-3}). A higher space time suggests that per $m^3\ h^{-1}$ syngas will pass through increasing amount of WC. The steam concentration in the syngas is then foreseeable to decrease drastically through the pilot-scale WC bed, which can lead to the reduction of the whole carbon conversion. The time interval for the replacement of wood char due to char loss thus still needs to be confirmed by pilot-scale testing in the future.

4. Conclusions

Wood char produced from fluidized bed pyrolysis exhibits promising catalytic activity for reforming the tar surrogates at typical SEG operation conditions. The toluene and naphthalene conversion reached 0.75 and 0.63, respectively, after the 1-h test at a temperature of 900 °C. It was found that wood char gasification is highly influenced by the steam concentration and temperature whereas the temperature is the main factor for promoting the gasification rate. Moreover, the elevated temperature is preferable during tar reforming over wood char for avoiding coke accumulation and producing extra H_2 and CO. Thus, a temperature over 850 °C is recommended as a suitable reforming temperature. A gasification reactivity model developed in this study confirmed that the Extended Random Pore Model is suitable for biochar gasification in the

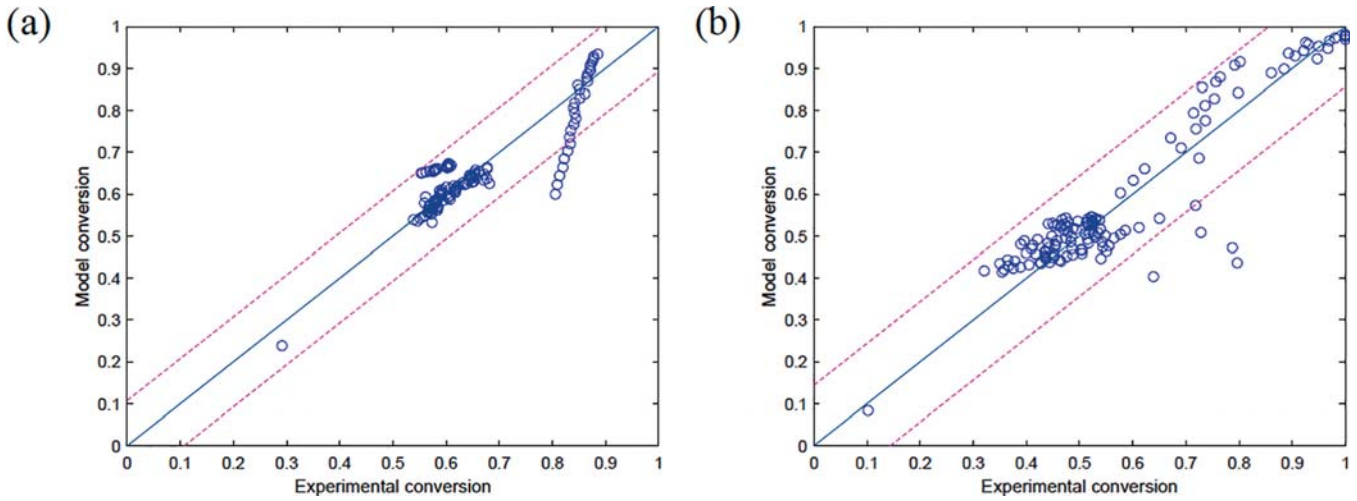

Fig. 13. Accuracy of the model to represent (a) toluene and (b) naphthalene conversion measurements. Points in dotted lines represent in 95% confidence interval.

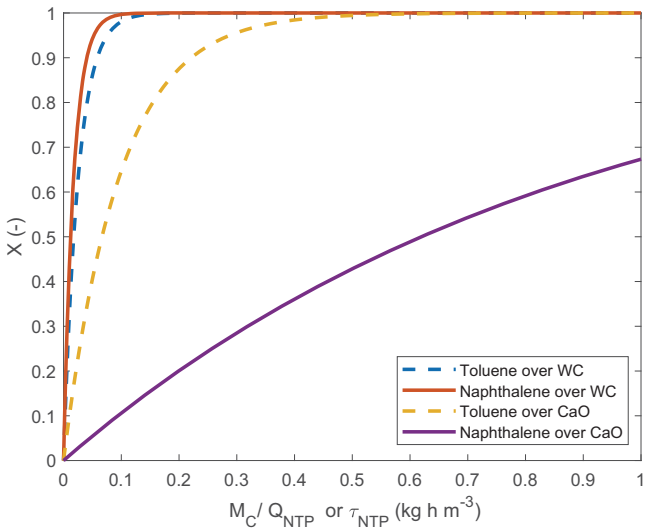

Fig. 14. Conversion of tar model compounds over wood char (at $X_C = 0.9$) and CaO as a function of the space time (τ_{NTP} for CaO; M_C/ Q_{NTP} for wood char) at 900 °C based on the SEG derived environment ($C_{H2O}/C_{H2} = 60\%/30\%$, $y_{TMC} = 10$ g $m^{-3}{}_{NTP}$, mass ratio of toluene to naphthalene = 90%/10%).

presence of steam, hydrogen, and tar. This model can be further applied for a two-stage gasification process where the second stage uses biochar as fuel/catalyst in the syngas surrounding environment. On the other hand, the change of C_{H2O} and C_{H2} had no significant effect on tar surrogates reforming over wood char. However, spontaneous gasification during tar reforming is highly related to the activation and deactivation of wood char. Mass loss, pore collapsing, and inorganics agglomeration due to continuous gasification leads to the catalytic deactivation of wood char. Carbon conversion, which represents the extent of gasification, was successfully included in the first-order kinetic model to calculate comparable conversions in the deactivation time range to those given by experimental results. According to the modified kinetic parameters of wood char and CaO, the volume design values of the tar reformer for wood char and CaO are found to be $1.17{\cdot}10^{-3}$ and $9.27{\cdot}10^{-33}$ m^3 / m^3 $h^{-1}{}_{NTP,syngas}$, respectively. These values represent the minimal reformer volume required to reach a theoretically complete tar conversion at 900 °C. Overall, the gasification model and tar reforming model developed in this study provide a novel approach for designing a tar reformer which can be successfully integrated with SEG process.

Declaration of Competing Interest

The authors declare that they have no known competing financial interests or personal relationships that could have appeared to influence the work reported in this paper.

Acknowledgement

The authors gratefully acknowledge the support from DAAD (German Academic Exchange Service) and the project NuCA (0324342A) funded by the German Ministry of Economic Affairs and Energy (BMWi).

References

[1] C. Hawthorne, N. Poboss, H. Dieter, A. Gredinger, M. Zieba, G. Scheffknecht, Operation and results of a 200-kWth dual fluidized bed pilot plant gasifier with adsorption-enhanced reforming, Biomass Conv. Bioref. 2 (3) (2012) 217–227, https://doi.org/10.1007/s13399-012-0053-3.
[2] G. Soukup, C. Pfeifer, A. Kreuzeder, H. Hofbauer, In situ CO 2 capture in a dual fluidized bed biomass steam gasifier – bed material and fuel variation, Chem. Eng. Technol. 32 (3) (2009) 348–354, https://doi.org/10.1002/ceat.200800559.
[3] C. Pfeifer, S. Koppatz, H. Hofbauer, Steam gasification of various feedstocks at a dual fluidised bed gasifier: Impacts of operation conditions and bed materials, Biomass Conv. Bioref. 1 (1) (2011) 39–53, https://doi.org/10.1007/s13399-011-0007-1.
[4] S. Steiert, FuE-Plattform "Biomass-to-Gas" – Energetische Nutzung biogener Reststoffe mit AER-Technologie zur Poly-Generation von Strom, Wasserstoff, Erdgassubstitut und Wärme, Schlussbericht, Zentrums für Sonnenenergie- und Wasserstoff-Forschung Baden-Württemberg (ZSW), Stuttgart, Germany, 2013.
[5] V.S. Sikarwar, M. Zhao, P. Clough, J. Yao, X. Zhong, M.Z. Memon, N. Shah, E. J. Anthony, P.S. Fennell, An overview of advances in biomass gasification, Energy Environ. Sci. 9 (10) (2016) 2939–2977, https://doi.org/10.1039/C6EE00935B.
[6] A.V. Bridgwater, The technical and economic feasibility of biomass gasification for power generation, Fuel 74 (5) (1995) 631–653, https://doi.org/10.1016/0016-2361(95)00001-L.
[7] H. Depner, Untersuchungen zur katalytischen Umsetzung flüchtiger Schwelprodukte in Rohgasen der Verkokung und Vergasung fester Brennstoffe, Doctoral thesis, TH Karlsruhe, Karlsruhe, Germany, 1998.
[8] A. Jess, Catalytic upgrading of tarry fuel gases: a kinetic study with model components, Chem. Eng. Process. Process Intensif. 35 (6) (1996) 487–494, https://doi.org/10.1016/S0255-2701(96)04160-8.
[9] N. Armbrust, N. Poboss, T. Eder, M. Zieba, G. Scheffknecht, Comparison of Two Methods of Sampling and Analyzing Tars During AER Biomass Gasification. 19th European Biomass Conference and Exhibition, Berlin, Germany, 6-10 June 2011.
[10] A. Diehl, Experimentelle Untersuchung der Reformierung von Teeren an Katalystisch Aktiven Substanzen, Ph.D. Thesis, Uni Stuttgart, Stuttgart, Germany, 2012.
[11] T.A. Milne, R.J. Evans, N. Abatzoglou, Biomass Gasifier "Tars": Their Nature, Formation, and Conversion, Report No. NREL/TP570-25357, National Renewable Energy Laboratory, Colorado, 1998.
[12] M. Speidel, H. Fischer, Steam reforming of tars at low temperature and elevated pressure for model tar component naphthalene, Int. J. Hydrogen Energy 41 (30) (2016) 12920–12928, https://doi.org/10.1016/j.ijhydene.2016.05.023.

[13] D. Feng, Y. Zhao, Y.u. Zhang, S. Sun, S. Meng, Y. Guo, Y. Huang, Effects of K and Ca on reforming of model tar compounds with pyrolysis biochars under H2O or CO2, Chem. Eng. J. 306 (2016) 422–432, https://doi.org/10.1016/j.cej.2016.07.065.
[14] D. Feng, Y. Zhao, Y.u. Zhang, Z. Zhang, H. Che, S. Sun, Experimental comparison of biochar species on in-situ biomass tar H2O reforming over biochar, Int. J. Hydrogen Energy 42 (38) (2017) 24035–24046, https://doi.org/10.1016/j.ijhydene.2017.08.013.
[15] D. Feng, Y. Zhao, Y.u. Zhang, Z. Zhang, S. Sun, Roles and fates of K and Ca species on biochar structure during in-situ tar H2O reforming over nascent biochar, Int. J. Hydrogen Energy 42 (34) (2017) 21686–21696, https://doi.org/10.1016/j.ijhydene.2017.07.096.
[16] Y.-H. Chen, M. Schmid, T. Kertthong, G. Scheffknecht, Reforming of toluene as a tar model compound over straw char containing fly ash, Biomass Bioenergy 141 (2020) 105657, https://doi.org/10.1016/j.biombioe.2020.105657.
[17] S. Mani, J.R. Kastner, A. Juneja, Catalytic decomposition of toluene using a biomass derived catalyst, Fuel Process. Technol. 114 (2013) 118–125, https://doi.org/10.1016/j.fuproc.2013.03.015.
[18] Y. Shen, Y. Fu, Advances in in situ and ex situ tar reforming with biochar catalysts for clean energy production, Sustainable Energy Fuels 2 (2) (2018) 326–344, https://doi.org/10.1039/c7se00553a.
[19] Z. Abu El-Rub, E.A. Bramer, G. Brem, Review of catalysts for tar elimination in biomass gasification processes, Ind. Eng. Chem. Res. 43 (22) (2004) 6911–6919.
[20] P.N. Bhandari, A. Kumar, D.D. Bellmer, R.L. Huhnke, Synthesis and evaluation of biochar-derived catalysts for removal of toluene (model tar) from biomass-generated producer gas, Renewable Energy 66 (2014) 346–353, https://doi.org/10.1016/j.renene.2013.12.017.
[21] D. Feng, Y. Zhao, Y.u. Zhang, Z. Zhang, L. Zhang, S. Sun, In-situ steam reforming of biomass tar over sawdust biochar in mild catalytic temperature, Biomass Bioenergy 107 (2017) 261–270, https://doi.org/10.1016/j.biombioe.2017.10.007.
[22] N.B. Klinghoffer, M.J. Castaldi, A. Nzihou, Catalyst properties and catalytic performance of char from biomass gasification, Ind. Eng. Chem. Res. 51 (40) (2012) 13113–13122, https://doi.org/10.1021/ie3014082.
[23] Y.-H. Chen, M. Schmid, C.-C. Chang, C.-Y. Chang, G. Scheffknecht, Lab-scale investigation of palm shell char as tar reforming catalyst, Catalysts 10 (5) (2020) 476, https://doi.org/10.3390/catal10050476.
[24] D. Fuentes-Cano, A. Gómez-Barea, S. Nilsson, P. Ollero, Decomposition kinetics of model tar compounds over chars with different internal structure to model hot tar removal in biomass gasification, Chem. Eng. J. 228 (2013) 1223–1233, https://doi.org/10.1016/j.cej.2013.03.130.
[25] D. Shekhawat, J.J. Spivey, D.A. Berry (Eds.), Fuel Cells: Technologies for Fuel Processing, 1st ed., Elsevier Science, London, 2011.
[26] D. Feng, Y. Zhao, Y.u. Zhang, S. Sun, Effects of H2O and CO2 on the homogeneous conversion and heterogeneous reforming of biomass tar over biochar, Int. J. Hydrogen Energy 42 (18) (2017) 13070–13084, https://doi.org/10.1016/j.ijhydene.2017.04.018.
[27] Grand View Research, Biochar Market Size, Share & Trends Analysis Report By Technology (Gasification, Pyrolysis), By Application (Agriculture (Farming, Livestock)), By Region, And Segment Forecasts, 2019–2025, 2019.
[28] X.i. Zeng, R. Shao, F. Wang, P. Dong, J. Yu, G. Xu, Industrial demonstration plant for the gasification of herb residue by fluidized bed two-stage process, Bioresour. Technol. 206 (2016) 93–98, https://doi.org/10.1016/j.biortech.2016.01.075.
[29] N.B. Klinghoffer, M.J. Castaldi, A. Nzihou, Influence of char composition and inorganics on catalytic activity of char from biomass gasification, Fuel 157 (2015) 37–47, https://doi.org/10.1016/j.fuel.2015.04.036.
[30] X.i. Zeng, F. Wang, Z. Han, J. Han, J. Zhang, R. Wu, G. Xu, Assessment of char property on tar catalytic reforming in a fluidized bed reactor for adopting a two-stage gasification process, Appl. Energy 248 (2019) 115–125, https://doi.org/10.1016/j.apenergy.2019.04.122.
[31] P. Fu, S. Hu, J. Xiang, W. Yi, X. Bai, L. Sun, S. Su, Evolution of char structure during steam gasification of the chars produced from rapid pyrolysis of rice husk, Bioresour. Technol. 114 (2012) 691–697, https://doi.org/10.1016/j.biortech.2012.03.072.
[32] P.A. Simell, E.K. Hirvensalo, V.T. Smolander, A.O.I. Krause, Steam reforming of gasification gas tar over dolomite with benzene as a model compound, Ind. Eng. Chem. Res. 38 (4) (1999) 1250–1257, https://doi.org/10.1021/ie980646o.
[33] E.P. Barrett, L.G. Joyner, P.P. Halenda, The determination of pore volume and area distributions in porous substances. I. Computations from nitrogen isotherms, J. Am. Chem. Soc. 73 (1) (1951) 373–380, https://doi.org/10.1021/ja01145a126.
[34] S. Storck, H. Bretinger, W.F. Maier, Characterization of micro- and mesoporous solids by physisorption methods and pore-size analysis, Appl. Catal. A 174 (1-2) (1998) 137–146, https://doi.org/10.1016/S0926-860X(98)00164-1.
[35] G. Taralas, M.G. Kontominas, Kinetic modelling of VOC catalytic steam pyrolysis for tar abatement phenomena in gasification/pyrolysis technologies, Fuel 83 (9) (2004) 1235–1245, https://doi.org/10.1016/j.fuel.2003.11.010.
[36] D. Świerczyński, S. Libs, C. Courson, A. Kiennemann, Steam reforming of tar from a biomass gasification process over Ni/olivine catalyst using toluene as a model compound, Appl. Catal. B 74 (3-4) (2007) 211–222, https://doi.org/10.1016/j.apcatb.2007.01.017.
[37] G. Taralas, M.G. Kontominas, Numerical modeling of tar species/VOC dissociation for clean and intelligent energy production, Energy Fuels 19 (1) (2005) 87–93, https://doi.org/10.1021/ef040048o.
[38] G. Taralas, M.G. Kontominas, X. Kakatsios, Modeling the thermal destruction of toluene (C7H8) as tar-related species for fuel gas cleanup, Energy Fuels 17 (2) (2003) 329–337, https://doi.org/10.1021/ef0201533.
[39] M. Morin, X. Nitsch, S. Pécate, M. Hémati, Tar conversion over olivine and sand in a fluidized bed reactor using toluene as model compound, Fuel 209 (2017) 25–34, https://doi.org/10.1016/j.fuel.2017.07.084.
[40] S. Nilsson, A. Gómez-Barea, D.F. Cano, Gasification reactivity of char from dried sewage sludge in a fluidized bed, Fuel 92 (1) (2012) 346–353, https://doi.org/10.1016/j.fuel.2011.07.031.
[41] T. Yu, A. Abudukeranmu, A. Anniwaer, Y.A. Situmorang, A. Yoshida, X. Hao, Y. Kasai, A. Abudula, G. Guan, Steam gasification of biochars derived from pruned apple branch with various pyrolysis temperatures, Int. J. Hydrogen Energy 45 (36) (2020) 18321–18330, https://doi.org/10.1016/j.ijhydene.2019.02.226.
[42] S.D. Ferreira, J. Junges, B. Scopel, C. Manera, E. Osório, I.P. Lazzarotto, M. Godinho, Steam gasification of biochar derived from the pyrolysis of chrome-tanned leather shavings, Chem. Eng. Technol. 42 (12) (2019) 2530–2538, https://doi.org/10.1002/ceat.201800660.
[43] P.O. Morf. Secondary Reactions of Tar during Thermochemical Biomass Conversion, Switzerland, 2001.
[44] Y.-H. Chen, C.-C. Chang, C.-Y. Chang, M.-H. Yuan, D.-R. Ji, J.-L. Shie, C.-H. Lee, Y.-H. Chen, W.-R. Chang, T.-Y. Yang, T.-C. Hsu, M. Huang, C.-H. Wu, F.-C. Lin, C.-H. Ko, Production of a solid bio-fuel from waste bamboo chopsticks by torrefaction for cofiring with coal, J. Anal. Appl. Pyrol. 126 (2017) 315–322, https://doi.org/10.1016/j.jaap.2017.05.015.
[45] C. Fushimi, T. Wada, A. Tsutsumi, Inhibition of steam gasification of biomass char by hydrogen and tar, Biomass Bioenergy 35 (1) (2011) 179–185, https://doi.org/10.1016/j.biombioe.2010.08.017.
[46] M. Barrio, B. Gbel, H. Rimes, U. Henriksen, J.E. Hustad, L.H. Srensen, Steam Gasification of Wood Char and the Effect of Hydrogen Inhibition on the Chemical Kinetics, in: A. V. Bridgwater (Ed.), Progress in Thermochemical Biomass Conversion, Blackwell Science Ltd, Oxford, 2001, p.32–46.
[47] I.I. Ahmed, A.K. Gupta, Kinetics of woodchips char gasification with steam and carbon dioxide, Appl. Energy 88 (5) (2011) 1613–1619, https://doi.org/10.1016/j.apenergy.2010.11.007.
[48] L. Zhang, J. Huang, Y. Fang, Y. Wang, Gasification reactivity and kinetics of typical chinese anthracite chars with steam and CO2, Energy Fuels 20 (3) (2006) 1201–1210, https://doi.org/10.1021/ef050343o.
[49] A. Gómez-Barea, B. Leckner, Modeling of biomass gasification in fluidized bed, Prog. Energy Combust. Sci. 36 (4) (2010) 444–509, https://doi.org/10.1016/j.pecs.2009.12.002.
[50] Y. Zhang, S. Hara, S. Kajitani, M. Ashizawa, Modeling of catalytic gasification kinetics of coal char and carbon, Fuel 89 (1) (2010) 152–157, https://doi.org/10.1016/j.fuel.2009.06.004.
[51] Z. Yang, M. Gao, Y. Wang, Y. Bai, F. Li, Identification for the behavior of maximum reaction rate during the initial stage of coal char gasification, J. Therm. Anal. Calorim. 128 (2) (2017) 1183–1194, https://doi.org/10.1007/s10973-016-6006-5.
[52] Y.-H. Chen, M. Schmid, G. Waizmann, S. Hafner, G. Scheffknecht, Tar Reforming over CAO and Straw Char Produced Inherently in Steam-oxygen Biomass Gasification Processes Using Toluene as Model Component. 27th European Biomass Conference and Exhibition, Lisbon, Portugal, 27-30 May 2019. doi: 10.5071/27thEUBCE2019-2BO.14.2.
[53] X.i. Zeng, Y. Ueki, R. Yoshiie, I. Naruse, F. Wang, Z. Han, G. Xu, Recent progress in tar removal by char and the applications: a comprehensive analysis, Carbon Resources Conversion 3 (2020) 1–18, https://doi.org/10.1016/j.crcon.2019.12.001.
[54] L. Devi L, K. J. Ptasinski, F.J.J.G. Janssen, Decomposition of Naphthalene as a Biomass Tar over Pretreated Olivine: Effect of Gas Composition, Kinetic Approach, and Reaction Scheme. Ind. Eng. Chem. Res. 44 (24) (2005) 9096-9104. doi: 10.1021/ie050801g.
[55] C. Li, K. Suzuki, Tar property, analysis, reforming mechanism and model for biomass gasification—an overview, Renew. Sustain. Energy Rev. 13 (3) (2009) 594–604, https://doi.org/10.1016/j.rser.2008.01.009.
[56] L.L. Devi, Catalytic removal of biomass tars:olivine as prospective in-bed catalyst for fluidized-bed biomass gasifiers, Technische Universiteit Eindhoven (2005).
[57] Z. Abu El-Rub, E.A. Bramer, G. Brem, Experimental comparison of biomass chars with other catalysts for tar reduction, Fuel 87 (10-11) (2008) 2243–2252, https://doi.org/10.1016/j.fuel.2008.01.004.

3 Results and Discussion

All findings from the published papers are summarized and discussed with regard to the application of biochar for tar reforming. The discovery including the catalytic performance of biochars in different conditions, reforming kinetics of tar model compounds over biochars, and gasification rate of biochars during the reforming is presented in this chapter. The design of a tar reformer is also presented here based on the results and developed models from the papers. In the end, proposals for further work are presented.

3.1 The properties of applied biochar catalysts

Different kinds of biochars from three manufacturing methods, including in-situ biochar from the gasification process, pyrolyzed biochar, and metal-impregnated biochar, were analyzed and applied as tar-reforming catalysts in this study. In-situ biochar from the gasification process, straw char containing fly ash (SCFA), was produced referring to steam-oxygen gasification conducted by Schmid et al. [20]. Straw pellets were gasified by the SOG process applying silica sand as fluidized bed and method described by Schmid et al. The 20 kW fuel input bubbling fluidized bed facility was used for conducting the gasification, and details of the configuration and process can be found elsewhere [20]. SCFA was the fly ash from the primary cyclone of the 20 kW facility. The cyclone efficiently collected SCFA during SOG, which did not return to the bubbling fluidized bed. It was a mixture of spent straw char, soot, ash, and silica sand attrition. As respects pyrolyzed biochars, three different types of biomasses (wood, straw, and palm shell) were pyrolyzed until 850 °C for biochars production (wood char (WC), straw char (SC), and palm shell char (PSC)). The palm shell was then selected as biomass support for metal

impregnation. This research adopted a low-cost impregnation method with K_2CO_3 and $Fe(NO_3)_3$-$9H_2O$ (to prepare K- and Fe-loaded palm shell char). The amounts of K_2CO_3 and $Fe(NO_3)_3$-$9H_2O$ added in the solution were decided by making K and Fe occupy 5 wt.% of the metal impregnated palm shell assuming that all potassium or iron ions in the solution could evenly cover the surface of the palm shell. 5% K and 5% Fe metal impregnated palm shell chars (5%K-PSC and 5%Fe-PSC) were subsequently pyrolyzed at a ramping temperature until 850 °C. On the other hand, the bed material of the SEG process, CaO, has been proven that it can reduce tar production and convert heavy tar into light tar. CaO, which is obtained from the calcination of limestone at 900 °C, was also tested here as the reference catalyst representing mineral rock catalyst. The characteristics of all examined materials in this study are listed in Table 3.1.

Table 3.1 Characteristics of applied materials.

Analyses	Compositions	Straw char containing fly ash	Wood char	Straw char	Palm shell char	5%K-Palm shell char	5%Fe-Palm shell char	CaO[d]
Proximate Analysis [a] (wt.%)	Fixed carbon	20.4	77.54	53.5	89.7	59.8	69.3	-
	Volatile matters	8.9	10.50	8.09	3.38	13.4	7.32	-
	Ash	67.8	5.36	31.1	4.61	16.9	17.8	94.4
	Equilibrium moisture [b]	3.0	6.58	7.30	2.00	9.94	5.58	6.40
Ultimate Analysis [a] (wt.%)	C	25.7	83.8	56.7	89.8	67.5	75.3	0.313
	H	0.7	1.23	1.15	0.708	1.70	0.974	0.679
	O[c]	0.5	2.57	1.81	1.82	3.02	-	-
	N	0.4	0.428	1.02	0.905	0.873	0.745	<0.4
	S	0.5	0.009	0.345	0.075	0.017	0.047	-
	Cl	1.5	0.020	0.579	0.079	0.047	0.028	-
Ash components [a] (wt.%)	Al_2O_3	2.6	0.095	0.407	1.72	0.014	0.058	0.384
	BaO	0.1	0.019	0.008	0.004	0.0001	0.0001	-
	CaO	8.6	2.03	1.62	0.215	0.430	2.08	91.6
	Fe_2O_3	2.0	0.059	0.656	0.939	0.021	12.1	0.224
	K_2O	6.5	1.24	4.24	0.532	11.0	0.340	0.059
	MgO	1.5	0.342	1.10	0.054	0.057	0.087	0.579
	MnO_2	0.1	0.255	0.525	0.002	0.004	0.020	0.007
	Na_2O	0.2	0.014	0.685	0.060	0.033	0.016	0.017
	P_2O_5	2.1	0.215	0.731	0.028	0.029	0.045	0.050
	SO_3	1.4	0.008	0.803	0.17	0.031	0.071	0.059
	SiO_2	38.0	0.656	18.1	3.22	1.74	2.68	1.95
	SrO	-	0.006	0.005	0.008	0.001	0.002	0.026
	TiO_2	0.1	0.004	0.028	0.077	0.001	0.00	0.019
BET total surface area (m^2/g)		116.6	350.7	-	469.6	6.93	220.7	8.77
Pellet size (mm)		0.01–0.3	4.4 (avg.)	2–5	2–5	2–5	2–5	3.2 (avg.)

[a] In wet basis. [b] Equilibrium moisture content of the sample in air. [c] Balance of C, H, N, S, Cl, H_2O, including ash. [d] Sum of H_2O, oxides, organics = 100.5 %.

Straw char containing fly ash is an exception of pure biochars among all examined materials since it is from the actual fluidized-bed gasification process. Straw char containing fly ash has a significant carbon mass fraction of 26 % after SOG, while the highest mass fraction is ash with 68%. It was found that

potassium occupied the most content in the ash of straw pellets. However, the ash component analysis shows that SiO_2 is the highest component between all metal oxides in straw char containing fly ash with a mass fraction of 38 % much more than the mass fraction of 6.5 % for K_2O among the total ash content, suggesting a contribution of silica sand attrition. According to Blott et al. [53], the specific surface area of quartz sands is in the range of 1.0 to 4.0 $m^2\ g^{-1}$. However, a much higher surface area of 116.6 $m^2\ g^{-1}$ for SCFA is observed, compared to the sand. As biochar possesses a higher surface area than mineral materials, straw char might have a dominant distribution in straw char containing fly ash, which contributes the most of the surface area. Straw char containing fly ash has thus the potential as a tar-reforming catalyst due to the abundant active sites from straw char. However, straw char containing fly ash is a mixture of fine particles making the application in a classical fixed bed difficult in a practical process. These fine particles should be suitably used in an additional fluidized bed tar reformer connected with the gasifier or in the "freeboard" of the gasifier where the syngas can pass through with many fine particles, contributing to tar reforming.

Pyrolyzed biochars are all pure chars in pellet form which can be properly filled in a fixed bed with syngas passing through for tar reforming. All pyrolyzed biochars have high carbon content and the presence of AAEM contents in ash components. Since the higher volatile matter makes biomass more susceptible to tar formation during steam reforming, the low volatile and high fixed carbon content in pyrolyzed biochars is suitable for the following tar-reforming catalyst usage. The surface area of pyrolyzed biochar is relatively higher than straw char containing fly ash and CaO, which indicates that the pure biochars have much better pore distribution than mineral materials.

On the other hand, both K and Fe-supported palm shell char had higher ash contents of 16.9 wt.% and 17.8 wt.%, respectively, than palm shell char with

4.61 wt.%. After palm shell char was impregnated with potassium and iron-containing solutions, 11.0 wt.% of K_2O and 12.1 wt.% of Fe_2O_3 were observed by metal analysis of prepared ashes from 5%K- palm shell char and 5%Fe- palm shell char, respectively, while palm shell char had only 0.532 wt.% of K_2O and 0.939 wt.% of Fe_2O_3 in ash. These results verify that the metal loading method used in this study can successfully load potassium or iron on the palm shell char. Although ash content had a significant rise after palm shell was soaked with K and Fe, the major component in both, metal-loaded palm shell char is still carbon. According to the surface area analysis of three palm shell chars, 5%K-palm shell char has a tiny surface area of 6.9 $m^2\ g^{-1}$, which might be due to potassium agglomeration, resulting in the disappearance of the porous structure. The surface areas of 5%Fe-palm shell char are slightly lower than palm shell char, suggesting a pore reduction caused by impregnation.

Except for straw char containing fly ash, other active materials all have similar pellet size for making the comparison of catalytic activity under the same dimension. Since commercial catalysts are majorly manufactured in pellet form and utilized in the fixed-bed reformer, this study decided later to focus on granular biochars as the tar-reforming catalyst for the future design of a tar reformer. Considering other advantages, lower cost and less complexity are two persuasive reasons for constructing a fixed-bed reactor instead of a fluidized-bed reactor.

3.2 The gasification reactivity of biochar during the reforming of tar model compounds

The innovative method for calculating the gasification rate during tar reforming is introduced in detail in Paper Ⅱ and Paper Ⅲ. The gasification rates of three biochars point out that straw char (SC) has the most drastic gasification with carbon conversion (X_C) = 0.60 in 90 min reforming, which may be due to the highest ash content among these three biochars with abundant AAEM groups dispersed on the surface. Some research has already confirmed that AAEM groups enhance the gasification rate of biochars [54,55]. This surmise also agrees with wood char (WC), which is more susceptible to steam for gasification with X_C = 0.35 in 90 min reforming than palm shell char (PSC) because of a higher content of AAEM groups. With the least content of AAEM groups, the gasification rate (r_G/M_C) of PSC remains almost constant during the whole-time reforming range. At 850 °C, X_C at 90 min of PSC (=0.21) is much lower than those of WC and SC, demonstrating a stabilized characteristic at high temperature and rich steam concentration environments.

It was found that the primary gasification of WC and SC took place in the beginning, and r_G/M_C became constant afterward. The surface area might soar tensely in this gasification time range, corresponding to the increase of activity of biochars at the starting time range. This study then proved that biochar catalysts can be parallelly gasified to raise the amount of H_2 and CO to increase their contents in the bio-syngas during the reforming of tar model compounds.

A thorough investigation of the gasification reactivity of WC during tar reforming in SEG derived environment was then carried out. Because WC exhibits the best catalytic activity (section 3.3) among three pyrolyzed biochars, the gasification model is on the basis of the testing of wood char. After the calculation of the gasification rate at different conditions, it is found that

temperature plays a big role in promoting the gasification rate of carbon during the reforming. The increase of steam concentration (C_{H2O}) from 15 % to 40 % at 850 °C also promotes the gasification rate, and X_C at t = 60 min rises from 0.25 to 0.46. However, there is no significant increase in the gasification rate during the 1-h test when C_{H2O} rises from 30 % to 40 %, indicating that gasification reactivity is moderated at a high steam concentration (> 30 %).

In Paper Ⅲ, two previous modeling methods were integrated here for developing the empirical equations of gasification reactivity during reforming of tar model compounds over wood char. The model was formulated based on the reactivity at 20% carbon conversion according to Nilsson et al. [56]. Subsequently, the Extended Random Pore Model (ERPM) [57,58] was adopted to fit the reactivity (r_G/r_{G20}) curve line since this method gave a good agreement with r_G/r_{G20} at different operating conditions. The model-derived carbon conversion curves have high consistency with the experimental data, suggesting a predictable X_C with increasing time. ERPM is thus confirmed to be a suitable method for gasification of biochar in the presence of steam, hydrogen, and tar. Additional production of H_2 and CO from biochar catalyst and the time interval for the dosing of fresh biochar catalyst to maintain a stable gas space time are then possible to predict by this method. This model also can be further improved for the application in the two-stage gasification process for simulating the gasification reactivity of biochar in the second-stage gasifier.

On the other hand, since the gasification reactivity of biochar can be considerably enhanced by loading metal [54], the impact of potassium and iron on biochar gasification during tar reforming was also investigated. A continuous three-stage tar reforming at three temperatures was thus conducted to investigate the effect of temperature and r_G/M_C on tar conversion. A significant difference in the gasification rate between 5%K-PSC and 5%Fe-PSC was thus observed. At each stage, steam activation of Fe-loaded PSC quickly

occurs with an extremely high gasification rate in the beginning, while the mass loss is much less than 5%K-PSC during long-term reforming on account of a rapid drop of r_G/M_C. 5%Fe-PSC has a considerable decrease of r_G/M_C from 0.035 to 0.003 min^{-1} at 840 °C, and the value then maintains constant close to r_G/M_C of PSC. According to Yu et al. [59], iron in its reduced forms on the char surface can be oxidated into magnetite during short reforming time with steam, which reduces the activity of char for reacting with steam and hence leads to a sink of r_G/M_C. In contrast, with potassium on the surface of PSC, a high gasification rate, which is twelve times greater than that of PSC at 850 °C, appears with nearly a constant value through the reforming. It was found that conversion of tar model compounds decreased apparently along with the increase of X_C when applying 5%K-PSC. A drastic mass loss is thus proved to result in catalytic deactivation because of the drop-in residence time. As a result, rapid mass loss of char catalysts because of gasification during tar reforming must be avoided to maintain the activity of char catalysts. In the site of reforming at a low temperature of 750 °C, the gasification rate of K-loaded PSC is still much faster than that of PSC at 850 °C. Consequently, the proper temperature (below 750 °C) should be considered to reduce the severe mass loss of 5%K-PSC while applying them as a catalyst in tar reforming.

3.3 The gasification-caused deactivation of biochar

According to references in Introduction, spontaneous gasification of biochar during tar reforming is highly associated with the deactivation of the catalytic activity of biochar. Here, wood char (WC) was selected for figuring out whether the deactivation factors occurred after reforming. As one of the negative influences on tar reforming, mass loss of wood char has been proven through the tar surrogates reforming confirmed in Section 3.2. Other deactivation factors were then investigated by surface property analyses. According to the surface structure of WCs, although the surface area had a slight increase after the reforming at 850 °C, micropore surface area is found to drop from 266 m^3 g^{-1} to 155 m^3 g^{-1}. In contrast, the mesopore surface area rises from 26 m^3 g^{-1} to 297 m^3 g^{-1}. The ratio of micropore to mesopore area has a decrease from 10.2 to 0.52 after the reforming, indicating a collapse of micropores through the long-time gasification. This phenomenon, which is related to the catalytic deactivation of char catalyst, was also found by Zeng et al. [48]. As micropores are highly related to the efficiency of tar reforming over chars, the conversion of tar model compounds might also be affected by the change of the pore distribution. In addition, the scanning electron microscope (SEM) provided sufficient information on the elemental composition and the surface property of the fresh and reacted WC. No coke or pore blockage are observed on the surface of reacted WC. High numbers of white inorganic clusters are observed on the reacted WC, suggesting that the inorganics agglomeration on the char surface took place during the 1-h test of tar surrogates reforming. SEM–energy dispersive X–ray spectroscopy (SEM-EDX) was applied to prove the presence of the elements and show the dispersion of the inorganic on the material's surface by a color distribution. More intensive distribution of Ca and K, which are the major ash components in WC, are found on the surface of the reacted WC. The images illustrate that the reacted WC

shows a completely different surface property with densely concentrated inorganics agglomeration compared to fresh WC. More inorganics migrated on the surface during the reforming that can also lead to negative impacts on the performance of tar reforming.

In summary, the phenomenon for the catalytic deactivation of WC, including mass loss, pore collapse, and inorganics agglomeration, were all confirmed after the 1-h reforming. Thus, a decline in the conversion of tar model compounds can be anticipated during the reforming.

3.4 The effect of main syngas components (H_2O and H_2) and the catalytic performance of biochars on the reforming of tar model compounds

According to Section 1.3, syngas from SEG and SOG contains high concentrations of H_2O and H_2. Since the existence of the individual gas can give rise to different reaction paths in tar reforming, different H_2O to H_2 ratios were investigated to understand the main reaction selectivity. Straw char containing fly ash (SCFA) was used as the examined char catalyst in H_2O to H_2 ratios for toluene reforming. Toluene conversion and reaction selectivity during toluene reforming over SCFA at various hydrogen concentrations (C_{H2}) = 0 %, 2.5 %, 5 %, and 10 % (850 °C; steam concentration (C_{H2O}) fixed at 5 %) was firstly tested. Toluene conversion has no significant difference with the change of C_{H2} in this research. However, it is worth mentioning that hydrogen has an enormous influence on the selectivity of toluene reforming. The selectivity of C_6H_6 and CH_4 (S_{C6H6} and S_{CH4}) increase from 0.14 to 0.44 and from 0.03 to 0.07, respectively, along with rising $C_{H2,}$ indicating that toluene hydrodealkylation plays a major role. Therefore, at a high range of C_{H2} (above 5 %), C_6H_6 was the major component formed from toluene reforming, among other carbon-containing species. In the presence of H_2, steam reforming of toluene was suppressed, and hence less and less CO and CO_2 were produced. Steam reforming was drastically weakened by increasing C_{H2} because the primary reaction was switched to hydrodealkylation. This effect might also lead to the change of toluene conversion when hydrogen is present. A fixed C_{H2} = 10 % was also tested with three different C_{H2O} = 5 %, 10 %, and 20 % to investigate the influence of the steam to hydrogen volumetric ratio (C_{H2O}/C_{H2}) on the selectivity. The selectivity of C_6H_6 and CO (S_{C6H6} and S_{CO}) at different C_{H2O}/C_{H2} are illustrated in Fig. 3.1, suggesting that C_{H2O}/C_{H2} has a significant influence on the selectivity.

Higher C_{H2O}/C_{H2} leads to the preference for steam reforming of toluene rather than hydrodealkylation of toluene. As a result, S_{CO} significantly increases while S_{C6H6} drops along with C_{H2O}/C_{H2} increasing in the range from 0.5 to 2. At high C_{H2O}/C_{H2} = 2, SCFA exhibited better activity on the breakdown of the aromatic ring, which is one of the main challenges in tar reforming, with a lower S_{C6H6} below 0.35 compared to S_{C6H6} of 0.45 at C_{H2O}/C_{H2} = 0.5. The finding here suggests that the conversion from aromatics to light gas components over SCFA can be enhanced with an additional steam flow for raising the value of C_{H2O}/C_{H2} in raw syngas. With different C_{H2O}/C_{H2} of syngas derived from various biomass gasification processes, the selectivity of tar reforming might also have different trends. According to the aforementioned findings, compared to the H_2O to H_2 volumetric ratio of SOG (30%:30%), SEG derived syngas has a much higher value (60%:30%), which can be more inclined to steam reforming of tar through thermal reforming over biochars. To investigate the potential of biochar catalyst for tar reforming in SEG derived syngas, a typical H_2O to H_2 volumetric ratio = 2 was set as the target condition for further test. With regards to tar, toluene and naphthalene were used as the tar model compounds because they are the major tar components in SEG derived syngas which also represents secondary and tertiary tars [2]. The total concentration of tar model compounds was 10 g m^{-3}_{NTP} on account of the typical tar concentration. Naphthalene concentration of 250 ppmv was considered here based on a representative SEG derived tar fraction [60]. Hence, a mass ratio of toluene to naphthalene applied in this study was 90 %/10 %. In a lab-scale examination, gas cleaning of a mixture gas containing H_2O, H_2, tar model species, and nitrogen over different granular biochars was carried out in a fixed bed reactor.

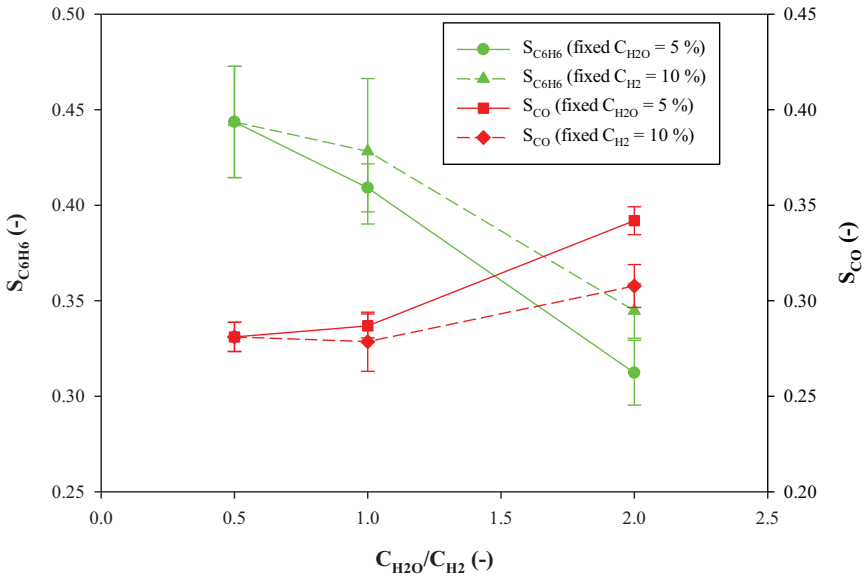

Fig. 3.1. Effect of steam to hydrogen concentration ratio on selectivity during toluene reforming over SCFA (T = 850 °C).

By sorting average conversions of both toluene and naphthalene (X_T and X_N) at different temperatures, the catalytic activities of the reforming of tar model compounds over all biochars (WC, SC, and PSC) are compared here. WC has the best catalytic activity for tar reforming with the highest X_T and X_N of roughly 0.7 at 880 °C. On the other hand, X_T and X_N increase along with the temperature, suggesting that naphthalene and toluene can be better reformed at high temperatures.

The average conversions of 5%K- and 5%Fe-PSC from the tests were discussed in order to understand whether conversion can be enhanced in the presence of additional K and Fe. 5%K-PSC has an excellent catalytic activity with high X_T and X_N = 0.7 at moderate temperature = 780 °C. However, both conversions decrease to 0.54, and 0.47, respectively, at 840 °C, caused by rapidly decreasing char amount owing to drastic char gasification. With the iron on the surface, the catalytic activity was also promoted, giving higher conversions of

toluene and naphthalene than PSC. These findings correspond to the references [32–34,36] that potassium and iron enhance the ability of tar decomposition over biochars in a steam-hydrogen rich environment.

Benzene has been known as an intermediate which is cracked mainly from aromatic tars through dealkylation. With better catalysts, benzene can be further decomposed to light gas components indicating that S_{C6H6} can also be regarded as a proper index to evaluate whether tar tends to decompose to light gas components with certain catalysts or not. S_{C6H6} of three different PSCs are smaller than 0.2 compared to relatively high values between 0.20 and 0.54 obtained from CaO in the temperature range from 700 °C to 900 °C. Moreover, the reforming of tar model compounds over WC and SC also exhibited similar selectivity of benzene with values below 0.2, suggesting that biochars are inclined to break down benzene further and present high selectivity to light components due to unique surface possessing AAEM groups. In addition, apparent drops of S_{C6H6} of PSC and CaO occur at 850 °C to 900 °C, meaning that, at a high-temperature range above 850 °C, not only a high conversion rate can be approached over PSC and CaO, but benzene is also much easier to decompose.

After the performance of different biochars for tar reforming was discussed, the effect of gasification-caused deactivation on reforming conversion was subsequently examined. Reforming of tar model compounds over WC was thus conducted at different conditions in 1 h. A two-step reforming is confirmed. An activation step is observed at the beginning where X_T and X_N increase to a maximum value and follow by a deactivation step with gradually sinking conversions. At the first step, the steam activation of WC for increasing surface area and pores is directly carried out. However, at the second step, considerable carbon loss, the collapse of micropores, and inorganics agglomeration lead to the catalytic inactivation of WC and a decline of tar

surrogates conversions. In comparison with naphthalene reforming, toluene reforming over WC exhibits a better resistance of inactivation on the WC's surface. This finding indicates naphthalene, which represents a tertiary tar and a heavy tar, might be more susceptible to the catalytic deactivation of WC. When tests were conducted at 850 °C under different H_2O and H_2 concentrations, no apparent difference in maximum conversions was detected. Thus, inhibition impact on the reforming performance of tar over WC from hydrogen is not necessary to be considered in the SEG derived environment. With a promising catalytic activity and a negligible effect by hydrogen inhibition, WC was therefore confirmed to be a more suitable catalyst than CaO for the reduction of tar presented in SEG derived syngas. In addition, it was found that X_T and X_N increased along with rising temperatures over both CaO and WC from 800 °C to 900 °C.

3.5 Kinetics of the reforming of tar model compounds over biochars

Kinetic constants can be calculated using kinetic models, along with the relationship between tar concentration and reaction temperature. In a recent review paper [31], the kinetics of tar model compounds reforming over char catalysts were assessed from the previous publication. It indicated that the research on the reaction kinetics of tar removal is very scarce at present. Generally, for the typical tar model compounds, such as phenol, toluene, and naphthalene, the first-order reaction model is appropriate in describing the reaction process. By using the same model, it is also beneficial for comparing the results with the literature [39,61]. As a result, the first-order kinetic model was then applied in this study for comparison with the literature. Kinetic constants of different biochars and mineral materials from different researches are listed in Table 3.2.

The gas space times for the reforming over different biochars are different. However, with two parameters, the activation energy (E_a) and the pre-exponential factor (k_0), the performance of different active materials tested in this study can be easily compared by establishing the relationship between gas space time and conversion. Since the space time of the reforming over straw char containing fly ash (SCFA) is much shorter than other studies, so a relatively low toluene conversion is expected. SCFA was tested by pure steam reforming with only one tar specie, toluene, for kinetic formulation. The relevance between space time and the conversion of toluene at 850 °C was then constructed. Since SCFA is fine particles with a particle size below 0.5 mm, biochars with the similar size listed in Table 3.2 are then compared with SCFA in Fig.3.2, although the reforming processes, conditions, and tested tar compounds in different research are distinct. At 850 °C, all chars have high

conversion exceeding 0.8 with space time above 0.1 kg h m^{-3}, while only SCFA and sawdust biochar [8] reach complete conversion of the tar compound at 0.05 kg h m^{-3}, confirming that SCFA can be regarded as a suitable catalyst for tar reduction as demonstrated by high conversion rate in short space time.

With respect to pyrolyzed biochar pellets (WC, PSC, SC) (Figure 3.3), simulated SEG derived environment with toluene and naphthalene as tar model surrogates were applied for developing the kinetics. The theoretical space time for the complete conversion of naphthalene is longer than that of toluene, indicating that this tertiary tar with a stable structure is harder to break down. At 850 °C, WC has the best catalytic activity for naphthalene reforming among natural materials, and CaO demonstrates a similar activity to PSC. Due to the best catalytic ability, WC was thus selected as the target biochar for further experiments.

Table 3.2 Comparison of char catalysts applied in this study with the literature. (Data from the tar model specie in boldface letter)

Catalyst type	Reactants	Temperature (°C)	Conversion (–)	Ea (kJ/mol)	k_0 (m^3 kg^{-1} h^{-1})	Space time (kg h m^{-3})	Pellet size (mm)
Straw char containing fly ash	**Toluene**, H_2O	750–900	0.06–0.21	78	$8.7 \cdot 10^5$	0.0008	0.01–0.3
Straw char	**Toluene** &Naphthalene, H_2O, H_2	830-880	0.21-0.56	260	$2.3 \cdot 10^{13}$	0.02	2-5
Straw char	Toluene &**Naphthalene**, H_2O, H_2	830-880	0.07-0.35	372	$1.6 \cdot 10^{18}$	0.02	2-5

Palm shell char	**Toluene** &Naphthalene, H_2O, H_2	850-900	0.31-0.81	319	$7.8 \cdot 10^{15}$	0.03	2-5
Palm shell char	Toluene &**Naphthalene**, H_2O, H_2	850-900	0.15-0.77	479	$9.6 \cdot 10^{22}$	0.03	2-5
Wood char	**Toluene** &Naphthalene, H_2O, H_2	730-880	0.26-0.70	89	$1.3 \cdot 10^{6}$	0.01	4.4 (avg.)
Wood char	Toluene &**Naphthalene**, H_2O, H_2	730-880	0.22-0.68	97	$2.6 \cdot 10^{6}$	0.01	4.4 (avg.)
Pine bark biochar [61]	**Toluene**, H_2O	650–900	0.19–0.94	91	$2.6 \cdot 10^{5}$	0.09	0.212–0.42
Commercial biochar [39]	**Naphthalene**, H_2O	700–900	~0.75–1.0	61	$7.6 \cdot 10^{4}$	0.04	0.5–0.8
Coal char [21]	**Toluene** & Naphthalene, H_2, H_2O	750–950	–	91	$4.0 \cdot 10^{6}$	0.014[a]	1–2.8
Coconut char [21]	**Toluene** & Naphthalene, H_2, H_2O	750–950	–	75	$2.8 \cdot 10^{5}$	0.044[a]	1–2.8
Dried sewage sludge char [21]	**Toluene** & Naphthalene, H_2, H_2O	750–950	–	88	$6.0 \cdot 10^{5}$	0 .048[a]	2–2.8
Sawdust biochar [62]	**Tar from pyrolysis of biomass**, H_2O	650–800	0.81–0.96	35	$1.8 \cdot 10^{4}$	~0.009	0.15–0.25
18.7% Fe–biochar [36]	**Toluene**, H_2O	450–900	–	48	$5.4 \cdot 10^{3}$	0.09	0.2–0.4

Olivine [63]	**Naphthalene**, H_2O, CO_2, CO, H_2	825–900	~0.3–0.75	141	$1.7 \cdot 10^{7}$	–	–
Ni/olivine [6]	**Toluene**, H_2O	560–850	0.3–1.0	196	$3.1 \cdot 10^{13}$	–	0.25–0.315
CaO[a] [43]	**Toluene** &Naphthalene, H_2O, H_2	750-900	0.14-0.98	218	$1.5 \cdot 10^{11}$	0.135	3.2 (avg.)
CaO[a] [43]	Toluene &**Naphthalene**, H_2O, H_2	750-900	0.15-0.68	130	$5.9 \cdot 10^{6}$	0.135	3.2 (avg.)

[a]Calculated by bulk density (kg m^{-3}) and residence time (s)

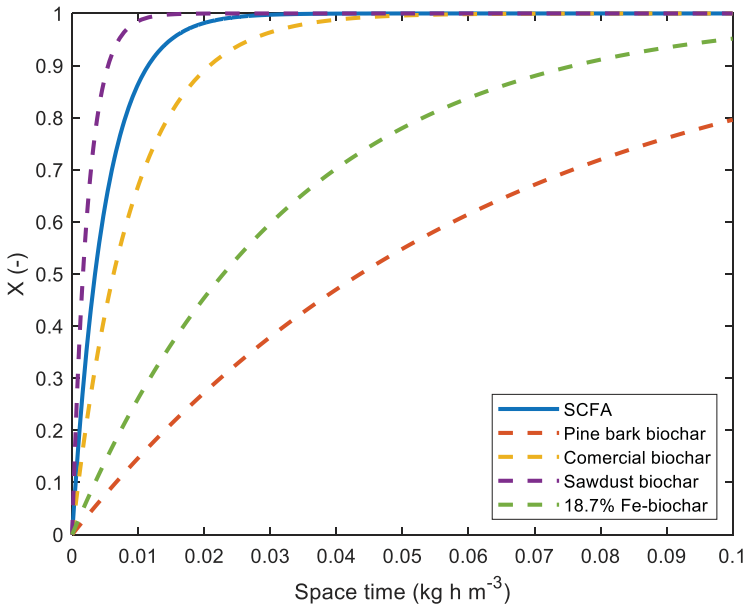

Fig. 3.2. Theoretical conversion of the tar compound over different fine char-based materials as a function of gas space time at 850 °C, calculated from the kinetics given in Table 5.

(a)

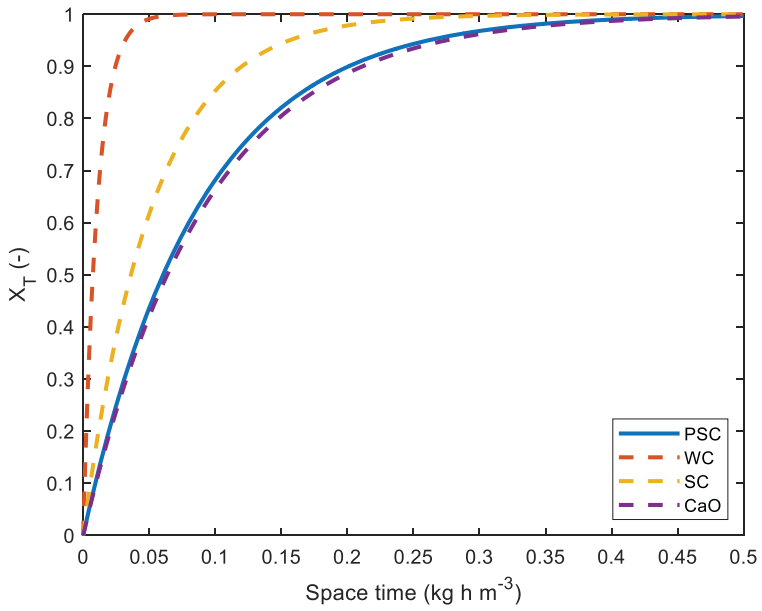

(b)

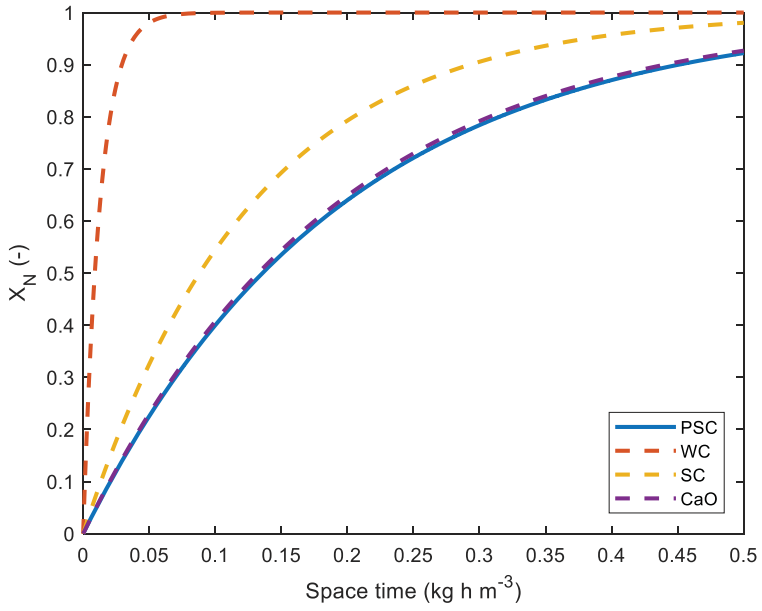

Figure 3.3 (a) Toluene; and (b) naphthalene conversion as a function of theoretical residence time at 850 °C for different active materials.

As far as we know, since catalytic deactivation takes place parallelly during tar reforming, a kinetic considering the deactivation should be established to exhibit the alternation of the catalytic performance through the time. Char deactivation, including char mass loss, micropore collapsing, and carbon disappearance on the surface (agglomeration of inorganics), are directly related to the gasification of wood char during the long-term reforming of tar surrogates. Thus, carbon conversion (X_C), which is associated with the extent of gasification, has been regarded as a crucial parameter to determine the catalytic deactivation of WC taking place after the maximum conversion. As no coke deposition on the WC surface has been observed because of spontaneous gasification, the catalytic deactivation due to soot formation was not considered. An empirical equation of the reforming rate of model tar species over WC in the time range of the deactivation was thus derived based on the first-order kinetic model and X_C. As the catalytic activity of WC is highly dependent on the carbon content, the space time for kinetic calculation is substituted with the carbon space time (carbon mass of WC divided by total gas flow rate), neglecting the mass of ash which occupies only 5.7 % on a dry basis.

Since the change of C_{H2O} and C_{H2} has no noticeable influence on the tar surrogates conversion, carbon conversion, space time, and temperature are assumed to be the main variables for the calculation of the reforming rate by modifying the first-order kinetic equations. Toluene and naphthalene conversions in the deactivation time range (X_T and X_N after the respective maximums during the 1-h test) and their corresponding X_C are then substituted into the first-order kinetic model to calculate the pre-exponential factor (k_o) and the activation energy (E_a) (Table 6). 1-X_C is used as a deactivation function for adjusting the apparent kinetic rate constant (k). This modified model is then compared with all the data from experiments. Although calculated toluene

conversions are found to be lower than experimental conversions at high X_C (> 0.8), the model conversions still fit reasonably well to those given by experimental measurements under various conditions. X_C is, therefore, proved to be a vital parameter for predicting the conversion rate. In comparison with the kinetics of wood char without the consideration of deactivation in Table 3.3, the activation energy and pre-exponential factor are found to increase considerably after considering the catalytic deactivation of wood char in this study. Thus, a high energy condition is actually required for tar reforming over wood char. Elevated temperature is thus essential to maintain high tar conversion during the time range of the catalytic deactivation.

Table 3.3 Kinetic parameters of toluene and naphthalene over wood char considering gasification-caused deactivation.

Materials	Tar species	k_o	E_a
		$m^3\ kg^{-1}\ h^{-1}$	$kJ\ mol^{-1}$
Wood char	Toluene	$1.90 \cdot 10^{15}$	284.8
	Naphthalene	$2.92 \cdot 10^{22}$	442.5

Lastly, metal modified biochar is discussed here. The advantage of loading with potassium and iron on biochar is that activation energy for the reforming of tar model compounds becomes much lower (shown in Table 3.4), meaning that tar reforming over 5%K- and 5%Fe-PSC can be accomplished at more moderate temperatures compared to PSC. The energy consumption thus decreases for a long-time reforming. In order to avoid considerable mass loss of PSC due to gasification at high temperatures, metal-loaded PSC is, therefore, more suitable for low-temperature tar reforming. 5%K-PSC and 5%Fe-PSC are

hence compared to PSC at a low temperature of 750 °C with the relationship between residence time and conversion, as can be seen in Figure 3.4. A complete conversion of naphthalene for 5%K- and 5%Fe-loaded PSC is reached with theoretical space time = 0.27 and 1.22 kg h m^{-3}, respectively, while PSC shows a weak activity with X_N = 0.05 at theoretical space time = 1.5 kg h m^{-3}, proving potassium and iron are prominent promoters for not only reducing the required reforming temperature but also significantly enhancing the catalytic activity of PSC.

Table 3.4 Effect of temperature on fractional conversions and first-order rate constants for tar reforming over different catalysts. Calculation by toluene conversions and naphthalene conversions.

Tar model compound	Catalyst Type	Temperature (°C)	Conversion (-)	Ea (kJ/mol)	k_0 (m^3 kg^{-1} h^{-1})	R^2
Toluene	PSC	850–900	0.31–0.81	318.9	$7.8 \cdot 10^{15}$	0.973
	5%K-PSC	740–780	0.51–0.70	116.3	$3.06 \cdot 10^{7}$	-
	5%Fe-PSC	740–850	0.26–0.52	82.7	$2.07 \cdot 10^{5}$	0.999
Naphthalene	PSC	850–900	0.15–0.77	478.9	$9.6 \cdot 10^{22}$	0.996
	5%K-PSC	740–780	0.54–0.70	99.1	$4.27 \cdot 10^{6}$	-
	5%Fe-PSC	740–850	0.18–0.43	100.6	$1.11 \cdot 10^{6}$	0.999

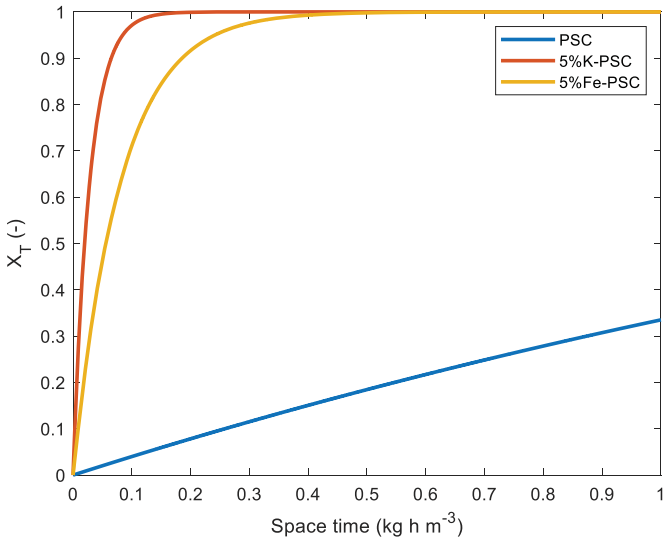

(a)

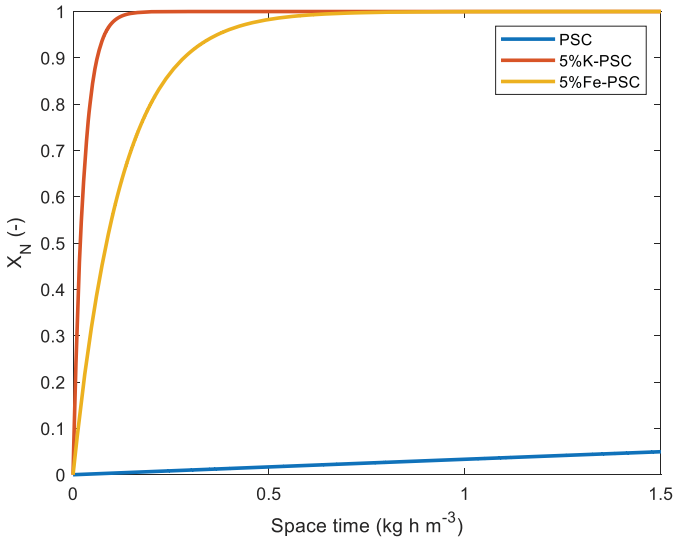

(b)

Figure 3.4 (a) Toluene; and (b) naphthalene conversion as a function of theoretical residence time at 750 °C for PSC, 5%K-PSC, and 5%Fe-PSC.

3.6 The design of the tar reformer

Based on the above-mentioned developed models, the required volume of the tar reformer loaded with wood char or CaO at a typical SEG condition (C_{H2O}/C_{H2} = 60 %/30 %) can be calculated. Since high-temperature operation can reduce the volume required for the reformer and enhance the qualities of the syngas (e.g., hydrogen concentration and heating value) by WC gasification, 900 °C was chosen as a suitable temperature for the tar reforming. The carbon conversion of wood char is assumed to be acceptable until X_C = 0.9, and then the reacted WC should be replaced by the fresh WC for maintaining stable bed space time and reforming performance. The reforming of model tar species over CaO is compared to WC by setting up the relationship between conversion rate and the space time. The mass of WC required for a high conversion rate is far less than that needed for CaO. This result indicates that WC is a more sustainable and cost-effective tar reforming material than CaO. Approximately 0.3 kg_{WC} / m^3 $h^{-1}{}_{NTP,syngas}$ (0.3 kg of WC per m^3 h^{-1} of syngas at NTP) is regarded as a minimum required load in the tar reformer according to Fig. 14 in **Paper Ⅲ**, where a complete conversion of toluene and naphthalene is achieved. Since the bulk density of WC used in this study was roughly 213 kg m^{-3}, the value with $1.17 \cdot 10^{-3}$ m^3 / m^3 $h^{-1}{}_{NTP,syngas}$ should be considered for the volume design of the tar reformer. As for CaO, 8.85 kg_{CaO} / m^3 $h^{-1}{}_{NTP,syngas}$ is required for a complete conversion of naphthalene, which means the estimated volume design is $9.27 \cdot 10^{-3}$ m^3 / m^3 $h^{-1}{}_{NTP,syngas}$ (bulk density of CaO is roughly 955 kg m^{-3}). On the other hand, it is still a challenge to predict the actual carbon loss in a pilot-scale WC reformer by using the gasification reactivity model developed in this study since a large amount of WC (0.3 kg) is required for 1 m^3 h^{-1} of the syngas. There is a 20 times difference in the space time between the value adopted in this lab-scale study (0.015 kg h m^{-3}) and the calculated value for the practical reformer (0.3 kg h m^{-3}). A higher space time suggests that per m^3 h^{-1} syngas will pass

through an increasing amount of WC. The steam concentration in the syngas is then foreseeable to decrease drastically through the pilot-scale WC bed, which can lead to the reduction of the whole carbon conversion. The time interval for the replacement of wood char due to char loss thus still needs to be confirmed by pilot-scale testing in the future.

3.6.1 Heat demand for tar reforming of SEG derived syngas over wood char

After a lab-scale investigation of char catalysts for the application of tar reforming, a practical tar reformer was planned to be coupled with Elwira-Diva (20 kW dual fluidized beds in the University of Stuttgart) for field research of tar reforming over wood char. SEG process will be conducted in Elwira-Diva, and the produced raw syngas from Elwira subsequently go through cyclones and a filter for particulate matter capture. Afterward, the raw syngas will then be tested in the tar reformer.

Although the kinetic model of tar reforming over WC has been derived, the heat demand of the whole tar conversion process should also be assessed for the design of the reformer. There are two major heat demands for tar reforming over wood char. The first part is to preheat the raw syngas to the reforming temperature. Because the raw syngas is cooled down to circa 300 °C after passing through the cyclones and the filter, a preheating process is necessary to increase the temperature of the raw syngas until the reforming temperature rapidly. Previous preheater design for Diva-Elwira was generally used spiral pipes surrounded in a furnace. However, the heat transfer of this way has a low efficiency because of the low heat-transfer area and large diameter of the pipe. Thus, a much higher temperature of the furnace should be reached to provide enough energy for preheating, which leads to bending and damage to the pipe.

In this study, the preheater is designed with two combined pipes and directly integrated with the main reformer to diminish the heat loss. It consists of two pipes to form a film ring area for letting the flow of the raw syngas go through to reduce the heat transfer distance. The external surface of the preheater is the main area to receive the heat from the heat source which is beneficial for increasing the effective heat-contacting area compared to the spiral pipe. The heat demand of preheating (Q_{preH}) can be calculated by the heat capacity (C_{p_syn} = 2715 J kg^{-1} K^{-1}, average heat capacity of 300 and 900°C) of SEG derived syngas, the mass flow rate of inflow syngas ($\dot{m}$), and the temperature difference (ΔT_P) required for preheating (Eq.(1)). The syngas composition refers to Table 1.3. Basic properties of the referring syngas including specific heat capacity, thermal conductivity, dynamic viscosity, and density were all calculated based on the equations (Appendix) according to VDI book [68]. Since the empirical flow rate of produced gas from Elwira is 3-5 $m^{3,NTP}$ h^{-1}, the trial reformer targets to treat around 1 $m^{3,NTP}$ h^{-1} of the partial gas where the mass flow rate is **0.63 kg/h** assuming the raw syngas is an ideal gas. Due to the fluctuating production of syngas from gasification, a twice mass flow rate of **1.26 kg/h** is set up as the flow rate for the calculations of the design. According to the kinetic study of tar reforming over wood char, the desired reforming temperature is 900 °C for enhancing char gasification and preventing soot deposition. ΔT_P of the heated syngas is therefore 873 K through the preheater. The theoretical heat demand ($\dot{Q}_{preH}$) for preheating is subsequently obtained with a value of **570 W**.

$$\dot{Q}_{preH} = \dot{m} \times C_{P\_syn} \times \Delta T_P \qquad \text{Eq.(1)}$$

According to Section 3.2, wood char can be gasified during tar reforming. A large heat might be required for the wood char gasification when abundant char catalysts are loaded in the reformer. Hence, the second part of the heat demand is to offer the energy for spontaneous wood char gasification during tar reforming. Apart from the gasification of wood char, reforming of tar and

methane in raw syngas are all considered in the required reaction heat. Because the main oxidant is steam, steam reforming reactions of the char, tar, and CH_4 are identified as the primary reactions, and the heat demand for other reactions are all neglected. Wood char, which contains 84 wt.% carbon content on a wet basis, is regarded as pure carbon for simulation. A catalyst bed weight has been predicted by the kinetic model of wood char previously, where 0.3 kg wood char per $m^{3}_{,NTP}$ h^{-1} raw syngas is needed for complete conversion of tar at 900 °C. According to the previous gasification model of wood char during tar reforming at the condition of 30 vol% steam, 15 vol% H_2, and 900 °C, rapid carbon conversion of around 90% can be reached in 1 h, leading to the replacement of the char bed per hour. Thus, the continuous carbon flow rate of 0.3 kg h^{-1} is assumed in this simulation for calculating the heat demand of wood char gasification. Carbon (0.3 kg h^{-1} per $m^{3}_{,NTP}$ h^{-1} raw syngas), tar (10 g h^{-1} per $m^{3}_{,NTP}$ h^{-1} raw syngas; represented by naphthalene), and methane (2.04 mol h^{-1} per $m^{3}_{,NTP}$ h^{-1} raw syngas) are all assumed to be completely reacted through steam reforming (R(10), (4), and (11)) in the system. Reaction heats of different reactions at 900 °C are derived by Factsage. The total heat demand ($\dot{Q}_{ref}$) due to steam reforming in tar reformer is **1116 W** per $m^{3}_{,NTP}$ h^{-1} syngas while this value is much higher in the actual situation as the condition for these calculations founds on the complete conversion of carbon, tar, and methane. In any case, a huge heat requirement during tar reforming by using char as catalyst should be taken into account in the design. Stainless-steel (HWF 1.4841) is applied in this study for the design of the tar reformer and preheater because of its high-temperature tolerance (up to 1150 °C).

$C + H_2O \rightarrow CO + H_2$ $\Delta H°_{900\,°C} = 136$ kJ mol^{-1} (R10)

$C_{10}H_8 + 10H_2O \rightarrow 10CO + 14H_2$ $\Delta H°_{900\,°C} = 1234$ kJ mol^{-1} (R4)

$CH_4 + H_2O \rightarrow CO + 3H_2$ $\Delta H°_{900\,°C} = 227$ kJ mol^{-1} (R11)

3.6.2 Design of the tar reformer

When gas flow in the reformer is closer to plug flow, a more evenly distributed flow is going through the reformer bed, which benefits the heterogeneous interaction between catalyst and gas. Dimensionless Peclet number (Pe) can be applied to describe the flow behavior in the reformer, where ideal plug flow gives an infinite value of Pe.

$$\mathrm{Pe} = \frac{\frac{V_S}{\varepsilon(d)} \times D}{D_l}, \qquad \text{Eq.(2)}$$

where D is the inside diameter of the circular reformer; D_l is thermal diffusivity; $\varepsilon(d)$ (-) is porosity in the catalyst bed with the function of pellet diameter d; V_S is superficial velocity. $\frac{D}{d}$ is regarded as an important parameter. The gas fluid is closer to the plug flow when $\frac{D}{d}$ increases. According to the lab-scale test, tar reforming over WC tested in the experimental rig with a diameter of 3 cm ($\frac{D}{d}$ = 10), which treated 0.2 $m^3\ h^{-1}$ simulated syngas, showed a fittable result with the assumption of plug flow in the first-order kinetic model. Since a larger diameter of the reformer is required to handle the syngas with a higher flow rate over 1 $m^3\ h^{-1}$ from Elvira to avoid pressure block and shorten the length of the required catalyst bed, a large reformer diameter is considered here, which also benefits the plug flow assumption. The pressure drop of the packed bed is not so significant due to the pellet form of the wood char (characteristic diameter of pellet, d = 0.003 m). A reasonable reformer's diameter of around 10 cm is then chosen here to give a suitable height for the catalyst bed in the reformer of 0.16 m per $m^3\ h^{-1}$ syngas, and $\frac{D}{d}$ in this pilot scale is around 33 (much higher than that in the lab scale, indicating a better gas flow distribution). Therefore, 4'' pipe based on the standard "HWF 1.4841" is chosen with an inner diameter (D) of 107.1 mm and an outer diameter of 114.3 mm. Moreover, the production amount of syngas can be variated during the operation. 0.32 m is a

required bed length for the tar reforming of 2 $m^{3}_{,NTP}$ h^{-1} syngas with wood char pellets as the catalyst.

Due to the endothermic reforming reactions and the large diameter of the reformer, the temperature drop from the internal wall of the reformer to the center can be tremendous. A reliable model created by Nilles and Martin for calculating the temperature difference in a packed bed reactor is adopted here (Eq.(3)) [64,65]. The Nusselt number is the ratio of convective to conductive heat transfer at a boundary in a fluid. After figuring out Nu_{ref}, the heat transfer coefficient (α_{syn_ref}) of the syngas in the reformer is calculated by Eq. (4). According to the general definition of the heat transfer coefficient shown in Eq. (5), it is observed that the temperature dropping (ΔT_{ref}) of around 373 K might occur during the reforming from the internal wall of the reformer to the center, based on the treatment for 2 $m^{3}_{,NTP}$ h^{-1} syngas. The huge decrease of reforming temperature in a radical direction to the pipe's center can significantly influence the tar reforming efficiency. Thus, the actual temperature profile in the reactor is worth detecting for the investigation of the char catalyst application.

$$Nu_{ref} = \left(1.3 + \frac{5}{D/d}\right)\frac{\lambda_{bed}}{\lambda_{syn\_ref}} + 0.19{Re_{ref}}^{0.75}{Pr_{ref}}^{1/3} \quad \text{Eq.(3)}$$

$$Nu_{ref} = \frac{\alpha_{syn\_ref} \cdot d}{\lambda_{syn\_ref}} \quad \text{Eq.(4)}$$

$$\alpha_{syn\_ref} = \frac{\dot{Q}_{ref}}{A_{ref} \cdot (\Delta T_{ref})} \quad \text{Eq.(5)}$$

where λ_{bed} (= 0.38 W m^{-1} K^{-1} for wood char) [66] and λ_{syn_ref} (= 0.24 W m^{-1} K^{-1} according to Appendix) are the thermal conductivity of wood char and syngas in the reformer, respectively. Re_{ref} (= 4.5) and Pr_{ref} (= 0.46) are the Reynolds number and Prandtl number of the syngas in the reformer. A_{ref} (= 0.108 m^2 for the length of 0.32 m) is the heat transfer area of the reformer's internal wall.

As far as we know, char catalyst can be used as a low-cost protector to reform most of the tar before commercial catalysts. The design of the reformer also takes the combination of the commercial catalysts for methane reforming into account. A mixing catalyst testing, char catalyst bed (tar reforming) and nickel catalyst bed (methane reforming), with inert material in between, is planned to be examined in the future. As a result, 3 times the theoretical char bed length (1 m) is determined for this design. The heating shell will also be separated into 3 parts for heating three different bed regions individually (Fig. 3.8), which is suitable for controlling the temperature range in different heights of the reformer when applying the char catalysts and nickel catalysts at different levels.

The actual tar reformer is displayed in Figure 3.5. A simple pipe with an inside diameter of 107.1 mm constitutes the main reformer (Table 3.5). A perforated plate is inserted in the bottom of the reformer as a support for the tar-reforming catalysts. The accurate length for the catalyst bed inside the reformer is 1040 mm. The cap of the reformer possesses several channels directly coupled with the temperature probes to detect the temperatures at different levels in the reformer. The reformed syngas passing through the catalyst bed enters a flue gas pipe with subsequent connections of analyzing devices. The catalyst can be easily added into the reformer from the hopper which is combined with the flue gas pipe.

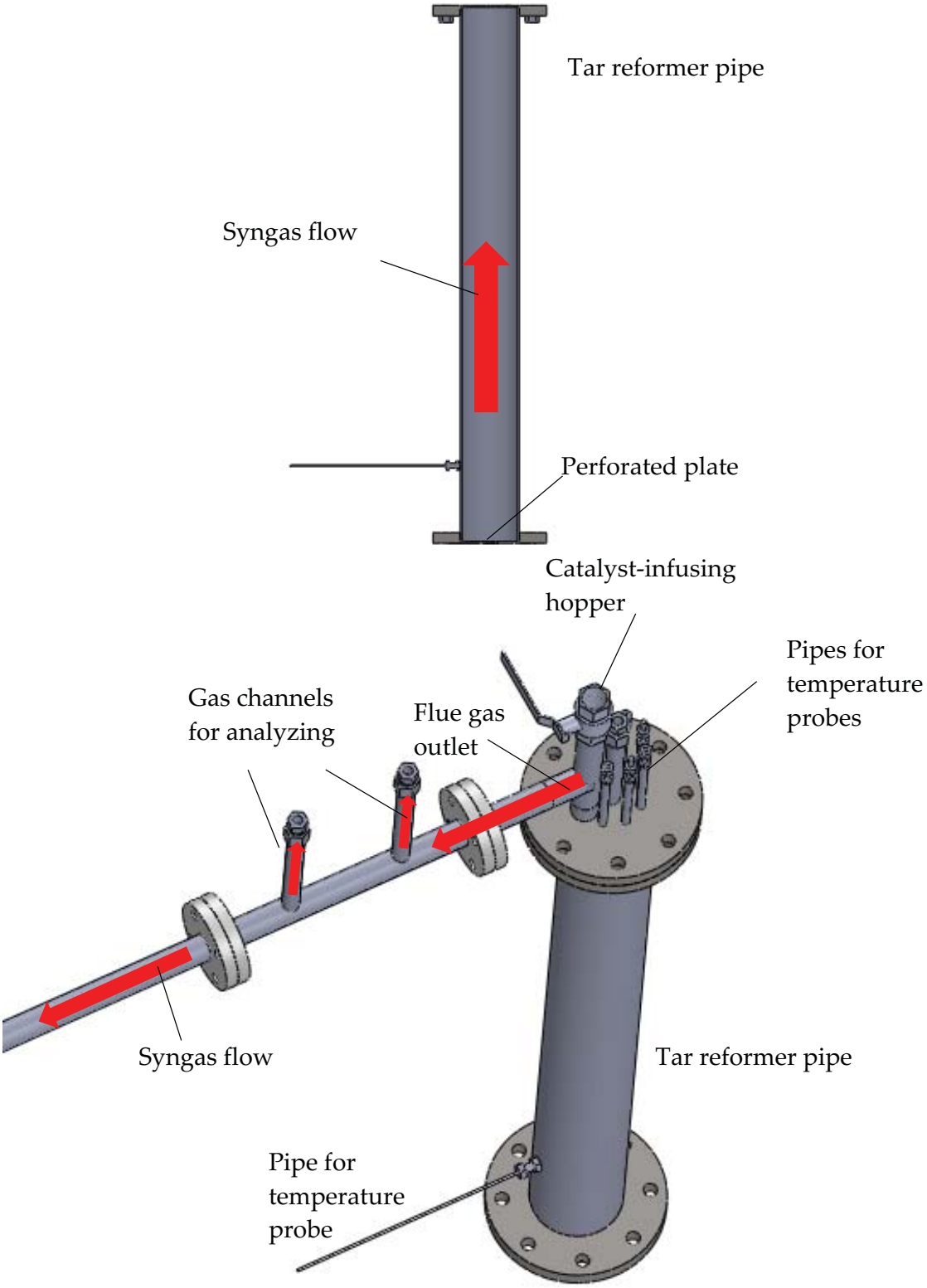

Figure 3.5 The design of the tar reformer

3.6.3 Design of the preheater

The suitable length of the preheater is decided by considering the heat required for the raw syngas ramping up from 300 to 900 °C (all properties of the referring syngas in this section were taken by the average of values at 300 and 900 °C.). The designed preheater is mainly composed of two pipes with close diameters. The ring area between Pipe1 and Pipe2 is the main film for heat transfer from the outside heat source to the raw syngas passing through (Fig. 3.6).

The derivation of Nusselt number (Nu_{preH}) in the ring area has been developed according to Martin [67]. In a laminar flow where Re is less than 2300 (as in this case, Re_{preH} = 77), Nu_{preH} can be calculated by Eq.(6) when the heat is transferred from Pipe1 to Pipe2. The heat transfer coefficient (α_{syn_preH}) in the ring film is then obtained. At last, utilizing the values of $\dot{Q}_{preH}$ for preheating and surface area (A_{preH}) of Pipe1's internal wall, the temperature difference between T_a and T_i (shown in Fig. 3.6) thus comes out. Since the diameter and the length of the preheaters' pipes have a significant influence on the temperature difference, a suitable design should be carried out to avoid considerable variation of the temperature profile. As the design of Pipe1 should be the same size as the reformer, a thoughtful selection of Pipe2's diameter is necessary to maintain a narrow distance in the film ring region. The characteristics of both pipes are listed in Table 3.5. On the other hand, as the longer the Pipe1 is, the more the heat transfer area is, a proper length is determined to be around 0.4 m (429 mm) for the whole preheater. The temperature variation (ΔT_{preH}) from T_a to T_i is then calculated with a low value of 300 K, and a homogeneous temperature profile can be hence reached in the preheated syngas.

$$Nu_{preH} = 3.66 + 1.2 \cdot \left(\frac{d_i}{d_a}\right)^{0.5} \quad \text{Eq.(6)}$$

$$Nu_{preH} = \frac{\alpha_{syn\_preH} \cdot d_h}{\lambda_{syn\_preH}} \quad \text{Eq.(7)}$$

$$\alpha_{syn\_preH} = \frac{\dot{Q}_{preH}}{A_{preH} \cdot (\Delta T_{preH})} \quad \text{Eq.(8)}$$

Where d_i and d_a are Pipe2's outside diameter and Pipe1's inside diameter, respectively. λ_{syn_preH} (= 0.18 W m^{-1} K^{-1}) is the thermal conductivity of the syngas in the preheater. d_h (hydraulic diameter) is equal to (d_a - d_i). A_{preH} (0.135 m^2 for the length of 0.4 m) is the heat transfer area of Pipe1's internal wall.

The actual design of the preheater is illustrated in Figure 3.7. Pipe1 and Pipe2 are constructed as the previous description. Another pipe (Pipe3) is fixed in the center as a path for guiding the low-temperature raw syngas to the primary heating area (the film ring area between Pipe1 and Pipe2). Heated syngas then flows into a mixing chamber before penetrating the perforated plate into the tar reformer.

Table 3.5 The characteristics of pipes in the reformer and preheater

Part	External diameter (mm)	Wall thickness (mm)	Inner diameter (mm)	Material
Main reformer	114.3	3.6	107.1	HWF 1.4841
Pipe1	114.3	3.6	107.1 (d_a)	HWF 1.4841
Pipe2	101.6 (d_i)	4	93.6	HWF 1.4841

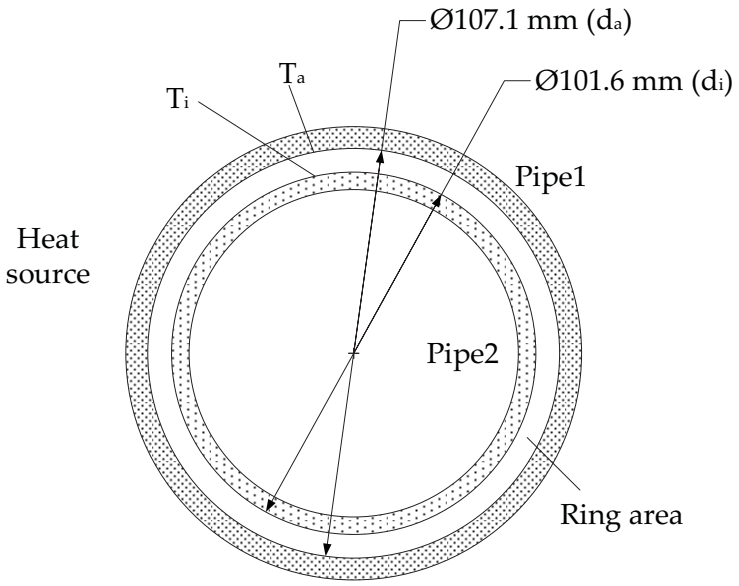

Figure 3.6 The ring area constituted by two pipes in the preheater for heat transfer.

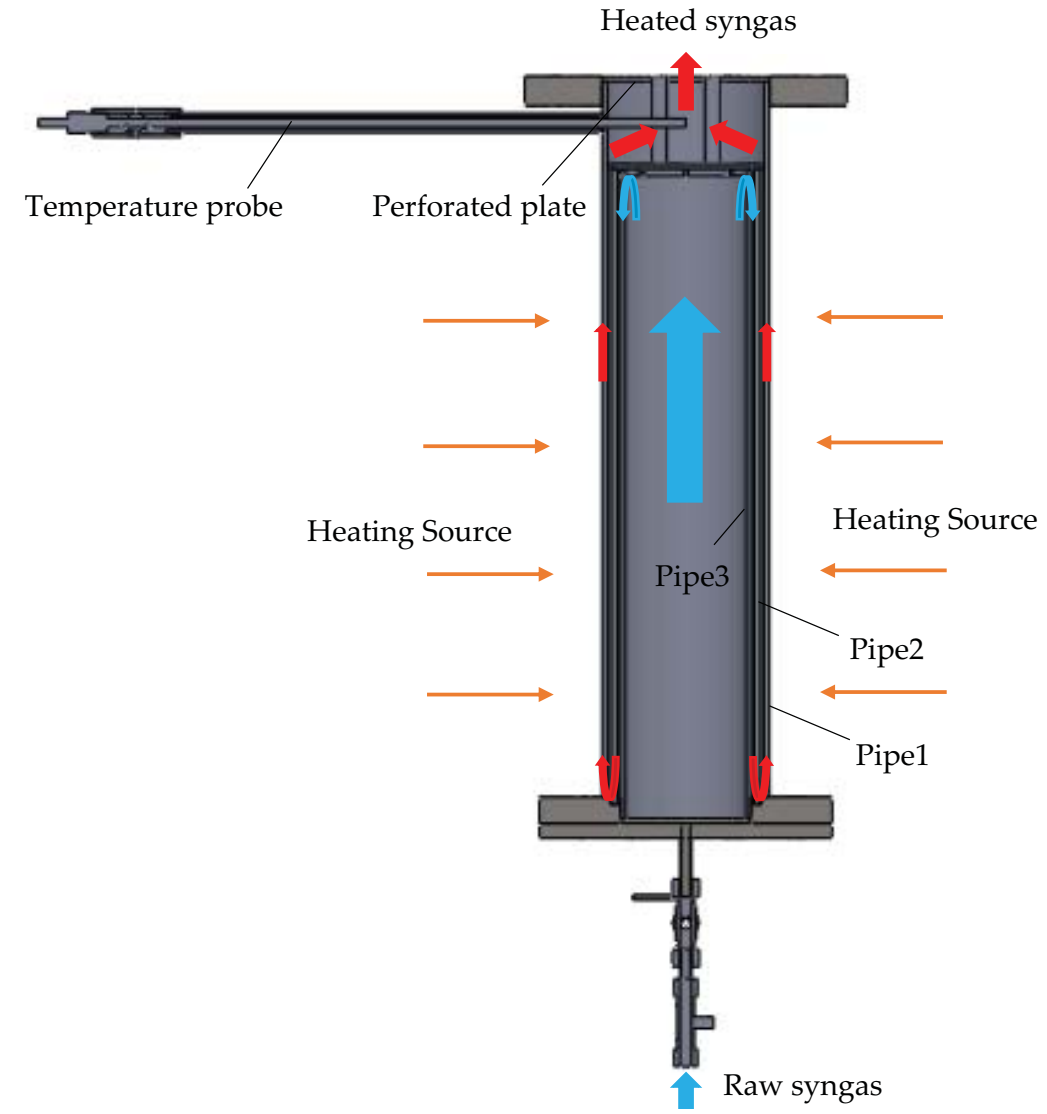

Figure 3.7 The design of the Preheater.

3.6.4 Heat source

Heat transfer from the heat source to the reformer and preheater is mainly controlled by thermal radiation. Since the temperatures on the external wall and internal wall of stainless pipe have no evident difference due to thin thickness and promising conductivity, the temperature variation can be directly calculated by Stefan–Boltzmann law between the heat source and the

internal wall. The minimum temperature ($T_{HS,m}$) of the heat source can be hence calculated. Both $T_{HS,m}$ for the preheater and reformer are derived via Eq.(9) with the values of 950 ℃ and 1019 ℃, respectively. Heating shells that are equipped with heating elements exhibiting high-temperature (> 1100 ℃) releasing ability are the proper choice for this design considering the slight heat loss to the external environment although an ideal insulation layer will cover the heating shell.

$$\dot{Q} = \sigma \cdot A \cdot ({T_{HS,m}}^4 - {T_{wall,in}}^4) \qquad \text{Eq.(9)}$$

Where $\dot{Q}$ is $\dot{Q}_{ref}$ or $\dot{Q}_{preH}$. σ is Stefan–Boltzmann constant. A is A_{ref} or A_{preH}. $T_{HS,m}$ is the minimum temperature of heat source for the tar reformer or preheater. $T_{wall,in}$ is the temperature on the internal wall surface of the reformer or T_a on Pipe1 of the preheater.

3.6.5 The diagram of the tar reformer integrated with the preheater

The reformer is illustrated in Figure 3.8. The heating shells and insulation layers are put on the plate support. The heating shells for the reformer are separated into 3 parts while the preheater is surrounded with only one heating shell as shown in Figure 3.7. This facility is now put on the 10 m floor of the University of Stuttgart's power plant for further testing. The pipe for the entrance of the raw syngas is connected with Elwira.

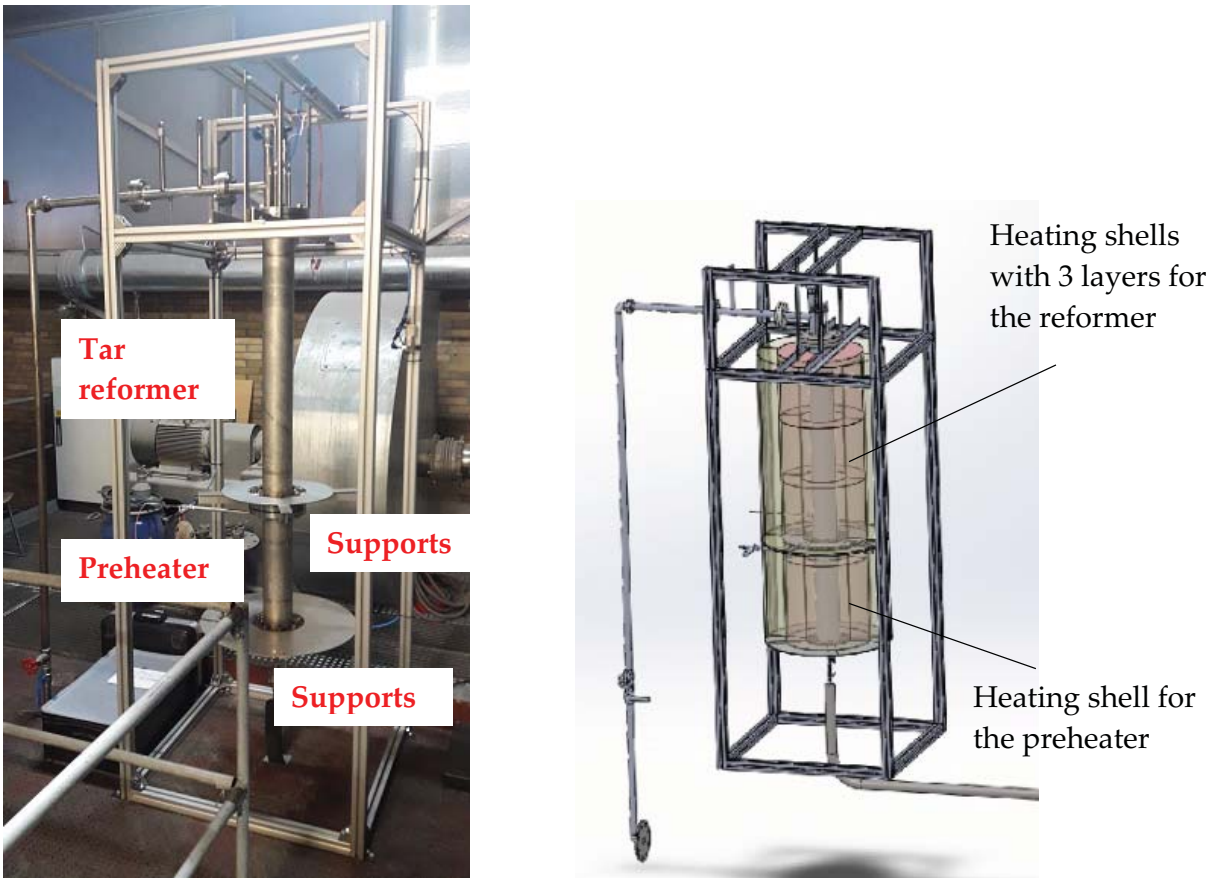

Figure 3.8 The picture of the tar reformer system.

4 Summary and Conclusions

This research successfully examined different biochars for the utilization in tar reforming. In–situ biochar mixture produced inherently from steam oxygen gasification has been proven as a reusable material to enhance the overall performance of the original gasification process. Pyrolyzed biochars are capable of applying as tar–reforming catalysts at high-temperature range between 850 and 900 °C in a fixed bed after sorption enhanced gasification. New methods for gasification rate enumerating, gasification model developing, and tar–reforming kinetics calculating are completely presented here. These empirical equations are then adopted for a tar–reformer design. On the other hand, palm shell char supported potassium and iron exhibits promoting catalytic performance on tar reforming with lower reforming temperature compared to raw palm shell char.

Several novel findings in this research are listed below:

- Straw char containing fly ash (SCFA) collected from the cyclone after steam-oxygen gasification has the potential to be reused as a tar–reforming catalyst. However, the fine particle form due to fluidization in steam-oxygen gasification is much more suitable for the application in a fluidized bed reactor. Char surface, which provides the main surface area in straw char containing fly ash, plays a big role in toluene reforming.
- Gasification of straw char containing fly ash and selectivity of toluene reforming over straw char containing fly ash are highly related to the steam to hydrogen volumetric ratio in the sample gas. Although toluene can be catalytically reformed over straw char containing fly ash accompanied with the spontaneous gasification in a simulated SOG environment with C_{H2O}/C_{H2} = 1, adding additional steam into the SOG

derived syngas before the tar reformer should be considered for formulating C_{H2O}/C_{H2} larger than 1 when applying recycled SCFA as tar–reforming catalyst. The reduction of the aromatic structure and enhancement of the gasification rate by increasing C_{H2O}/C_{H2} are beneficial for the downstream utilization and the total carbon conversion of the fuel.

- Toluene and hydrogen show an inhibiting effect on steam gasification. Tar in the syngas can diminish the gasification rate of biochar catalysts in a connecting tar reformer.
- The deactivation of straw char containing fly ash and the reforming selectivity are highly related to the alternation of the surface property.
- Different biochars (wood char, straw char, and palm shell char) exhibit different gasification reactivity during tar reforming due to the significant difference of AAEM group content.
- As for the reforming selectivity, toluene and naphthalene over pyrolyzed biochars are mainly decomposed to light components with low benzene selectivity.
- Parallel gasification of biochars during the reforming of tar model compounds is highly related to the activation and deactivation of biochars. Initial gasification can increase the surface area and micropores. However, mass loss, pore collapsing, and ash agglomeration after continuous gasification lead to the deactivation of biochars.
- It is worth developing K- and Fe- loaded biochars for reducing the reforming temperature. These metal promoters significantly enhance the catalytic activity of palm shell char, while intense gasification carried out on potassium loaded palm shell char results in a rapid mass loss. Iron is a relatively tender promoter on the palm shell char suitable for long-term

operation with a quick activation only at the very beginning during the reforming of toluene and naphthalene mixture.

- Elevated temperature and steam fraction promote gasification during tar reforming.
- Wood char gasification with H_2O, H_2, and tar model compounds fits the Extended Random Pore Model.
- Insignificant hydrogen inhibition on tar reforming over wood char is observed, while tar reforming over CaO exhibits an apparent hydrogen inhibition.
- Carbon conversion of biochar due to gasification is a crucial parameter for the kinetics of tar reforming considering deactivation.
- The design of a tar reformer is performed based on the developed kinetic model of wood char. The required volume of the wood char bed per $m^3\ h^{-1}_{STP}$ syngas is calculated. The consideration of heat demands for tar reforming over wood char is also presented in this study.

Via these comprehensive investigations of biochar application in tar reforming, the basic concept for utilizing biochars in a tar reformer is established. After a pilot-scale reformer is constructed, the biochar shall be tested at a high-temperature level with real syngas produced in biomass gasification on a technical scale (i.e. approx. 5-7 kg/h fuel). Validating them under practical biomass gasification conditions at the technical scale is the major future work of this study. This will help to render biomass gasification more efficient and economical.

References

[1] Molino A, Chianese S, Musmarra D. Biomass gasification technology: The state of the art overview. Journal of Energy Chemistry 2016;25(1):10–25.

[2] Milne TA, Evans RJ, Abatzoglou N. Biomass Gasifier "Tars": Their Nature, Formation, and Conversion. National Renewable Energy Laboratory: Golden, Colorado, U.S; 1998.

[3] Sikarwar VS, Zhao M, Clough P, Yao J, Zhong X, Memon MZ et al. An overview of advances in biomass gasification. Energy & Environmental Science 2016;9(10):2939–77.

[4] Bridgwater AV. The technical and economic feasibility of biomass gasification for power generation. Fuel 1995;74(5):631–53.

[5] Anis S, Zainal ZA. Tar reduction in biomass producer gas via mechanical, catalytic and thermal methods: A review. Renewable and Sustainable Energy Reviews 2011;15(5):2355–77.

[6] Świerczyński D, Libs S, Courson C, Kiennemann A. Steam reforming of tar from a biomass gasification process over Ni/olivine catalyst using toluene as a model compound. Applied Catalysis B: Environmental 2007;74(3-4):211–22.

[7] Abu El-Rub Z, Bramer EA, Brem G. Review of Catalysts for Tar Elimination in Biomass Gasification Processes. Industrial & Engineering Chemistry Research 2004;43(22):6911–9.

[8] Coll R, Salvadó J, Farriol X, Montané D. Steam reforming model compounds of biomass gasification tars: conversion at different operating conditions and tendency towards coke formation. Fuel Processing Technology 2001;74(1):19–31.

[9] Anis S, Zainal ZA. Tar reduction in biomass producer gas via mechanical, catalytic and thermal methods: A review. Renewable and Sustainable Energy Reviews 2011;15(5):2355–77.

[10] van de Kamp WL, de Wild PJ, Knoef HAM, Neeft JPA, Kiel JHA. Tar Measurement in Biomass Gasification, Standardisation and Supporting R&D. Research Centre of the Netherlands, 2006 report ECN-C-06-046: The Netherlands; 2006.

[11] Neeft JPA, Knoef HAM, Zielke U, Sjöström K, Hasler P, Simell PA, Dorrington MA, Thomas L, Abatzoglou N, Deutch S, Greil C, Buffinga GJ, Brage C, Suomalainen M. Guideline for sampling and analysis of tar and particles in biomass producer gases. In: Bridgwater AV (Ed.), Progress in Thermochemical Biomass Conversion. Blackwell Science Ltd.: Oxford, UK; 2001. 162.

[12]Dayton D. A Review of the Literature on Catalytic Biomass Tar Destruction: Colorado, US: National Renewable Energy Laboratory. Report No. NREL/TP- 510-32815; 2002.

[13] Soltes EJ, Milne TA (eds.). Pyrolysis Oils from Biomass. Washington, DC: American Chemical Society; 1988.

[14] Hawthorne C, Poboss N, Dieter H, Gredinger A, Zieba M, Scheffknecht G. Operation and results of a 200-kWth dual fluidized bed pilot plant gasifier with adsorption-enhanced reforming. Biomass Conversion and Biorefinery 2012;2(3):217–27.

[15] Poboss N, Swiecki K, Charitos A, Hawthorne C, Zieba M, Scheffknecht G. Experimental investigation of the absorption enhanced reforming of biomass in a 20 kWth dual fluidized bed system. International Journal of Thermodynamics 2012;15(1):53–9.

[16] Soukup G, Pfeifer C, Kreuzeder A, Hofbauer H. In Situ CO 2 Capture in a Dual Fluidized Bed Biomass Steam Gasifier - Bed Material and Fuel Variation. Chemical Engineering and Technology 2009;32(3):348–54.

[17] Pfeifer C, Koppatz S, Hofbauer H. Steam gasification of various feedstocks at a dual fluidised bed gasifier: Impacts of operation conditions and bed materials. Biomass Conversion and Biorefinery 2011;1(1):39–53.

[18] Steiert S. FuE-Plattform "Biomass-to-Gas" – Energetische Nutzung biogener Reststoffe mit AER-Technologie zur Poly-Generation von Strom, Wasserstoff, Erdgassubstitut und Wärme. Schlussbericht. Zentrums für Sonnenenergie-und Wasserstoff-Forschung Baden-Wüttemberg (ZSW): Stuttgart, Germany; 2013.

[19] Armbrust N, Poboss N, Eder T, Zieba M, Scheffknecht G. Comparison of Two Methods of Sampling and Analyzing Tars During AER Biomass Gasification: ETA-Florence Renewable Energies. In Proceedings of the 19th European Biomass Conference and Exhibition, Berlin, Germany, 6–10 June 2011.

[20] Schmid M, Beirow M, Schweitzer D, Waizmann G, Spörl R, Scheffknecht G. Product gas composition for steam-oxygen fluidized bed gasification of dried sewage sludge, straw pellets and wood pellets and the influence of limestone as bed material. Biomass and Bioenergy 2018;117:71–7.

[21] Fuentes-Cano D, Gomez-Barea A, Nilsson S, Ollero P. Decomposition kinetics of model tar compounds over chars with different internal structure to model hot tar removal in biomass gasification. Chemical Engineering Journal 2013;228:1223–33.

[22] Shekhawat D, Spivey JJ, Berry DA (ed.). Fuel cells: Technologies for fuel processing. Elsevier Science: Amsterdam, London; 2011.

[23] Taralas G, Kontominas MG. Kinetic modelling of VOC catalytic steam pyrolysis for tar abatement phenomena in gasification/pyrolysis technologies. Fuel 2004;83(9):1235–45.

[24] Taralas G, Kontominas MG. Numerical modeling of tar species/VOC dissociation for clean and intelligent energy production. Energy & Fuels 2005;19(1):87–93.

[25] Taralas G, Kontominas MG, Kakatsios X. Modeling the thermal destruction of toluene (C7H8) as tar-related species for fuel gas cleanup. Energy & Fuels 2003;17(2):329–37.

[26] Simell PA, Hirvensalo EK, Smolander VT, Krause AOI. Steam Reforming of Gasification Gas Tar over Dolomite with Benzene as a Model Compound. Industrial & Engineering Chemistry Research 1999;38(4):1250–7.

[27] Aznar MP, Caballero MA, Gil J, Martín JA, Corella J. Commercial Steam Reforming Catalysts To Improve Biomass Gasification with Steam−Oxygen Mixtures. 2. Catalytic Tar Removal. Industrial & Engineering Chemistry Research 1998;37(7):2668–80.

[28] Guan G, Kaewpanha M, Hao X, Abudula A. Catalytic steam reforming of biomass tar: Prospects and challenges. Renewable and Sustainable Energy Reviews 2016;58:450–61.

[29] Kurkela E, Kurkela M, Hiltunen I. Steam–oxygen gasification of forest residues and bark followed by hot gas filtration and catalytic reforming of tars: Results of an extended time test. Fuel Processing Technology 2016;141:148–58.

[30] Kostyniuk A, Grilc M, Likozar B. Catalytic Cracking of Biomass-Derived Hydrocarbon Tars or Model Compounds To Form Biobased Benzene, Toluene, and Xylene Isomer Mixtures. Industrial & Engineering Chemistry Research 2019;58(19):7690–705.

[31] Zeng X, Ueki Y, Yoshiie R, Naruse I, Wang F, Han Z et al. Recent progress in tar removal by char and the applications: A comprehensive analysis. Carbon Resources Conversion 2020;3:1–18.

[32] Feng D, Zhao Y, Zhang Y, Sun S, Meng S, Guo Y et al. Effects of K and Ca on reforming of model tar compounds with pyrolysis biochars under H2O or CO 2. Chemical Engineering Journal 2016;306:422–32.

[33] Feng D, Zhao Y, Zhang Y, Zhang Z, Che H, Sun S. Experimental comparison of biochar species on in-situ biomass tar H2O reforming over biochar. International Journal of Hydrogen Energy 2017;42(38):24035–46.

[34] Feng D, Zhao Y, Zhang Y, Zhang Z, Sun S. Roles and fates of K and Ca species on biochar structure during in-situ tar H2O reforming over nascent biochar. International Journal of Hydrogen Energy 2017;42(34):21686–96.

[35] Klinghoffer NB, Castaldi MJ, Nzihou A. Catalyst Properties and Catalytic Performance of Char from Biomass Gasification. Industrial & Engineering Chemistry Research 2012;51(40):13113–22.

[36] Kastner JR, Mani S, Juneja A. Catalytic decomposition of tar using iron supported biochar. Fuel Processing Technology 2015;130:31–7.

[37] Nordgreen T, Liliedahl T, Sjostrom K. Metallic iron as a tar breakdown catalyst related to atmospheric, fluidised bed gasification of biomass. Fuel 2006;85(5-6):689–94.

[38] Klinghoffer NB, Castaldi MJ, Nzihou A. Influence of char composition and inorganics on catalytic activity of char from biomass gasification. Fuel 2015;157:37–47.

[39] Abu El-Rub Z, Bramer EA, Brem G. Experimental comparison of biomass chars with other catalysts for tar reduction. Fuel 2008;87(10-11):2243–52.

[40] Krerkkaiwan S, Mueangta S, Thammarat P, Jaisat L, Kuchonthara P. Catalytic Biomass-Derived Tar Decomposition Using Char from the Co-pyrolysis of Coal and Giant Leucaena Wood Biomass. Energy Fuels 2015;29(5):3119–26.

[41] Nitsch X, Commandré J-M, Valette J, Volle G, Martin E. Conversion of Phenol-Based Tars over Biomass Char under H2 and H2O Atmospheres. Energy Fuels 2014;28(11):6936–40.

[42] Bhandari PN, Kumar A, Bellmer DD, Huhnke RL. Synthesis and evaluation of biochar-derived catalysts for removal of toluene (model tar) from biomass-generated producer gas. Renewable Energy 2014;66:346–53.

[43] Chen Y-H, Schmid M, Chang C-C, Chang C-Y, Scheffknecht G. Lab-Scale Investigation of Palm Shell Char as Tar Reforming Catalyst. Catalysts 2020;10(5):476.

[44] Feng D, Zhao Y, Zhang Y, Sun S. Effects of H2O and CO2 on the homogeneous conversion and heterogeneous reforming of biomass tar over biochar. International Journal of Hydrogen Energy 2017;42(18):13070–84.

[45] Research and Markets. Biochar Market Size, Share & Trends Analysis Report By Technology (Gasification, Pyrolysis), By Application (Agriculture (Farming, Livestock)), By Region, And Segment Forecasts, 2019 - 2025. 2019.

[46] Zeng X, Shao R, Wang F, Dong P, Yu J, Xu G. Industrial demonstration plant for the gasification of herb residue by fluidized bed two-stage process. Bioresource technology 2016;206:93–8.

[47] Chen Y-H, Schmid M, Kertthong T, Scheffknecht G. Reforming of toluene as a tar model compound over straw char containing fly ash. Biomass and Bioenergy 2020;141:105657.

[48] Zeng X, Wang F, Han Z, Han J, Zhang J, Wu R et al. Assessment of char property on tar catalytic reforming in a fluidized bed reactor for adopting a two-stage gasification process. Applied Energy 2019;248:115–25.

[49] Fu P, Hu S, Xiang J, Yi W, Bai X, Sun L et al. Evolution of char structure during steam gasification of the chars produced from rapid pyrolysis of rice husk. Bioresource technology 2012;114:691–7.

[50] Ravenni G. Application of biomass char to tar conversion and producer gas upgrading to syngas. Ph.D. Thesis, Technical University of Denmark: Kgs. Lyngby; 2018.

[51] Ravenni G, Elhami OH, Ahrenfeldt J, Henriksen UB, Neubauer Y. Adsorption and decomposition of tar model compounds over the surface of gasification char and active carbon within the temperature range 250–800 °C. Applied Energy 2019;241:139–51.

[52] Brandt P, Larsen E, Henriksen U. High Tar Reduction in a Two-Stage Gasifier. Energy Fuels 2000;14(4):816–9.

[53] Blott SJ, Al-Dousari AM, Pye K, Saye SE. Three-Dimensional Characterization of Sand Grain Shape and Surface Texture Using a Nitrogen Gas Adsorption Technique. Journal of Sedimentary Research 2004;74(1):156–9.

[54] Suzuki T, Nakajima H, Ikenaga N-o, Oda H, Miyake T. Effect of mineral matters in biomass on the gasification rate of their chars. Biomass Conversion and Biorefinery 2011;1(1):17–28.

[55] Yip K, Tian F, Hayashi J-i, Wu H. Effect of Alkali and Alkaline Earth Metallic Species on Biochar Reactivity and Syngas Compositions during Steam Gasification †. Energy Fuels 2010;24(1):173–81.

[56] Nilsson S, Gomez-Barea A, Fuentes Cano D. Gasification reactivity of char from dried sewage sludge in a fluidized bed. Fuel 2012;92(1):346–53.

[57] Gómez-Barea A, Leckner B. Modeling of biomass gasification in fluidized bed. Progress in Energy and Combustion Science 2010;36(4):444–509.

[58] Zhang Y, Hara S, Kajitani S, Ashizawa M. Modeling of catalytic gasification kinetics of coal char and carbon. Fuel 2010;89(1):152–7.

[59] Yu J, Tian F, Chow M, McKenzie L, Li C. Effect of iron on the gasification of Victorian brown coal with steam: enhancement of hydrogen production. Fuel 2006;85(2):127–33.

[60] Speidel M, Fischer H. Steam reforming of tars at low temperature and elevated pressure for model tar component naphthalene. International Journal of Hydrogen Energy 2016;41(30):12920–8.

[61] Mani S, Kastner JR, Juneja A. Catalytic decomposition of toluene using a biomass derived catalyst. Fuel Processing Technology 2013;114:118–25.

[62] Feng D, Zhao Y, Zhang Y, Zhang Z, Zhang L, Sun S. In-situ steam reforming of biomass tar over sawdust biochar in mild catalytic temperature. Biomass & Bioenergy 2017;107:261–70.

[63] Devi L. Catalytic removal of biomass tars: Olivine as prospective in-bed catalyst for fluidizedbed Catalytic removal of biomass tars: Olivine as prospective in-bed catalyst for fluidized-bed biomass gasifiers. Eindhoven, The Netherlands; 2005.

[64] Martin H, Nilles M. Radiale Wärmeleitung in durchströmten Schüttungsrohren. Chemie Ingenieur Technik 1993;65(12):1468–77.

[65] Martin, H., Nilles, M. Wärmeübertragung an der Wand durchströmter Schuttungsrohre. VDI-Eds: Düsseldorf, Germany; 1991.

[66] Muñoz-Hernández A, Diaz G. Modeling of thermal runaway of carbonaceous materials: Graphite, biochar, and wood. AIP Advances 2018;8(9):95312.

[67] Martin H. Vorlesung Wärmeübertragung 2; 1990.

[68] VDI e.V. VDI-Wärmeatlas, Eleventh Edition. Springer Verlag: Berlin Heidelberg, Germany; 2013

Appendix

1. Specific heat capacity of gas component i ($C_{p,i}$) and gas mixture ($C_{p,mix}$):

$$\frac{C_{p,i}}{R_i} = \mathrm{B} + (\mathrm{C} - \mathrm{B}) \cdot \left(\frac{T}{A+T}\right)^2 \cdot [1 - \frac{A}{A+T} \cdot (D + E \cdot \frac{T}{A+T} + F \cdot \left(\frac{T}{A+T}\right)^2 + G \cdot \left(\frac{T}{A+T}\right)^3)]$$

$$C_{p,mix} = \sum_i m_i \cdot C_{p,i}$$

where R_i (J kg^{-1} K^{-1}) is ideal gas constant of gas component i and T (K) is the temperature of gas mixture. Constants in the equation are listed in Table A1. m_i is the mass fraction of gas component i.

Table A1 Constants of specific heat capacity of ideal gas component i.

Gas component i	A	B	C	D	E	F	G
H_2O	706.3032	5.1703	-6.0865	-6.6011	36.2723	-63.0965	46.2085
H_2	392.8422	2.4906	-3.6262	-1.9624	35.6197	-81.3691	62.6668
CO	407.9796	3.5028	2.8524	-2.3018	32.9055	-100.1815	106.1141
CO_2	514.5073	3.4923	-0.9306	-6.0861	54.1586	-97.5157	70.9687
CH_4	1530.8043	4.2039	-16.615	-3.5668	43.0563	-86.5507	65.5986
N_2	432.2027	3.516	2.8021	-4.1924	42.0153	-114.25	111.1019
Air	2548.932	3.5248	-0.6366	-3.4281	49.8238	-120.3466	98.8659

2. Thermal conductivity of gas component i (λ_i) and gas mixture (λ_{mix}):

$$\frac{\lambda_i}{w/(m \cdot K)} = \mathrm{A} + \mathrm{B} \cdot \frac{T}{K} + C \cdot \left(\frac{T}{K}\right)^2 + D \cdot \left(\frac{T}{K}\right)^3 + E \cdot \left(\frac{T}{K}\right)^4$$

$$\lambda_{mix} = \sum_i V_i \cdot \lambda_i$$

where V_i the is volume fraction of gas component i. Constants in the equation are listed in Table A2.

Table A2 Constants of thermal conductivity of ideal gas component i.

Gas component i	A	B	C	D	E
H_2O	0.013918	-0.00004699	2.58066E-07	-1.83149E-10	5.5092E-14
H_2	0.000651	0.0007673	-6.8705E-07	5.0651E-10	-1.3854E-13
CO	-0.000783	0.00010317	-6.759E-08	3.945E-11	-9.47E-15
CO_2	-0.003882	0.00005283	7.146E-08	-7.031E-11	1.809E-14
CH_4	0.008154	0.00000811	3.5153E-07	-3.3865E-10	1.4092E-13
N_2	-0.000133	0.00010149	-6.065E-08	3.361E-11	-7.1E-15
Air	-0.000908	0.00011161	-8.4333E-08	5.6964E-11	-1.5631E-14

3. Dynamic viscosity of gas component i (η_i) and gas mixture (η_{mix}):

$$\frac{\eta_i}{Pa \cdot s} = A + B \cdot \frac{T}{K} + C \cdot \left(\frac{T}{K}\right)^2 + D \cdot \left(\frac{T}{K}\right)^3 + E \cdot \left(\frac{T}{K}\right)^4$$

$$\eta_{mix} = \sum_i V_i \cdot \eta_i$$

where constants in the equation are listed in Table A3.

Table A3 Constants of dynamic viscosity of ideal gas component i.

Gas component i	A	B	C	D	E
H_2O	6.4966E-06	-1.5102E-08	1.15935E-10	-1.008E-13	3.1E-17
H_2	1.8024E-06	2.7174E-08	-1.3395E-11	5.85E-15	-1.04E-18
CO	1.384E-07	7.4306E-08	-6.2996E-11	3.948E-14	-1.032E-17
CO_2	-1.8024E-06	6.5989E-08	-3.7108E-11	1.586E-14	-3E-18
CH_4	-7.759E-07	5.0484E-08	-4.3101E-11	3.118E-14	-9.81E-18
N_2	-1.02E-07	7.4785E-08	-5.9037E-11	3.23E-14	-6.73E-18
Air	-1.702E-07	7.9965E-08	-7.2183E-11	4.96E-14	-1.388E-17

4. Density of ideal gas component i (ρ_i) and gas mixture (ρ_{mix}):

$$\rho_i = \frac{\bar{M} \cdot P}{R \cdot T}$$

$$\rho_{mix} = \sum_i V_i \cdot \rho_i$$

where $\bar{M}$ and P are molar weight of gas component i and atmosphere pressure, respectively.

P.S. Design of the preheater takes the average of the values calculated by the temperature of inlet temperature (300 °C) and desired final temperature (900 °C). Design of the reformer only considers the desired temperature in the reformer (900 °C).